

**IDENTIFICATION AND CHARACTERIZATION OF THE BIOCHEMICAL AND
PHYSIOLOGICAL FUNCTIONS OF ACYL-COA DEHYDROGENASE 10**

by

Kaitlyn Nicole Kormanik

BS Biology, Wilkes University, 2009

Submitted to the Graduate Faculty of
Graduate School of Public Health in partial fulfillment
of the requirements for the degree of
Doctor of Philosophy

University of Pittsburgh

2014

UNIVERSITY OF PITTSBURGH
GRADUATE SCHOOL OF PUBLIC HEALTH

This dissertation was presented

by

Kaitlyn Nicole Kormanik

It was defended on

April 17, 2014

and approved by

Dissertation Director: Jerry Vockley, M.D. Ph.D., Professor
Pediatrics, School of Medicine, Professor, Graduate School of Public Health,
University of Pittsburgh

Al-Walid Mohsen, Ph.D., Associate Professor, Pediatrics
School of Medicine, University of Pittsburgh

Candace Kammerer, Ph.D., Professor, Human Genetics
Graduate School of Public Health, University of Pittsburgh

Zsolt Urban, Ph.D., Associate Professor, Human Genetics
Graduate School of Public Health, University of Pittsburgh

David Finegold, Ph.D., Professor, Pediatrics
School of Medicine, University of Pittsburgh

Copyright © by Kaitlyn N. Kormanik

2014

**IDENTIFICATION AND CHARACTERIZATION OF THE BIOCHEMICAL AND
PHYSIOLOGICAL FUNCTIONS OF ACYL-COA DEHYDROGENASE 10**

Kaitlyn Nicole Kormanik, PhD

University of Pittsburgh, 2014

ABSTRACT

The acyl-CoA dehydrogenase, ACAD, genes encode enzymes that are essential to cellular metabolism as evidenced by the identification in the past 20 years of genetic defects associated with nine members of this gene family. In total, these defects constitute the most common inborn errors of metabolism identified through newborn screening and so are concerns to public health. Recently, two new ACADs, ACAD10 and 11, of unknown function have been identified. This discovery raises the specter of additional unrecognized disorders since prior studies on these two ACADs suggested a novel role in metabolism. Recently, ACAD10 has been linked to type 2 diabetes in Pima Indians, which draws additional attention to its role in metabolism and public health importance.

Both ACAD10 and ACAD11 are highly conserved but with unique additional large protein domains compared to other ACADs, likely encoded from multiple coding domains. ACAD10 antigen in mice is present in lung, muscle, kidney, and pancreas, and localized to mitochondria, while a weak signal is also observed in peroxisomes of mouse lung. Human tissues including lung, kidney, liver, muscle, and pancreas reveal antigen present in mitochondria, and a weak antigen signal in peroxisomes in kidney and pancreas.

To investigate the role of ACAD10 in metabolism further, I have generated an *Acad10* deficient mouse and have characterized it through pathological, biochemical, and molecular studies. Deficient animals are viable and fertile, but become obese. Pathological studies reveal

inflammatory liver disease and secondary splenic extramedullary hematopoiesis. Skeletal muscle findings were abnormal, consistent with deficient mice have elevated creatine kinase when fasting, indicative of rhabdomyolysis. Metabolomics analysis identified elevated levels of a variety of acylcarnitine species in deficient mouse samples consistent with mild, global energy dysfunction. Most dramatically, animals develop a syndrome consistent with insulin insensitivity characteristic of type 2 diabetes mellitus in humans. A better understanding of the biochemical pathways and physiological role of ACAD10, as well as the pathophysiology of disorders occurring among this new ACAD family member will allow identification and treatment of patients with ACAD10 deficiency, as well as its role in obesity and type 2 diabetes.

TABLE OF CONTENTS

ACKNOWLEDGEMENTS	XVII
ABBREVIATIONS.....	XIX
1.0 INTRODUCTION.....	1
1.1 MITOCHONDRIAL FATTY ACID OXIDATION.....	1
1.1.1 Structural aspects of ACADs.....	4
1.1.2 Mouse Models of ACAD Deficiencies	5
1.2 ACAD 10 AND 11.....	6
1.2.1 Multiple transcripts from ACAD10 and ACAD11 genes.....	6
1.2.2 Tissue distribution of ACAD10 and ACAD11 transcripts	9
1.2.3 Subcellular location and mitochondrial fractionation of ACAD11 protein isoforms	10
1.2.4 Computer modeling of ACAD10 and ACAD11.....	13
1.3 PLANT ACADS.....	14
1.4 ACAD LOCALIZATION ON GLUT4-CONTAINING VESICLES	15
2.0 EVIDENCE FOR INVOLVEMENT OF MEDIUM CHAIN ACYL-COA DEHYDROGENASE IN THE METABOLISM OF PHENYLBUTYRATE	16
2.1 ABSTRACT.....	16
2.2 INTRODUCTION	17

2.3	MATERIALS AND METHODS	20
2.3.1	Purification of recombinant human MCAD	20
2.3.2	The electron transfer flavoprotein (ETF) purification	21
2.3.3	Fibroblast cell culture and extract preparation.....	21
2.3.4	ETF fluorescence reduction assay.....	22
2.3.5	Phenylbutyryl-CoA synthesis	22
2.3.6	Monitoring the interaction of MCAD with substrates	23
2.3.7	Molecular modeling.....	24
2.4	RESULTS	24
2.4.1	Interaction of MCAD with substrates, the reductive half-reaction	24
2.4.2	Interaction of MCAD: Substrate ternary complex with ETF, the oxidative half reaction	27
2.4.3	The ETF fluorescence reduction assay of cell extract	28
2.5	DISCUSSION.....	28
2.6	ACKNOWLEDGEMENTS	33
3.0	CLONING AND EXPRESSION OF ACAD10 IN <i>E. COLI</i>.....	34
3.1	ABSTRACT.....	34
3.2	INTRODUCTION	35
3.3	MATERIALS AND METHODS	37
3.3.1	Cloning and Expression	37
3.3.2	Transient transfection and overexpression in HEK293T cells with pcDNA ACAD10	39
3.3.3	His-Tag Protein Purification	41

3.3.4	Production and Purification of Anti-ACAD10 Antiserum	41
3.3.5	Western Blot analysis	42
3.3.6	Identification of Proteins by Tandem Mass Spectrometry (MS/MS)	43
3.4	RESULTS	44
3.4.1	ACAD10 cDNA amplification and expression	44
3.4.2	First half reaction	48
3.5	DISCUSSION	53
4.0	CHARACTERIZATION OF AN ACAD10 DEFICIENT MOUSE MODEL: PATHOLOGICAL AND BIOCHEMICAL ANALYSES	56
4.1	ABSTRACT	56
4.2	INTRODUCTION	57
4.2.1	Mitochondrial fatty acid oxidation and diabetes	57
4.3	MATERIALS AND METHODS	59
4.3.1	Subcellular Location of ACAD10 Protein in Human Tissues	59
4.3.2	Subcellular Location of ACAD10 Protein in Mouse Tissues.....	60
4.3.3	Generation of Mutant Mice	61
4.3.4	Clinical Characterization.....	61
4.3.5	Micro MRI Imaging	61
4.3.6	Histopathology	62
4.3.7	Immunohistochemical and immunofluorescent staining of paraffin- embedded sections of mouse tissues	62
4.3.8	Biochemical Analysis.....	63
4.3.9	Glucose and Insulin Regulation Studies	64

4.3.10	Microscopy	65
4.3.11	Electron Transport Chain complexes	65
4.3.11.1	Preparation of Mitochondria from Organs	65
4.3.11.2	Blue native gel electrophoresis (BNGE).....	65
4.3.11.3	Complex I and V gel in situ activity stain	66
4.3.12	qPCR Expression studies	67
4.4	NEUROBEHAVIORAL TESTING.....	67
4.4.1	Open Field Testing.....	67
4.4.2	DigiGait Testing.....	68
4.5	RESULTS	70
4.5.1	ACAD10 Protein	70
4.5.2	<i>Acad10</i> Deficient Mouse Model	75
4.5.3	Clinical Characterization.....	76
4.5.4	Histopathology	79
4.5.5	Transmission Electron Microscopy	84
4.5.6	Biochemical Phenotype	85
4.5.7	Intraperitoneal glucose tolerance test (IPGTT).....	89
4.5.8	Inflammation.....	91
4.5.9	Electron Transport Chain complexes (Liu, Wang et al.).....	95
4.5.10	Quantitative PCR (qPCR)	97
4.6	NEUROBEHAVIORAL ANALYSES	100
4.6.1	Open Field Testing.....	100
4.6.2	Digigait Testing.....	104

4.6.3	Micro-MRI Brain	107
4.7	DISCUSSION.....	109
	APPENDIX A : TATN-1 MUTATIONS REVEAL A NOVEL ROLE FOR TYROSINE AS A METABOLIC SIGNAL THAT INFLUENCES DEVELOPMENTAL DECISIONS AND LONGEVITY IN CAENORHABDITIS ELEGANS.....	114
	APPENDIX B : QUANTITATIVE PCR	182
	APPENDIX C : DIGIGAIT IMAGING SYSTEMS - INDICES.....	186
	APPENDIX D : ACYLCARNITINE MS/MS SPECTRA FOR MOUSE WHOLE BLOOD AND HEART SAMPLES.....	201
	APPENDIX E : COMPLETE ACYLCARNITINE RAW DATA.....	207
	BIBLIOGRAPHY	349

LIST OF TABLES

Table 1. Comparison of FAO deficiencies in mouse models	6
Table 2. Kinetic Constants of Recombinant Human MCAD Using Octanoyl-CoA and Phenylbutyryl-CoA as Substrates and the ETF Fluorescence Reduction Assay	27
Table 3. Human ACAD10 Plasmid Constructs	38
Table 4. ACAD10 Plasmid Primers.....	38
Table 5. Fold change in gene expression in ACAD10 deficient fat tissue compared to control	100

LIST OF FIGURES

Figure 1. Mitochondrial Fatty Acid β -Oxidation Pathway	2
Figure 2. ACAD10 Map	7
Figure 3. Relative expression of ACAD10 mRNA species vs. GUSB in 21 human tissues	8
Figure 4. Distribution of ACAD10 and 11 mRNA and protein in human tissues	10
Figure 5. Immunoblotting of mitochondrial subfractions from different tissue lysates	11
Figure 6. Immunofluorescent staining of ACAD11 in human neuroblastoma and skin fibroblast	12
Figure 7. Comparison of the amino acid residues in the active site of ACAD11	13
Figure 8. Schematic showing a proposed overall pathway for metabolism of phenylbutyrate to its final metabolite	18
Figure 9. Monitoring the formation of the charge transfer complex with purified MCAD upon addition of increasing amounts of octanoyl-CoA.	25
Figure 10. Monitoring the formation of the charge transfer complex with purified MCAD upon addition of increasing amounts of phenylbutyryl-CoA.	26
Figure 11. Detailed proposed pathway of metabolism of phenylbutyrate to its active form, phenylacetate.....	30
Figure 12. Stick representation of MCAD active site residues and ligands with phenylbutyryl- CoA modeled in place of octanoyl-CoA.....	31
Figure 13. Plasmid Map.....	39
Figure 14. ACAD10 Human Plasmid Constructs Map.....	45

Figure 15. Expression of ACD10-ACAD & ACAD11-ACAD domains as His-tag proteins	46
Figure 16. Expression of N-terminus truncated ACAD10 long version in E. coli	47
Figure 17. Overexpression of ACAD10 in HEK293	48
Figure 18. Binding of glutaryl-CoA to ACAD10 short protein.....	49
Figure 19. Binding of HMG-CoA to ACAD10 short protein binding.....	50
Figure 20. Binding of succinyl-CoA to ACAD10 short protein.....	51
Figure 21. Binding of malonyo-CoA to ACAD10 short protein.....	52
Figure 22. Binding of acetoacetyl-CoA to ACAD10 short protein.....	53
Figure 23. Open field testing chamber.....	68
Figure 24. DigiGait testing equipment.....	69
Figure 25. Immunofluorescent staining of ACAD10 in human tissues.....	71
Figure 26. Immunofluorescent staining of ACAD10 in Human tissues.....	72
Figure 27. Western blot survey of human tissues for ACAD10 production.....	73
Figure 28. ACAD11 confocal microscopy on mouse liver and kidney	73
Figure 29. Subcellular fractionation and western blotting of wild type mouse liver tissue.....	74
Figure 30. Subcellular localization of ACAD10 varies in different tissues	75
Figure 31. PCR genotyping of mutant animals.....	76
Figure 32. ACAD10 ^{-/-} and WT mice average body weight measured in grams (g).....	77
Figure 33. Intrabdominal fat accumulation is increased in mutant mice.....	77
Figure 34. Micro-MRI imaging of Acad10 mouse abdominal cavity	78
Figure 35. Mouse food intake	79
Figure 36. Histopathology of tissues from ACAD10 deficient mice.....	80
Figure 37. Organ tissue weights.....	81

Figure 38. Western blot survey of ACAD10 in mouse brain, pancreas, and kidney	82
Figure 39. Western blot survey of ACADs in mouse liver, heart, muscle, and brain	83
Figure 40. Western blot survey of various mouse and human tissues for ACAD11	84
Figure 41. Transmission electron microscopy of control and <i>Acad10</i> deficient mouse tissues ...	85
Figure 42. Acylcarnitines in tissue and blood from wild type and deficient mice.	86
Figure 43. Glucose concentrations in wild type and <i>Acad10</i> ^{-/-} mouse serum	87
Figure 44. Insulin concentration in <i>Acad10</i> ^{-/-} and wild type mice	88
Figure 45. Insulin concentration in <i>Acad10</i> ^{-/-} and wild type mice	88
Figure 46. Intraperitoneal glucose tolerance test on <i>Acad10</i> deficient and wild type female mice	89
Figure 47. Intraperitoneal glucose tolerance test on <i>Acad10</i> deficient and wild type male mice.	90
Figure 48. Total blood glucose level in mice during IPGTT as determined by area under the curve.....	91
Figure 49. Blood CPK level in fed and fasted <i>Acad10</i> ^{-/-} and wild type mice	92
Figure 50. C-reactive protein concentration in wild type and <i>Acad10</i> deficient mice	93
Figure 51. Cytokine levels in blood from wild type and deficient mice.....	94
Figure 52. Cytokine levels in blood from wild type and mutant male mice.....	95
Figure 53. Characterization of electron transport chain complexes by blue native gel electrophoresis	96
Figure 54. Quantitative PCR in <i>Acad10</i> deficient mouse fat tissue.....	97
Figure 55. Quantitative PCR in <i>Acad10</i> deficient mouse muscle tissue	98
Figure 56. Quantitative PCR in <i>Acad10</i> deficient mouse liver tissue	99
Figure 57. Open field zones in testing chamber.	101

Figure 58. Open field ambulatory measures in female mice	102
Figure 59. Open field vertical measures in female mice	102
Figure 60. Open field measures of stereotypic movements in female mice	103
Figure 61. Open filed resting measures in female mice.....	103
Figure 62. Digigait indices I	104
Figure 63. Digigait indices II	105
Figure 64. Digigait indices III.....	106
Figure 65. Digigait indices IV	107
Figure 66. Micro-MRI of mouse brain	108
Figure 67. Diagram of daf-2/IGFR signaling pathway and tyrosine metabolic pathway.....	118
Figure 68. Tyrosine aminotransferase mutations enhance eak dauer and lifespan phenotypes..	121
Figure 69. The tatn-1 mutant enhances dauer formation and lifespan of worms with impaired daf-2/IFGR signaling.....	125
Figure 70. tatn-1 effects on development do not require changes in PI3 kinase signaling.....	129
Figure 71. aak-2 activity is necessary and sufficient for tatn-1 effects on development and longevity	131
Figure 72. tatn-1 acts by daf-16/FOXO dependent and independent mechanisms.....	134
Figure 73. tatn-1 mutants and crh-1/CREB mutants share gene expression profiles and effects on dauer formation.....	140
Figure 74. Control of TATN-1 protein expression by daf-2/IGFR signaling, diet and temperature	143
Figure 75. tatn-1 acts by increasing tyrosine levels.....	148

Figure 76. Model for the regulation of TATN-1 expression, tyrosine levels, and the resulting effects of tyrosine effects on cell signaling pathways	152
Figure 77. qPCR raw data for ACAD10 deficient mouse fat tissue	183
Figure 78. qPCR raw data for ACAD10 deficient mouse muscle tissue	184
Figure 79. qPCR raw data for ACAD10 deficient mouse liver tissue	185
Figure 80. Wild type Mouse Whole Blood Acylcarnitine Chromatogram I.....	201
Figure 81. Acad10 ^{-/-} Mouse Whole Blood Acylcarnitine Chromatogram I	202
Figure 82. Wild type Mouse Whole Blood Acylcarnitine Chromatogram II	203
Figure 83. Acad10 ^{-/-} Mouse Whole Blood Acylcarnitine Chromatogram II	204
Figure 84. Wild type Mouse Heart Acylcarnitine Chromatogram I.....	205
Figure 85. Acad10 ^{-/-} Mouse Heart Acylcarnitine Chromatogram I.....	206

ACKNOWLEDGEMENTS

I would like to express my deepest gratitude to my research advisor Dr. Jerry Vockley for his guidance and constant support in helping me to conduct and complete this work. I would also like to express much thankfulness and appreciation to Dr. Al-Walid Mohsen for his constant encouragement and expertise. In addition, I want to offer special thanks to my academic advisors Dr. Candace Kammerer, Dr David Finegold, and Dr Zsolt Urban for serving on my advisory committee, and for all of their generous advice and feedback regarding my work. Additionally, I would like to acknowledge all the members of the Vockley lab for their support over the years. I want to thank Dr. Edda Thiels and Eloise Peet in the Rodent Behavioral Analysis Core (RBAC)/Department of Neurobiology at the University of Pittsburgh for their guidance and expertise on the behavioral testing of the mice. I am extremely grateful for the patience they had with me as I learned testing of the animals in the Rodent Behavioral Analysis Core. I would like to recognize Dr Kimimasa Tobita who taught me micro-MRI imaging techniques for used in my experimental animal studies.

Special thanks also to Drs. Eric Goetzman, Kristen Skvorak, Lina Gonzalez, Chikara Otsuba, Suzanne Bertera, and Yudong Wang who were instrumental in willing to provide me advice and expertise throughout the process. I am very grateful for all of the support staff and faculties in the Department of Human Genetics and the Graduate School of Public Health who have helped me during my graduate studies. Many thanks to all the people I have come to know at the University of Pittsburgh, and whose friendship and companionship I will always enjoy and remember.

Finally, I owe my sincere appreciation to my family who has supported and encouraged me over the years. I especially want to thank my husband Nathan for the inspiration and motivation during the final years of my studies. I want to extend my deepest appreciation to my mother and father for their love, affection, and constant support during my life and studies, because without them I could not have accomplished my goals.

This work was funded in part by Public Health Service award number NIH R01 DK54936 (JV).

ABBREVIATIONS

aa- amino acid
ACAD9-acyl-CoA dehydrogenase 9
ACAD10-acyl-CoA dehydrogenase 10
ACAD11-acyl-CoA dehydrogenase 11
ACADs - acyl-CoA dehydrogenases
ACADD- acyl-CoA dehydrogenases deficiency
ACN-acetonitrile
AcN(S)-acylcarnitine(s)
APH- aminoglycoside phosphotransferase domain
ATP-adenosine triphosphate
BNGE-blue native gel electrophoresis
bp-base pair
CK-creatine kinase
CoA-coenzyme A
CRP-C-reactive protein
2D-two dimension
DAPI- 4',6-diamidino-2-phenylindole
DMEM-Dulbecco's Modified Eagle Medium
EDTA- ethylenediaminetetraacetic acid
ELISA- enzyme-linked immunosorbent assay
ETC-electron transport chain
ETF-electron transferring flavoprotein
FAD- flavin adenine dinucleotide
FADH- flavin adenine dinucleotide (hydroquinone form)
FAO- fatty acid β -oxidation
FAOD-fatty acid β -oxidation disorders
FBS-fetal bovine serum
FFPE- formalin fixed paraffin embedded
GDH-glutaryl dehydrogenase
GLUT4-glucose transporter type 4
GO - gene ontology
GWAS – genome-wide association study
H₂O₂-hydrogen peroxide
HEK293T- human embryonic kidney cells
HPLC-high performance liquid chromatography
IBA- indole-3-butyric acid

IBD-isobutyryl dehydrogenase
IBR- indole butyric receptor
IEM- inborn errors of metabolism (IEM)
IPGTT-interperitoneal glucose tolerance test
IPTG- Isopropyl β -D-1-thiogalactopyranoside
IR-insulin resistance
IRAP- insulin-regulated aminopeptidase
IVD-isovaleryl dehydrogenase
KD app-dissociation constant
Kd/kDa- kilodaltons
LCAD-long chain acyl-CoA dehydrogenase
LC-MS/MS-liquid chromatography-mass spectrometry/mass spectrometry
MCAD-medium-chain acyl- CoA dehydrogenase
MS - mass spectrometry
NADH- nicotinamide adenine dinucleotide
NBS-newborn screening
OXPHOS-oxidative phosphorylation
PBS- phosphate buffered saline buffer
PCR-polymerase chain reaction
PPAR α -peroxisome proliferator-activated receptor- α
PVDF- polyvinylidene difluoride membrane
RT-PCR- real time PCR
RP-HPLC-reverse phase high performance liquid chromatography
SBCAD-short branched chain acyl-CoA dehydrogenase
SCAD-short chain acyl-CoA dehydrogenase
SDS-PAGE- sodium dodecyl sulfate polyacrylamide gel electrophoresis
SNP – single nucleotide polymorphism
T2DM- type 2 diabetes mellitus
TBS- tris-buffered saline
TCA- tricarboxylic acid
TWEEN- polysorbate 20 (polysorbate surfactant)
UHPLC MS/MS- ultra high performance liquid chromatography-mass spectrometry/mass spectrometry
V-volts
VLC
AD-very long chain acyl-CoA dehydrogenase

1.0 INTRODUCTION

Mitochondrial β -oxidation of fatty acids is critical for maintaining energy balance in organisms. While fatty acids are essential components of membrane structure and energy storage, their functions in cellular signaling, protein activation, and regulation of inflammatory, immune and other stress responses are no less important. These other roles often involve unusual complex lipids that are strictly regulated, often through their acyl-CoA intermediates. The goal of this project was to characterize the role of acyl-CoA dehydrogenases 10 and 11 on the metabolism of acyl-CoAs, and to identify the consequences of its failure in a model organism.

1.1 MITOCHONDRIAL FATTY ACID OXIDATION

Fatty acid β -oxidation (FAO) is a series of enzymatic reactions that occurs in the mitochondria and peroxisomes of all living eukaryotic organisms. β -oxidation in mitochondria generates reducing equivalents that are tied to adenosine triphosphate (ATP) synthesis via the electron transport chain (ETC) (Atkinson, Kapralov et al.), whereas β -oxidation in peroxisomes is associated with the production of hydrogen peroxide (H_2O_2) (Coates and Tanaka 1992, Reddy and Hashimoto 2001). Mitochondrial β -oxidation allows generation of energy from the degradation of fatty acids when the cellular glucose supply is low (Houten and Wanders 2010). Fatty acid synthesis is tightly linked to dietary intake, and during fasting, fatty acid synthesis is

halted, and in turn, fatty acid oxidation is induced (Lehninger 1982). During this process, a variety of substrate transporters and enzymes ultimately lead to the degradation of fatty acids, resulting in the production of FADH_2 and NADH that provide reducing equivalents directly to the ETC, and acetyl-CoA, which is available to enter the Krebs cycle (tricarboxylic acid cycle, TCA) where additional reducing equivalents are generated for production of ATP. ATP is the main source of energy for the organism (Lehninger 1982).

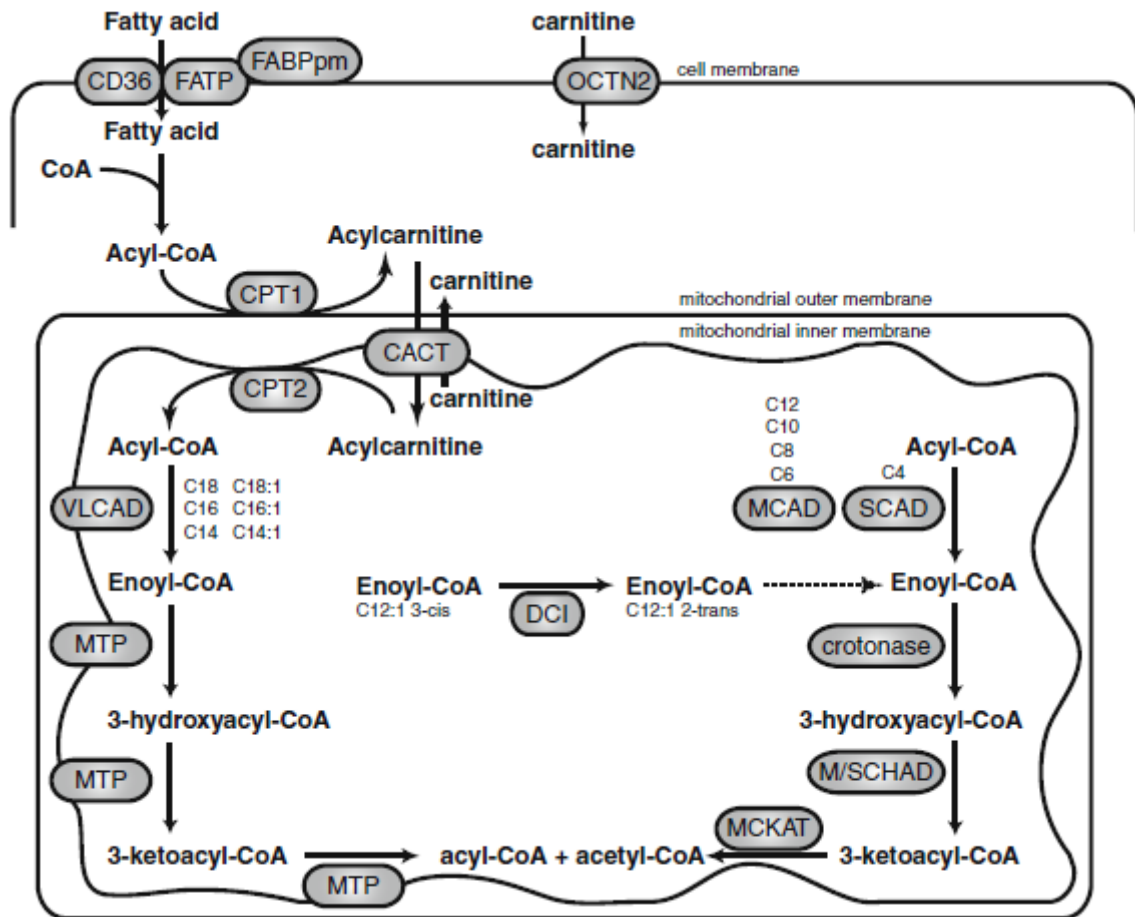


Figure 1. Mitochondrial Fatty Acid β -Oxidation Pathway

Fatty acids consist of a chain of carbons with a carboxyl group attached at one end that serves as a reactive group for incorporation of coenzyme A into the molecule (Houten and

Wanders 2010). Coenzyme A (CoA) is a cofactor that destabilizes the carbon-to-carbon bonds, allowing for reactions to occur at the third carbon in the chain (Houten and Wanders 2010). Free fatty acids are released from body triglyceride stores, then transported to cells via carrier proteins, imported into cells, and imported into the mitochondrial matrix as an activated acyl-CoA substrate (Vockley and Whiteman 2002). There, a series of four enzymatic steps removes an acetyl-CoA moiety from the carbon backbone and leaves an acyl-CoA molecule that is two carbons shorter.

In the first step of β -oxidation within the mitochondrial matrix, acyl-CoA dehydrogenases convert acyl-CoA esters to trans-2-enoyl-CoA, reducing its FAD cofactor to FADH₂ (Lehninger 1982, Swigonova, Mohsen et al. 2009). The trans-2-enoyl-CoA is hydrolyzed by enoyl-CoA hydratase forming a 3-hydroxyacyl-CoA (GallusReactome 2010). The third step involves a second oxidation; 3-hydroxyacyl-CoA is converted to 3-ketoacyl-CoA by 3-hydroxyacyl-CoA dehydrogenase, generating a molecule of NADH (GallusReactome 2010). Reducing equivalents captured in FADH₂ and NADH enter the respiratory chain at complexes I and III, respectively. The final step of the cycle is catalyzed by a ketoacyl-CoA thiolase and releases the two-carbon acetyl-CoA and a 2-carbon shorter acyl-CoA ready for another round of β -oxidation (GallusReactome 2010). Acetyl-CoA has a variety of metabolic fates, one of which is utilization by the TCA cycle, leading, in turn, to the generation of additional reducing equivalents for energy production through oxidative phosphorylation (OXPHOS). Thus, the 18-carbon substrate palmitic acid (C16:0) for example will cycle through this process a total of eight times to reach completion and can generate up to 123 molecules of ATP through oxidative phosphorylation.

Acyl-CoA dehydrogenases catalyze the α,β -dehydrogenation of acyl-CoA esters, utilizing FAD to transfer electrons to electron transferring flavoprotein, and in turn to the ETC. Several acyl-CoA dehydrogenases function in fatty acid oxidation cycle, each with a unique substrate optimum. Very long, medium, and short chain ACDs (VLCAD, MCAD, and SCAD) catalyze the first step of mitochondrial β -oxidation in the mitochondrial matrix with substrate chain length optima of 16, 8, and 4 carbons, respectively (Coates and Tanaka 1992). In contrast to VLCAD, ACAD9 and LCAD are most active against unsaturated long and branched medium chain substrates, respectively (Coates and Tanaka 1992). Other highly homologous ACADs, isovaleryl-CoA (IVD), short/branched chain acyl-CoA (SBCAD), and isobutyryl-CoA dehydrogenases (IBD) (Ibdah, Paul et al.), catalyze the third step in leucine, isoleucine, and valine metabolism, respectively, while glutaryl-CoA dehydrogenase (GDH) functions in lysine and tryptophan catabolic pathways (Coates and Tanaka 1992).

1.1.1 Structural aspects of ACADs

The crystal structures of MCAD, *Mega- losphaera elsendii* butyryl-CoA dehydrogenase, GDH, IVD, SCAD, VLCAD, and IBD have been published and are highly conserved (Tiffany, Roberts et al. 1997, Battaile, Molin-Case et al. 2002, Battaile, Nguyen et al. 2004, McAndrew, Wang et al. 2008). In MCAD, the fatty acyl portion of the octanoyl-CoA substrate is buried inside the polypeptide chain and is surrounded by V259 and Y375 on opposite sides, E376 at the top, and the flavin ring at the bottom. The structure also reveals that the FAD has an extended conformation with interaction of the flavin ring C2 carbonyl oxygen with residue Thr136 of the mature peptide chain. The overall polypeptide fold of IVD and SCAD are similar to that of MCAD and to a bacterial SCAD. The identity of the catalytic base of IVD has been confirmed to

be E254, and the location of the catalytic residue together with a glycine at position 374, which is a tyrosine in all other members of the ACAD family, appears to be important for conferring the branched-chain substrate specificity of IVD.

1.1.2 Mouse Models of ACAD Deficiencies

In the literature, several mouse models of ACAD deficiencies have been developed to help characterize the disease (Houten and Wanders 2010). The majority of these models have been created by genetic manipulation, however, two of them contain spontaneous mutations (Houten and Wanders 2010). Table I. below defines several of these models and how they relate to the disease as observed in humans (Koizumi, Nikaido et al. 1988, Schiffer, Prochazka et al. 1989, Wood, Amendt et al. 1989, Kuwajima, Kono et al. 1991, Kurtz, Rinaldo et al. 1998, Cox, Hamm et al. 2001, Ibdah, Paul et al. 2001, Janssen and Stoffel 2002, Exil, Roberts et al. 2003, Nyman, Cox et al. 2005, Tolwani, Hamm et al. 2005, Ji, You et al. 2008, Miinalainen, Schmitz et al. 2009, Houten and Wanders 2010).

Table 1. Comparison of FAO deficiencies in mouse models

Disease	Human Deficiency	Mouse Mode	Reference
OCTN2/Primary carnitine deficiency	+	+	Koizumi et al. 1988; Kuwajima et al. 1991
CPT1a	+	§	Nyman et al. 2005
CPT1b		§	Ji et al. 2008
LCHAD/MTP	++	++	Ibdah et al. 2001
VLCAD	++	±	Cox et al. 2001; Exil et al. 2003
LCAD	?	+	Kurtz et al. 1998
MCAD		±	Tolwani et al. 2005
SCAD	?(?)	±	Wood et al. 1989; Schiffer et al. 1989
DCI	?	±	Janssen and Stoffel 2002
DECR	++(?)	±	Miinalainen et al. 2009

§ Embryonic lethal

? Unknown

? No phenotype or asymptomatic

± Mild, + moderate, ++ severe

1.2 ACAD 10 AND 11

1.2.1 Multiple transcripts from *ACAD10* and *ACAD11* genes

The function of two additional genes annotated in the human genome and predicted to be ACADs (*ACAD10* and *11*) is unknown (Swigonova, Mohsen et al. 2009, He 2011). These two genes share 46% amino acid homology between each other and are widely conserved across evolution. *ACAD10* and *ACAD11* genes with homology to the ACAD, APH, and HDL domains

are still found in lower organisms, such as fungi (Swigonova, 2009). Both genes are located within complicated loci containing multiple predicted exons and protein domains. Upstream of the conserved ACAD domains, there is a putative aminoglycoside phosphotransferase (APH) domain in both ACAD10 and ACAD11, which also could be a homoserine kinase type II domain (Figure 2) (He, 2011).



Figure 2. ACAD10 Map

The human ACAD10 genes consists of multiple predicted domains, including an APH domain, mitochondrial targeting signal (M), ACAD N-terminal domain (ACDN), ACAD middle domain (ACDM), and ACAD C-terminal domain (ACDC). There is also a predicted hydrolase superfamily domain (HDL) identified at the N-terminus of some alternative protein forms of ACAD10. These domains are drawn as colored boxes with the number of associated amino acids specified.

The N-terminus of ACAD10 is longer than ACAD11, and it contains a predicated hydrolase domain ahead of the APH/homoserine kinase type II domain. Database searches of transcribed sequences from these genes have identified the presence of multiple transcripts that differ mostly at either the 5' or 3' end (He, 2011).

To examine the presence of these transcripts *in vivo*, real-time PCR with primer pairs targeted to unique exon junctions in the different transcripts was used to measure the expression level of alternative transcripts of ACAD10 and 11 in 21 different human tissues (He 2011).

Multiple transcripts from the *ACAD10* gene were detected and the relative abundance of each transcript differed in the various human tissues (Figure 3; (He 2011)). Primer set 7/8 target the region corresponding to the predicted APH domain (He, 2011). Primers 13/14 target a region shared by most transcripts in the genetic databases at the junction between the APH domain and

conserved ACAD N- terminal domain (He, 2011). Primers 21/22 amplified a region mapped to a conserved C-terminal ACAD domain containing the catalytic base (He, 2011). In contrast, primers 21/22' target an alternatively spliced species that eliminate exon 22, leading to loss of the predicted ACAD catalytic domain (He, 2011). In all tissues, expression of the transcripts amplified by primers 7/8 was higher than those by primers 21/22 (He, 2011). Thus, a large portion of the transcripts that contain sequences for an APH domain at the N-terminus do not have sequences for the ACAD domain at the C-terminus (He, 2011). Expression of the fragment defined by p21/22 was much higher than p21/22' showing that the majority of transcripts encoding ACAD domains contain sequences potentially supporting ACAD enzymatic function (He, 2011). Interestingly, in some tissues (*e.g.*, small intestine and thymus) the expression level of transcripts containing fragment 7/8 was higher than those amplified by primers 13/14, suggesting that these tissues may express a previously unrecognized protein species comprised of only an APH domain without ACAD sequences (He, 2011). Figure 3 below represents the expression of each fragment.

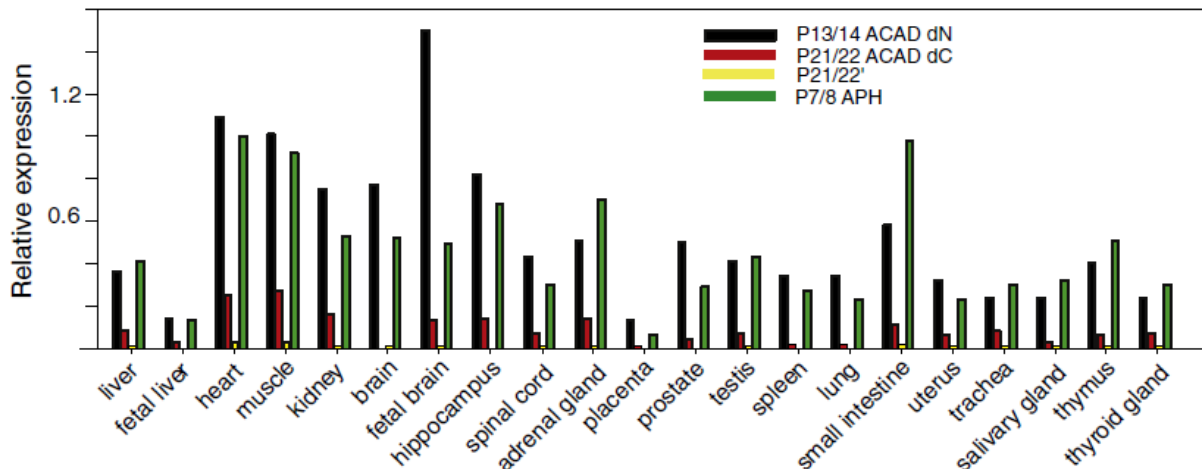


Figure 3. Relative expression of ACAD10 mRNA species vs. GUSB in 21 human tissues

Each colored bar represents the expression of a fragment amplified by a different set of primers as indicated by the legend. The data represent the mean of three qPCR experiments with a robust %CV less than 1.35%

1.2.2 Tissue distribution of ACAD10 and ACAD11 transcripts

To begin to understand the *in vivo* functions of ACAD10 and 11, the tissue expression pattern of the two genes in 21 different human tissues was examined using real-time RT-PCR (He 2011). Information currently available on both genes in public databases proved to be incomplete, hindering the ability to quantitate each of the specific transcripts. Therefore probes p13/14 (ACAD10) and p11/12 (ACAD11) were used to target the sequences that are common to most of the identified transcripts thus measuring the total expression of each gene. ACAD11 had the highest level of expression in adult brain, 1.3 times the expression of the housekeeping gene GUSB (used as the internal control) (He, 2011). Thereafter, expression levels in other tissues were normalized to the brain. ACAD11 additionally had significant levels of expression in adult liver, heart, and kidney. ACAD10 had much lower levels of expression than ACAD11 with the highest level in muscle (0.3 times the expression of GUSB). Figure 4 below shows the expression of ACAD10 in other tissues relative to muscle. Interestingly, ACAD10 was expressed more highly in fetal brain than adult, a pattern similar to that seen for LCAD and also was highly expressed in heart and kidney (He, 2011).

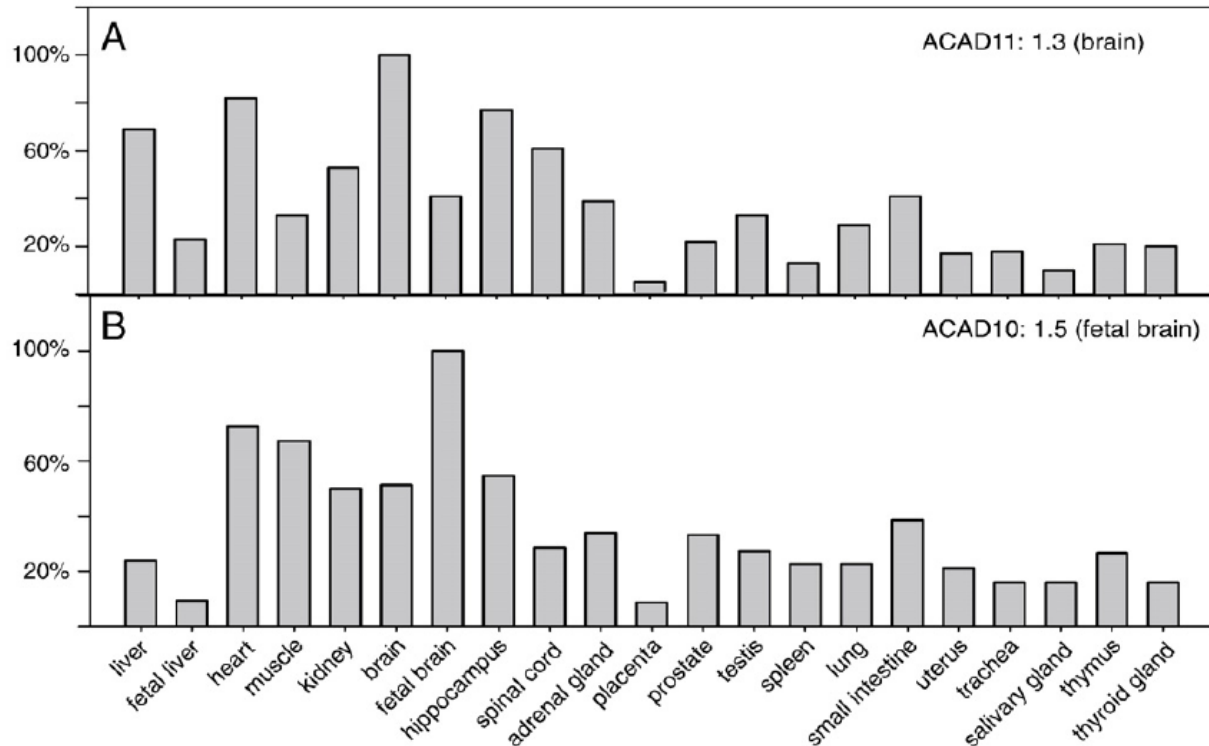


Figure 4. Distribution of ACAD10 and 11 mRNA and protein in human tissues

Levels of ACAD11 (A) and ACAD10 (B) mRNA were measured in 21 human tissues by real-time RT-PCR and normalized to the relative level of expression in the highest expression tissue. Primers P11/12 were used for measuring ACAD11 expression level and primers P13/14 were used for measuring ACAD10 levels. Both probes target the common region among all the known transcripts. The highest expression tissue of ACAD11 was found in brain (ratio to the housekeeping gene GUSB = 1.3), and the highest expression of ACAD10 was in fetal brain (relative expression to GUSB = 1.5).

1.2.3 Subcellular location and mitochondrial fractionation of ACAD11 protein isoforms

The presence of multiple ACAD10 and 11 transcripts in various tissues raises the possibility that some might generate protein species that localize to different subcellular compartments (He 2011). To examine this, two separate rabbit polyclonal antisera were raised against synthetic ACAD11 peptides corresponding to a portion of the sequence of the N-terminal domain of the mature mitochondrial ACAD11 (He, 2011). The peptide sequences are common to potential ACAD11 protein isoforms translated from all identified ACAD11 transcripts, but not

homologous to other ACADs including ACAD10 (He, 2011). Western blot analysis with this antiserum identified an ACAD11 protein species corresponding in size to the mature mitochondria form seen in our *in vitro* import studies. This form primarily localized to the membrane fraction of mitochondria isolated from both human cerebellum and kidney, but not in the mitochondrial matrix fraction (Figure 5) (He, 2011).

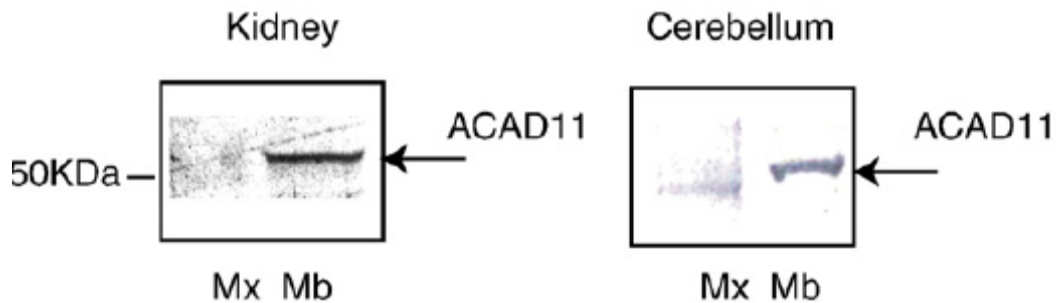


Figure 5. Immunoblotting of mitochondrial subfractions from different tissue lysates

An antibody to an ACAD11 peptide gave the highest signal in human kidney and brain. It appeared mainly in mitochondrial membrane (Mb), rather than matrix fraction (Mx).

Immunofluorescence staining of ACAD11 in human neuroblastoma and skin fibroblasts revealed a marked difference in subcellular location of ACAD11 proteins (Figure 6 A-J) (He, 2011). ACAD11 protein in neuroblastoma cells co-localized with mitochondrial ATPase (Figure 6 A-C) (He, 2011). In contrast, majority of the ACAD11 signal in fibroblasts did not colocalize with mitochondrial ATPase (Figure 6 D-F) (He, 2011).

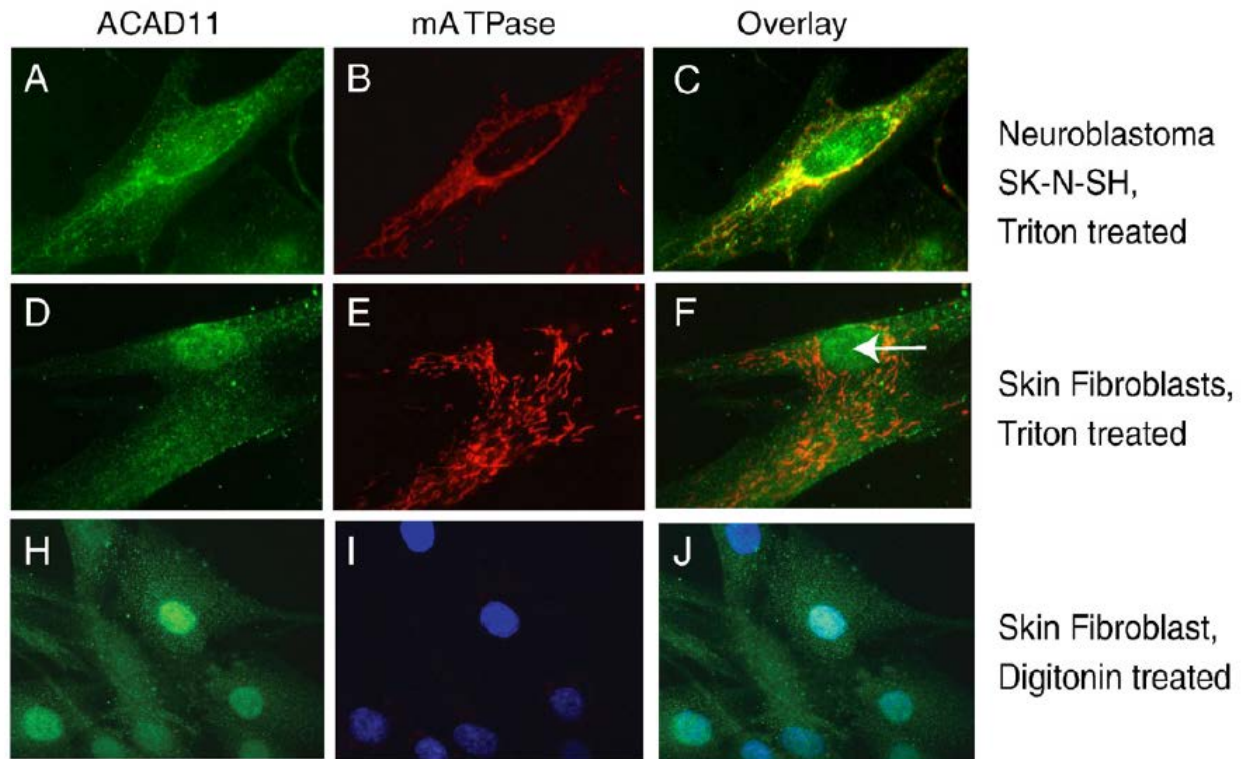


Figure 6. Immunofluorescent staining of ACAD11 in human neuroblastoma and skin fibroblast

Fluorescent staining of human neuroblastoma (SK-N-SH) (A), skin fibroblast (D) with antibodies to an ACAD11 peptide is shown in green. (B and E) Fluorescent staining of the same human cells against mitochondrial ATPase antibody is shown in red. C is the merged image of A and B, and F is the merged image of D and E. The nucleus is indicated by white arrows. Human skin fibroblast were also treated with digitonin to only dissolve only the outer membrane, and then stained with ACAD11 peptide antibody (H), mitochondrial ATPase antibody (I). J is the merged image of H and I, showing ACAD11 stains other single membrane organelles besides mitochondria. DAPI was used for nuclear staining in panels H-J.

Interestingly, in both human skin fibroblast and human neuroblastoma, additional ACAD11 specific staining actually appeared near the cytoplasmic membrane with a punctate pattern typical of membrane associated vesicles, most prominently seen with digitonin treatment (which preferentially solubilizes the cytoplasmic membrane). Finally, ACAD11 antibodies strongly stained nuclei regardless of cell solubilization conditions (Figure 6 H-J), a pattern also seen for ACAD9 (He, 2011). The striking difference in subcellular location of ACAD11 among various cell and tissue types emphasizes that expression of the mitochondrial form of ACAD11 as the product of alternative splicing is tissue specific, in agreement with RNA expression

studies (He, 2011). Consistent with these observations, a global proteomic survey of subcellular organelles of six major organs in mouse localized predicted ACAD10 protein to the membrane (microsomal) fraction and mitochondria, while ACAD11 sequences were identified in peroxisomes and mitochondria (He, 2011).

1.2.4 Computer modeling of ACAD10 and ACAD11

Computer modeling of ACAD10 and ACAD11 predict that an amino acid change from glutamate to aspartate (Figure 7) occurred in the catalytic site of these two members of the ACAD family (He 2011). This change is predicted to lead to different substrate specificity than seen in the other ACADs. To examine this prediction, a fragment comprising the mature mitochondrial coding region was cloned and over expressed in a prokaryotic system.

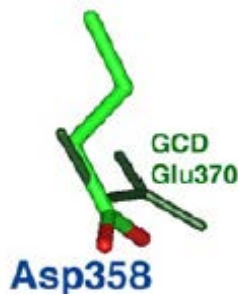


Figure 7. Comparison of the amino acid residues in the active site of ACAD11

A predicted model and GCD crystal structural model. Amino acids in ACAD11 are shown as colored sticks. Dark green highlights the relative positions of Glu370, the catalytic residue common to many of the ACADs.

Extracts expressing the mature ACAD10 insert were only active with R or S, 2-methyl-C15-CoA (R or S, 2-methyl-pentadecanoyl-CoA) among a broad series of other substrates including the optimum ones for all of the other ACADs. The measured activity (1.4 mU/mg at 150 M substrate concentration) was considerably lower and required higher substrate

concentration than that obtained with other expressed ACADs towards their optimum substrates, suggesting that the dehydrogenation reaction between ACAD10 and *R* or *S*, 2 methyl- C15-CoA is unlikely the optimal function for ACAD10 *in vivo*.

1.3 PLANT ACADS

Plants perform a variation of fatty acid oxidation localized to the peroxisomes utilizing acyl-coA oxidases, which is thus analogous to human peroxisomes (Zolman, Nyberg et al. 2007). Acyl-CoA oxidases are structurally similar to ACAD enzymes except that they utilize water as the electron acceptor for the oxidized enzyme, generating hydrogen peroxide in the process. The auxin indole-3-butyric acid (IBA, a plant growth factor) has been identified as a substrate of peroxisomal fatty acid β - oxidation in plants. The metabolism of IBA has been shown to be dependent on a peroxisomal protein (IBR) homologous to the ACADs, specifically ACAD10 and 11 (Zolman, Nyberg et al. 2007). The plant and mammalian proteins both contain an APH domain at the N-terminus and ACAD domain at the C-terminus (Zolman, Nyberg et al. 2007). The *IBR* ACAD domain is most similar to the ACAD domain found in MCAD and other branched chain acyl-CoA dehydrogenases active against substrates containing characteristic aromatic rings (Zolman, Nyberg et al. 2007).

1.4 ACAD LOCALIZATION ON GLUT4-CONTAINING VESICLES

In addition to their usual location in the mitochondrial matrix, acyl-CoA dehydrogenases have been shown to be associated with cytoplasmic GLUT4-containing vesicles where they interact with two dileucine motifs on insulin-regulated aminopeptidase (IRAP) (Katagiri, Asano et al. 2002). Glucose transporter type 4 is a protein encoded by the *GLUT4* gene, and is expressed primarily in fat and muscle tissues (Katagiri, Asano et al. 2002). In cells, glucose equilibrium is maintained by the GLUT4 response to insulin (Haga, Ishii et al. 2011). The IRAP containing GLUT4 vesicles respond to insulin stimulation by translocating to the cell surface. IRAP has a specific protein structure containing a dileucine motif. The dileucine motif in IRAP plays a critical role in regulating GLUT4 trafficking. Several ACADs have been identified as being associated with the dileucine motif portion of IRAP, including LCAD, MCAD, and SCAD (Katagiri, Asano et al. 2002). Mutation of the dileucine motif of IRAP (amino acids 55-82) destroys this interaction (Katagiri, Asano et al. 2002).

While these findings potentially connect some of the ACADs with insulin dependent transportation of glucose within cells, the physiologic role of the ACAD proteins in this setting is unclear (Katagiri, Asano et al. 2002). Of note, *ACAD10* has been linked to insulin resistance and lipid oxidation in the Pima Indian population, but its localization to GLUT4 vesicles has not been investigated (Bian, Hanson et al. 2010). *ACAD10* was one of 30 genes further examined after demonstrating a significant signal for diabetes in a genome-wide association study (Bian, Hanson et al. 2010). In this GWAS, a single nucleotide polymorphism (SNP), rs632650, was found to map within intron 2 of *ACAD10* (Bian, Hanson et al. 2010). A functional association of *ACAD10* with GLUT4-containing vesicles could provide a possible link between this ACAD and an insulin-regulated pathway.

2.0 EVIDENCE FOR INVOLVEMENT OF MEDIUM CHAIN ACYL-COA DEHYDROGENASE IN THE METABOLISM OF PHENYLBUTYRATE

This work has been previously published in the following location, (Kormanik, Kang et al. 2012). Copyright permission was obtained to include the manuscript in this thesis dissertation.

Kormanik K, Kang H, Cuebas D, Vockley J, Mohsen AW. "Evidence for involvement of medium chain acyl-CoA dehydrogenase in the metabolism of phenylbutyrate." *Mol Genet Metab.* 2012 Dec;107(4):684-9. doi: 10.1016/j.ymgme.2012.10.009. Epub 2012 Oct 18.

2.1 ABSTRACT

Sodium phenylbutyrate is used for treating urea cycle disorders, providing an alternative for ammonia excretion. Following conversion to its CoA ester, phenylbutyryl-CoA is postulated to undergo one round of β -oxidation to phenylacetyl-CoA, the active metabolite. Molecular modeling suggests that medium chain acyl-CoA dehydrogenase (MCAD; EC 1.3.99.3), a key enzyme in straight chain fatty acid β -oxidation, could utilize phenylbutyryl-CoA as substrate. Moreover, phenylpropionyl-CoA has been shown to be a substrate for MCAD and its intermediates accumulate in patients with MCAD deficiency. We have examined the involvement of MCAD and other acyl-CoA dehydrogenases (ACADs) in the metabolism of phenylbutyryl-CoA. Anaerobic titration of purified recombinant human MCAD with phenylbutyryl-CoA caused changes in the MCAD spectrum that are similar to those induced by

octanoyl-CoA, its bona fide substrate, and unique to the development of the charge transfer ternary complex. The calculated apparent dissociation constant (K_D app) for these substrates was 2.16 μM and 0.12 μM , respectively. The MCAD reductive and oxidative half reactions were monitored using the electron transfer flavoprotein (ETF) fluorescence reduction assay. The catalytic efficiency and the K_m for phenylbutyryl-CoA were $0.2\text{mM}^{-1}\cdot\text{sec}^{-1}$ and 5.3 μM compared to $4.0\text{mM}^{-1}\cdot\text{sec}^{-1}$ and 2.8 μM for octanoyl-CoA. Extracts of wild type and MCAD-deficient lymphoblast cells were tested for the ability to reduce ETF using phenylbutyryl-CoA as substrate. While ETF reduction activity was detected in extracts of wild type cells, it was undetectable in extracts of cells deficient in MCAD. The results are consistent with MCAD playing a key role in phenylbutyrate metabolism.

2.2 INTRODUCTION

Impairment of urea synthesis in humans is caused by defects in the activity of enzymes in the urea cycle including carbamylphosphate synthetase, ornithine transcarbamylase, argininosuccinic acid synthetase, argininosuccinate lyase, and arginase and leads to hyperammonemia. High levels of ammonia in blood may lead to encephalopathy and death (Diaz, Krivitzky et al. 2013).

Sodium phenylbutyrate is the active ingredient in Buphenyl® (Hyperion, Pharmaceuticals) and is currently used for treating primary hyperammonemia caused by certain urea cycle defects (Adam, Almeida et al. 2013). Sodium phenylbutyrate may also be useful in treating secondary hyperammonemia that accompanies other inborn errors. In addition, phenylbutyrate has been and is being investigated in numerous clinical settings including modulation of fetal hemoglobin gene expression in sickle cell and in thalassemia, treatment of myelodysplastic syndromes and

acute myeloid leukemia, cerebral and liver ischemic injury protection, among others (SD Gore 2001, M Vilatoba and JL 2005, G Egger 2007, Y Saito 2009). As of this writing >30 trials involving sodium phenylbutyrate are listed on the www.clinicaltrial.gov website. The mechanism proposed for ammonia clearance by phenylbutyrate administration involves its activation to phenylbutyryl-CoA, conversion to phenylacetyl-CoA, and conjugation with glutamine (Figure 8) for excretion by the kidneys (X Qi 2004).

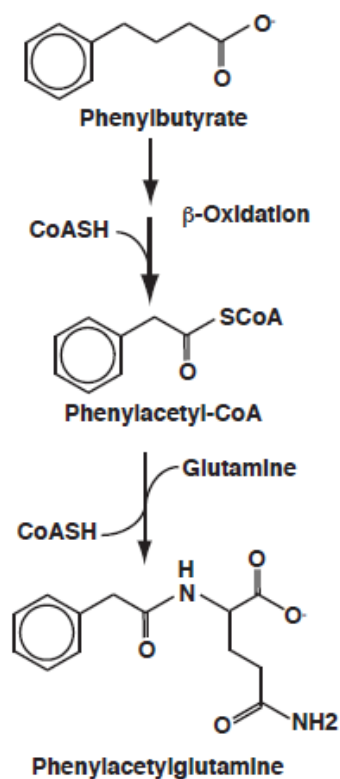


Figure 8. Schematic showing a proposed overall pathway for metabolism of phenylbutyrate to its final metabolite

The conversion of phenylbutyryl-CoA to phenylacetyl-CoA is presumed to occur through one cycle of β -oxidation in mitochondria. The first step in the β -oxidation cycle is the α,β -dehydrogenation of fatty acid CoA esters catalyzed by members of the acyl-CoA dehydrogenase

(ACAD) family of enzymes. Nine members of this enzyme family have been identified, each with characteristic substrate specificity profile (J Willard , Y Ikeda 1983, Y Ikeda 1983, K Ikeda 1985, K Izai 1992, R Rozen 1994, J Zhang 2002, TV Nguyen 2002). Short, medium, long, saturated very long, unsaturated very long chain acyl-CoA dehydrogenases (SCAD, MCAD, LCAD, VLCAD and ACAD9) have substrate optima of C4, C8, C12, C16, and C16:1 (unsaturated very long chain among others) acyl-CoA esters, respectively, but can utilize other substrates (Y Ikeda 1983, Y Ikeda 1985, Y Ikeda 1985, R Ensenauer 2005). The crystal structures of SCAD, MCAD, and VLCAD have been published, (PDB ID: 1JQI, 3MDE, and 43B96, respectively) (J-J Kim 1993, KP Battaile 2002, RP McAndrew 2008). The remaining four enzymes in the family are involved in amino acid metabolism and their crystal structures have been published as well, (PDB ID: 1IVH, 1SIR, 1RX0, and 2JIF) revealing a relatively restrictive active sites, rendering them highly specific for their bonafide substrates (KA Tiffany 1997, KP Battaile 2004, Z Fu 2004, ACW Pike 2007). It has been observed that patients with MCAD deficiency characteristically accumulate both the glycine and carnitine conjugates of phenylpropionate, a bacterial metabolite from bowel flora that is absorbed into the blood stream (P Rinaldo 1988). Mass spectrometry based enzymatic assay of MCAD deficient patient fibroblast cells using phenylpropionyl-CoA as substrate showed lack of conversion to its α,β -unsaturated product (TG Derks 2008). While the crystal structure of SCAD and VLCAD and homology 3D modeling of ACAD9 show that the active site would not accommodate the phenylbutyryl acyl moiety, the active site of MCAD would. These findings and the structural similarities between phenylpropionate and phenylbutyrate implicate MCAD in the metabolism of phenylbutyryl-CoA. In this study we tested the ability of purified human recombinant ACADs to bind and use phenylbutyryl-CoA as a substrate. We demonstrate that MCAD indeed uniquely

utilizes phenylbutyryl-CoA as a substrate. In addition, we show the inability of extracts prepared from MCAD-deficient fibroblast to act upon this substrate.

2.3 MATERIALS AND METHODS

2.3.1 Purification of recombinant human MCAD

Expression and purification of recombinant human MCAD was performed as previously described for isovaleryl-CoA dehydrogenase with minor modifications (A-W Mohsen 1995). *E. coli* JM105 cells (Amersham Biosciences Corp; Piscataway, NJ) containing the human MCAD high expression vector p*Ke*MCAD (Y Matsubara 1989) and a GroEL/GroES expression plasmid were grown overnight in a 200-ml LB broth pre-culture that was used to inoculate 4 x 2-L cultures in 2-YT broth. The cells were left to grow overnight at 37°C with shaking and MCAD expression was induced the next morning using IPTG at a final concentration of 0.5 mM for 3 hrs. Cells were harvested by centrifugation and resuspended in 2:1 weight to volume of 100 mM potassium phosphate pH 8.0, 150 mM EDTA. Cells were then lysed by sonication on ice. Including high amounts of EDTA in the cell lysis buffer is for protecting residues with groups, *e.g.*, cysteine thiols and methionine sulfide groups, vulnerable to modification by oxygen reactive species generated during sonication cell suspension. This was effective in improving enzyme preparations resulting higher specific activity and consistent kinetic behavior (A-W Mohsen 1999). Cellular debris was removed by centrifugation at 250,000 x *g* for 60 minutes. The final supernatant was dialyzed for 4 hours with vigorous stirring in 50 mM potassium phosphate pH 8.0, at 4°C. The sample was then loaded on a 16 x 40 mm DEAE Sepharose FF column

preequilibrated in 50 mM potassium phosphate pH 8.0, using an ÄKTA UPC-900 pump FPLC system (Amersham Biosciences Corp; Piscataway, NJ). After washing with 300 ml of 50 mM potassium phosphate pH 8.0, MCAD was eluted with a 300 ml linear gradient from 50 to 500 mM potassium phosphate pH 8.0. Green fractions with a 270/447 nm ratio <12 containing MCAD were pooled, concentrated, and dialyzed against 25 mM potassium phosphate, pH 8.0. Pooled fractions of essentially pure MCAD (270/447 nm ratio = 5.5), were concentrated and stored at -80°C . Other recombinant human ACADs were similarly purified except that the protocol was terminated after the DEAE-Sepharose column for LCAD as the enzyme was unstable. LCAD protein purity ~70% at this stage.

2.3.2 The electron transfer flavoprotein (ETF) purification

Porcine ETF was purified as previously published (J Vockley 2000), except that the dialysis buffer used after both the 40-60% ammonium sulfate fractionation and DE-52 cellulose anion-exchange chromatography steps consisted of unbuffered 15 mM dibasic potassium phosphate and 5% glycerol.

2.3.3 Fibroblast cell culture and extract preparation

Wild type and MCAD deficient cells (homozygous for the K304E mutation) with the designation GM085401 and GM07844, respectively, were obtained from Coriell Institute for Medical Research, Camden, NJ. Cells were cultured in DMEM medium supplemented with glutamine and ampicillin and streptomycin, and 20% fetal bovine serum. Cells were harvested from a T175 flask by sonication with a buffer consisting of 50 mM Tris buffer and 10 mM EDTA, pH 8.0.

The cell debris was removed by centrifugation and the cell free extract was assayed for protein and enzyme activity as described below.

2.3.4 ETF fluorescence reduction assay

The ETF reduction assay was performed using a Jasco FP-6300 spectrofluorometer (Easton, MD) with a cuvette holder heated with circulating water at 32°C. The assay was otherwise performed as described (FE Frerman 1985), at the indicated substrate concentrations. The enzyme was diluted 1200-fold into a buffer containing 50 mM Tris, pH 8.0, 5 mM EDTA and 50% glycerol, and 10 µl were used for each assay. The ETF concentration in the reaction mixture was 2 µM. Spectra Manager 2 software (Jasco Inc) was used to collect data and calculate reaction rate and Microsoft Excel was used to calculate the kinetic parameters.

2.3.5 Phenylbutyryl-CoA synthesis

CoASH, octanoyl-CoA, C₁₂-CoA and phenylbutyric acid were obtained from Sigma (St. Louis, MO.) 2,6-dimethylheptanoic acid was obtained from Matreya LLC (Pleasant Gap, PA). The phenylbutyryl-CoA and 2,6-dimethylheptanoyl-CoA esters were prepared by the mixed anhydride method as described previously (Schulz 1974) and was purified by HPLC using a Luna 5 µm C18(2) column (25 cm x 0.46 cm) and a linear gradient (10-60%) of acetonitrile into 50 mM ammonium phosphate, pH 5.5, at a flow rate of 1.5 mL/min over 30 min.

2.3.6 Monitoring the interaction of MCAD with substrates

Formation of the charge transfer ternary complex was monitored by observing the increase in absorbance at the 570 nm area, concomitant with the decrease of absorbance at 447 nm area, of the purified MCAD in 120 mM potassium phosphate spectrum under anaerobic conditions using a JascoV-650 Spectrophotometer. Phenylbutyryl-CoA solution dissolved in water to 0.53 mM was titrated into the MCAD sample one μL at a time using a 50 μL Hamilton syringe attached to an automatic dispenser. Ten seconds of equilibration time were allowed after mixing before the sample was scanned at 250 to 800 nm. Final substrate concentrations varied as indicated in figure legends. All data were adjusted for the dilution resulting from substrate addition. Substrates were titrated, but with different final concentrations as indicated in the figure legends. The dissociation constant ($K_{D \text{ app}}$) was calculated with the Stockell equation as described previously (MC McKean 1979):

$$\frac{d}{p} = K_{D \text{ app}} \frac{1}{e-p} + n$$

where **d** is the total ligand concentration, **e** is the total molar concentration of enzyme, **p** is the fraction of enzyme sites that bind ligand multiplied by **e**, and **n** is the number of binding sites. The absorbance at 447 nm when all enzyme sites are occupied with ligand was determined separately by adding large excess of octanoyl-CoA and used to calculate the fraction of enzyme with bound ligand at various readings and assuming that at large excess of added substrate would equal to **e**.

2.3.7 Molecular modeling

Computer modeling of MCAD was performed using a Silicon Graphics Fuel workstation (Mountain View, CA) with the *Insight II* 2005 software package and MOE software, from Chemical Computing Group, Montreal, Canada, and the atomic coordinates of pig MCAD (3MDE) in the dimer form as a molecule (J-J Kim 1993). Carbon atoms at positions C5-C8 of the octanoyl-CoA ligand, which co-crystallized with MCAD, were replaced with a phenyl group. The phenylbutyryl-CoA ligand conformation in the active site was refined using the Discover module. Human LCAD 3D structure was modeled using MCAD atomic coordinates as template and the *Insight II* modeling software.

2.4 RESULTS

2.4.1 Interaction of MCAD with substrates, the reductive half-reaction

Formation of the charge transfer complex, the reductive half-reaction, is evident from the spectral scans of MCAD at various phenylbutyryl-CoA concentrations (Figures 9 and 10, respectively).

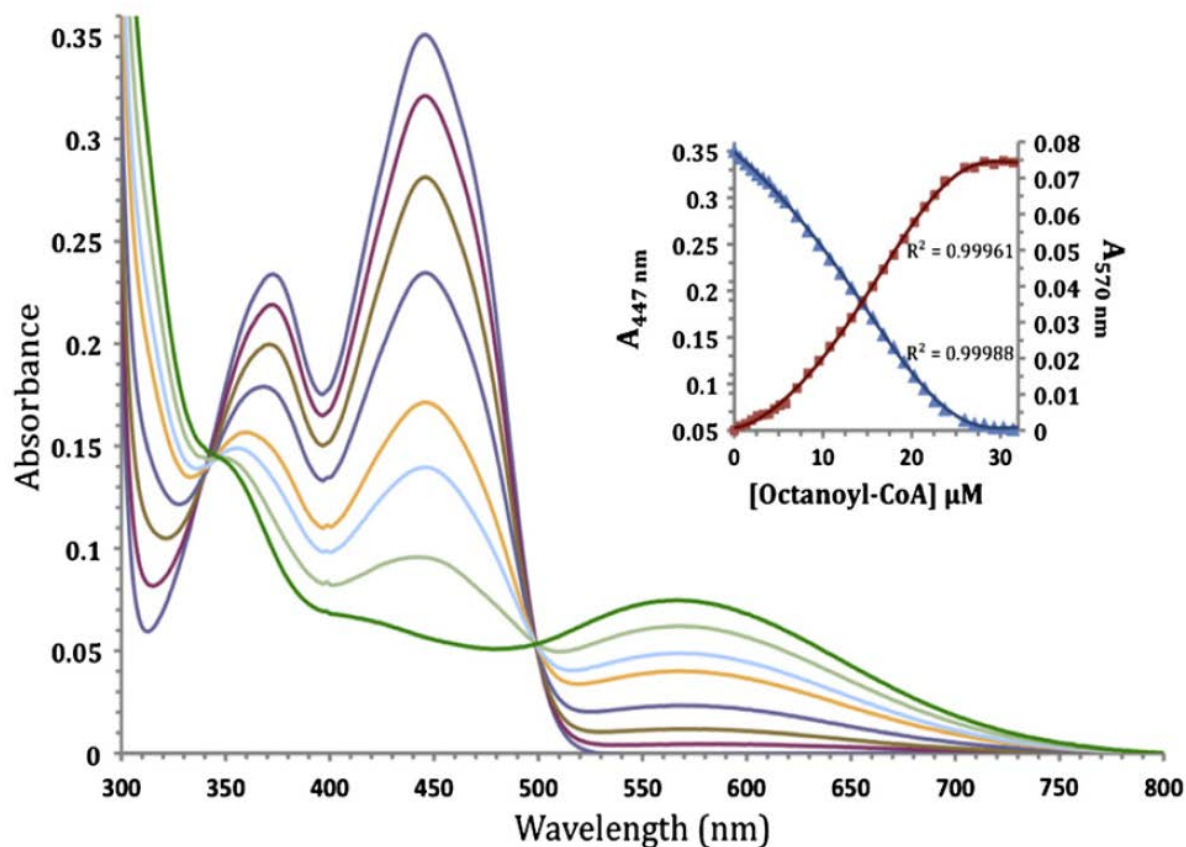


Figure 9. Monitoring the formation of the charge transfer complex with purified MCAD upon addition of increasing amounts of octanoyl-CoA.

The absorbance maxima at ~370 nm and ~447 nm are reduced and a new peak centered at 570 nm appears with addition of increasing substrate. Selected scans are shown with octanoyl-CoA concentration at 0, 3.25, 7.1, 10.8, 15.6, 18.0, 21.5, and 28.2 μM . The inset shows the kinetics of these changes. Equation for the decrease at 447 nm is: $y = -1 \times 10^{-9}x^6 + 1 \times 10^{-7}x^5 - 2 \times 10^{-6}x^4 + 2 \times 10^{-5}x^3 - 0.0003x^2 - 0.008x + 0.3489$. Equation for the increase at 570 nm is: $y = 6 \times 10^{-10}x^6 - 5 \times 10^{-8}x^5 + 1 \times 10^{-6}x^4 - 2 \times 10^{-5}x^3 + 0.0003x^2 + 0.0003x + 0.0008$. Enzyme concentration was 25.2 μM .

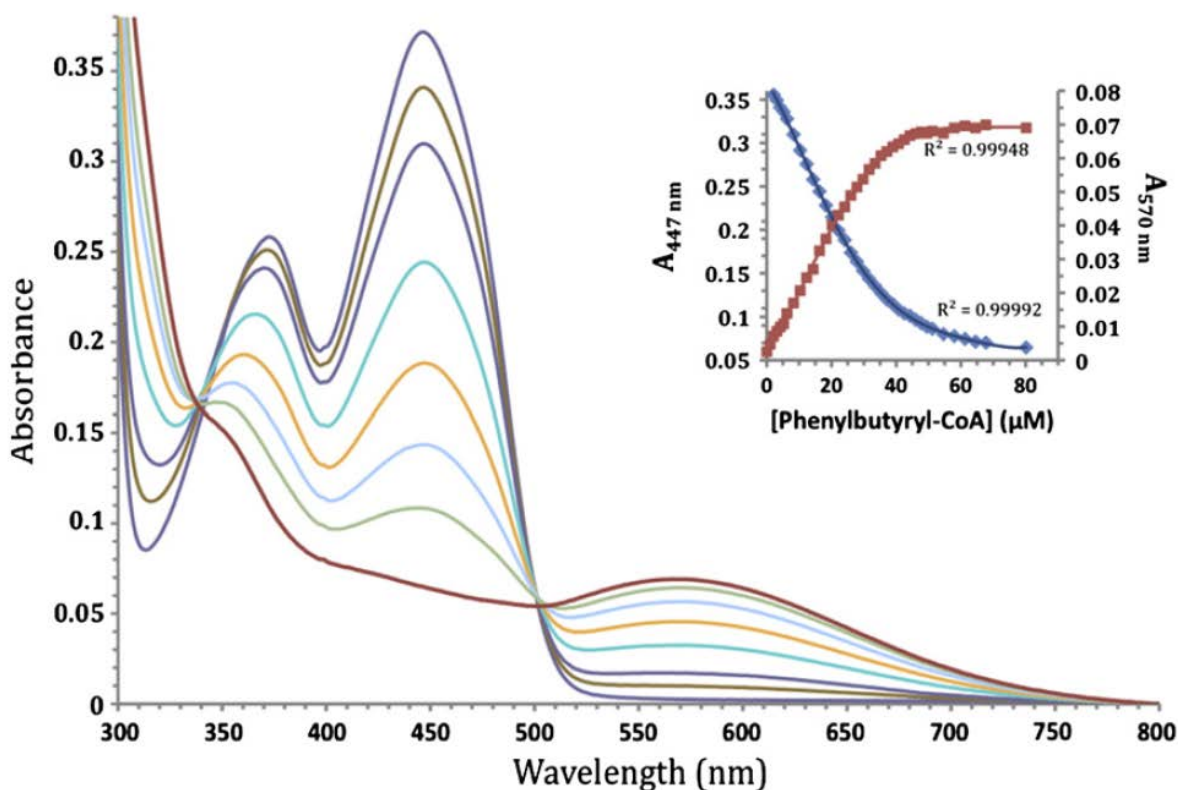


Figure 10. Monitoring the formation of the charge transfer complex with purified MCAD upon addition of increasing amounts of phenylbutyryl-CoA.

The absorbance maxima at ~370 nm and ~447 nm are reduced and a new peak centered at ~570 nm appears with addition of increasing substrate. Selected scans are shown with phenylbutyryl-CoA concentration at 0, 4.2, 8.3, 16.3, 24.1, 31.6, 40.7, and 80.2 μM . The inset shows the kinetics of these changes. Equation for the decrease at 447 nm is: $y = 5 \times 10^{-10} x^5 - 1 \times 10^{-7} x^4 + 9 \times 10^{-6} x^3 - 0.0002 x^2 - 0.0061 x + 0.3707$. Equation for the increase at 570 nm is: $y = -1 \times 10^{-10} x^5 + 3 \times 10^{-8} x^4 - 3 \times 10^{-6} x^3 + 7 \times 10^{-5} x^2 + 0.0012 x + 0.0036$. Enzyme concentration was 25.2 μM .

The progressive decrease and increase of absorbance at 447 nm and 570 nm, respectively, are similar to those induced by octanoyl-CoA. The octanoyl-CoA binding curve is sigmoidal in contrast to the phenylbutyryl-CoA binding curve, possibly reflecting differences in enzyme mechanism of interaction. The plot of d/p versus $1/e-p$ (the Stockell plot) was nonlinear. A line drawn at the straight area of the curve where the substrate:subunit ratio was 1:1 estimates the apparent dissociation constant ($K_{D \text{ app}}$) being 0.12 μM and 2.16 μM for octanoyl-CoA and

phenylbutyryl-CoA, respectively. Other mathematical derivatives of the absorbance data all indicated that the binding sites are non-equivalent.

Table 2. Kinetic Constants of Recombinant Human MCAD Using Octanoyl-CoA and Phenylbutyryl-CoA as Substrates and the ETF Fluorescence Reduction Assay

Substrate	K_m (μM)	V_{max} ($\mu\text{mol}\cdot\text{min}^{-1}$)	k_{cat}/K_m Per mol FAD ($\mu\text{M}^{-1}\cdot\text{min}^{-1}$)
Octanoyl-CoA	2.8	16.20	2.40×10^5
Phenylbutyryl-CoA	5.3	1.35	0.11×10^5

2.4.2 Interaction of MCAD: Substrate ternary complex with ETF, the oxidative half reaction

Using ETF as the electron acceptor in the standard enzymatic assay detailed above, transfer of electrons was confirmed as evident from the reduction of ETF fluorescence in the presence of various concentrations of phenylbutyryl-CoA. The catalytic efficiency and K_m for the phenylbutyryl-CoA were $0.2 \text{ mM}^{-1}\cdot\text{sec}^{-1}$ and $5.3 \mu\text{M}$ compared to $4.0 \text{ mM}^{-1}\cdot\text{sec}^{-1}$ and $2.8 \mu\text{M}$ for octanoyl-CoA, respectively.

Molecular modeling of human LCAD shows possible accommodation of the acyl moiety of the phenylbutyryl-CoA, with the exception of residue L264, which would have one of its side chain methyl hydrogens $\sim 1.3\text{\AA}$ away from a phenyl ring hydrogen and so would hinder binding. To test if the LCAD active site has enough plasticity to accommodate this potential substrate, we measured its activity with LCAD using the ETF fluorescence reduction assay. While the partially

purified recombinant human LCAD was active in the presence of various substrates including C₁₂-CoA and 2,6-dimethylheptanoyl-CoA, it was not active in the presence of phenylbutyryl-CoA. Purified SCAD, MCAD, and ACAD9 also showed no activity with phenylbutyryl-CoA as substrate.

2.4.3 The ETF fluorescence reduction assay of cell extract

ETF fluorescence reduction was observed using extracts from wild type fibroblast cells in the presence of 30 μ M of phenylbutyryl-CoA, octanoyl-CoA, or palmitoyl-CoA. (The latter substrate was used as internal control and is a substrate of VLCAD.) Enzyme specific activity measured using these substrates was 3.41 (0.53), 4.01 (1.34), 9.10 (2.13) *n*moles ETF reduced \cdot min⁻¹ \cdot mg⁻¹, respectively. No activity was observed using similar amounts of extract from fibroblast cells deficient in MCAD with either phenylbutyryl-CoA or octanoyl-CoA. The measured enzyme specific activity of palmitoyl-CoA oxidation in extract from these cells was 3.91 (1.34) *n*moles ETF reduced \cdot min⁻¹ \cdot mg⁻¹.

2.5 DISCUSSION

Following the conversion of phenylbutyrate to the CoA ester, one cycle of β -oxidation is expected to result in phenylacetyl-CoA and acetyl-CoA as the final products (Figure 11). Phenylacetyl-CoA is hydrolyzed to phenylacetate, which becomes conjugated with glutamine and is excreted in urine (Figure 8). An analysis of this first step in the β -oxidation of phenylbutyryl-CoA is important because the first step in the β -oxidation of fatty acids is

postulated to be rate-limiting (P Macheroux 1997), and thus the metabolism of Buphenyl to its active form, phenylacetate, may also be modulated by similar factors that affects energy metabolism at the same step.

The effect of phenylbutyryl-CoA on the MCAD absorbance spectrum at relatively low concentrations is monitored *via* the decrease of absorbance at 447 nm and increase of absorbance at 570 nm. This confirms productive binding of phenylbutyryl-CoA to MCAD in the reductive half reaction with lack of product release. This effect is similar to that induced by octanoyl-CoA binding to MCAD, and indicative of the transfer of a proton and a hydride to the flavin ring and formation of the charge transfer complex, which is comprised of the enzyme, reduced FAD, and enoyl product and detected by the intense absorbance band centered at 570 nm (SM Lau 1987, S Ghisla 2004).

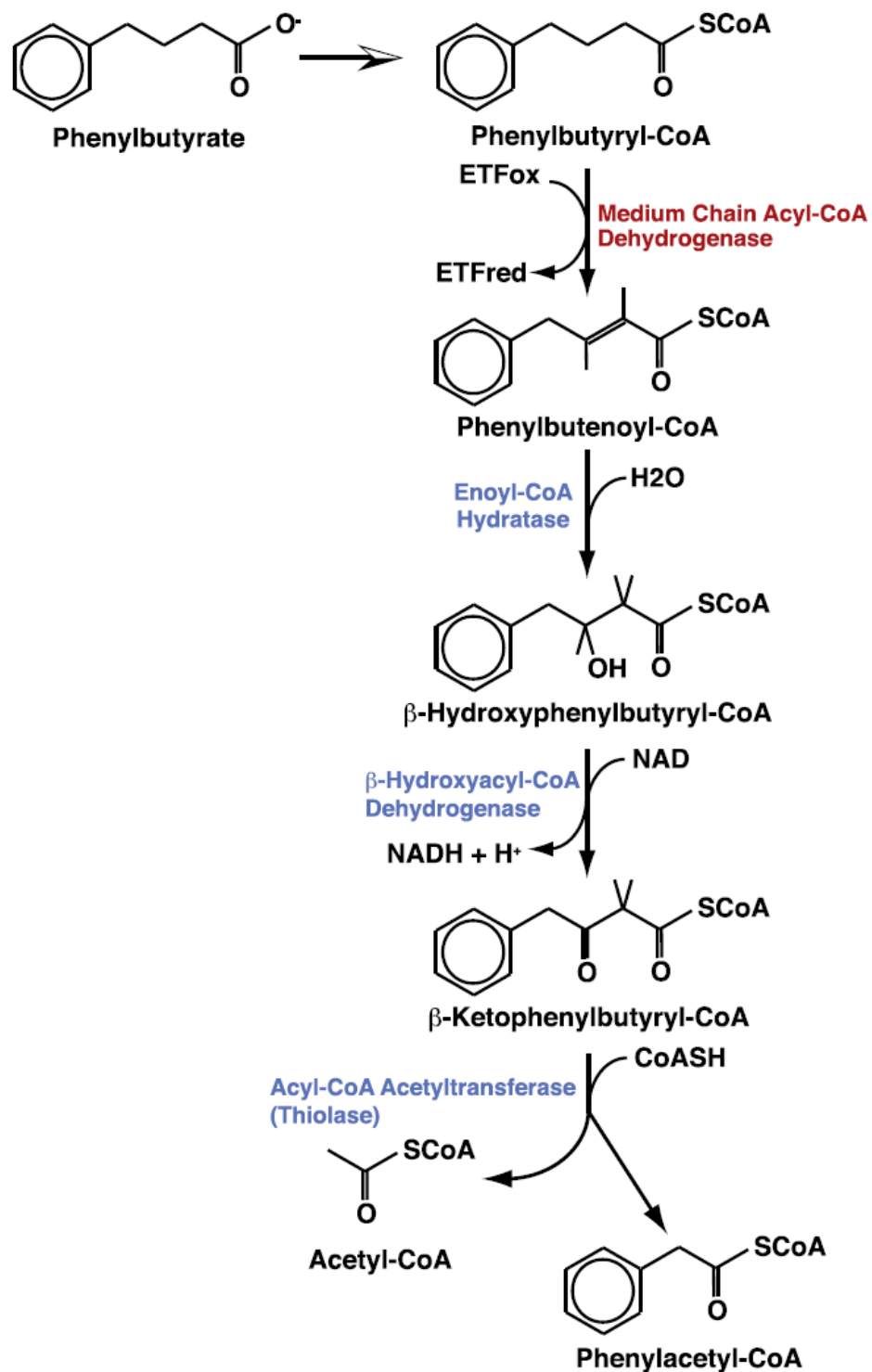


Figure 11. Detailed proposed pathway of metabolism of phenylbutyrate to its active form, phenylacetate

The inset in Figure 9 shows a sigmoidal shaped curve when octanoyl-CoA, but not

phenylbutyryl-CoA, was used as substrate. This may imply positive cooperativity between the first and second subunits with octanoyl-CoA binding that does not occur with phenylbutyryl-CoA. Although other interpretations of sigmoidal behavior in this setting are possible, including presence of various MCAD forms or other effector molecules, the argument is weakened by the fact that the only difference between the two reactions is the substrate itself. Impurities in the substrate preparation are also not likely to induce such an effect as such impurities would be present at ineffectively low concentrations at the low substrate concentrations range, between 0.25-1 and 4:1 substrate:MCAD tetramer ratio.

Reduction of ETF by the charge transfer complex in the oxidative half-reaction shows that electrons from the bound phenylbutyryl-CoA can be efficiently transferred to ETF and that the product, phenylbutenoyl-CoA, is released to complete the reaction. In contrast, none of the other ACADs are capable of catalyzing this reaction.

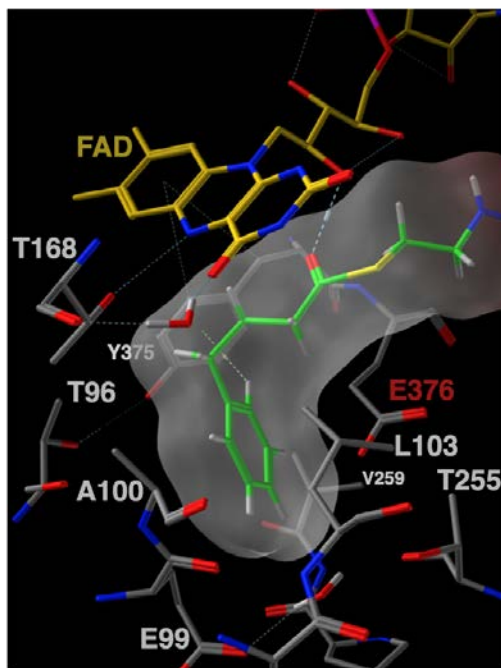


Figure 12. Stick representation of MCAD active site residues and ligands with phenylbutyryl-CoA modeled in place of octanoyl-CoA

The crystal structure of pig MCAD with bound octanoyl-CoA (PDB: 3MDE, [20]) was used to create the model using MOE modeling software. The E376 carboxylate is the active site catalytic base responsible for the substrate C2 proton abstraction to initiate catalysis.

Modeling of a phenylbutyryl moiety in the active site in place of the octanoyl moiety observed in the MCAD crystal structure shows the phenyl moiety accommodated in the acyl moiety binding site pocket with a conformation perpendicular to the aromatic ring of Y375 (Figure 12). Other residues involved in binding the phenyl moiety include E99, A100, Leu103, and V259. Furthermore, modeling predicts that the phenyl ring *para* and/or *meta* positions are candidate expansion sites for adding a functional group that may improve binding, while addition at the *ortho* position would prevent the derivative from binding to MCAD.

Based on the kinetic parameters of MCAD with phenylbutyryl-CoA as substrate, individuals with MCAD deficiency are likely to experience a functionally relevant decrease in the ability to metabolize the medication, though indications for use in these patients are likely to be rare. Of note, since octanoyl-CoA has been reported to provide thermal stability to the MCAD K304E mutant (I Nasser 2004), it is possible that phenylbutyryl-CoA would behave similarly and may be of benefit *in vivo* in patients carrying at least one copy of this mutation. This requires additional investigation in cellular or whole body systems. It is unknown if carriers for MCAD deficiency, a much more common situation, will display altered metabolism of phenylbutyrate. In other indications where the functional effects of phenylbutyrate are less well characterized, modulation of MCAD activity might be of benefit to alter drug metabolism and/or its half-life and increase its efficacy, depending on the mechanism of action of the medication in each disorder. Detailed biochemical studies to determine the drug's mode of action and its pharmacokinetics for such indications are thus crucial.

2.6 ACKNOWLEDGEMENTS

The project described was supported in part by Award Number R21 HD056004 from the Eunice Kennedy Shriver National Institute of Child Health & Human Development (A-WM) and RO1DK78755 and DK54936 (JV). The content is solely the responsibility of the authors and does not necessarily represent the official views of the Eunice Kennedy Shriver National Institute Of Child Health & Human Development or the National Institutes of Health. The project was also supported in part by an unrestricted research grant from Hyperion Therapeutics, Inc. (JV), and a Missouri State University Faculty Research Award, number F07036 (DC).

3.0 CLONING AND EXPRESSION OF ACAD10 IN *E. COLI*

3.1 ABSTRACT

Acyl-CoA dehydrogenases 10 (ACAD10) and 11 (ACAD11) transcripts encoding 1059-aa (118Kd) and 780-aa (87Kd) proteins predicted to be structurally related have been identified in databases but their function is unknown. A polymorphism in the *ACAD10* gene has been linked to obesity in Pima Indians and hence the physiological role of both proteins draws interest. We cloned human ACAD10 and 11 full length coding transcripts in *E. coli*, but they failed to support production of identifiable protein. Expression of inserts coding for ACAD10 S637-I1059 and ACAD11 S355-I780 sequences representing the ACAD domain was successful. The purified proteins have absorbance spectra typical of flavoproteins but were unstable. Antibodies were generated against each protein and eight mouse tissues were surveyed for presence of antigens using western blotting and immunofluorescence staining. Rabbit anti-ACAD10 antibodies detected ~100Kd and ~125Kd-bands in extracts from pancreas and brain, respectively. Anti-ACAD11 antibodies detected a 75Kd-band in all tissues, with kidney and lung showing the strongest signal. Subcellular localization (mitochondria or peroxisomes) was tissue specific. The ACAD11 antigen localized exclusively to peroxisomes. Removing a predicted ACAD10 N-terminus signal peptide from the full coding sequence resulted in production of a ~100Kd protein in *E. coli*, while expressing a sequence for the predicted 75Kd ACAD11 resulted in the

production of a 65Kd antigen. Purification and characterization of the native forms of these proteins will provide key insights into their structure and function.

3.2 INTRODUCTION

The acyl-CoA dehydrogenase (ACAD) family of flavoproteins consists of nine enzymes that are similar in structure and function (Swigonova, Mohsen et al. 2009). Seven are homotetramers (~400-amino acids per monomer) and two are homodimers (~640-amino acids per monomer).

They all catalyze the α,β -dehydrogenation of their corresponding acyl-CoA substrates.

Deficiencies in these proteins are major causes of inborn errors of metabolism (Vockley and Whiteman 2002). Five of these enzymes, VLCAD, ACAD9, LCAD, MCAD, and SCAD, catalyze the first step in the fatty acid β -oxidation spiral with each tolerating some variation in the acyl carbon chain length specificity and branching (Swigonova, Mohsen et al. 2009). More recently, a new ACAD gene, *ACAD10*, has been reported. It is even more highly conserved across species than the other ACADs, suggesting an essential role in cellular metabolism (He 2011). A study with a full-heritage Pima Indian population sample identified an association between *ACAD10* variants and type 2 diabetes and lipid oxidation (Bian, Hanson et al. 2010)

The *ACAD10* gene maps to chromosome 12q24.1 and encodes a predicted transcript for a 1059 or 1090 amino acid protein (Xin Ye 2004, Ensembl 2013). In contrast to other ACADs, *ACAD10* has a unique gene structure with multiple coding domains that likely yield multiple functional proteins. The hypothetical protein consists of three primary domains: an N-terminus domain with hydrolase homology, a middle domain with protein kinase homology, and a conserved ~ 400-aa C-terminus domain that is highly homologous to ACAD. The ACAD C-

terminus domain shows conservation of key primary structural ACAD elements essential for FAD and CoA ligand binding. Two isoforms of ACAD10 have been identified in genetic databases; isoform a and isoform b (National Center for Biotechnology Information 2013). ACAD10 isoform a is the longest transcript produced and codes for the largest predicted protein while the protein encoded by isoform b is predicted to be shorter. A second novel ACAD, *ACAD11*, encodes a hypothetical protein that is only 780 aa in length and is homologous to the middle and C-terminus domain of ACAD10. The ACAD domain and the protein kinase-like, catalytic domain is highly conserved in a number of species including humans, rat, mouse, chimpanzee, Rhesus monkey, cattle, chicken, *Arabidopsis thaliana* and more (National Center for Biotechnology Information 2013). The lowest organism that contain all of the ACAD10 protein domains is fungi (Swigonova, 2009).

The purpose of this project was to use molecular cloning and prokaryotic expression studies to determine the functional forms of ACAD10 and characterize its biochemical and physical properties using an in vitro *E. coli* expression system. I hypothesized that in humans the *ACAD10* gene will support the expression of at least two major proteins (one containing all domains and another consisting of just the ACAD domains) that will differ in their subcellular localization. Prior studies suggest that the ACAD10 proteins containing only the ACAD domain will be localized to mitochondria. I predict that a full domain ACAD10 protein will be targeted to peroxisomes. Such dual targeting would be unique among the ACADs. Expression, purification and characterization of the various isoforms of ACAD10 will allow a better understanding of role of this protein in normal cellular metabolism and physiology.

3.3 MATERIALS AND METHODS

3.3.1 Cloning and Expression

For cloning and expression, kits from Qiagen (Valencia, CA) were used according to the manufacturer's protocols. Briefly, MGC Fully Sequenced Human *ACAD10* *cDNA* was purchased from ThermoFisher Scientific (Pittsburgh, PA) as template for PCR. *ACAD10* specific sequences were amplified with the Hot Star HiFidelity PCR kit (Qiagen, Valencia, CA) using a variety of forward and reverse primers specific to the various predicted *ACAD10* isoforms. For expression studies, PCR generated *ACAD10* and 11 products were purified using QIAGEN Plasmid Mini or Midi kit, then ligated into either pKK223-3, (GE Healthcare BioSciences, Pittsburgh, PA) or pET21a+, some containing a His₆ N-terminal tag (Novagen, Billerica, MA). The sequence of all constructs was verified by the University of Pittsburgh Genomics and Proteomics Core Laboratories. The sequencing data were visualized and confirmed using the MacVector software (MacVector, Inc, Cary, NC).

Table 3. Human ACAD10 Plasmid Constructs

ACAD10 PLASMIDS (human)	
Plasmid Name	Description
ACD10 Plasmid_v19	Full length ACD10
ACD10 Plasmid_v18	Full length ACD10
ACD10 Plasmid_v17	Full length ACD10
ACD10 Plasmid_v16	Removed 12-mer@ N-terminus (PTSII)
ACD10 Plasmid_v15	Removed 18-mer @ N-terminus (PTSII) + His Tag
ACD10 Plasmid_v14	Removed 18-mer @ N-terminus (PTSII)
ACD10 Plasmid_v13	Sitedirected Mutagenesis to put stop codon btwn domains
ACD10 Plasmid_v12 (minus HRI)	Adjusting pETv8 by cleaving residues HRI at C term
ACD10 Plasmid_11 (C-His)	C-His tagged generated using SDM
ACD10 Plasmid_10 in pcDNA3.1	Transfected full length ACD10 into pcDNA3.1 system
ACD10 Plasmid_9 (N-His)	N-His tagged generated using PCR cut & paste
ACD10 Plasmid_8	Full length ACD10 - NheI site instead of AgeI site (for N-His)
ACD10 Plasmid_7 aka Fragment 6	"Full length" ACAD10
Fragment 5	Short form of ACAD10 (ACD11-like mito form)
Fragment 4	Short form of ACAD10 (ACD11-like mito form)/ used for Ab

Table 4. ACAD10 Plasmid Primers

ACAD10 Plasmid Primers (human)	
Plasmid Name	Primers
ACD10 Plasmid_v19	hACD10_29mito_sig_fw & hACD10_3273rv
ACD10 Plasmid_v18	hACD10_38mito_sig_fw & hACD10_3273rv
ACD10 Plasmid_v17	hACD10_61mito_sig_fw & hACD10_3273rv
ACD10 Plasmid_v16	hACD10_37fw & hACD10_3AgeI_946-940rv
ACD10 Plasmid_v15	hACD10_55AgeIHisfw & hACD10_3AgeI_946-940rv
ACD10 Plasmid_v14	hACD10_55AgeI_fw & hACD10_3AgeI_946-940rv
ACD10 Plasmid_v13	D1D2_fwd & D1D2_rv
ACD10 Plasmid_v12 (minus HRI)	hACD10_787bExon7_fw & hACD10_minusHRI_rv
ACD10 Plasmid_11 (C-His)	hACD10_exon7_787b_fw & hACD10_HisCter_rv
ACD10 Plasmid_10 in pcDNA3.1	
ACD10 Plasmid_9 (N-His)	hACD10_NterNheINHis_fw & hACD10_3AgeI_946-940_rv
ACD10 Plasmid_8	hACD10_NheI_fw & hACD10_NheI_rv
ACD10 Plasmid_7 aka Fragment 6	
Fragment 5	hACD10_53mito_fw & pET_3MCS_rv
Fragment 4	hACD10_47mito_fw & pET_3MCS_rv

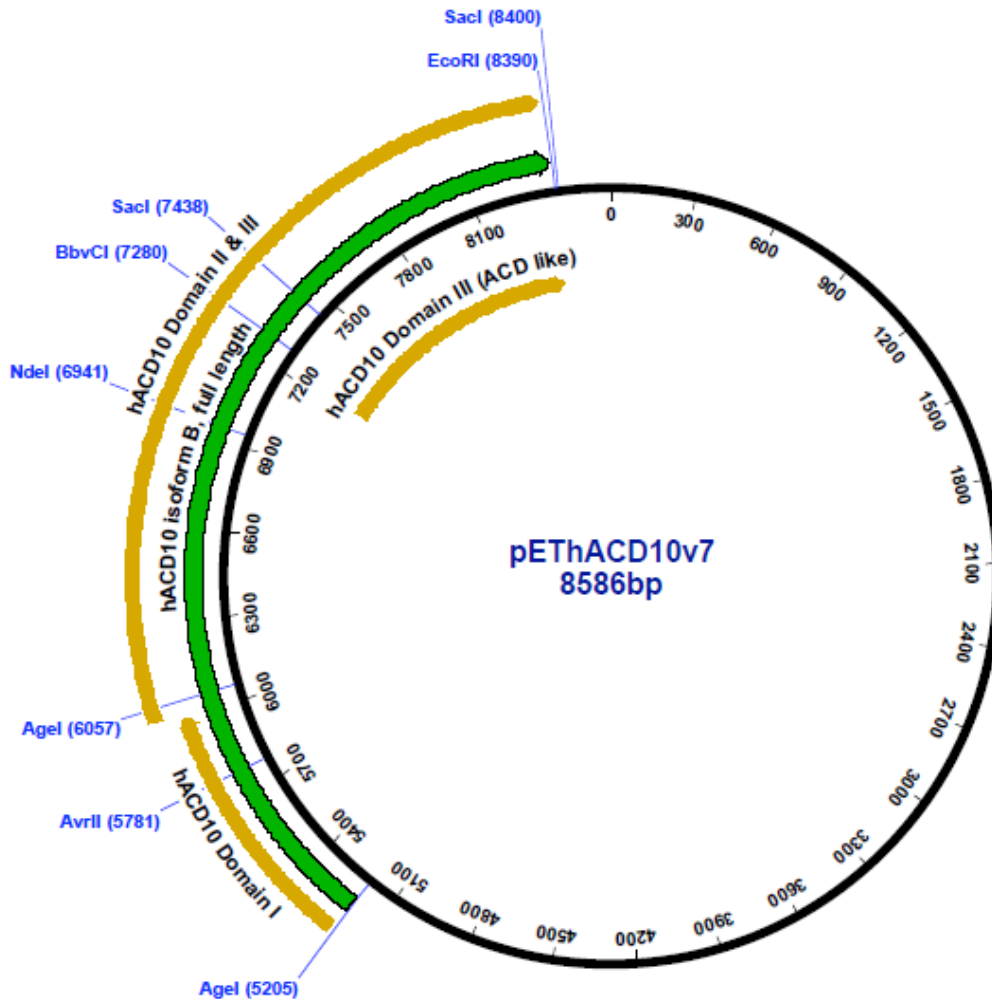


Figure 13. Plasmid Map

The *ACAD10* plasmid map represents several ACAD10 expression plasmids constructed and expressed, including one 89Kd peptide. Full length ACAD10 isoform B was constructed by inserting the N-terminus domain coding region at the 5'-end of the 89Kd peptide coding region, which required re-engineering the restriction enzyme sites at the insertion site to Age I without changing amino acid sequence.

3.3.2 Transient transfection and overexpression in HEK293T cells with pcDNA ACAD10

Human embryonic kidney cells (HEK293T) cells were cultured in regular DMEM media supplemented with 10% FBS (fetal bovine serum) and 1% penicillin. Upon confluence, cells were collected by trypsinization, counted, and electroporated each of 20×10^6 cells/mL with 20ug of

pcDNA ACAD10 test plasmid and pcDNA control, respectively. Electroporated cells were transferred to regular DMEM medium containing 450ug/mL neomycin and grown for 48 hours. A few flasks of transfected cells containing pcDNA ACAD10 and pcDNA control were induced using 5uM retinoic acid for 48 hours and the remaining cells were not induced. The cells were harvested and processed for western blotting and seeded for immunofluorescence staining. HEK293T pcDNA control, pcDNA10 uninduced and induced cells were seeded at a concentration of 5×10^4 cells/ml on tissue culture-treated glass cover slips and allowed to grow overnight at 37 °C in a 5% CO₂, 95% humidity incubator. Cells were fixed in 4% paraformaldehyde for 10 minutes followed by 0.1% Triton X100 cell permeabilization and further blocked after brief washings in 5% donkey serum (Jackson ImmunoResearch, West Grove, PA) for 1 hour on ice. This was followed by triple primary antibody incubation with: 1) anti-ACAD10 antibody (lab made) and 2) anti cytochrome c oxidase subunit 4 antibody (Abcam, Cambridge, MA) and 3) anti catalase peroxisome specific marker (Santa Cruz Biotechnology, Inc., Dallas, TX) at 4 °C overnight. After brief washing, cells were further incubated with donkey anti-rabbit secondary antibody Alexa Fluor 488 (Invitrogen, Grand Island, NY) for ACAD10, and donkey anti-mouse secondary antibody Alexa Fluor 555 (Invitrogen) for cytochrome c oxidase subunit 4, and donkey anti-goat secondary antibody Alex Fluor 647. Nuclei were counterstained with DAPI. The cover slips were then mounted using mounting media before imaging. All the images were taken using an Olympus Confocal FluoView FV1000 microscope at a magnification of 60X.

3.3.3 His-Tag Protein Purification

Protein purification was performed using Talon Metal Affinity resin column (Clontech Laboratories Inc, Mountain View, CA). Approximately 1.5-1.9g of plasmid preparations were lysed and added to the purification column for fraction collection at 4°C. Purified extracts were then dialyzed in 50mM Tris before performing a protein assay and running an SDS-PAGE gel used for expression of ACD10- & ACAD11-ACAD domains as His-tag proteins.

3.3.4 Production and Purification of Anti-ACAD10 Antiserum

Rabbit anti-mouse ACAD10 and 11 antibodies were produced to a peptide homologous to the ACAD homologous domain of the ACAD10 or 11 protein structures. Rabbit antiserum to purified ACAD9 was raised by Cocalico Biologicals, Inc. (Reamstown, PA) according to company protocols. Rabbits were given initial inoculations of each purified protein and boosted three to four times with the purified protein at 1- or 2-week intervals. Final serum activity was confirmed by Western blotting.

Both antibodies were affinity purified using blotting methods. Immun-blot PVDF (Millipore, Billerica, MA) membrane strips (0.5x2.0 cm) were placed in methanol for 2-3 minutes and then equilibrated in 1X TBS + 0.02% sodium azide buffer for 15 minutes. The membrane strips were placed in 0.75mL of ACAD10 antigen solution rotating at 4°C for 1 hour, washed with 70% ethanol, and dried for 30 minutes under the chemical fume hood. They were then rinsed in 5 mL of methanol for 2 minutes, 10 mL of TBS for 2 minutes, then 5 times in 15 mL of PBS each for 10 minutes. Up to four strips were placed in 1 mL of ACAD10 antigen antiserum and rotated gently on a Nutator (TCS Scientific Corporation, New Hope, PA) at 4°C

overnight. The next day the strips were removed, rinsed with water, and incubated in TB-TX buffer for 10 minutes. They were then washed 5 times in TBS-TX (1 0mL/wash) for 10 minutes each, and twice in 10 mL of TBS-EDTA for 10 minutes each. The strips were transferred to a tube containing 1 ml ice-cold 0.2 M glycine (pH 3.0), and glycine was pipetted over them for 2 minutes while collecting the eluent. The eluted antibody was neutralized with the same volume of 2 N NaOH. The eluting process was repeated a second time, then strips were washed with H₂O, dried, and stored at 4°C. The elutes were combined into an Amicon concentrator (Millipore, Billerica, MA) and the glycine/antibody solution was diluted with 10 mL PBS-azide. The Amicon concentrator was centrifuged at 2500 x g until the solution was reduced to 1 mL. The antibody solution was diluted to 10 mL final volume in PBS-azide + 0.25% BSA, concentrated to 1 ml, then diluted again to make a total volume of 3mL. The antibody was aliquoted into 0.3mL portions and stored at 4 °C or flash frozen in liquid nitrogen and stored at -80 °C. A western blot was performed to confirm final serum activity and determine a working dilution.

3.3.5 Western Blot analysis

To examine expression in *E. coli*, cultures of cells containing various *ACAD10* plasmids were grown in LB broth at 37 °C, induced for 3 hours at 37 °C, then harvested by centrifugation. The cell pellets were lysed by sonication in 50 mM Tris buffer, pH 8.0 on ice, and the sonicates were cleared by centrifugation at 14,000 x g for 30 min at 4 °C. Human and mouse tissues were homogenized in ice cold PBS, and were cleared by centrifugation. One hundred µg of protein from extracts were subjected to electrophoresis with SDS-PAGE, using a pre-cast 4-15% TGX gel (BioRad), and proteins were transferred electrophoretically to an Immun-Blot PVDF membrane. Rabbit anti-mouse ACAD10 and 11 antibodies were produced to a peptide

homologous to the ACAD homologous domain of the ACAD10 or 11 protein structures by Cocalico, Inc according to standard immunization protocols. The peptide made for the antiserum was expressed and purified from plasmid “short form Fragment 4” found in Table 3. The membrane was probed overnight with rabbit antiserum to ACAD10 or 11 at 1:500 dilution as primary antibody, then washed extensively with 1X TBS Tween 20 at room temperature. Following incubation with alkaline phosphatase-coupled goat anti-rabbit IgG antibody, the antigens were detected with NBT/BCIP color developing solution (Promega, Madison, WI).

3.3.6 Identification of Proteins by Tandem Mass Spectrometry (MS/MS)

Identification of ACAD10 and ACAD11 gel bands was performed by the University of Pittsburgh Proteomics Core Laboratory. Briefly, SDS-PAGE gels were stained with Coomassie blue, and bands of interest were excised, reductively alkylated with DTT/IAA, and digested with trypsin. Peptides were analysed using nano RP-HPLC interfaced with an LTQ XL linear ion trap mass spectrometer (Thermo Fisher Scientific). Spectra were analysed by the MASCOT (Matrix Science) search engine and identified peptides and proteins were further statistically validated with the Scaffold software.

3.4 RESULTS

3.4.1 ACAD10 cDNA amplification and expression

PCR amplified fragments of the predicted full length human ACAD10 and ACAD11 regions were cloned into BL21 GRO EL/ES vectors, respectively, and expressed in *E coli*, but neither protein was identifiable in cellular extracts. To examine the possibility that another isoform was in fact the bona fide active one, a variety of inserts containing different combinations of predicted proteins were created via PCR and tested for expression and function (Figure 14).

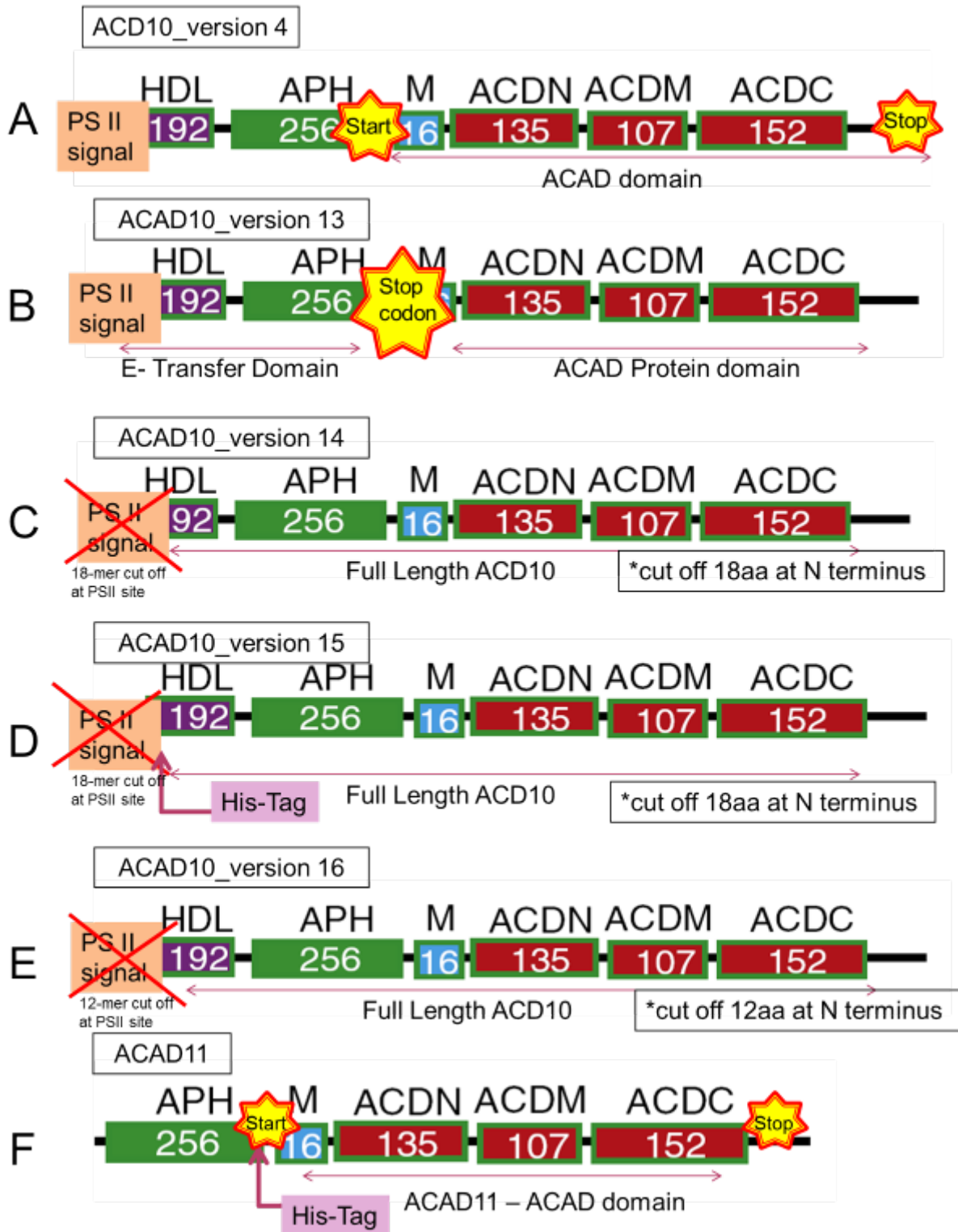


Figure 14. ACAD10 Human Plasmid Constructs Map

See the text for details regarding these constructs

To identify the substrate binding pocket and catalytic site, recombinant His-tag form of the ACAD-like domains (ACAD10 S637-I1059 and ACAD11 Q353-I780; designated ACAD10-C and ACAD11-C) were amplified, sub-cloned and expressed with an additional Met-His₆ tag at the N-terminus. The purified domains (predicted molecular mass 47 Kd) were yellow and had a typical flavin spectrum scanned between 250-800 nm demonstrated a reading of 1.660 at 280nm, but proved to be unstable as the protein precipitated before the next reaction could begin. The identity of the purified proteins was confirmed using MS/MS, and they were used to generate polyclonal rabbit antiserum. These antibodies were then used to analyze additional samples by SDS-PAGE and western blotting (Figure 15).

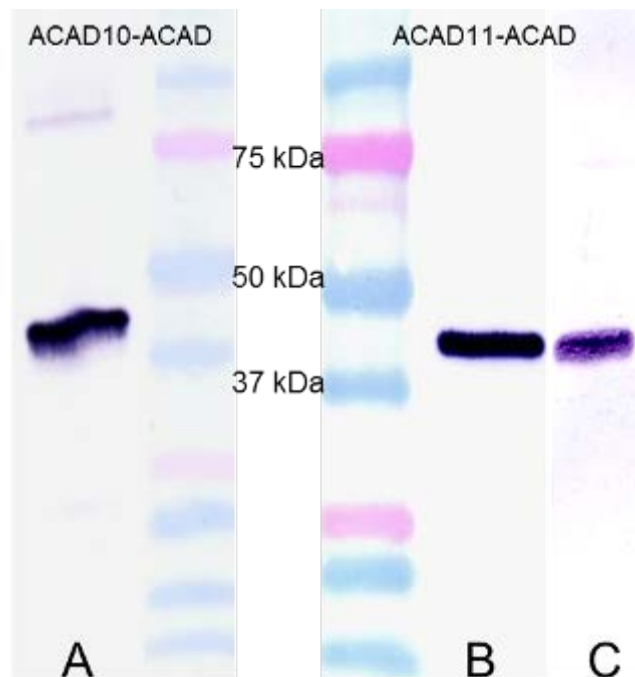


Figure 15. Expression of ACAD10-ACAD & ACAD11-ACAD domains as His-tag proteins

Western blot of a 4-15% SDS-PAGE gel. (A) Purified ACAD10-ACAD domain, 42 Kd form (0.5 μ g) was visualized with anti-ACAD10 antiserum, (B) ACAD11-ACAD domain, 47 Kd form (0.5 μ g) visualized with anti-His tag antibodies (C) ACAD11-ACAD domain, 47 Kd form (0.5 μ g) visualized with anti-ACAD11 antiserum

Expression of a truncated version of the ACAD10, missing the N-terminal domains including HDL, APH, and a part of the mitochondrial targeting domain that precede the ACAD domain led to production of an appropriate size protein band identified with western blotting (Figure 16).

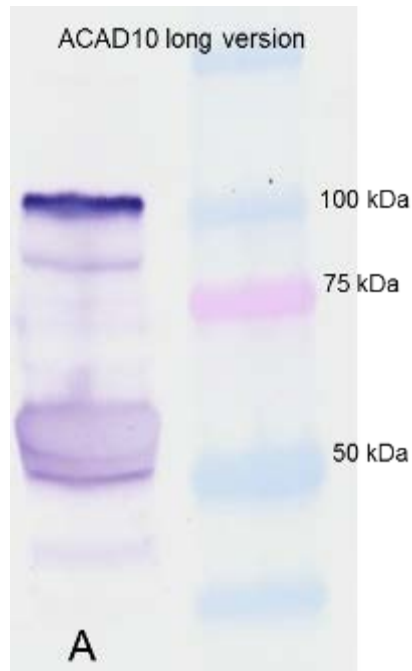


Figure 16. Expression of N-terminus truncated ACAD10 long version in E. coli

Western blot of a 4-15% SDS-PAGE gel. (A) Purified ACAD10 long version (10 μ g) ~100Kd form was visualized with anti-ACAD10 antiserum.

Overexpression in HEK293T (human embryonic kidney) cells of ACAD10 in a pcDNA3.1 vector system revealed that ACAD10 protein colocalized to mitochondria as demonstrated by immunofluorescent staining (Figure 17). Anti-VLCAD antibody was used as an internal control in these overexpression experiments.

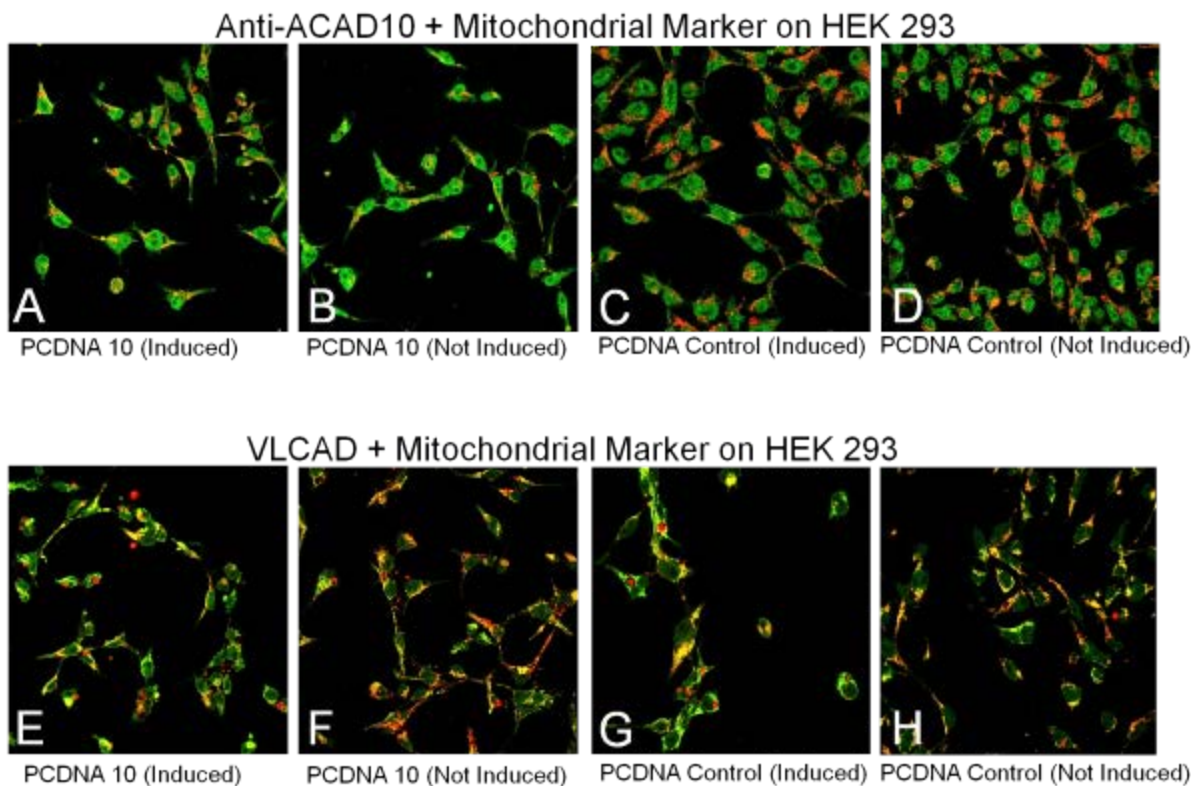


Figure 17. Overexpression of ACAD10 in HEK293

Control HEK293T cells were permeabilized with Triton X-100 and immunostained (green fluorescence) with antibodies to an ACAD10 peptide. (A-D). Fluorescent staining of induced or uninduced HEK293T cells with antibodies to the mitochondrial marker MTCO1 (red); colocalization of ACAD10 with mitochondria appears yellow. (E-H). Fluorescent staining of induced and uninduced HEK293T with anti-VLCAD antibodies (green) and antibodies to the mitochondrial marker anti MTCO1 (red). Colocalization of ACAD10 to the mitochondria appears yellow.

3.4.2 First half reaction

Screening for binding of a panel of acyl-CoA compounds the purified ACAD10 short form protein (which contains primarily the ACAD domain) was performed using absorbance spectral scanning. Purified protein has spectral maxima at ~370 nm and ~447 nm. These decreased after addition of glutaryl-CoA and HMG-CoA, evidence that these compounds were bound to the enzyme catalytic site and were able to, at least in part, establish the charge transfer complex

characteristic of the first half reaction (Figures 18 and 19). Incubation with succinyl-CoA, malonyl-CoA, and acetoacetyl-CoA led to no changes in the absorbance maxima, indicating lack of productive interaction with the enzyme (Figures 20-22).

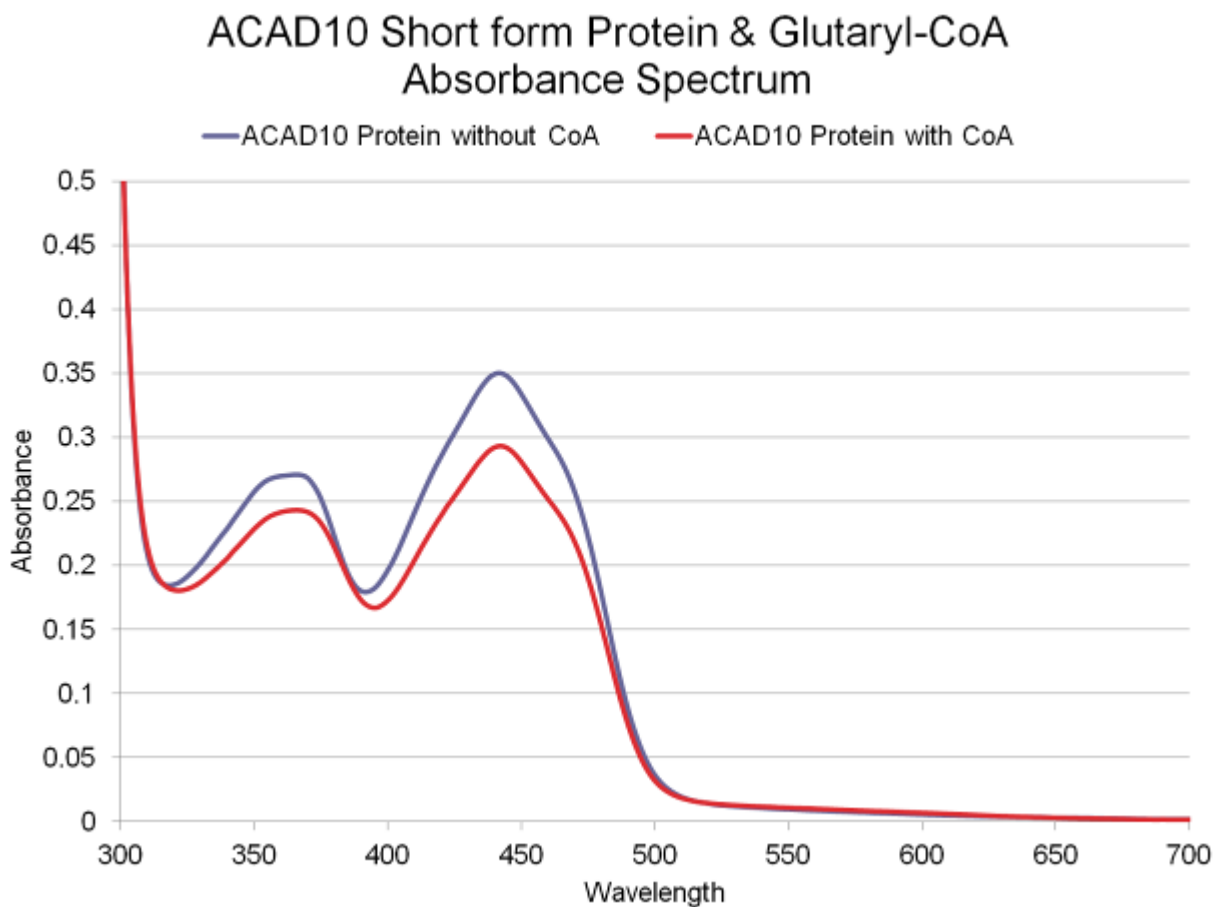


Figure 18. Binding of glutaryl-CoA to ACAD10 short protein.

An absorbance spectral scan from 300-700 nm.

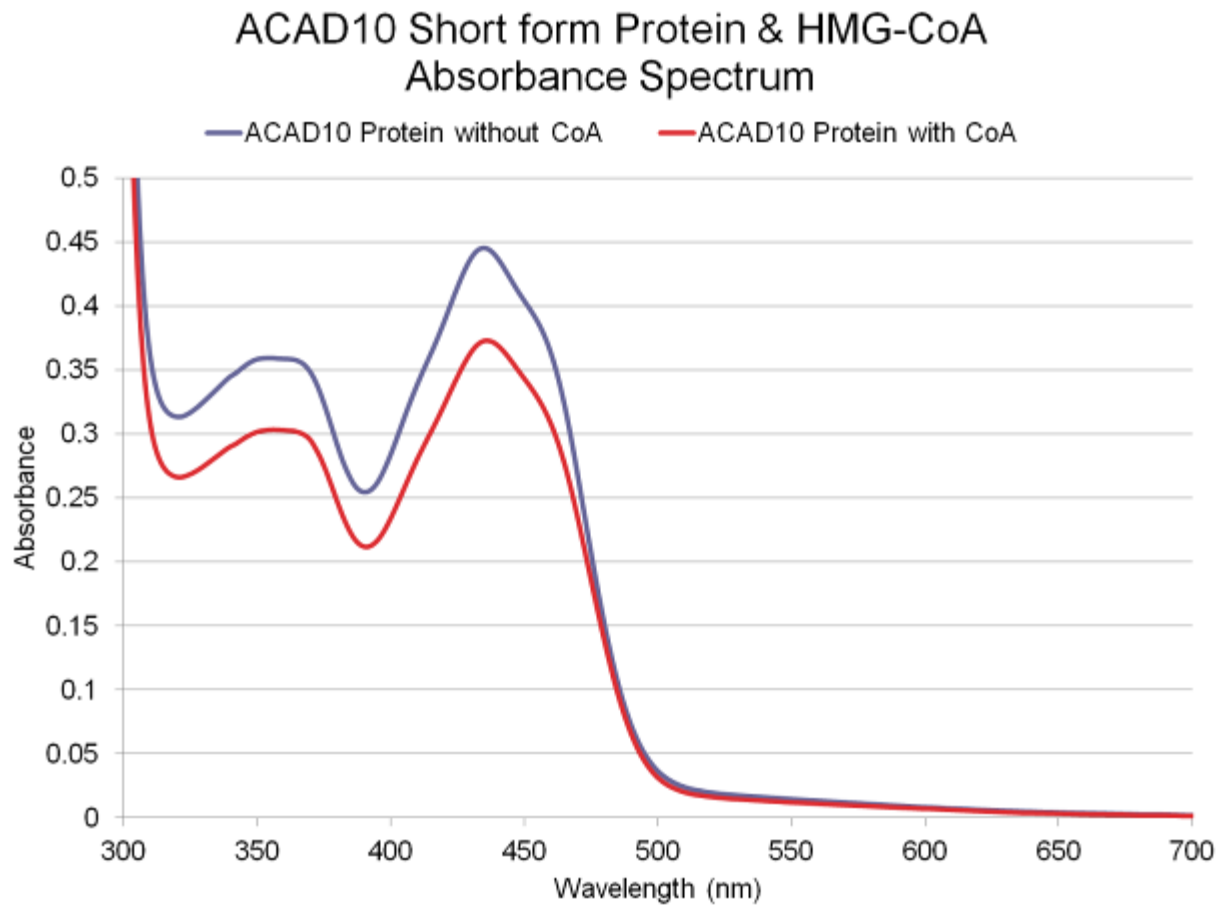


Figure 19. Binding of HMG-CoA to ACAD10 short protein binding.

An absorbance spectral scan from 300- 700 nm.

ACAD10 Short form Protein & Succinyl-CoA Absorbance Spectrum

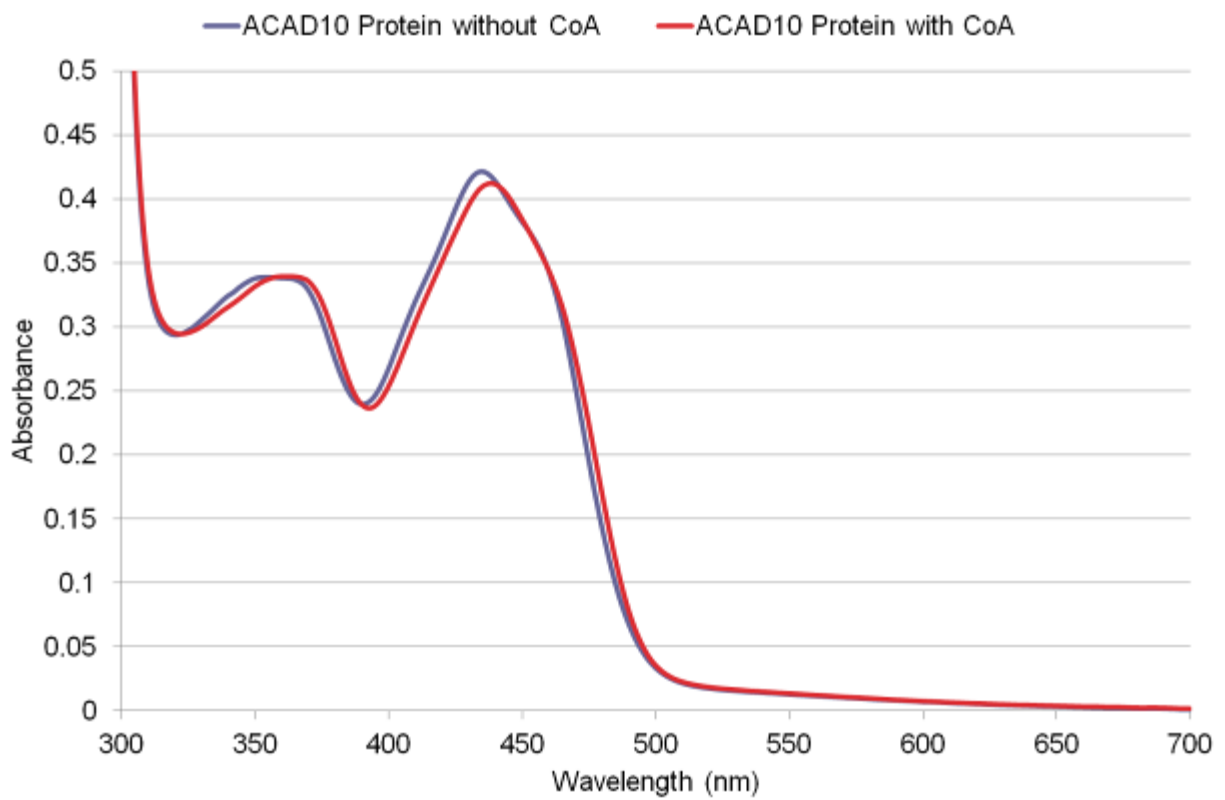


Figure 20. Binding of succinyl-CoA to ACAD10 short protein.

An absorbance spectral scan from 300- 700 nm.

ACAD10 Short form Protein & Malonyl-CoA Absorbance Spectrum

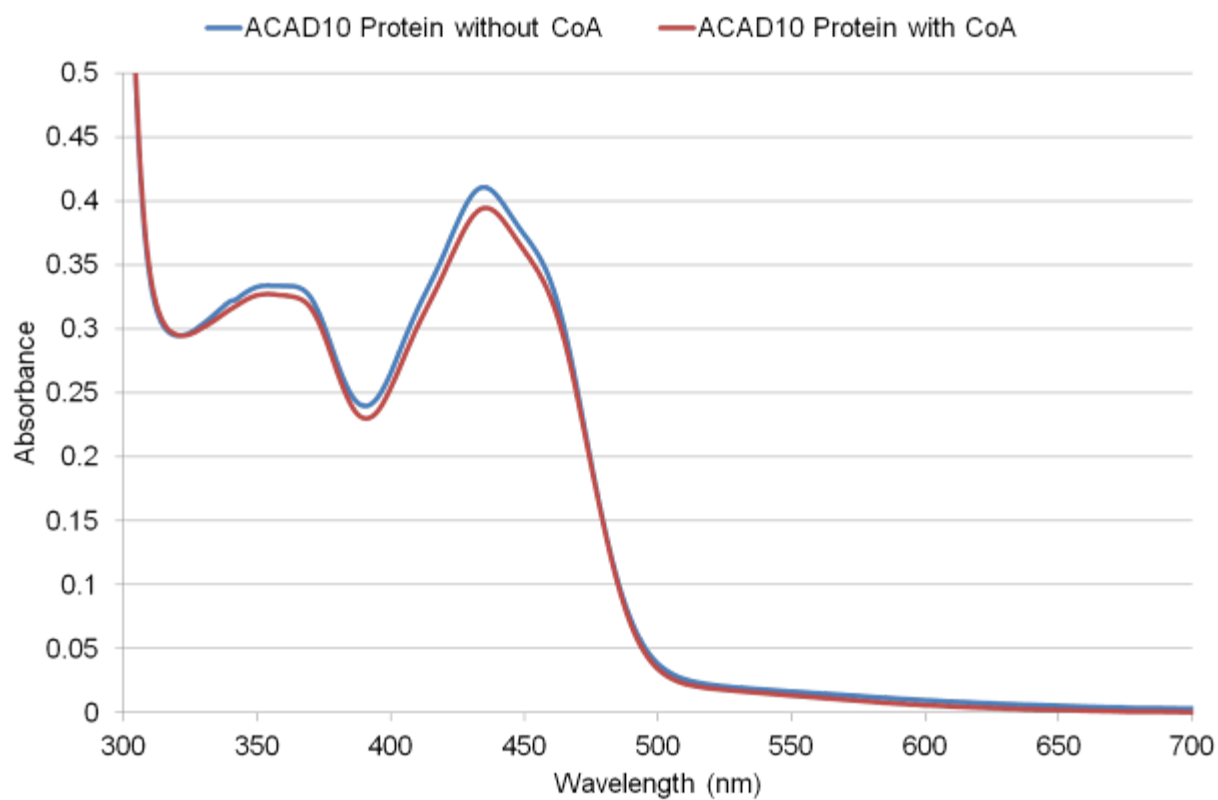


Figure 21. Binding of malonyl-CoA to ACAD10 short protein.

An absorbance spectral scan from 300- 700 nm.

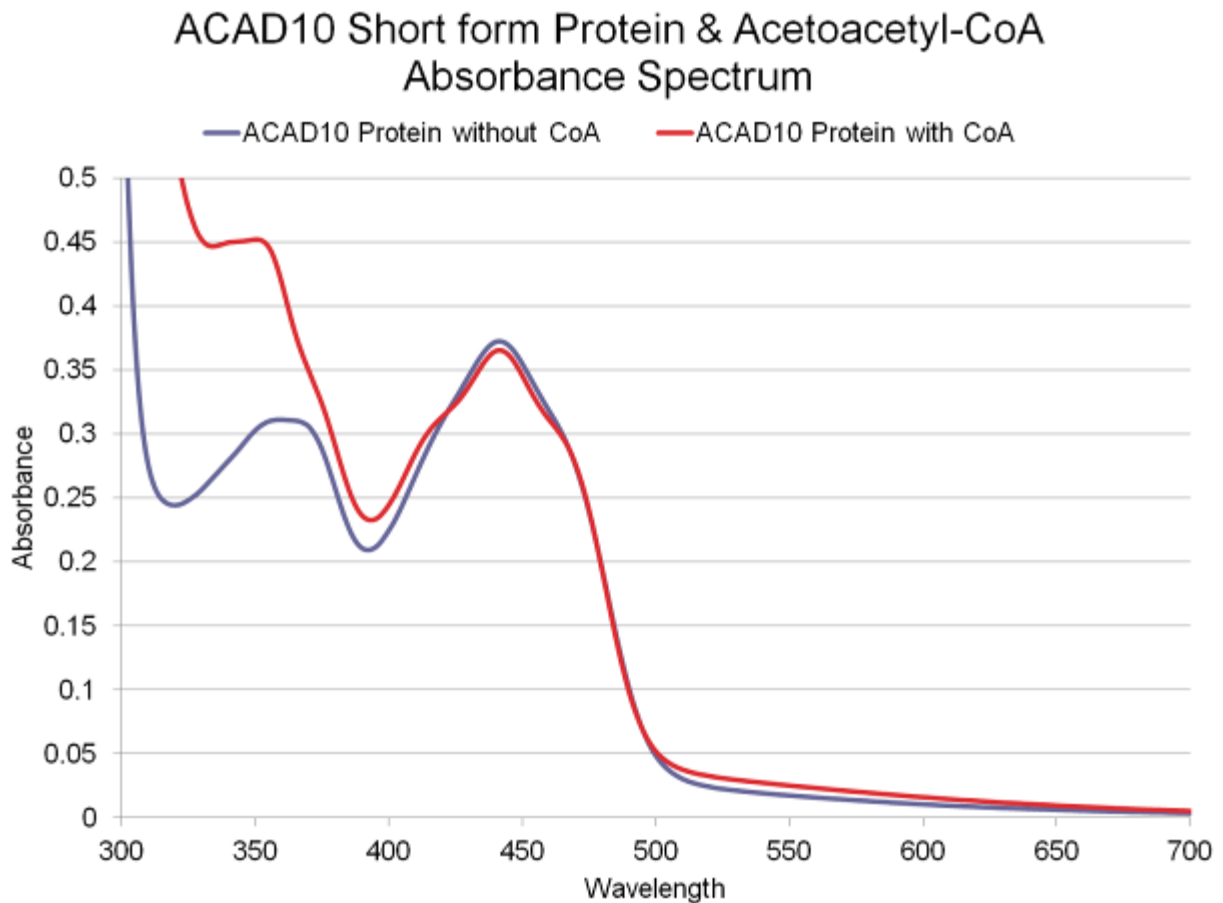


Figure 22. Binding of acetoacetyl-CoA to ACAD10 short protein.

An absorbance spectral scan from 300- 700 nm.

3.5 DISCUSSION

The *ACAD10* and *11* genes are unique among the ACADs in that each contains additional predicted domains other than those homologous to the ACAD coding region. Moreover, multiple versions of sequences from each gene are found in expression databases, consisting of variable combinations of the predicted protein domains (Ensembl 2013). Additionally, ACAD10 and 11

proteins have been localized to both peroxisomes and mitochondria in undirected proteomics studies. To better characterize these novel ACADS, various coding forms of each have been expressed in prokaryotic system, antisera have been produced, and their native forms have been explored in mouse and human tissue extracts. Prokaryotic expression studies confirmed that each protein contained an expected FAD cofactor, but none of the purified proteins were active. The proteins were unstable on storage, making extensive characterization impossible. In fact, many of the vectors tested led to no identifiable protein following expression. The expression vectors were designed to generate a variety of different forms of ACAD10, some predicted to be that seen in peroxisomes and others in mitochondria. I began attempting to express the full length ACAD10 protein; however, it was unstable in the full length form. Because of multiple domains and alternative splicing in mammalian cells, it is possible that the form used for these was in fact not the native one. I also created several of these inserts with the addition of His₆ tags to aid in expression, though none of these were stable either. I then began exploring the use of shorter ACAD10 protein fragments. I chose an ACAD domain insert specifically for its homology to the other ACADs, expecting it to behave in a similar manner when expressed. Unfortunately, all of these forms were unstable in the bacterial strains and rapidly degraded.

Mitochondrial import is directed by an N-terminal signal sequence characterized by positively charged amino acid residues and other properties (Omura 1998). Upon examination of the *ACAD10* gene, a potential mitochondrial targeting sequence is present, but it is not clear from database studies what form the transcript of a mitochondrial targeted protein might take, though my tissue studies clearly show that one is present. My prokaryotic expression studies failed to identify an active protein with ACAD activity, but not all possible combinations of exons were tested. Previous qPCR experiments were also unclear as to the nature of the mitochondrial form

of ACAD10. RNAseq experiments might be helpful to identify additional candidate transcripts. The amino terminus of ACAD10 contains a sequence homologous to a peroxisomal targeting signal. It has been shown that in proteins containing both a mitochondrial and peroxisomal targeting signal, the mitochondrial one is dominant (Omura 1998). Thus, any ACAD10 variants containing a mitochondrial targeting sequence are likely to in fact target to mitochondria, whereas all of the other forms will localize to peroxisomes.

ACAD11 has been confirmed to be a peroxisomal protein, though the existence of a small amount of a mitochondrial form cannot be excluded. Identification of an ACAD11 band at 75 kDa in tissue western blot experiments in contrast to the expected molecular mass of 87kDa for a full length protein suggests the existence of a shorter transcript generated by exon skipping of one or more protein domain, or alternative posttranslational modification including proteolytic processing of the full length protein. Additional tissue expression and prokaryotic expressions studies are necessary to differentiate these possibilities. The function of *ACAD11* remains unclear. As a peroxisomal protein, it is likely to be an oxidase rather than a dehydrogenase, but additional characterization must await expression and purification of a stable protein for further study.

4.0 CHARACTERIZATION OF AN *ACAD10* DEFICIENT MOUSE MODEL: PATHOLOGICAL AND BIOCHEMICAL ANALYSES

4.1 ABSTRACT

Pima Indians have the highest incidence of insulin resistance (IR) and type-2 diabetes mellitus (T2DM) of any reported population, but the pathophysiologic mechanism is unknown. Genetic studies have linked the *ACAD10* gene, among others, to this predisposition. *ACAD10* is related to a family of flavoenzymes active in fatty acid oxidation (FAO). Dysregulation of FAO and an increase in plasma acylcarnitines is recognized as important in the pathophysiology of IR and T2DM. In *Acad10* deficient mice, animals accumulate excess abdominal adipose tissue, develop an early inflammatory liver process, and exhibit fasting rhabdomyolysis. Skeletal muscle mitochondria are abnormal. Blood acylcarnitine analysis shows an increase in long chain species in older animals, as seen in adults with obesity and T2DM. *Acad10* deficient mice show an abnormal glucose tolerance test with elevated insulin levels in response to the glucose challenge. Our results identify *ACAD10* as an important genetic determinant of T2DM and provide a model to further explore pathophysiology and therapy.

4.2 INTRODUCTION

4.2.1 Mitochondrial fatty acid oxidation and diabetes

In the last half of the 20th century, the incidence of T2DM, previously unrecognized in the Pima Indians, began to rise. Multiple factors were postulated to be responsible including environmental factors such as diet and resultant obesity, along with a number of genetic determinants (Baier and Hanson 2004). *ACAD10* was one of 30 genes further examined after demonstrating a significant signal for diabetes in a genome-wide association study (Bian, Hanson et al. 2010). In this genome wide association scan (GWAS), a single nucleotide polymorphism (SNP), rs632650, was found to map within intron 2 of *ACAD10* (Bian, Hanson et al. 2010). The hypothetical ACAD10 protein is structurally related to the acyl-CoA dehydrogenase (ACAD) family of mitochondrial flavoproteins, which consists of nine enzymes that are similar in structure and function as they catalyze the α,β -dehydrogenation of their corresponding acyl-CoA substrates. Seven of these ACADs, LCAD, MCAD, SCAD, IVD, IBD, 2-methyl-BCAD, GDH, are homotetramers (~400-aa per monomer) and two, VLCAD and ACAD9, are homodimers (~640-aa per monomer). In addition to their usual location in the mitochondrial matrix, some ACADs including LCAD, MCAD, and SCAD have been shown to be associated with cytoplasmic GLUT4- containing vesicles where they interact with two dileucine motifs on insulin-regulated aminopeptidase (IRAP) (Katagiri, Asano et al. 2002). Mutation of the dileucine motif of IRAP (amino acids 55-82) eliminates this interaction (Katagiri, Asano et al. 2002). In cells, glucose equilibrium is maintained by the GLUT4 response to insulin (Haga, Ishii et al. 2011). The GLUT4 and IRAP containing vesicles respond to insulin stimulation by translocation to the cell surface. IRAP has a specific protein structure containing a

dileucine motif. The dileucine motif in IRAP plays a critical role in regulating GLUT4 trafficking. These findings connect some of the ACADs with insulin dependent transportation of glucose within cells, but the physiologic role of the ACAD proteins in this setting is unclear (Katagiri, Asano et al. 2002).

While skeletal muscle patterns of fatty acid utilization during fasting conditions have been shown to be associated with obesity-related insulin resistance and altered mitochondrial energy metabolism, including fatty acid oxidation, it has also been shown to play an important role in the development of T2DM (Kelley, Goodpaster et al. 1999)(Goodpaster 2013). We have recently shown that the pattern of acylcarnitines (ACNs), key metabolic intermediates of fatty acid oxidation, in the blood of obese and T2DM participants fall into two distinct patterns. First, the T2DM and obese participants have a similar accumulation of long-chain ACNs that arise from activity in the initial rounds of β -oxidation, consistent with increased flux at entry into mitochondrial β -oxidation. Diabetic participants also displayed a secondary accumulation of various shorter chain ACNs suggestive of inefficient fatty acid oxidation or interactions between β -oxidation and ETC. They also showed an inability to efficiently switch from fat metabolism during insulin clamp, as reflected in their inability to lower their ACNs as effectively as either the lean or obese subjects. In contrast, this pattern was not present in obese adolescents, who instead showed metabolic findings suggestive of upregulation of fatty acid oxidation (Mihalik, Goodpaster et al. 2010).

The function of two additional proteins annotated in the human genome and predicted to be ACADs (ACAD10 and 11) is unknown (Vockley , Swigonova, Mohsen et al. 2009, He 2011). These two genes share 46% homology and are widely conserved across evolution. Homology alignments have defined three domains. Both genes are located within complicated loci

containing multiple predicted exons and protein domains, including an ACAD domain. Previous published results and experiments described in the previous chapter of this thesis describe potential functions for *ACAD10* in the central nervous system, metabolism, and immunity. In addition to their usual location in the mitochondrial matrix, acyl-CoA dehydrogenases have been shown to be associated with cytoplasmic GLUT4- containing vesicles where they interact with two dileucine motifs on insulin-regulated aminopeptidase (Katagiri, Asano et al. 2002).

To characterize the physiologic role of *ACAD10* in intermediary metabolism and its possible link to T2DM, we have characterized an *ACAD10* gene trap knockout mouse model. Aging animals become obese on a normal diet and develop insulin resistant hyperglycemia in response to an intraperitoneal glucose challenge. Tissue and blood ACN profiles are similar to those previously described for adult humans with T2DM. Our findings identify *ACAD10* as new monogenic cause of T2DM in mice, and provide valuable insight into its potential role in the development of T2DM in Pima Indians.

4.3 MATERIALS AND METHODS

4.3.1 Subcellular Location of ACAD10 Protein in Human Tissues

A human tissue panel was obtained from the NIH's Eastern Division of the Cooperative Human Tissue Network (CHTNE). Formalin Fixed Paraffin Embedded (FFPE) human tissues were sectioned to 5 μ m thickness. The sections were deparaffinized, rehydrated, and subjected to antigen retrieval followed by cell permeabilization, then briefly washed with PBS and blocked. Tissues were stained by overnight incubation with three primary antibodies: anti-ACAD10, anti-cytochrome c oxidase subunit 4, and anti-catalase. ACAD10 purified antibody was used in a

1:1000 dilution and anti-MTCO1 antibody as a mitochondrial marker (Abcam), and catalase (N-17) (Santa Cruz Biotechnology, Inc.) were used in 1:250 dilutions for the lung. Two different antibody dilutions were used to obtain the best possible tissue images. ACAD10 purified antibody was used in a 1:500 dilution, and anti-MTCO1 antibody as a mitochondrial marker (Abcam), and catalase (N-17) (Santa Cruz Biotechnology, Inc.) were used in 1:250 dilutions for kidney, liver, muscle, and pancreas. After washing, sections were further incubated for 1 hour with secondary antibodies donkey anti-rabbit 488 for ACAD10, donkey anti-mouse Cy3 for mitochondria, and donkey anti goat Cy5. Nuclei were counterstained with DAPI. Aqueous anti-fade fluorescent mounting medium was applied and imaged. Slides were analyzed using an Olympus FluoView FV1000 confocal microscope (Olympus).

4.3.2 Subcellular Location of ACAD10 Protein in Mouse Tissues

Crude peroxisomal, mitochondrial, and purified peroxisomal fractions from ~10 mg of fresh control mouse liver tissue were separated using the PEROX1 Kit (Sigma-Aldrich, St Louis, MO) as per the manufacturer protocol, and 15 µg of total protein from each fraction were separated on a 12% SDS polyacrylamide gel, transferred to a PVDF membrane, and immunostained and visualized with ACAD10 antibodies as above. A western blot survey of ACAD10 expression in various human tissues was performed by homogenizing approximately 100 mg tissue in ice cold PBS using a Virtis HandiShear homogenizer followed by sonication using a microtip sonicator, and centrifugation at 30 minutes, maximum speed, at 4 °C. The supernatants (100 µg protein) were loaded onto SDS-PAGE gels, transferred to Immun-Blot PDVF membrane, and probed with 1:500 dilution of ACAD10 F-11 mouse monoclonal primary antibody (Santa Cruz Biotechnology, Inc.).

4.3.3 Generation of Mutant Mice

A heterozygote *Acad10* gene trap knockout mouse model generated in a total genome knockout mouse project was purchased from Taconic Laboratories (Bian, Kasumov et al. 2006). Six- to 8-week-old *Acad10* deficient (*Acad10*^{-/-}) 129SvEv/BL6 mice were purchased from Taconic (Germantown, NY). Heterozygous mice were viable and fertile. Genotyping was performed by isolating genomic DNA from the tail tip using standard methods followed by PCR with primers designed to specifically amplify an ACAD10 containing DNA fragment, and visualization using 1% agarose gel electrophoresis. PCR was able to reliably differentiate the genotype as either wild type, heterozygous, or homozygous for the disrupted *Acad10* gene. Wild type and homozygous lines were established by breeding to create experimental animals in the same SvEv129/BL6 mixed background strain. Mice were housed in pathogen-free conditions at Children's Hospital of Pittsburgh, Pennsylvania. All of the animal studies were conducted with the approval of the University of Pittsburgh Institutional Animal Care and Use Committee.

4.3.4 Clinical Characterization

Regular visual observations and weight measurements using a digital balance were performed to monitor health status and behaviors of wild type and *Acad10* deficient mice over time.

4.3.5 Micro MRI Imaging

Abdominal MRI was performed with a Horizontal bore 7-T MRI system (Bruker Biospin Corporation, Billerica, MA) 70/30 with full vital monitoring system to assess accumulation of

adipose tissue content in wild type and *Acad10* deficient mice. Briefly, animals were anesthetized with isoflurane and 100% oxygen gas via nose cone during MRI imaging. Animal body temperature, heart rate, respiratory rate, and arterial oxygen saturation were continuously monitored visually and with the real-time physiology monitoring system. Total scanning time was approximately 30 to 45 minutes per animal.

4.3.6 Histopathology

Wild type and *Acad10* deficient mice were sacrificed by cervical dislocation. Tracheas of the mice were exposed and cannulated (Pociask, Scheller et al. 2013). Lungs were perfused by instillation of PBS, and tissues were immediately dissected, flash frozen in liquid nitrogen for metabolic analysis, or preserved in 2.5% gluteraldehyde or 4% paraformaldehyde for histopathology (Pociask, Scheller et al. 2013). Tissues harvested included lung, liver, spleen, pancreas, brain, heart, bone, muscle, bone marrow, eyes, testes, and kidney. After fixation, organs were dehydrated and embedded in paraffin; 10 μ m sections were stained with hematoxylin and eosin, according to standard protocols. Gomorri staining was also performed on muscle tissue samples using standard techniques.

4.3.7 Immunohistochemical and immunofluorescent staining of paraffin-embedded sections of mouse tissues

Tissues were removed from mice and immersed in fixative overnight at 4 °C, samples were formalin-fixed, paraffin embedded, and 5 μ m sections were prepared and mounted on glass slides by the Department of Pathology, Children's Hospital of Pittsburgh..

Immunohistochemical staining was performed using overnight incubation at 4 °C with primary antibody, followed by incubation for 1 hour at room temperature with fluorescently labeled secondary antibodies as described in the previous chapter. Primary antibodies included rabbit polyclonal antibody against ACAD10, mouse anti-MTCO1 antibody as a mitochondrial marker (Abcam), and goat polyclonal IgG anti-catalase (N-17) (Santa Cruz Biotechnology, Inc.) as marker for peroxisomes. Primary antibodies were used at dilutions of 1:500 and secondary antibodies at a dilution of 1:3,000. Slides were analyzed using an Olympus FluoView FV1000 confocal microscope with a magnification of 60X (Olympus).

4.3.8 Biochemical Analysis

Acad10 deficient mouse tissues including heart, liver, lung, muscle, kidney, spleen, and pancreas were harvested and immediately flash frozen in liquid nitrogen. Samples were extracted and derivatized with pentafluorophenacyl trifluoromethanesulfonate. Acylcarnitine profiling by UHPLC MS/MS was performed as previously described (Minkler, Stoll et al. 2008). Values were quantified using 13 point calibration curves, and 72 acylcarnitines were reported.

Blood samples, (approximately 50-100 μ L) were collected in a serum separator tube (BD Microtainer) by performing a retroorbital bleed. After collection blood was subjected to centrifugation for four minutes at \sim 450 g. Serum was removed and frozen at -80 °C until use. Glucose and creatine kinase levels were determined by MS/MS by clinical laboratory in the Department of Pathology at the Children's Hospital of Pittsburgh of UPMC. C-reactive protein and insulin were measured with commercially available ELISA kits (Alpco Diagnostics, Salem, NH) according to the manufacturer instructions. Samples were assayed in triplicate. A panel of

23 cytokines was analyzed with a Luminex immunoassay kit (Bio-Rad, Austin, TX) according to the manufacturer's instructions.

Whole blood, plasma, urine, and various tissue samples were also collected and processed for acylcarnitine profiling. Whole blood, urine, and tissues were collected and immediately flash frozen prior to analysis. Plasma was flash frozen after separation from whole blood as described above. For analysis of (1) acylcarnitines (2) carnitine and butyrobetaine, and (3) total carnitine, samples were isolated by ion-exchange solid-phase extraction, derivatized with pentafluorophenacyl trifluoromethanesulfonate, separated by HPLC, and detected with an ion trap mass spectrometer (Minkler, Stoll et al. 2008). Acylcarnitines values were quantified using 13 point calibration curves, and approximately 72 acylcarnitines were reported. The internal standards used were d6-acetyl-, d3-propionyl-, undecanoyl-, undecanedioyl-, and heptadecanoylcarnitine (Minkler, Stoll et al. 2008). Tissues were reported in concentrations units of $\mu\text{mol}/\text{gram}$ wet weight. Urine, plasma, and whole blood were reported in units of nmol/mL .

4.3.9 Glucose and Insulin Regulation Studies

An intraperitoneal glucose tolerance test (IPGTT) was performed as previously described (Rehman, Wang et al. 2005). Briefly, mutant animals and age-matched controls were fasted for approximately 5.5 hours followed by an intraperitoneal administration of sterile filtered D-glucose at 2 g/kg body weight. The blood glucose levels were measured in tail blood samples at 0 (prior to glucose administration), 15, 30, 60, and 120 minutes after glucose administration using a handheld Precision Xtra glucometer (Abbott, Alameda, CA). Glucose levels of 70-150 mg/dl under normal conditions is considered normal in mice.

4.3.10 Microscopy

Light microscopy was performed in the Mouse histology core laboratory by the Children's Hospital of Pittsburgh of UPMC. Transmission electron microscopy was performed by the Center for Biologic Imaging at the University of Pittsburgh.

4.3.11 Electron Transport Chain complexes

4.3.11.1 Preparation of Mitochondria from Organs

Three control and *Acad10*^{-/-} mouse heart, brain, liver, and muscle tissues were harvested and placed in ice-cold PBS (1X) on ice at the time of harvest. The organs were washed twice with PBS and suspended in the mitochondrial separation buffer (Behboo, Carroll et al.) which consists of 0.25M sucrose, 1mM EDTA, 2.5% glycerol, 50mM phosphate buffer (pH 8.0) and freshly added protease inhibitor cocktail (Sigma, St Louis, MO). The organs were homogenized. The suspension was centrifuged at 2000 rpm for liver and brain, 1000 rpm for heart, and 1500 rpm for muscle in a Sorval SS34 rotor for 10 minutes. The supernatant was collected and centrifuged at 15,000 x g for 15 minutes at 4°C. The resulting pellet containing the mitochondria was washed twice with HB buffer, suspended in HB buffer and stored at -80 °C or in liquid nitrogen. The protein concentration of each sample was obtained using Bio-Rad DC Assay.

4.3.11.2 Blue native gel electrophoresis (BNGE)

Mitochondrial respiratory chain complexes and supercomplexes were characterized using BNGE (Graves, Wang et al. 2012). Eight mg of digitonin (MP Biomedicals, Solon, OH) were dissolved in 200 ml of 30 mM HEPES buffer, pH 7.4, 150 mM potassium acetate and 10% glycerol, heated

at 95°C, then cooled on ice. One mg of mitochondria, isolated as described above, was lysed by the addition of digitonin to a final ratio of 1:8 protein:digitonin. Following incubation on ice for 20 minutes, a Coomassie blue solution (5% Coomassie blue G250 in 750 mM 6-aminocaproic acid) was added (1/20 v/v), and the mixture was centrifuged at 14,000g for 20 minutes at 4 °C. The supernatant was then directly loaded onto a 3–12% Native PAGE Novex Bis-Tris gel (Invitrogen), and subjected to electrophoresis at 80 V for 4 hours at 4 °C in the buffer provided by the supplier. Following electrophoresis, gels were stained with Bio-Safe Coomassie G250 (Bio-Rad, Hercules, CA) for 30 minutes and exhaustively de-stained with water. Stained gels were scanned and the images analyzed. For confirmation of native complex identities, individual bands were excised from the above gels, incubated in Laemmli SDS- sample buffer (Bio Rad) for 30 minutes at room temperature and electrophoresed on a Criterion pre-cast gel (Bio Rad) and electrophoresed at 80 V for 2 hours followed by silver staining (Sigma-Aldrich).

4.3.11.3 Complex I and V gel in situ activity stain

For Complex I activity measurements, the blue native gel was placed in 3-4 ml of 2 mM Tris-HCl, pH 7.4 buffer containing 2.5 mg/ml nitrotertrazolinum blue chloride and freshly added 0.1 mg/ml NADH (Graves, Wang et al. 2012). The gel was incubated at 37 °C for 1-2 hours and then subjected to densitometric analysis. An average value from 3 gels was calculated. To quantify the ATPase activity of Complex V, gels were incubated in 3-4 ml of 34 mM Tris-glycine, pH 7.8, 14 mM MgSO₄, 0.2% Pb(NO₃)₂ with freshly added 8 mM ATP for 3 hours at 37 °C.

4.3.12 qPCR Expression studies

Wild type and *ACAD10* deficient mouse tissues including liver, muscle, and fat were harvested and immediately flash frozen in liquid nitrogen. RNA extraction was performed on all samples using Qiagen RNeasy Fibrous Tissue Mini Kit for muscle, and RNeasy Lipid Tissue Mini Kit for liver and fat (Valencia, CA). RNA concentration and quality was determined using Nanodrop. For cDNA synthesis and genomic DNA elimination in the RNA samples for use with the RT² Profiler PCR Arrays, the RT² First Strand Kit (Qiagen, Valencia, CA) was used. An RT² Profiler™ PCR Array Mouse Insulin Signaling Pathway (Qiagen, Valencia, CA) gene panel was tested following manufacturer's protocol. Real-time PCR was performed on an ABI 7900HT Sequence Detection System (PE Applied Biosystems, Foster City, CA) PCR assays were performed in 96 well optical plates following the manufacturer's recommendations.

4.4 NEUROBEHAVIORAL TESTING

4.4.1 Open Field Testing

To examine the locomotor function and behaviors of mutant mice in a new environment, animals were placed for 30 minutes in an open-field chamber testing chamber (28 x 28 x 40 cm) with a floor divided into equal-sized square fields, and the frequency of a variety of behaviors was determined (Figure 23). The lighting was set to 15-20 lux, similar to standard housing. The animal was removed from its home cage and placed into one of the four corners of the open-field

chamber and allowed to explore the chamber freely for 30 minutes, following which, it was returned to its home cage. Testing parameters included (1) ambulatory distance, (2) velocity, (3) real vertical time, (4) real stereotypic time, (5) distance per trip, (6) real resting time, (7) real ambulatory time, (8) ambulatory counts, (9) stereotypic counts, and (10) vertical counts.



Figure 23. Open field testing chamber

4.4.2 DigiGait Testing

A DigiGait (Mouse Specifics Inc, Quincy, MA) apparatus was used to examine locomotion on a motorized transparent treadmill belt with ventral plane treadmill videography to image the ventral view of animals as they walk (Figure 24). The motorized belt enabled numerous strides to be captured over a range of walking speeds (0.1 cm/s to 99.9 cm/s); goal boxes and other artifices to compel the animals to walk were not needed. Digigait software was used to compute the area of the advancing and retreating paws to quantify the spatial and temporal indices of gait, and reported >50 indices of gait for each limb a following the testing period (see Appendix B).

On day 1 each mouse was acclimated to the DigiGait chamber. The lights were off in the room, but the belt and overhead lighting fixture on the chamber were on. Animal containment plates were at their widest points. The animals were brought into the room and their micro-isolator cage lids were placed half way off for five minutes to allow for passive air transfer. Each animal was placed individually into the DigiGait chamber with the treadmill off for 10 minutes to explore. The mouse was then removed and put back to its cage. For days 2-5, each animal was acclimated to the DigiGait chamber in a similar fashion, except that belt speed was increased incrementally to 5 cm/s, 10 cm/s, 15 cm/s, and 29 cm/s on successive days. Ambulation was recorded on each day for 30 seconds, and the animal was returned to its home cage. One clip of data was analyzed for each animal and parameters for best visualization were set.

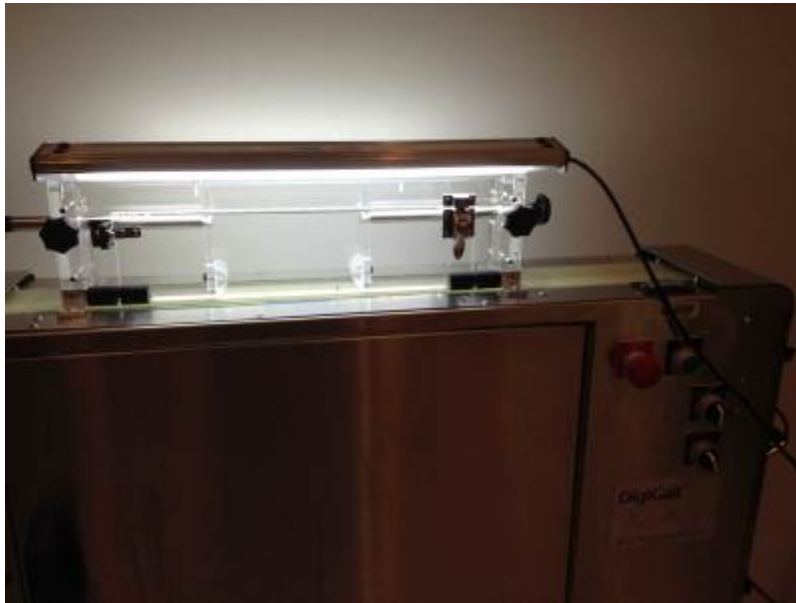


Figure 24. DigiGait testing equipment

4.5 RESULTS

4.5.1 ACAD10 Protein

Immunohistochemical staining results on a variety of human tissues using ACAD10 and ACAD11 antibodies are shown in Figures 25-27.

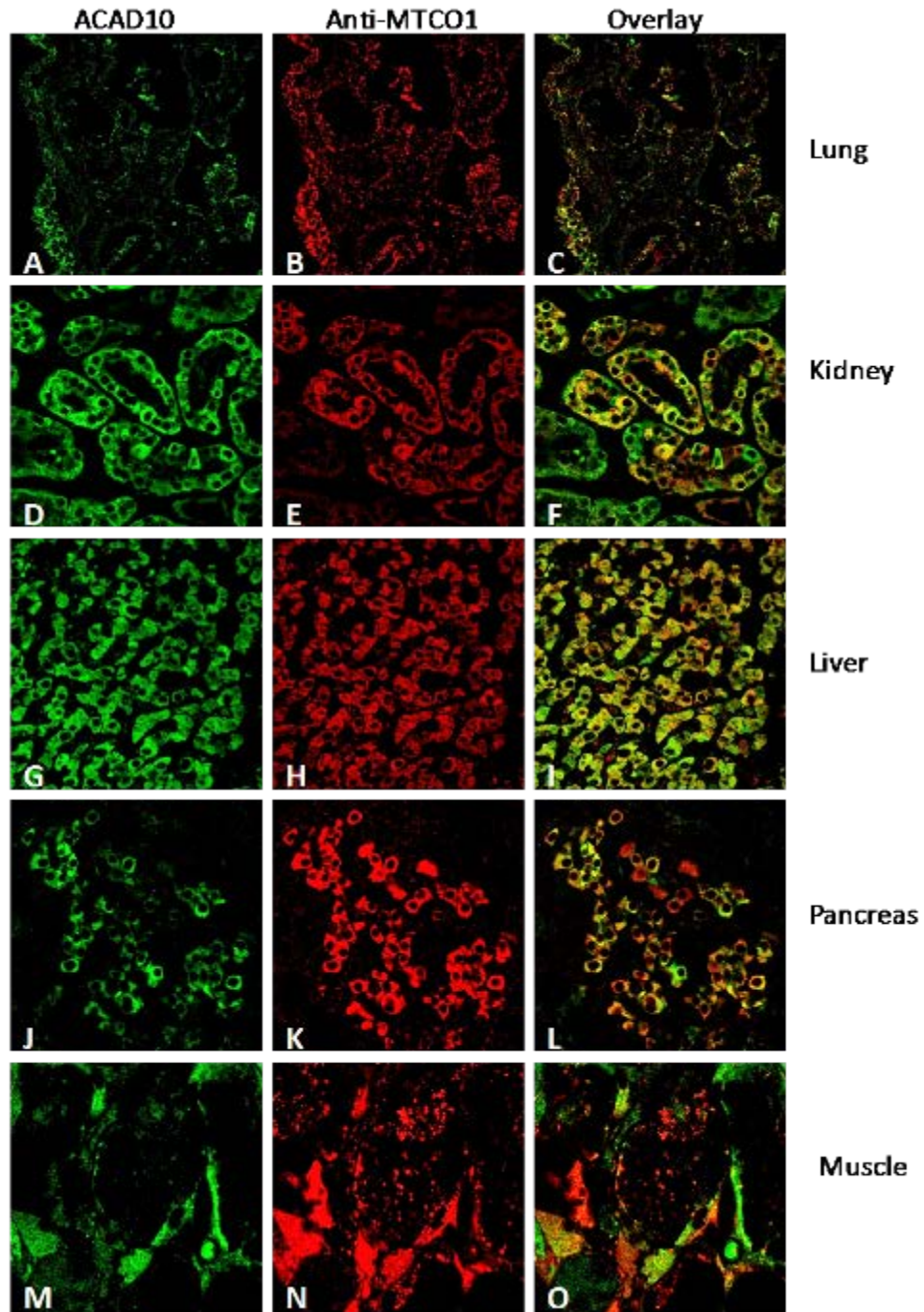


Figure 25. Immunofluorescent staining of ACAD10 in human tissues

Control human tissues (column A-M) were permeabilized with Triton X-100 and immunostained (green fluorescence) with antibodies to an ACAD10 peptide. Column (B-N) is fluorescent staining of the human tissues against anti-MTCO1 antibody is shown in red. Column (C-O) is the merged image of (A) and (B), and so on. There was significant co-localization of ACAD10 in mitochondria.

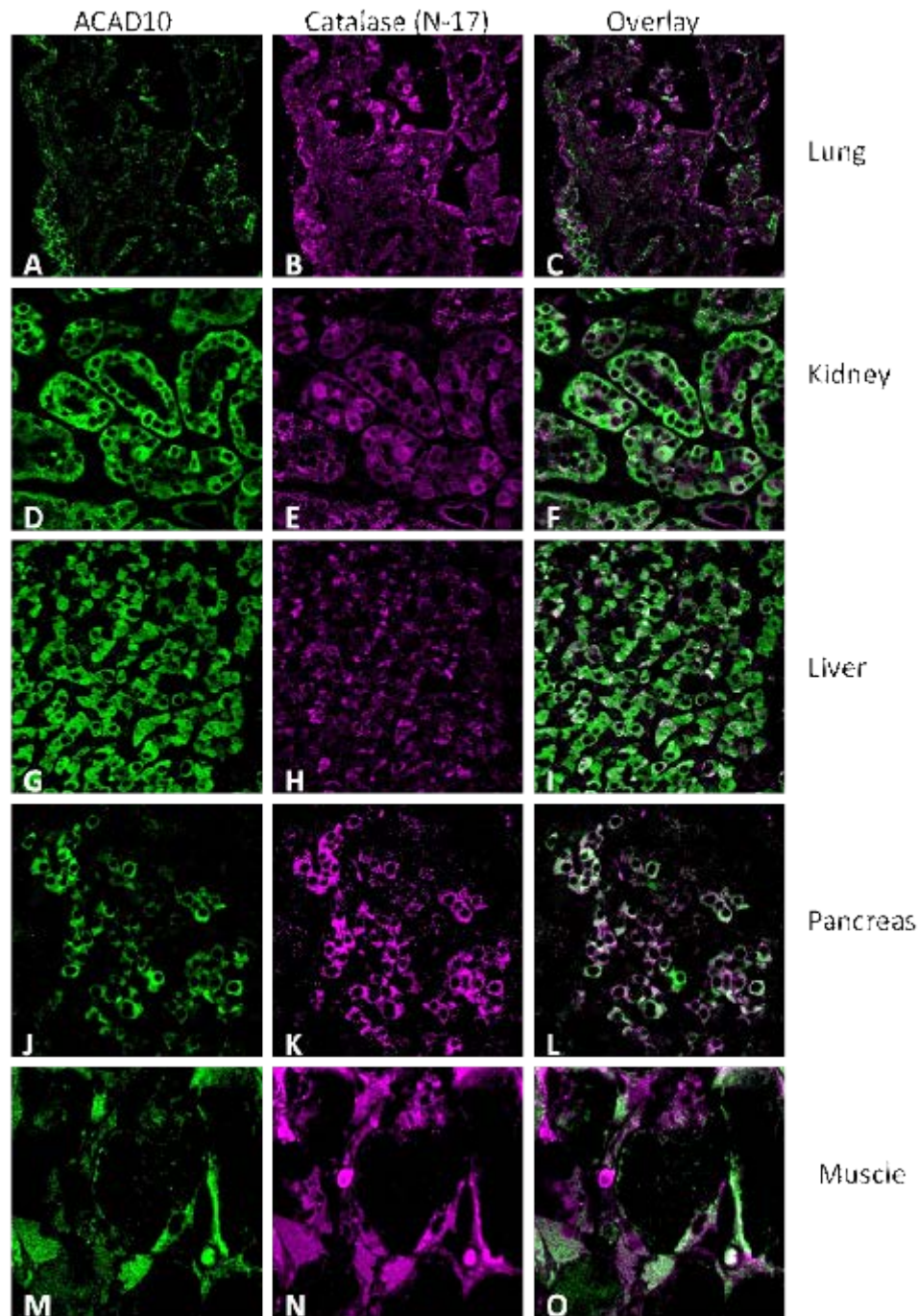


Figure 26. Immunofluorescent staining of ACAD10 in Human tissues

Control human tissues (column A-M) were permeabilized with Triton X-100 and immunostained (green fluorescence) with antibodies to an ACAD10 peptide. Column (B-N) is fluorescent staining of the human tissues against peroxisomal catalase (N-17) antibody is shown in magenta. Column (C-O) is the merged image of (A) and (B), and so on. In a few of the tissues there was faint colocalization of ACAD10 in peroxisomes observed.

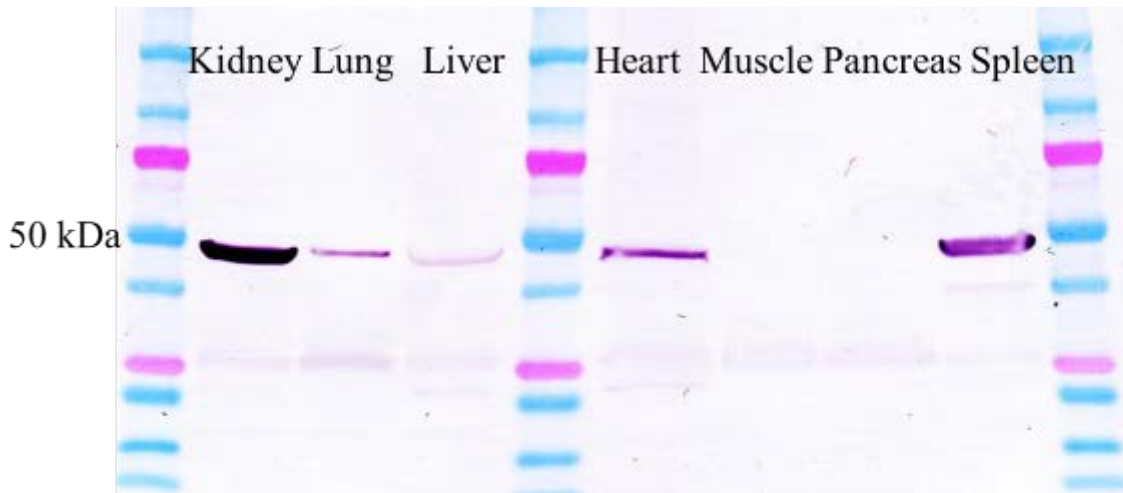


Figure 27. Western blot survey of human tissues for ACAD10 production

Western blot survey of ACAD10 in human tissues are shown on a 4-15% SDS-PAGE gel. 100 µg of tissue extract was applied per lane. Bands at ~50Kd were visualized with ACAD10 Santa Cruz F-11 mouse monoclonal primary antibody. All tissues except muscle and pancreas identified a predicted 50 Kd protein. Molecular mass marker size is listed to the left of the gel image.

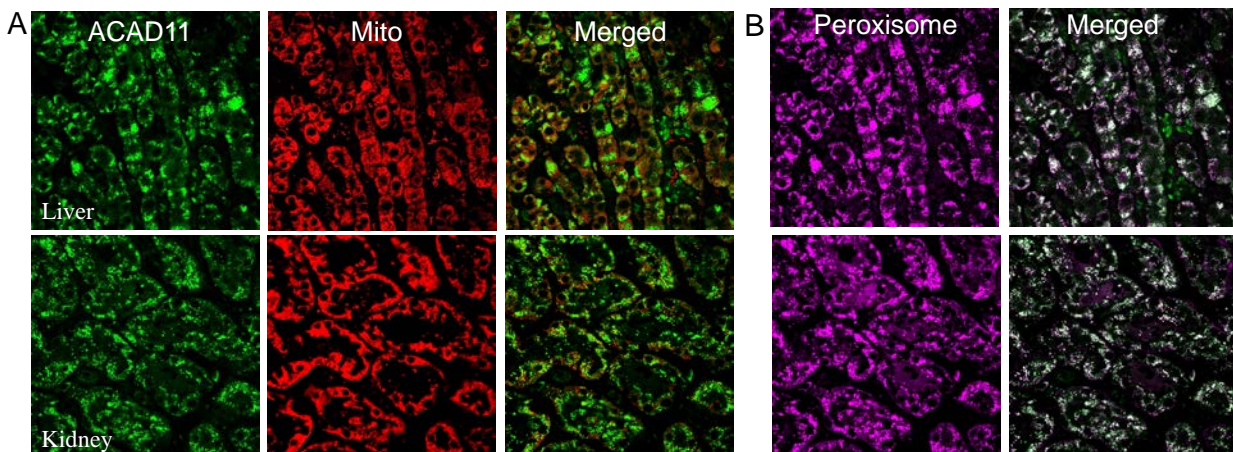


Figure 28. ACAD11 confocal microscopy on mouse liver and kidney

(A) Immunofluorescent staining of human liver and kidney with antiserum to ACAD11 (left column), the mitochondrial marker anti-MTCO1 (middle column), and the merged image (right column). (A) Tissues failed to show co-localization of ACAD11 with the mitochondrial marker. (B) Liver and kidney were stained with antibodies to the peroxisomal marker catalase (left column). The right column shows the merged images, and identifies colocalization of ACAD11 to peroxisomes in liver and kidney.

The function of ACAD10 protein is annotated in the human genome as an acyl-CoA dehydrogenase, but it has not been confirmed experimentally (Hashimoto, Fujita et al. 1999,

Swigonova, Mohsen et al. 2009, He 2011). Database searches of transcribed sequences from these genes have identified the presence of multiple transcripts that differed mostly at either the 5' or 3' end. One of the largest transcripts predicts a full length ACAD10 protein of 119Kd. Subcellular fractionation and western blotting was performed on wild type mouse liver tissue, and western blotting with ACAD10 antiserum identified a 119 Kd band in a combined mitochondrial/peroxisomal (M/P) fraction not present in a more purified peroxisomal fraction (P) (Figure 29). A smaller species was present in both fractions, and thus likely to be peroxisomal. We have noted 119, 100, 56, and 32 Kd ACAD10 isoforms are present in databases. We have observed bands at 119Kd in the mitochondrial fraction, but not in the pure peroxisomal fraction.

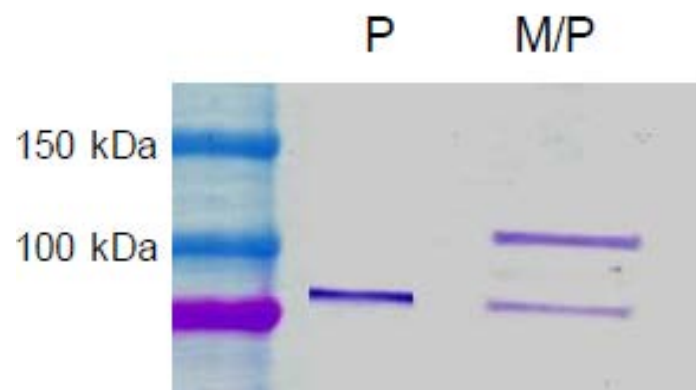


Figure 29. Subcellular fractionation and western blotting of wild type mouse liver tissue

ACAD10 purified antibody identified a predicted 119Kd full length ACAD10 protein in a combined mitochondrial/peroxisomal (M/P) fraction and a smaller protein in a more purified peroxisomal fraction (P). Molecular mass marker size is listed to the left of the gel image.

To further examine the subcellular location of ACAD10, immunohistochemical analysis was performed on a variety of control mouse tissues. Immunohistochemical staining demonstrated the presence of ACAD10 in mitochondria of muscle and kidney (Figure 30A). A faint ACAD10 signal was detected in mitochondria and peroxisomes of the lung and pancreas (Figure 30A and 30B), but was restricted to mitochondria in muscle and kidney (Figure 30A).

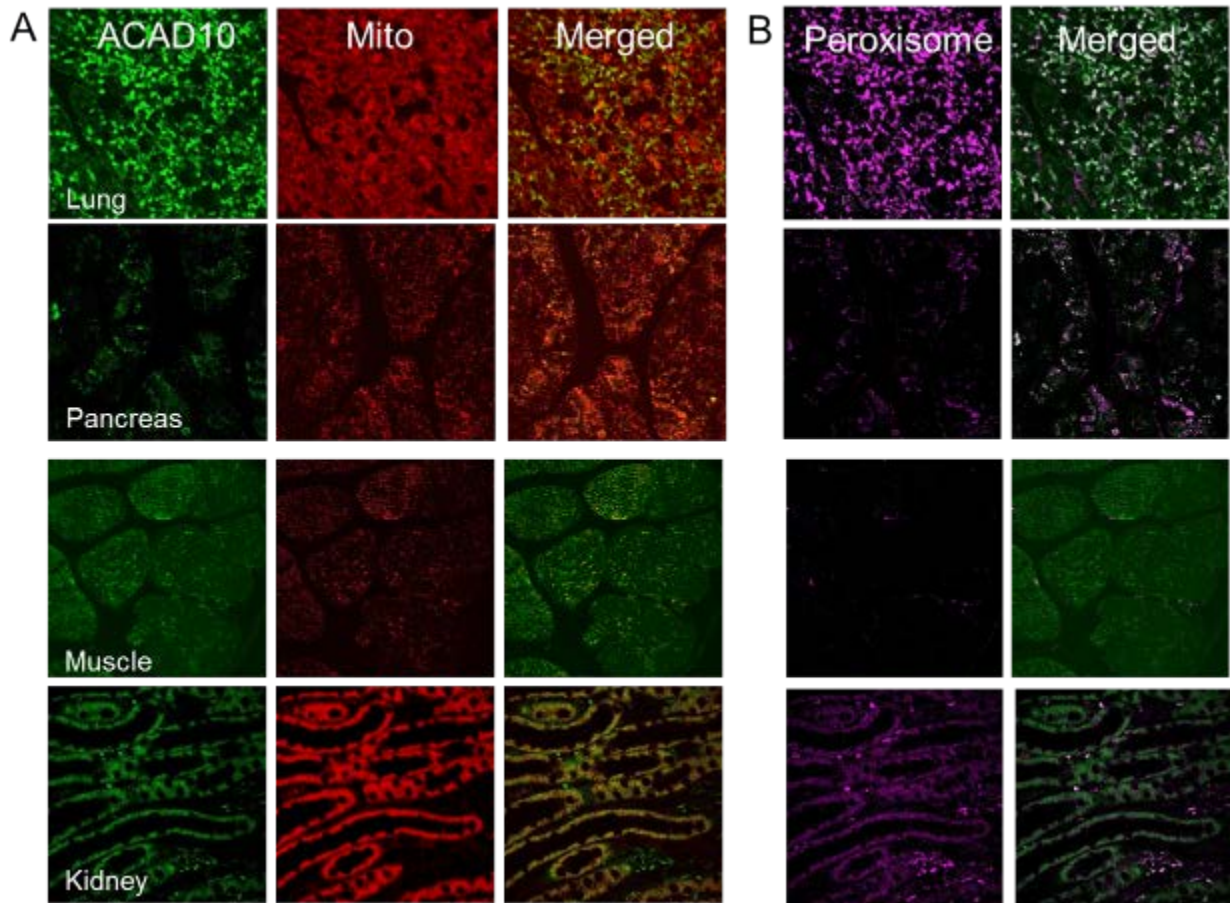


Figure 30. Subcellular localization of ACAD10 varies in different tissues

(A) Immunofluorescent staining of lung, pancreas, muscle, and kidney from wild type mice with antiserum to ACAD10 (left column), the mitochondrial marker anti-MTCO1 (middle column), and the merged image (right column). All tissues showed co-localization of ACAD10 with the mitochondrial marker. (B) In addition, lung and pancreas were stained with antibodies to the peroxisomal marker catalase (left column). The right column shows the merged images, and identifies colocalization of ACAD10 to peroxisomes as well as mitochondria in lung and pancreas.

4.5.2 *Acad10* Deficient Mouse Model

To determine the functional role of ACAD10, an *Acad10* gene trap knockout model produced in a total genome knockout mouse project was purchased (Taconic Farms, Germantown, NY).

Heterozygote animals were bred and PCR reactions using mouse genomic DNA to genotype offspring (Figure 31). Homozygous mutant animals proved to be viable and fertile.

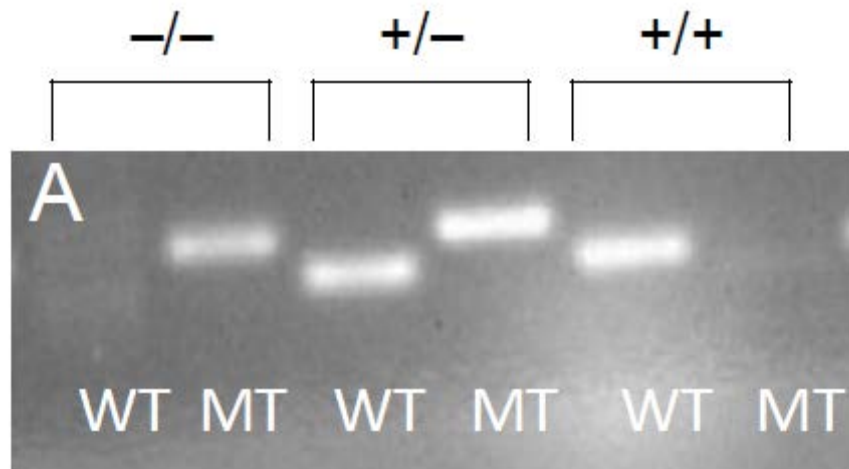


Figure 31. PCR genotyping of mutant animals

This is a 1% agarose gel electrophoresis of the larger fragment (195 bp) represents the wild type *Acad10* allele and the smaller (154 bp) the mutant allele, stained with ethidium bromide and photographed under UV light. Wild type (+/+), heterozygous (+/-), or homozygous mutant (-/-) could be distinguished.

4.5.3 Clinical Characterization

The *Acad10* deficient mice exhibited excess weight gain compared to wild type control animals, a difference that was more pronounced with age and sex (males > females) (Figures 32 and 33). Micro-magnetic resonance imaging and pathologic evaluation demonstrated greater accumulation of white adipose tissue in deficient mice, especially intra-abdominally (Figure 33).

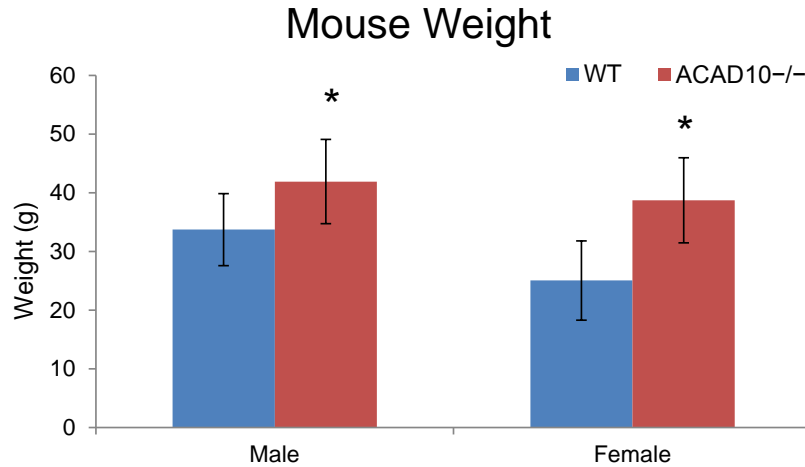


Figure 32. ACAD10^{-/-} and WT mice average body weight measured in grams (g)

The graph shows the weight (grams) of wild type and mutant male (blue) and female (red) animals measured at 6-8 months of age. The values are the mean and standard deviation of >7 animals each. The asterisk indicate significance difference. The difference between wild type and mutant male animals was statistically significant (two-tailed p-value=0.0006), as was the difference between the two female genotypes (two-tailed p-value=0.0007).

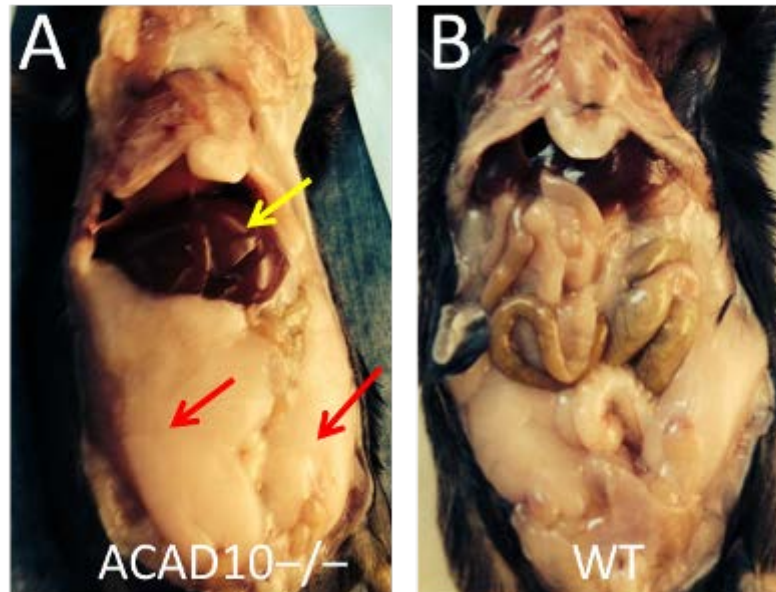


Figure 33. Intrabdominal fat accumulation is increased in mutant mice

Photograph of 2 male mice, age 10-15 months with abdominal incisions exposing the abdominal cavities. The liver (yellow arrow) is at the top of the figures. Intrabdominal fat (red arrows) is greatly increased in *Acad10*^{-/-} compared to wild type animals.

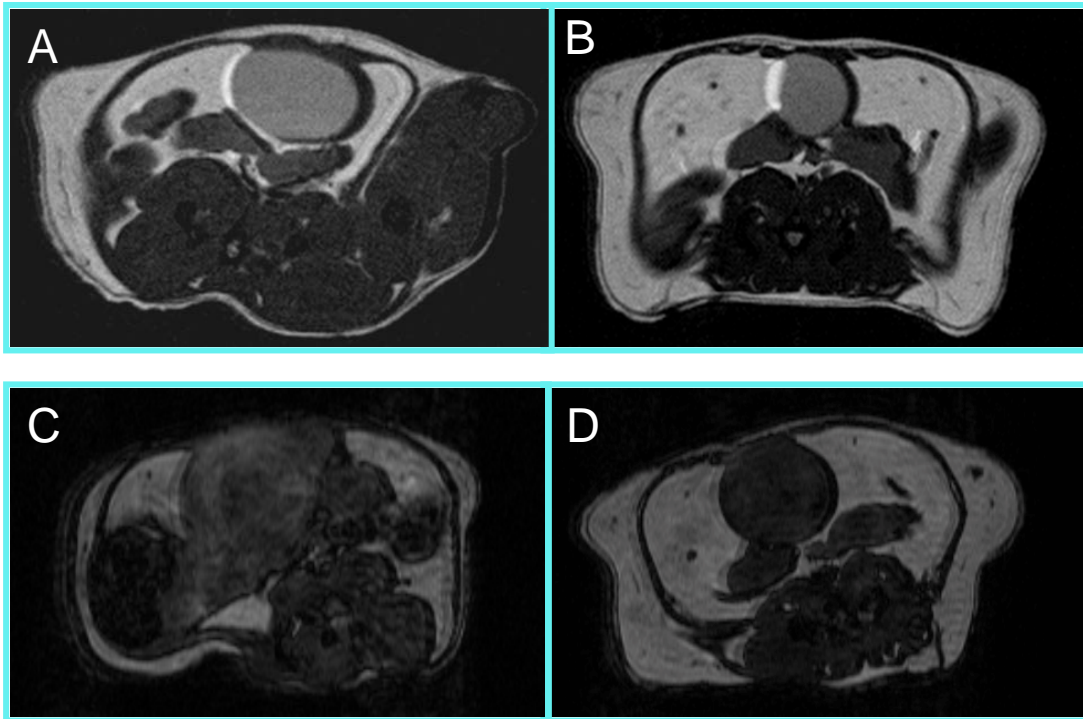


Figure 34. Micro-MRI imaging of Acad10 mouse abdominal cavity

Mice were visualized using Horizontal bore 7-T MRI system, Bruker Biospin 70/30 with full vital monitoring system. (A) is a wild type mouse at 2-3 months old and (B) is an *Acad10*^{-/-} mouse at 2-3 months old visualized using RARE-T2 Imaging. (C) is the same wild type mouse at 7-8 months old and (D) is the same *Acad10*^{-/-} mouse at 7-8 months old visualized using FISP-3D Imaging. The cross-sectional images are whole, live, mouse abdomen sections 11 of 15 for (A) and (B), and sections 40 of 128 for (C) and (D). The *Acad10* deficient mice visually show significant increase in adipose accumulation over time as compared to wild type control mice of the same background.

Increased weight over time in the *Acad10* deficient mice was not due to hyperphagia as they showed no significant differences in the amount of food consumed in wild type as compared to the mutants (Figure 35).

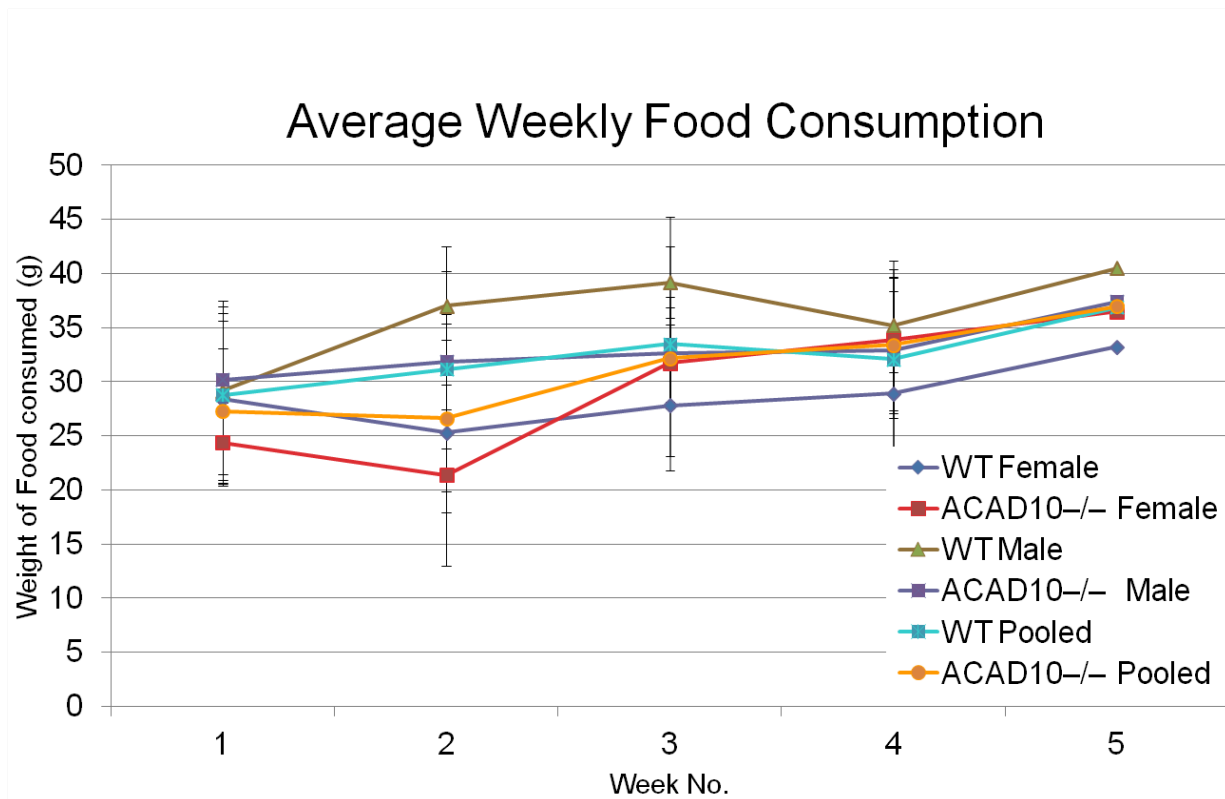


Figure 35. Mouse food intake

In a five week period mouse food levels from 6-7 mice per group were weighed weekly using a standard lab balance. All wild type and *Acad10* deficient mice were approximately 8 months old. The “WT pooled” and “*Acad10* deficient pooled” categories include combined data from both male and female mice. There were no significant differences in the amount of food consumed by wild type mice (any group) compared to *Acad10* deficient mice (any group).

4.5.4 Histopathology

A complete pathologic survey was performed on fed *Acad10* deficient mouse tissues from young (approximately 10-12 weeks old) and older (approximately 25-26 weeks and 1 year old) mice.

Haematoxylin and eosin staining revealed morphological abnormalities in deficient mice, including small multifocal necroinflammatory lesions and early abscess formation in liver parenchyma, extramedullary hematopoiesis with prominent megakaryocytes in spleen, and

multifocal extensive recent hemorrhage involving alveoli and bronchial tree in lung (Figure 36A). Alkaline phosphatase staining of muscle showed peripheral nuclei indicative of chronic damage; Gomorri trichrome demonstrated an increase in fat accumulation in deficient animals; and NADH dehydrogenase staining showed an increased number of poorly staining muscle fibers (Figure 36B). *Acad10* deficient mouse tissue weights were significantly higher than the weights of tissues found in wild type animals (Figure 37), suggesting the *Acad10* deficient mice tissue composition includes more fat.

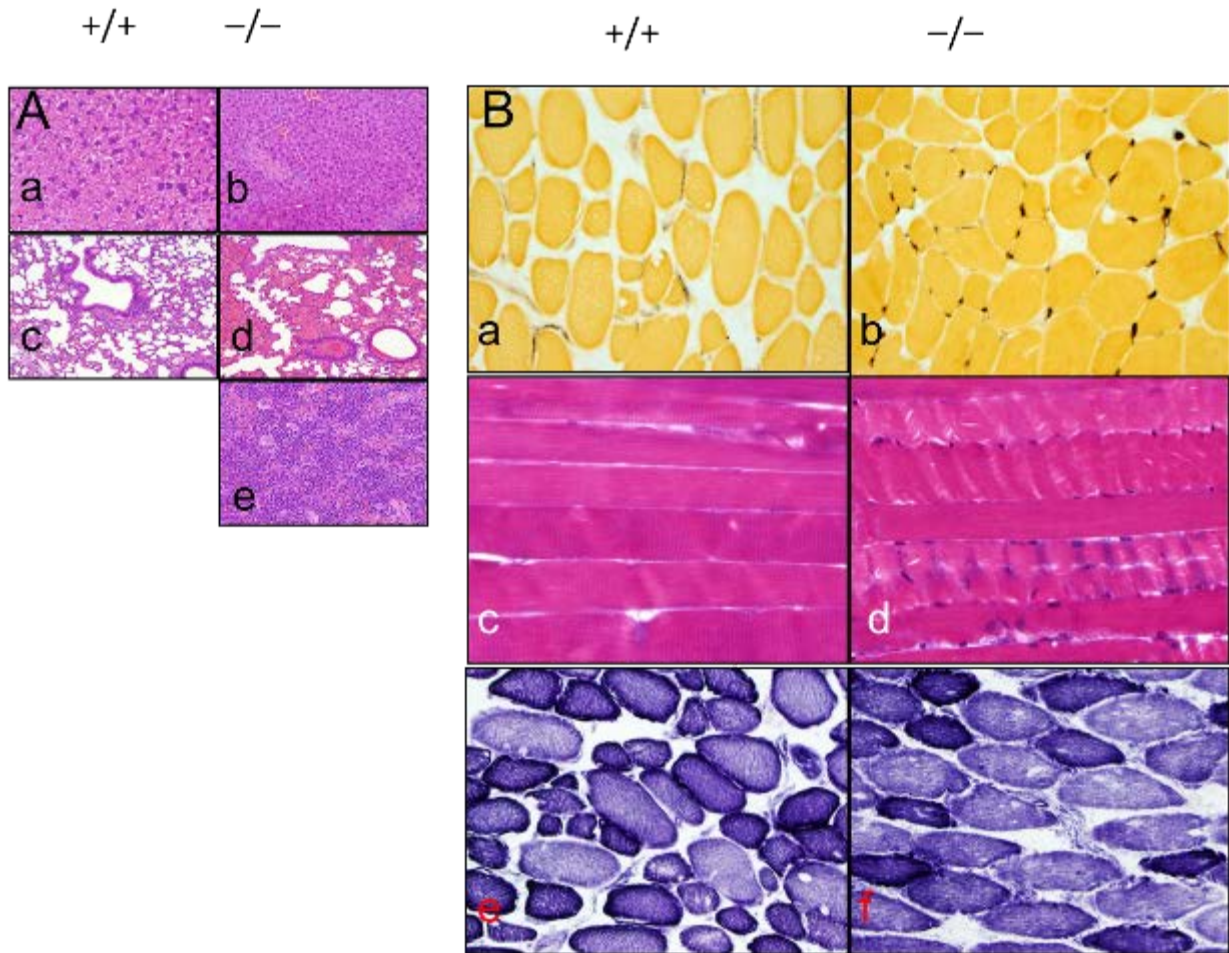


Figure 36. Histopathology of tissues from ACAD10 deficient mice

(A) Light microscopy with hematoxylin and eosin staining of wild type liver (a) and lung (c) and *Acad10* $-/-$ liver (b), lung (d), and spleen (e) showed the formation of small necroinflammatory lesions with the formation of early abscesses in liver, acute focal hemorrhaging in lung, and extramedullary hematopoiesis with prominent megakaryocytes in spleen. (B) Specialized staining techniques of wild type and deficient mouse tissues. a. & b.

Alkaline phosphatase staining showed peripheral nuclei indicative of chronic damage; c. & d. Gomorri trichrome shows increased fat accumulation (purple color) in deficient animals; e. & f. NADH dehydrogenase staining shows an increased number of poorly staining muscle fibers.

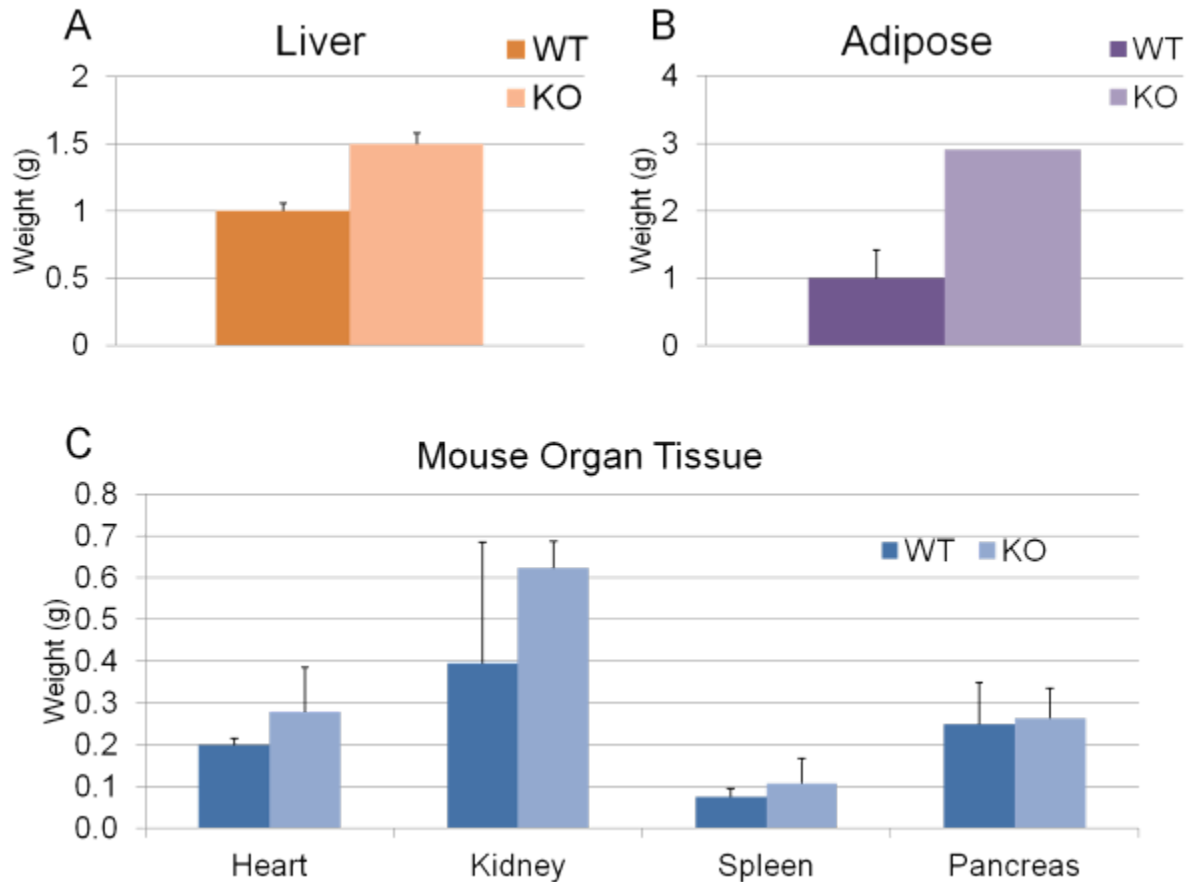


Figure 37. Organ tissue weights

Mouse organ tissues from 6 mice per group were weighed using a standard lab balance. All wild type and *Acad10* deficient mice were approximately 1 year old. The *Acad10* deficient (KO) demonstrated significant heavier tissues compared to wild type mice in (A) Liver, (B) Adipose, and (C) Heart.

Antigen purified anti-ACAD10 was used for visualization of western blots of 4-15% SDS polyacrylamide gels of several mouse tissues including liver, lung, muscle, brain, heart, kidney, pancreas, and spleen. ACAD10 antigen was detected in pancreas, kidney, and brain at a molecular mass of 100 Kd rather than the expected 119 Kd for full length ACAD10 containing all domains (Figure 38).

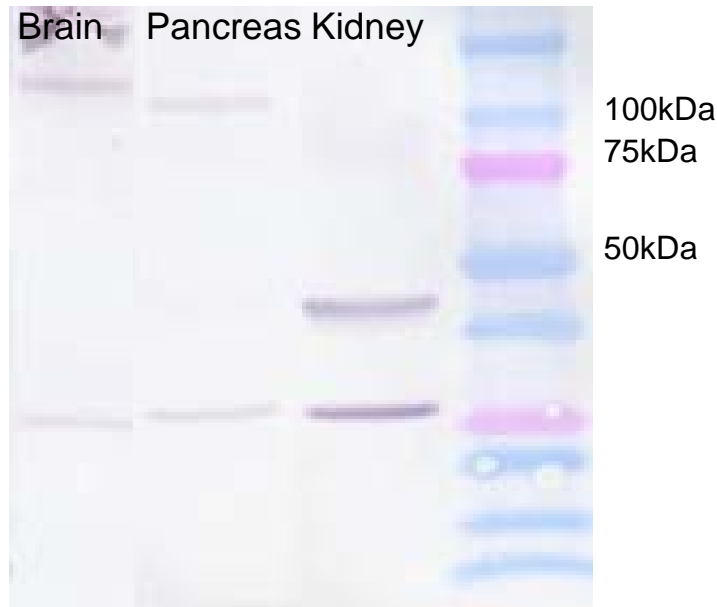


Figure 38. Western blot survey of ACAD10 in mouse brain, pancreas, and kidney

Western blot survey of ACAD10 in mouse tissue (only pancreas, kidney and brain are shown) of a 4-15% SDS-PAGE gel. 100 μ g of tissue extract were applied per lane. Bands at ~100Kd were visualized with ACAD10 purified anti-ACAD10-C to reduce background.

MitoProfile Total OXPHOS Rodent WB antibody cocktail (Abcam, Cambridge, MA), ATP Citrate synthase (C-20) (Santa Cruz Biotech Inc, Dallas, TX) VLCAD, and MCAD were used for visualization of western blots of 4-15% SDS polyacrylamide gels of several mouse tissues including heart, liver, muscle, and brain. Antigen was detected in all tissues at the appropriate molecular mass using the mitochondrial cocktail (expected sizes Complex V 55Kd, Complex III 48Kd, Complex IV 40Kd, Complex II 30Kd, Complex I 20Kd) and MCAD (expected 42Kd) (Figure 39). Similarly, ATP-citrate synthase (expected size 107Kd) was detected most highly in muscle tissue, while VLCAD (expected 62Kd) was observed in heart, liver, and muscle tissues.

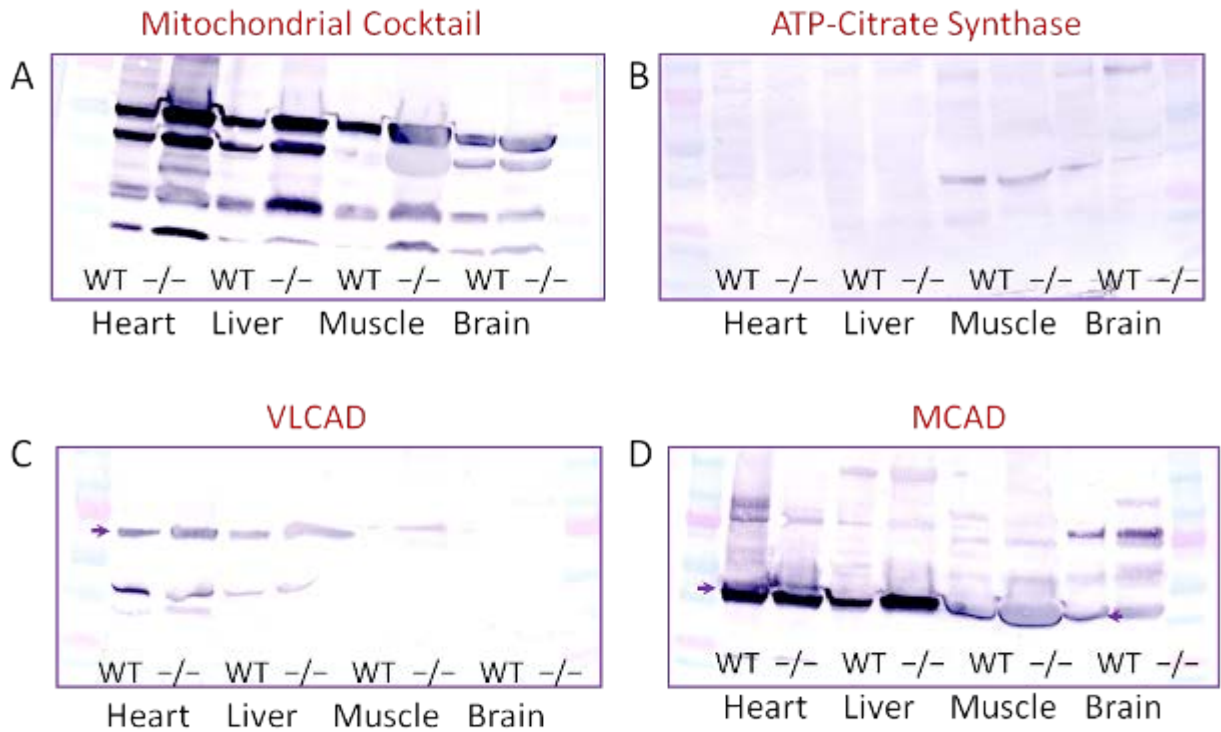


Figure 39. Western blot survey of ACADs in mouse liver, heart, muscle, and brain

A 4-15% SDS-PAGE gel with 50 μ g of tissue extract applied per lane was visualized with antiserum to the indicated protein. (A) ~55kDa, 48kDa, 40kDa, 30kDa, and 20kDa were visualized in heart, liver, muscle, and brain using a mitochondrial cocktail. (B) Staining with ATP-citrate synthase revealed an ~107Kd band. (C) and (D) Western blots with anti VLCAD and MCAD antisera, respectively showing the appropriate protein sizes of 62Kd and 42Kd, respectively.

Similarly, anti-ACAD11 antiserum was used to survey human and mouse tissue extracts including kidney, lung, liver, heart, muscle, pancreas, and spleen on western blots. ACAD11 antigen was detected in all mouse tissues examined and human kidney and liver at ~75 kDa in contrast to the expected molecular mass of 87 kDa (Figure 40). The identity of this band as ACAD11 was confirmed using MS/MS.

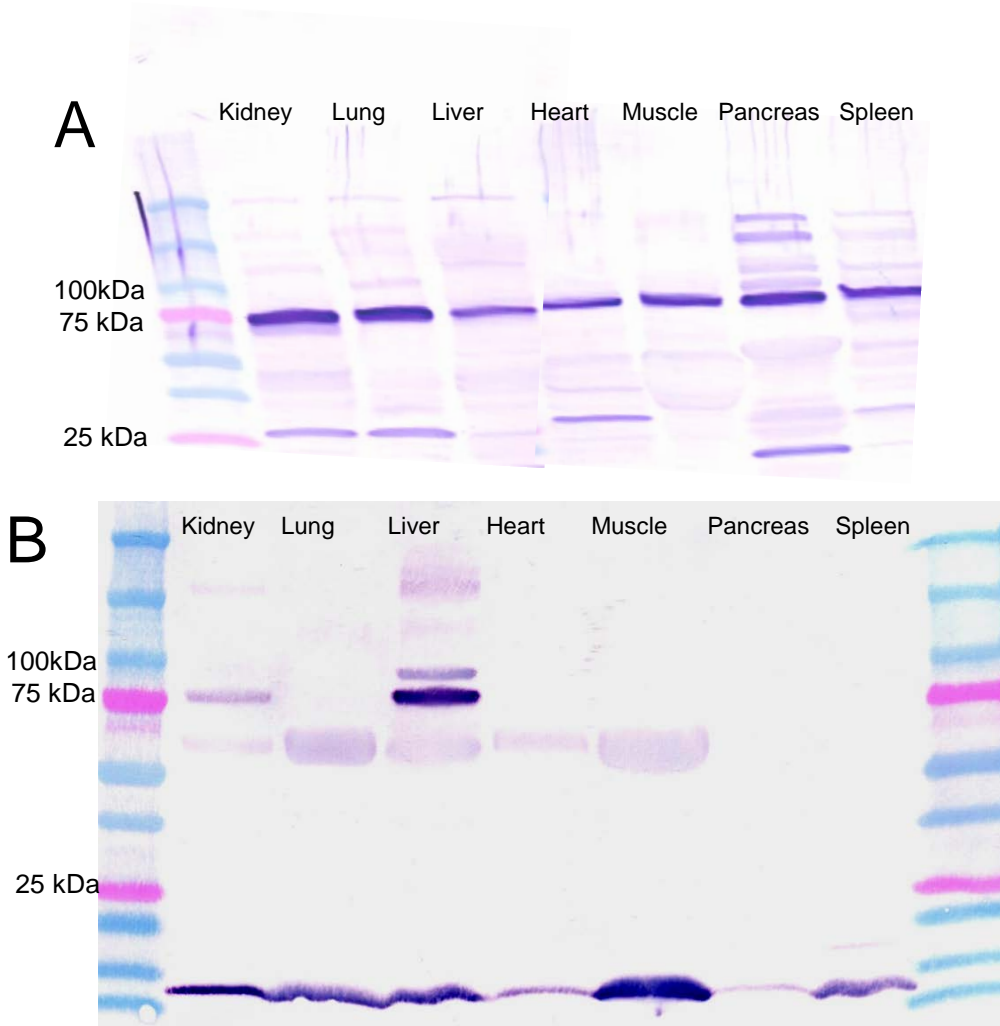


Figure 40. Western blot survey of various mouse and human tissues for ACAD11

Western blot survey of ACAD11 in (A) mouse and (B) human of a 4-15% SDS-PAGE gel. 100 μ g of tissue extract were applied per lane. In mouse, bands at ~75kDa were visualized in all tissues with ACAD11 purified anti-ACAD11-C to reduce background. In human, bands at ~75kDa were visualized in kidney and liver with the same antibody.

4.5.5 Transmission Electron Microscopy

Transmission electron microscopy performed at the Center for Biologic Imaging at the University of Pittsburgh identified lipid droplets in liver and muscle from *Acad10* deficient animals (Figure 41). The formation of lipid droplets was present in *Acad10* knockout liver and

muscle tissues (E and H). Lung tissue was morphologically abnormal with the presence of red blood cells consistent with hemorrhaging (G), while kidney was unremarkable (B and F).

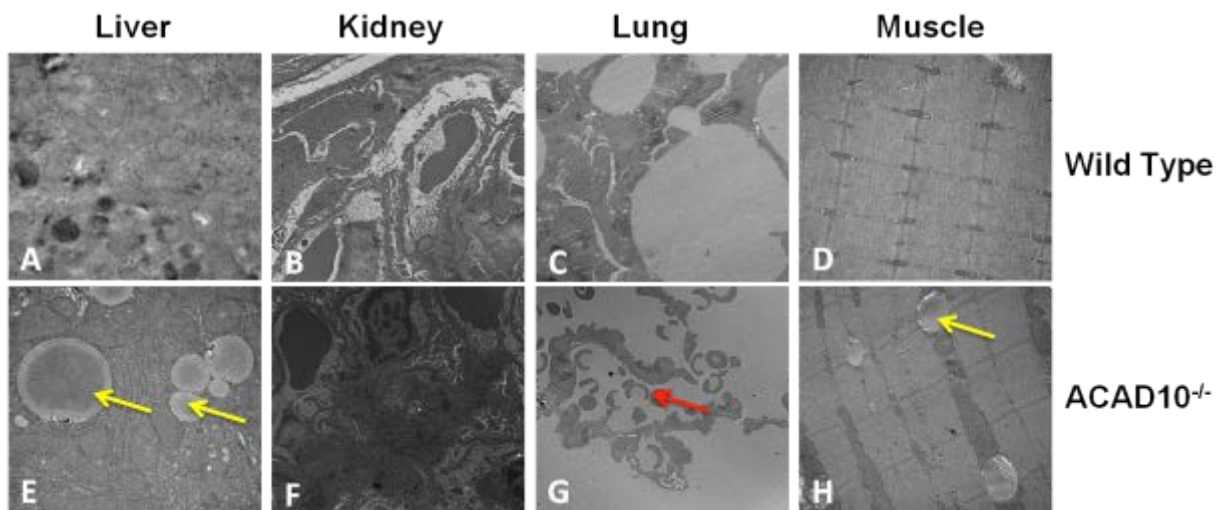


Figure 41. Transmission electron microscopy of control and *Acad10* deficient mouse tissues

Transmission electron microscopy of wild type mouse liver (a), kidney (c), lung (e), and muscle (g) was unremarkable. *Acad10* deficient liver (b) and muscle (h) showed the accumulation of lipid droplets (marked with yellow arrows) and enlarged mitochondria (white arrow). The kidney (d) was unremarkable, and lung (f) showed the presence of red blood cells (red arrow) and abnormal alveolar architecture.

4.5.6 Biochemical Phenotype

All other ACAD deficient mouse models exhibit characteristic patterns of blood and tissue acylcarnitine elevations consistent with the known substrate specificity of the deficient enzyme and reflecting the findings in human patients. Thus, I began biochemical phenotyping of the *Acad10*^{-/-} mice with similar analyses. Blood, urine and tissue extracts were analyzed by the Biochemical Genetics Laboratory at Case Western Reserve University (Dr. C. Hoppel, director) for acylcarnitine profiling. Levels of short, terminal branch chained acylcarnitines in blood and heart tissue in 3.9 and 5.7 month old animals were elevated (Figures 42). However, these patterns were not specific enough to allow identification of the optimum substrate for *ACAD10*.

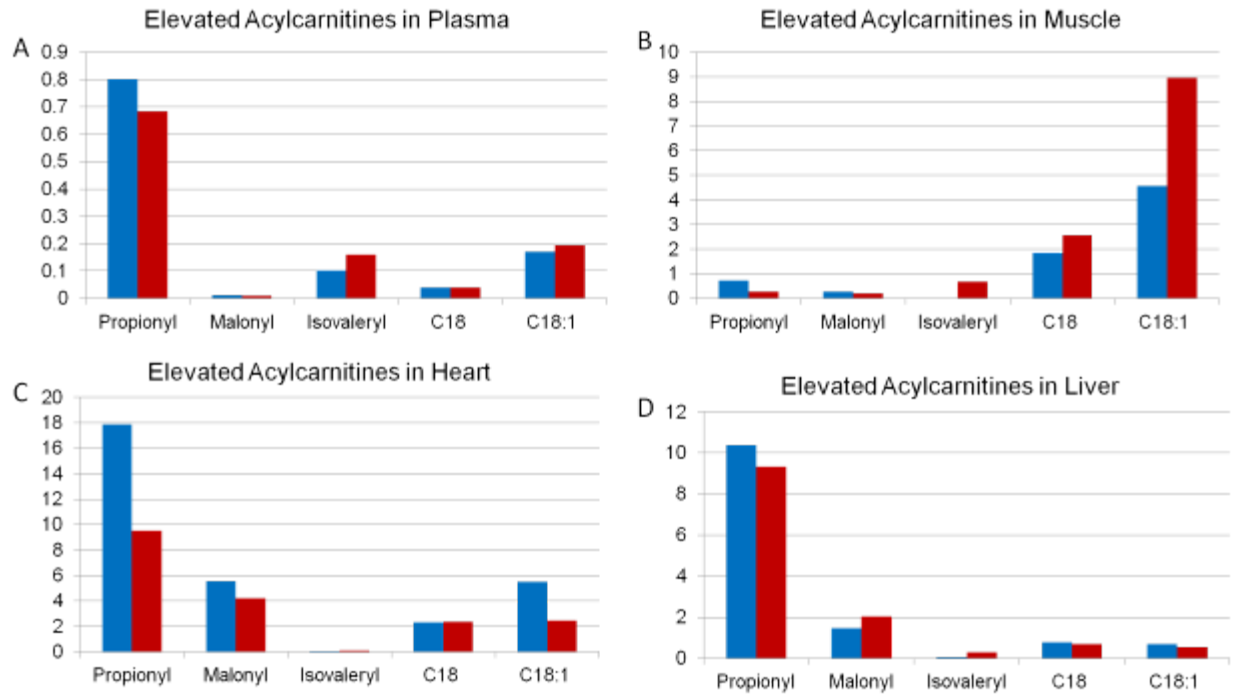


Figure 42. Acylcarnitines in tissue and blood from wild type and deficient mice.

Values of selected acylcarnitine species (average of two determinations) in heart measured at 3.9 and 5.7 months of age.

In light of the association of *ACAD10* variants with type 2 diabetes in Pima Indians, *Acad10* deficient mice were evaluated for glucose control and their glucose-insulin axis. The level of glucose in fasting *Acad10* knockout male mice was consistently slightly increased compared to wild type animals, but the difference was not statistically significant (Figure 43). *Acad10* deficiency females showed slightly elevated blood glucose compared to wild type females, but was not statistically significant.

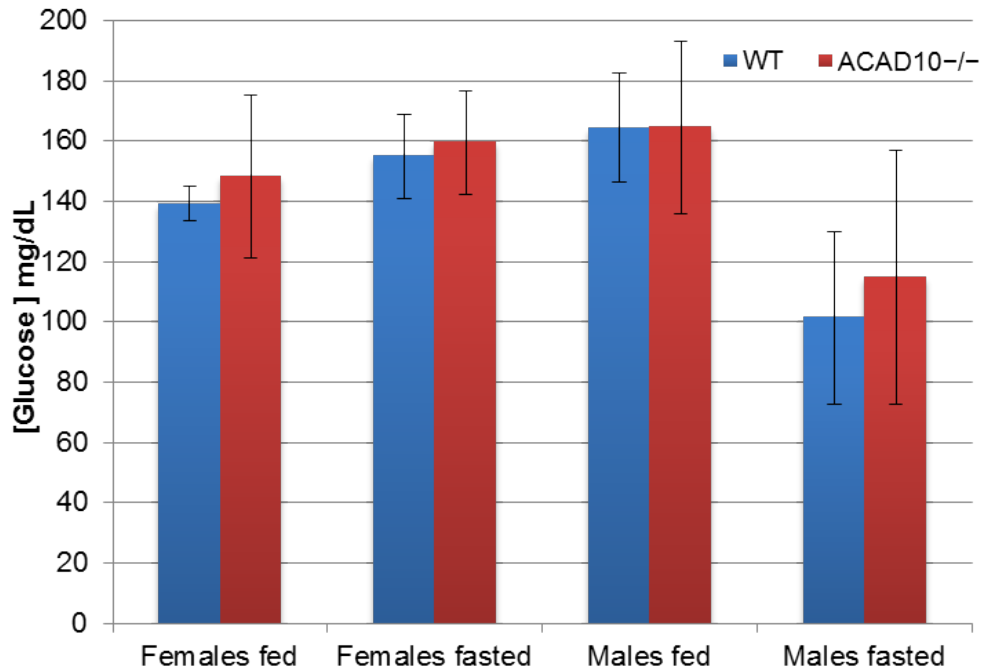


Figure 43. Glucose concentrations in wild type and *Acad10*^{-/-} mouse serum

Animals (8 months old) were fed ad lib and random blood glucose measurements were taken. Food was then removed from cages and blood glucose levels were measured after overnight fasting (~15 hours). The bars show the mean and standard deviation of 3-4 female mice and 5-6 male mice. Blue bars represent wild type animals and red, females. Glucose levels of each genotype and condition were compared to each other. While glucose concentration in fasted *Acad10* deficient male mice was slightly higher than for wild type, the difference was not statistically significant using an unpaired t-test (two-tailed p-values). *ACAD10* deficient females had significantly higher glucose levels than wild type females.

Fed animals of both genotypes showed a physiologically appropriate decrease in insulin concentrations, while in the fasting state there was an increase in insulin concentration in *Acad10* deficient mice compared to wild type (Figures 44 and 45).

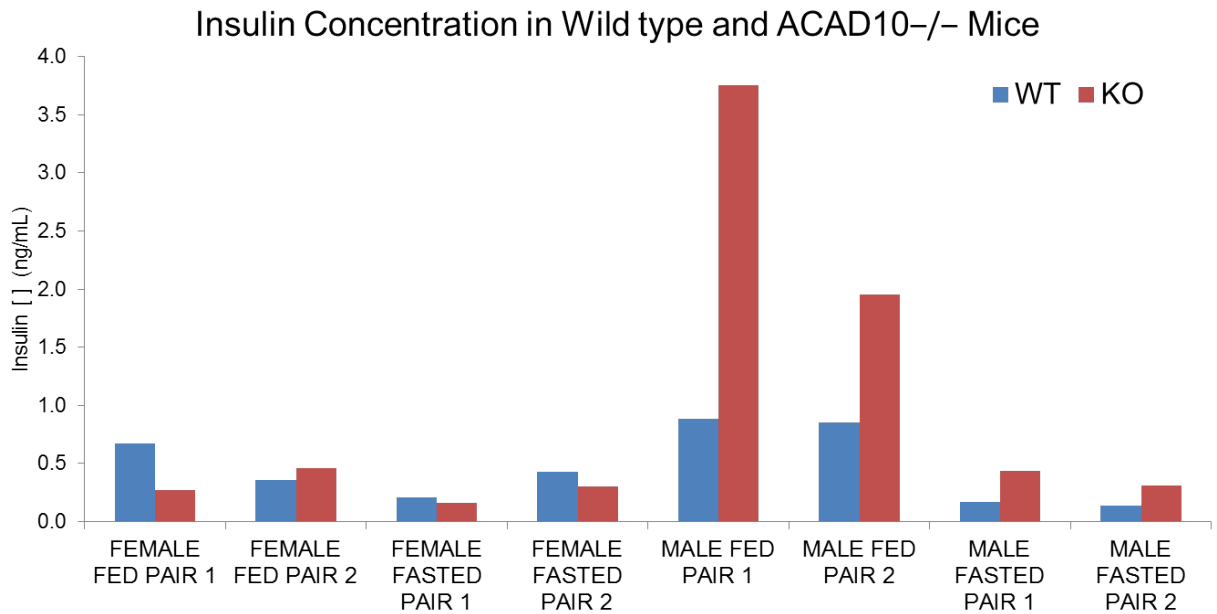


Figure 44. Insulin concentration in *Acad10*^{-/-} and wild type mice

Animals (~4 months old) were fed *ad lib*, or food was removed from cages and blood was drawn after fasting overnight (~15 hours). Blue bars represent wild type animals and red *Acad10*^{-/-}. Insulin levels of each genotype and condition were compared. Insulin concentration in fed and fasted *Acad10* deficient male mice was slightly higher than for wild type.

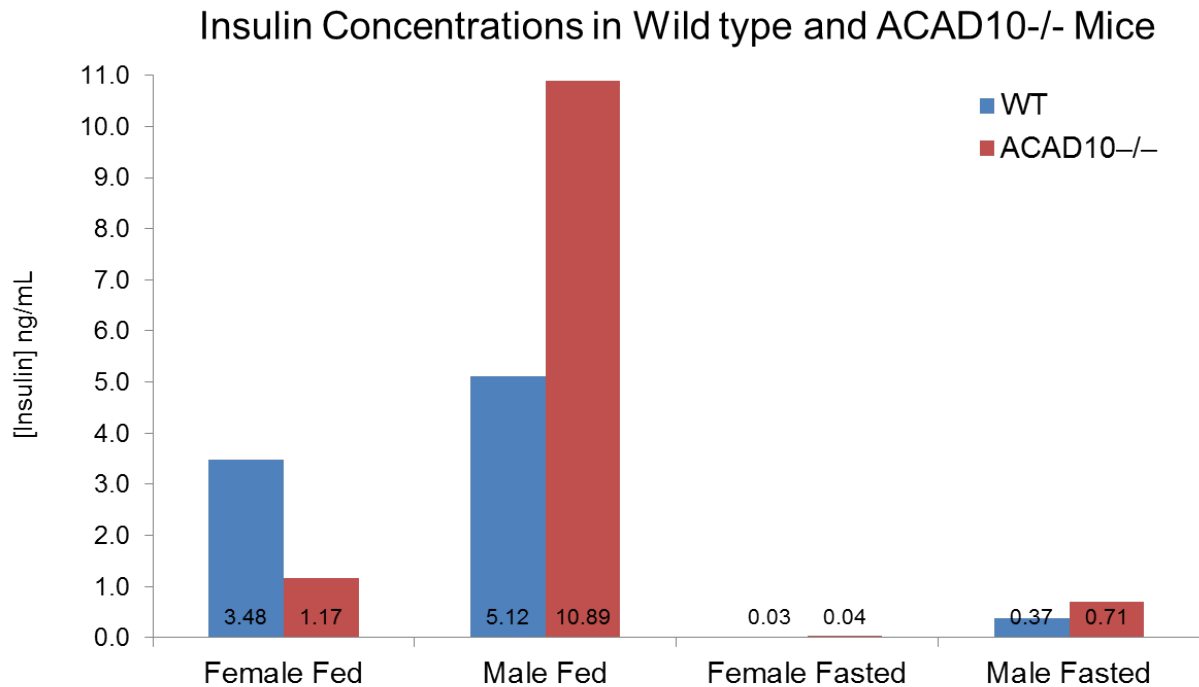


Figure 45. Insulin concentration in *Acad10*^{-/-} and wild type mice

Animals (~1yr old) were fed *ad lib*, or food was removed from cages and blood was drawn after fasting overnight (~15 hours). Blue bars represent wild type animals and red *Acad10*^{-/-}. Insulin levels of each genotype and condition were compared. Insulin concentration in fed and fasted *Acad10* deficient male mice was slightly higher than for wild type.

4.5.7 Intraperitoneal glucose tolerance test (IPGTT)

Given the abnormalities in fasting glucose and insulin, an intraperitoneal glucose tolerance test was performed on the mutant and wild type mice. *Acad10* deficient male mice demonstrated significantly elevated glucose compared to the wild type mice and returned to baseline levels more slowly (Figure 46-48). The *Acad10* deficient mice do not appear to clear glucose as effectively as the controls. The *Acad10* deficient female mice also demonstrated slightly less efficient glucose clearance than wild type females in the early time points of the IPGTT.

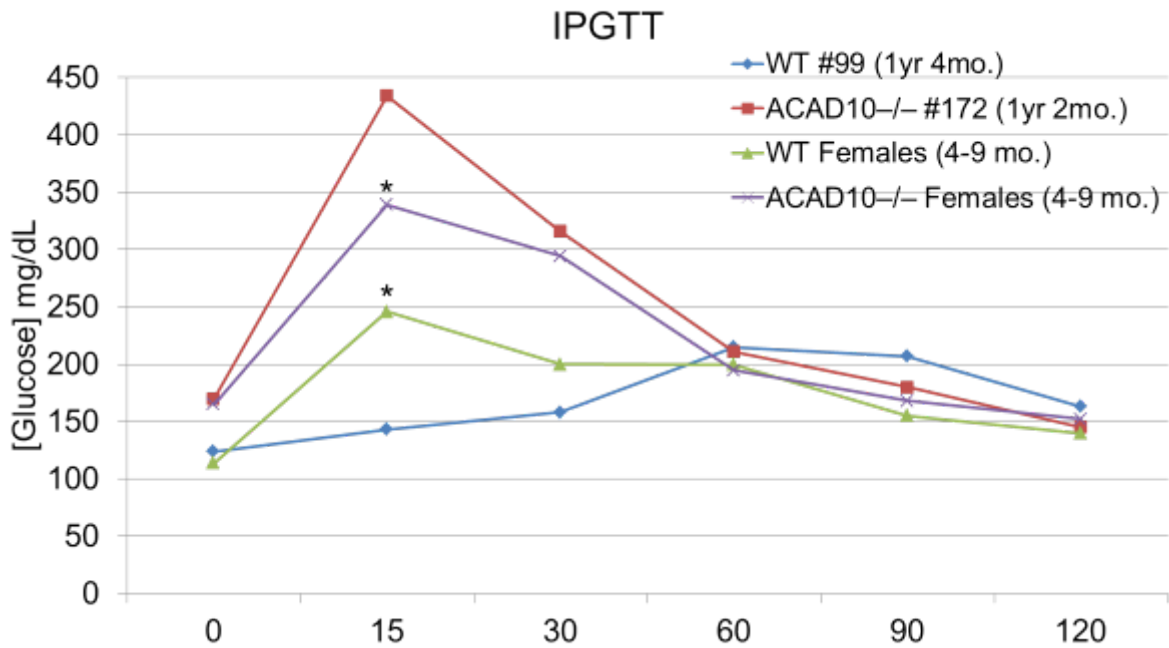


Figure 46. Intraperitoneal glucose tolerance test on *Acad10* deficient and wild type female mice

An IPGTT was performed as described in the methods. Wild type (Liu, Wang et al.) females old and young are shown in blue and green, respectively. *Acad10* deficient ($-/-$) old and young are shown in red and purple, respectively. Young *Acad10* deficient female mice show a statistically significant delay in glucose clearance compared to the young wild type females of the same genetic background (two-tailed p-value=0.0377 and 0.0134, respectively) at time 0 and 15 minutes, indicated by an asterisk.

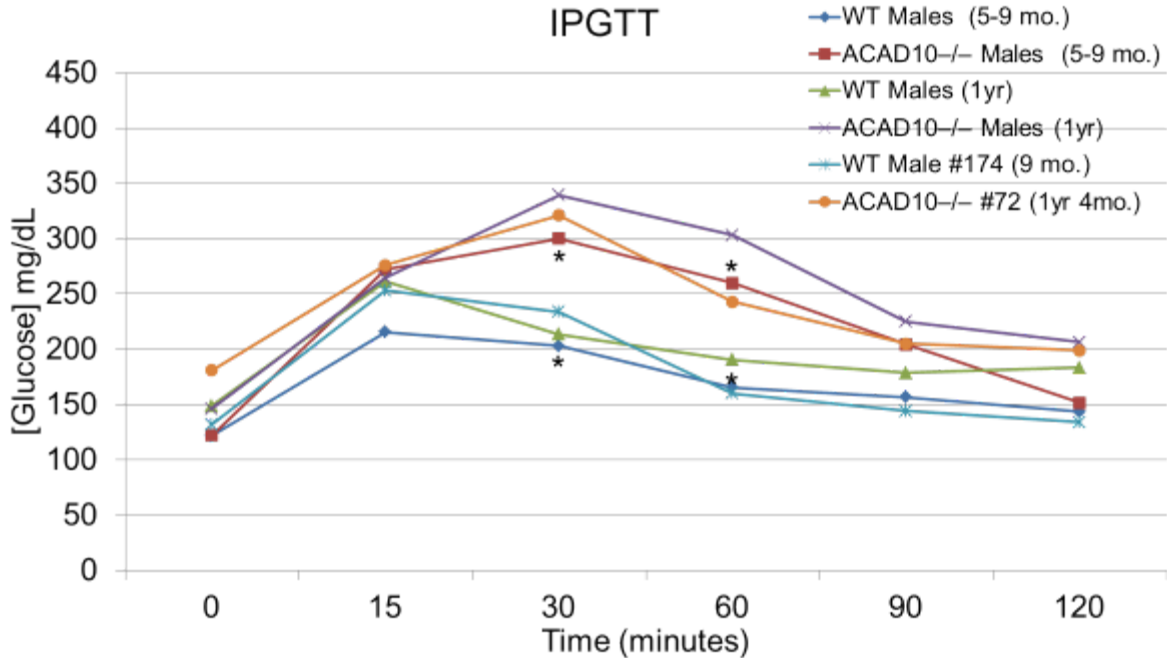


Figure 47. Intraperitoneal glucose tolerance test on *Acad10* deficient and wild type male mice

An IPGTT was performed as described in the methods. Wild type (Liu, Wang et al.) males old and young are shown in green/light blue and dark blue, respectively. *Acad10* deficient ($-/-$) old and young are shown in purple/orange and red, respectively. Young *Acad10* deficient male mice show a statistically significant delay in glucose clearance compared to the young wild type males of the same genetic background (two-tailed p-value=0.0201 and 0.0122, respectively) at time 30 and 60 minutes, indicated by an asterisk.

IPGTT Area under the Curve

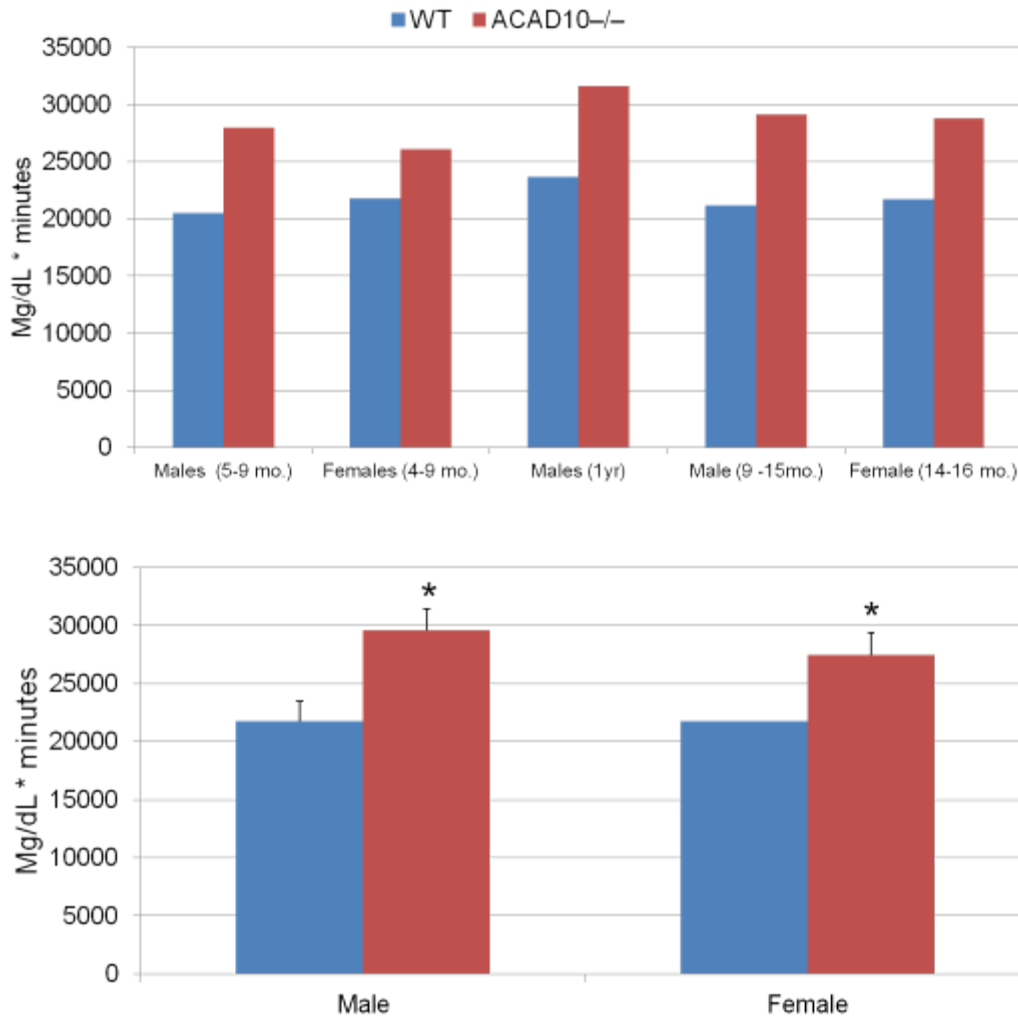


Figure 48. Total blood glucose level in mice during IPGTT as determined by area under the curve

Acad10 deficient (ACAD10^{-/-}) and wild type (WT) old and young are shown in red and blue, respectively. *Acad10* deficient mice show a significantly larger area under the curve compared to wild type in both males and females, and across all age groups.

4.5.8 Inflammation

Inflammation has been shown to play a significant role in the development of insulin resistant diabetes. Recurrent rhabdomyolysis is a common finding in human patients with ACAD deficiencies and other disorders of energy metabolism; therefore, we examined serum creatine

kinase (CPK) levels in *Acad10* deficient animals. Fed levels of CPK were normal in mutant animals. However, adult male *Acad10* deficient mice exhibited a dramatic increase in the CK levels with fasting (Figure 49).

To examine the inflammatory status in *Acad10* knockout mice, a highly sensitive ELISA assay was used to measure CRP (Figure 50). No significant difference was found between mutant and wild type animals. A broad panel of cytokines was normal or even reduced in *Acad10*^{-/-} male and female animals (Figure 51). *Acad10*^{-/-} male mice also showed significantly reduced cytokine levels (Figure 52). Additionally, quantification of C-reactive protein (CRP) in serum provides information on diagnosis, prognosis, and monitoring of disease (Eckersal 2000).

In total, these results suggest that the insulin resistance seen in *Acad10*^{-/-} animals is unrelated to an inflammatory process.

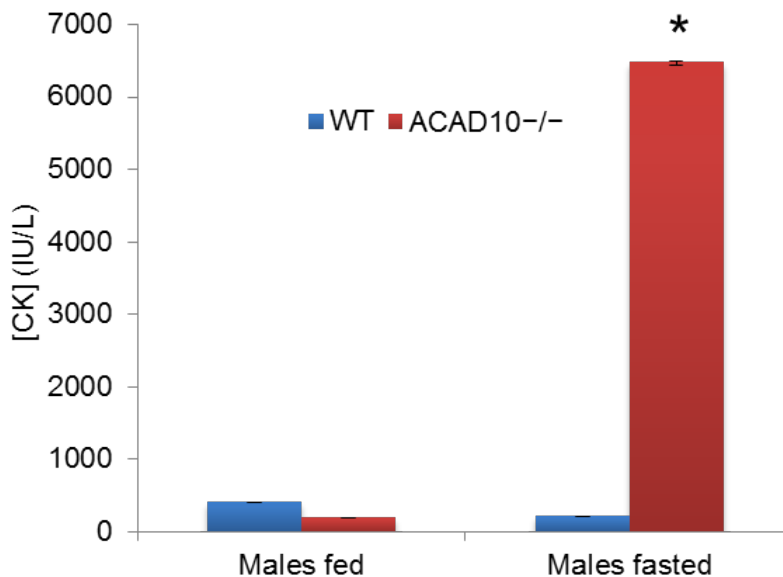


Figure 49. Blood CPK level in fed and fasted *Acad10*^{-/-} and wild type mice

Creatine kinase (CK) concentration in fasting *Acad10* deficient male mice shows a statistically significant increase (two-tailed p-value=0.0135) compared with other fed and fasted animals at 8 months of age.

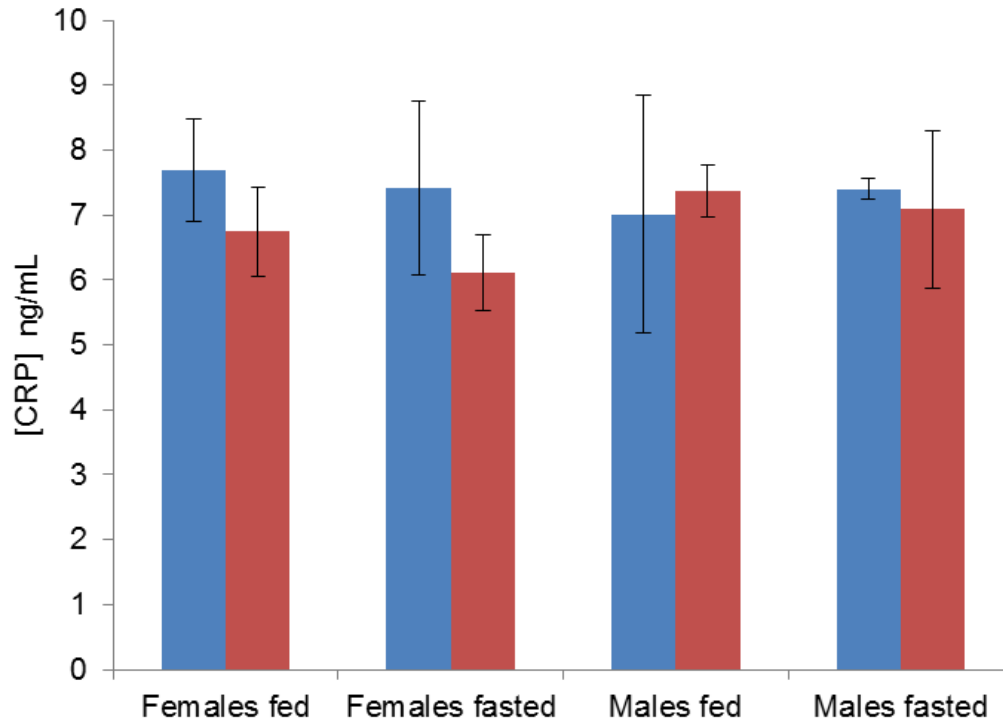


Figure 50. C-reactive protein concentration in wild type and *Acad10* deficient mice

Animals (~8 months old) were fed ad lib or food was removed from cages and blood was drawn after fasting overnight (~15 hours). The bars show the mean and standard deviation of 3 female mice and 3 male mice. Blue bars represent wild type animals and red *Acad10*^{-/-} *-/-*. CRP levels of each genotype and condition were compared to each other. Values between groups are not statistically significant, indicating lack of a generalized inflammation or infectious process in the *Acad10* deficient animals. Each group had 24 animals and the assay was performed in triplicate.

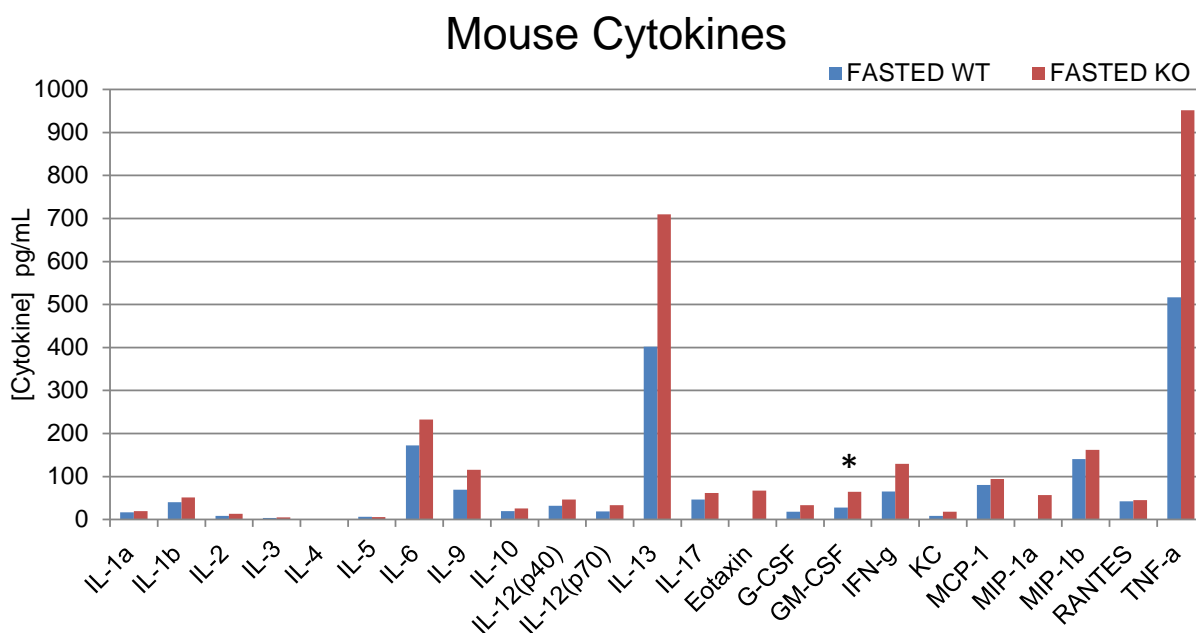
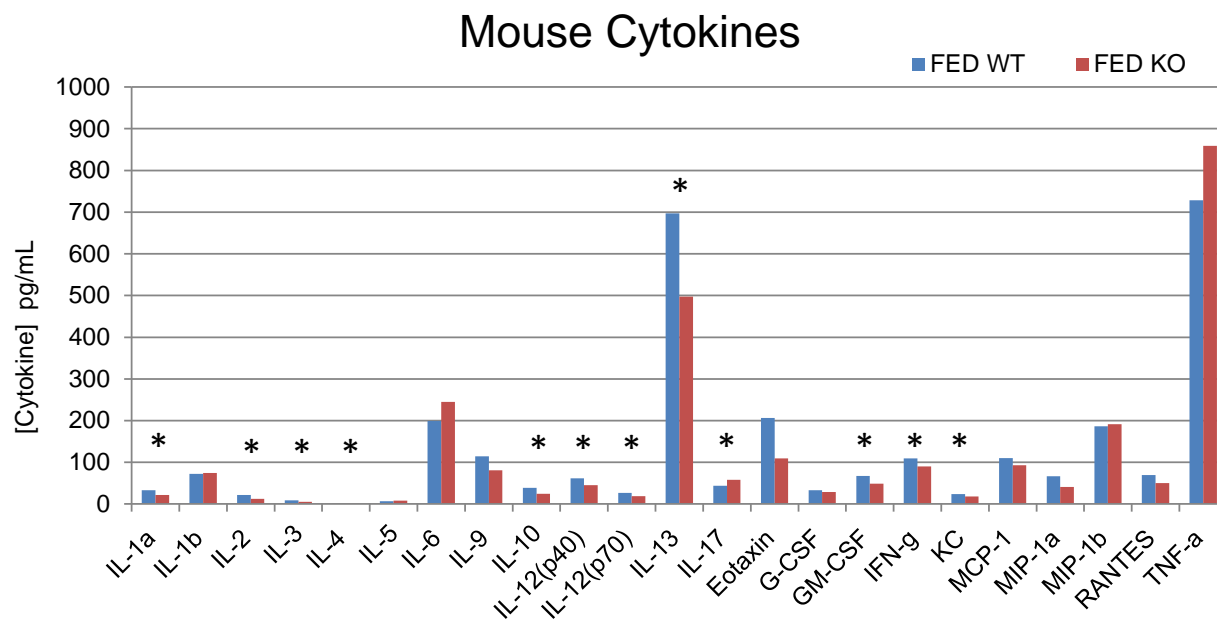


Figure 51. Cytokine levels in blood from wild type and deficient mice.

Male and female animals were fed ad lib or food was removed from cages and blood was drawn after overnight fasting (~15 hours). The bars show the mean and standard deviation of 3-4 female mice and 7 male mice for each group. Blue bars represent wild type animals and red *Acad10*^{-/-}. Cytokine levels of each genotype and condition were compared to each other. Values between groups with an asterisk are statistically significant.

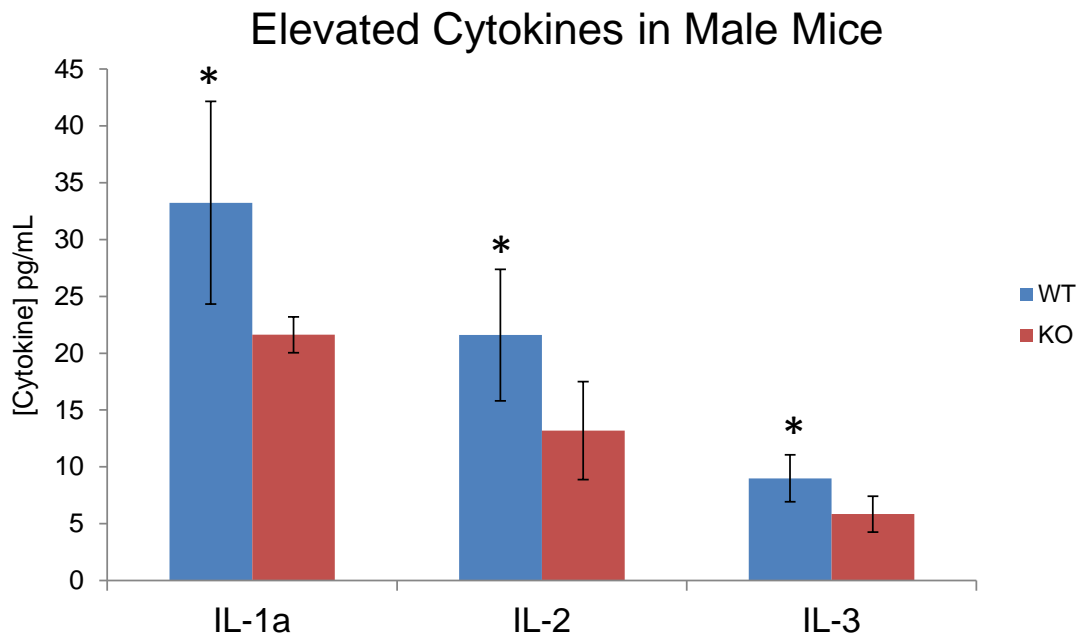


Figure 52. Cytokine levels in blood from wild type and mutant male mice

Male animals were fed ad lib and blood was drawn. The bars show the mean and standard deviation of 7 male mice for each group. Blue bars represent wild type animals and red *Acad10*^{-/-}. Cytokine levels of each genotype were compared to each other. Values between groups with an asterisk are statistically significant, indicating normal or reduced cytokine levels in the *Acad10* deficient animals.

4.5.9 Electron Transport Chain complexes (Liu, Wang et al.)

ETC abnormalities have previously been described in humans with obesity and T2DM (Goodpaster 2013). To examine ETC function in *Acad10* deficient mice, blue native gel electrophoresis (BNGE) was performed on mitochondrial extracts from heart, liver, muscle, and brain tissue (Figure 53). ETC complex I activity was found to be elevated in liver, muscle, and brain from deficient animals, suggestive of mitochondrial proliferation. Complex V activity was elevated in heart, liver and muscle, but decreased in brain, suggesting the possibility of as yet unrecognized neurologic problems.

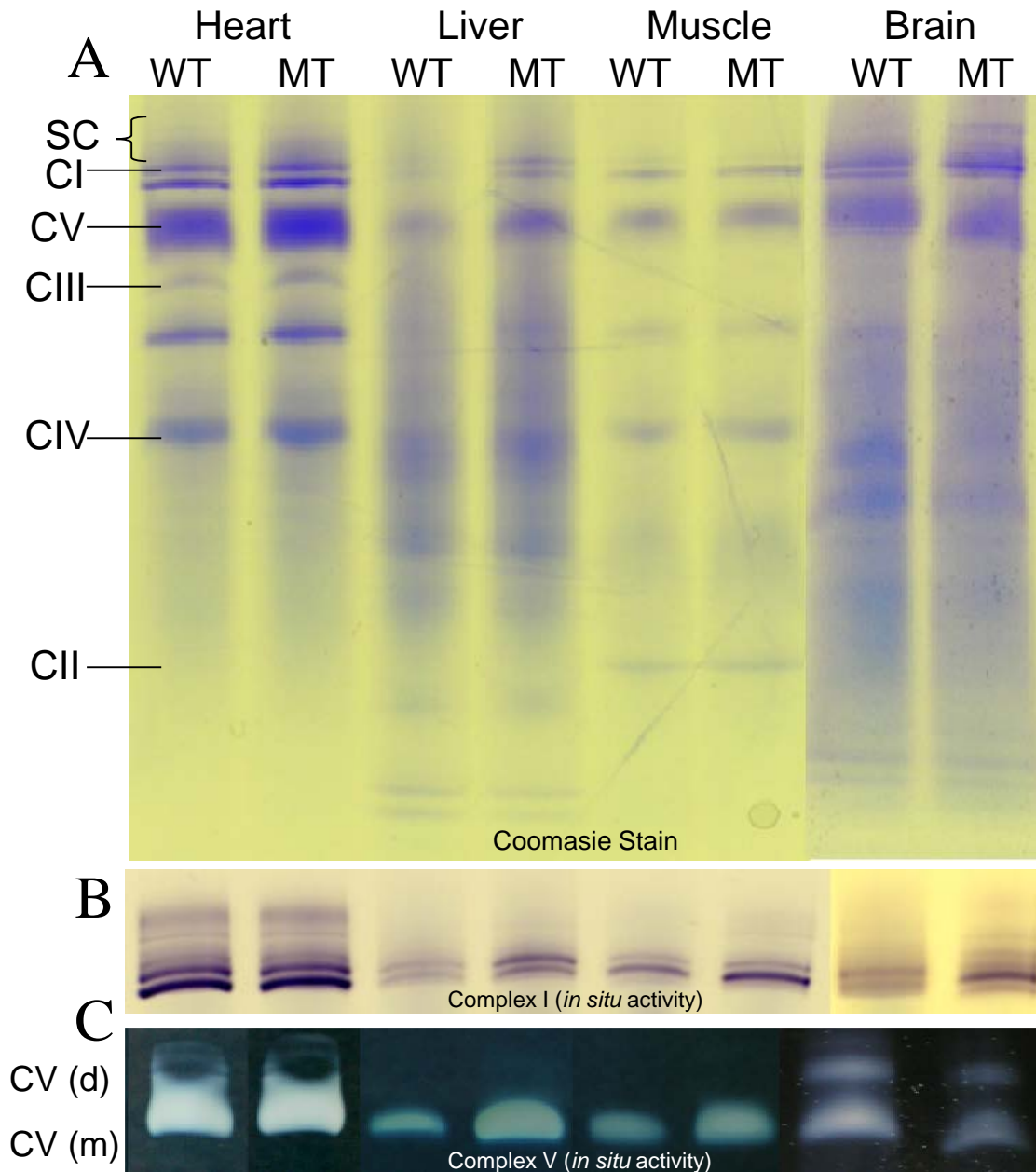


Figure 53. Characterization of electron transport chain complexes by blue native gel electrophoresis

(A) Blue native gel electrophoresis of heart, liver, muscle, and brain from mutant (MT) and wild type (Liu, Wang et al.). (B) Complex I (CI) *in situ* gel activity. Enzymatic activity staining was detected as isolated Complex I as well as the bands that represent higher order supercomplexes (SC). (C) Enzymatic Complex V (CV) *in situ* gel activity. "d" and "m" denote the active dimer and monomer forms of CV, respectively. All lanes contain ~0.06 μg of tissue extract. (CII, CIII, and CIV are respiratory chain complexes II, III, and IV, respectively).

4.5.10 Quantitative PCR (qPCR)

An insulin/T2D regulatory panel of genes was measured for expression in fat, liver, muscle, and brain. Analysis of fat tissues showed significant down regulation in expression of the genes Hnf1b, Glp1r, Hnf4a, Fbp1, and Aqp2 (Figure 54).

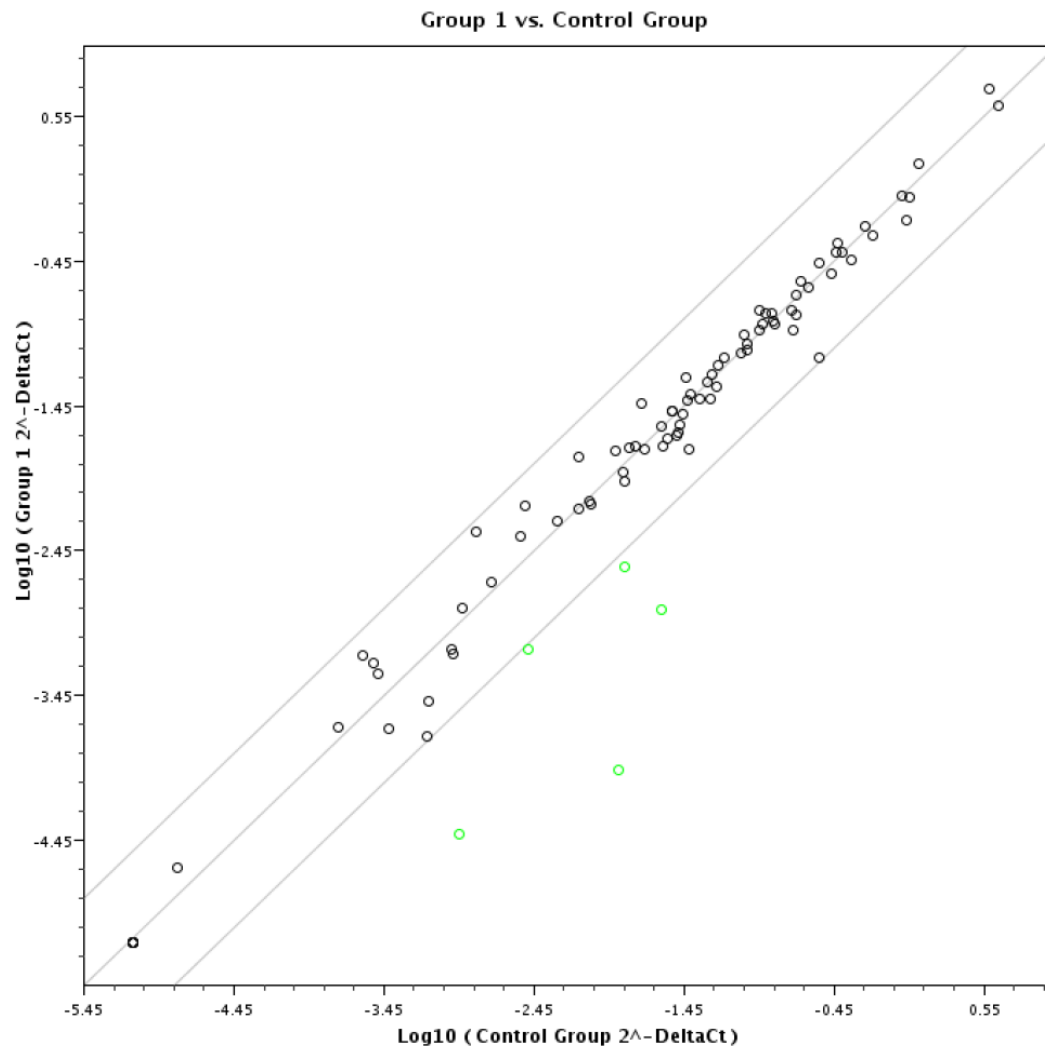


Figure 54. Quantitative PCR in *Acad10* deficient mouse fat tissue

This figure shows data points representing each gene's expression. Expression is relatively normal reasonably detected in all samples, except for the 5 highlighted in green, which are expressed at lower levels as described in the text.

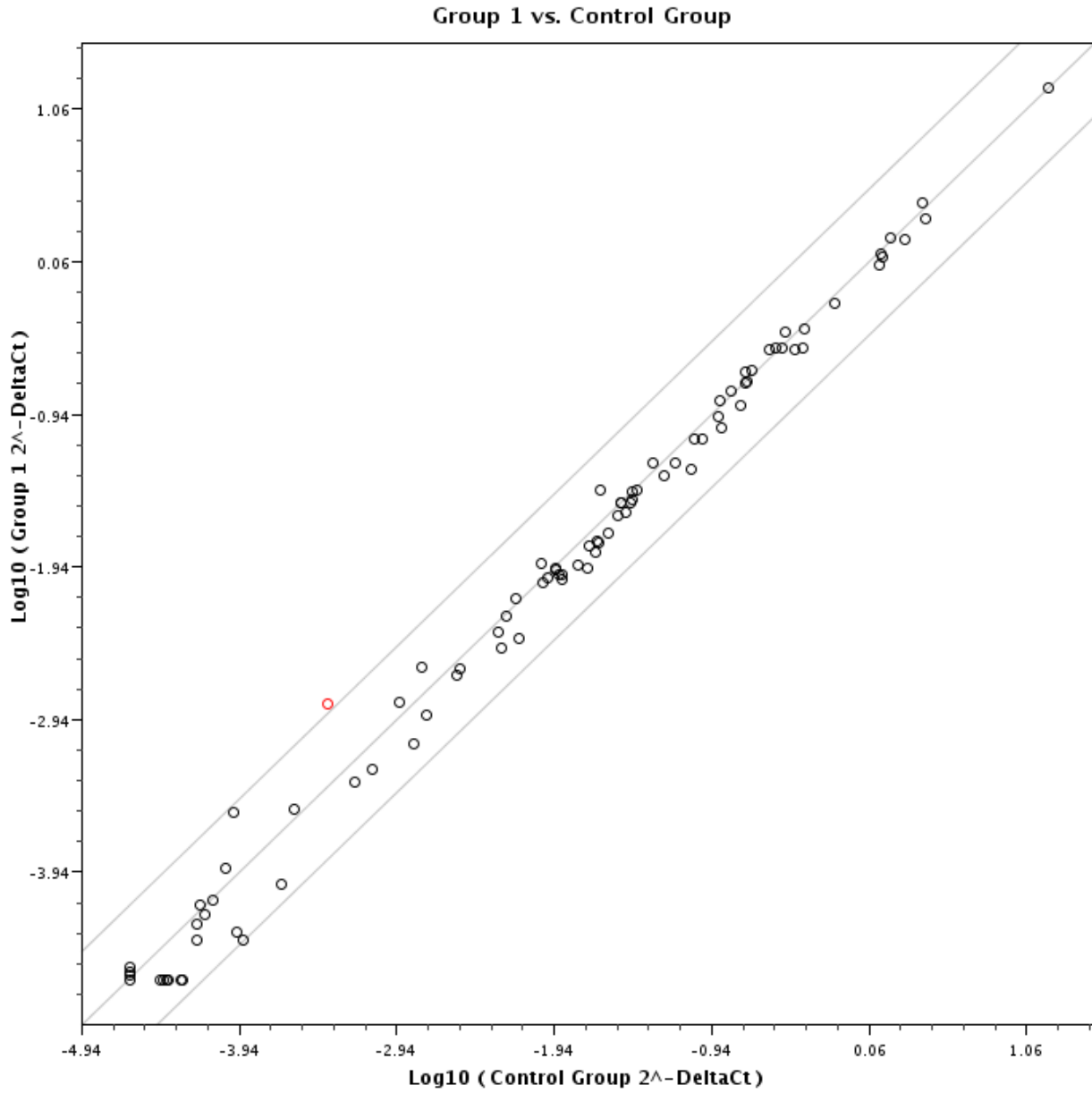


Figure 55. Quantitative PCR in Acad10 deficient mouse muscle tissue

This figure shows data points representing each gene's expression. Expression is relatively normal for all samples, except for the 1 highlighted in red, which is expressed at a higher level.

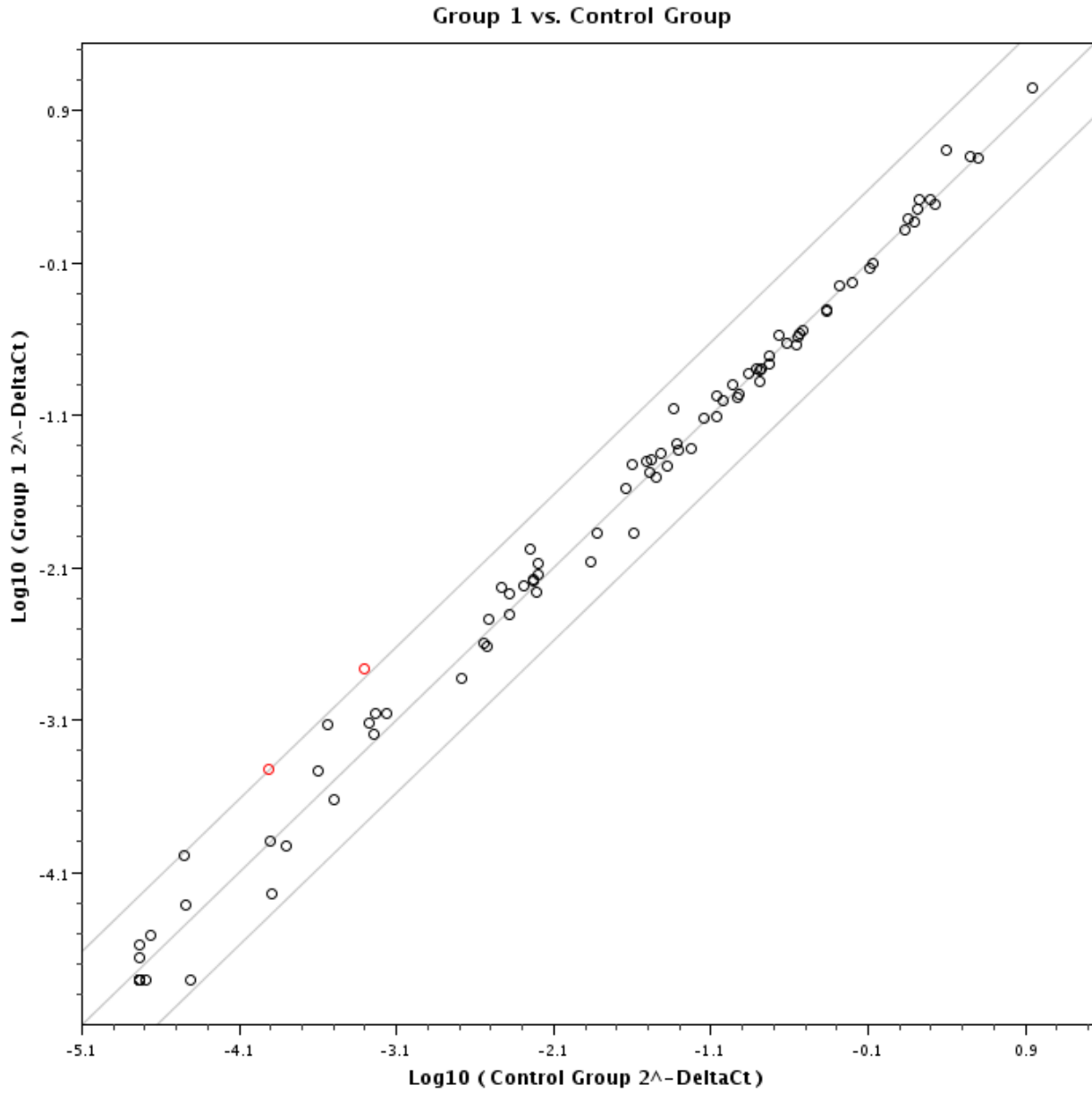


Figure 56. Quantitative PCR in Acad10 deficient mouse liver tissue

This figure shows data points representing each gene's expression. Expression is essentially normal for all samples, except for the 2 highlighted in red, which are expressed at higher levels.

Table 5. Fold change in gene expression in ACAD10 deficient fat tissue compared to control

Gene Expression in ACAD10 ^{-/-} vs Control				
Plate Position	Tissue	Gene Symbol	Fold Regulation	Comments
A07	Fat	Aqp2	-4.4537	Down
B05	Fat	Fbp1	-5.1396	Down
C01	Fat	Glpr1	-29.0071	Down
C05	Fat	Hnf1b	-118.3296	Down
C06	Fat	Hnf4a	-17.9802	Down
G04	Muscle	Tnf	2.54	Up
F05	Liver	Serpine1	3.45	Up
D03	Liver	Il6	3.07	Up

4.6 NEUROBEHAVIORAL ANALYSES

4.6.1 Open Field Testing

Acad10 shows significant expression in brain, but deficient animals showed no overt neurologic deficits. To better evaluate for subtle deficits, neurobehavioral testing was performed on mutant wild type mice. Open field testing parameters included (1) ambulatory distance, (2) velocity, (3) real vertical time, (4) real stereotypic time, (5) distance per trip, (6) real resting time, (7) real ambulatory time, (8) ambulatory counts, (9) stereotypic counts, and (10) vertical counts.

Analysis was performed by examining two different zones designated Zone 0 (box perimeter) and Zone 1 (box center) (Figure 57).

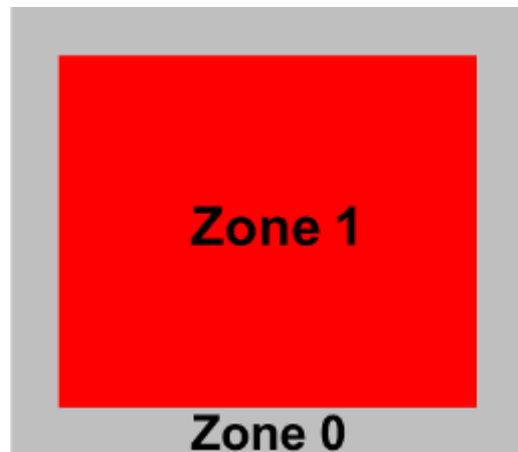


Figure 57. Open field zones in testing chamber.

Zone 0 is the outer perimeter of the testing chamber, where animals are expected to spend more time because they feel more protected by the surrounding walls. Zone 1 is considered a more dangerous zone because upon entering Zone 1 the animal is exposed on all sides.

Overall, female *Acad10* deficient animals demonstrate less activity in the center area of the open field testing box than wild type females suggesting higher anxiety. The mutants also demonstrated smaller measures of movement, consistent with animal hypoactivity. Reduced rearing (an act of exposing the underside of the body) is another indicator of anxiety and female *Acad10* deficient mice spent significant less time performing this activity than wild type females.

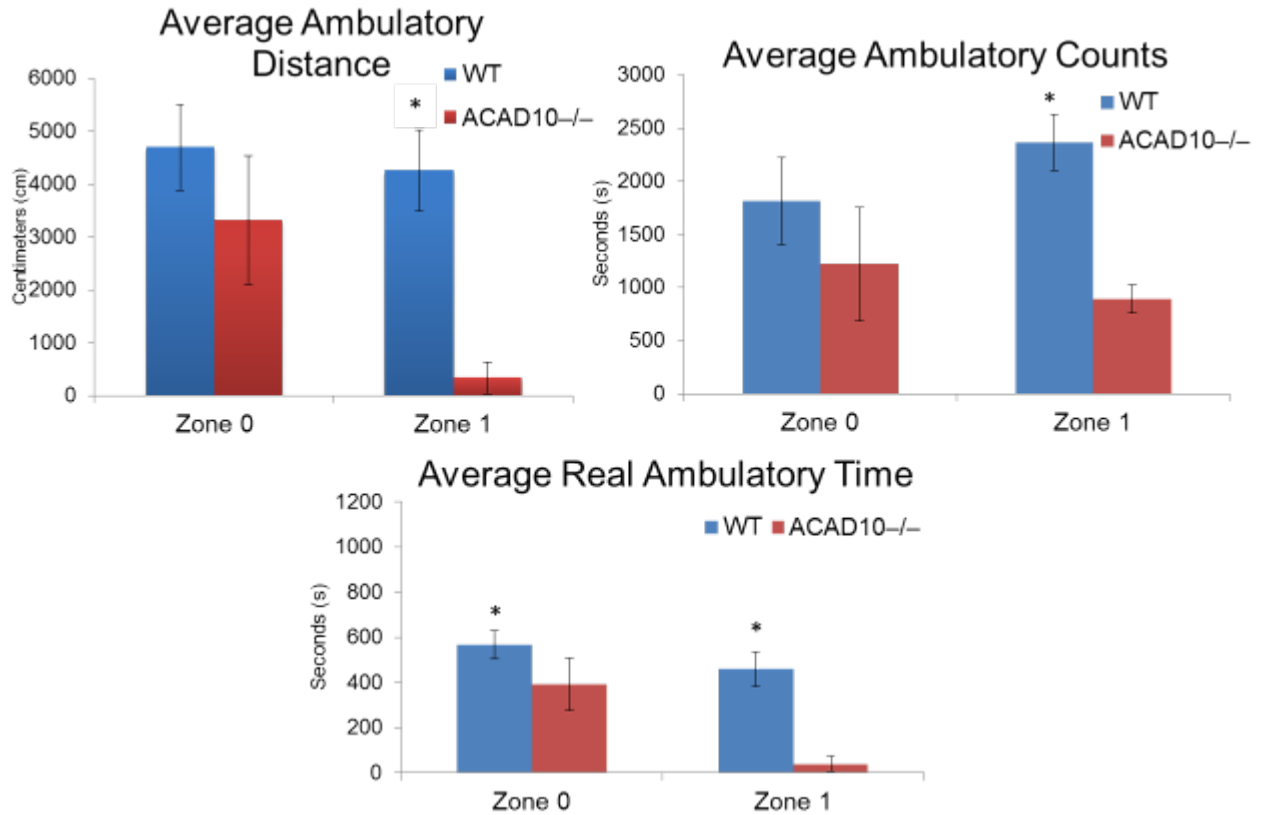


Figure 58. Open field ambulatory measures in female mice

Time (in seconds) or centimeters (cm) spent or traveled in each activity is depicted with wild type animals in blue and ACAD10^{-/-} deficient in red. The *Acad10* deficient female mice showed a statistically significant decrease in movement measures in Zone 1 (two-tailed p-value=0.0004, p-value= 0.0002, and 0.0003, respectively), indicated by an asterisk, as compared to wild type control mice of the same background. The *Acad10* deficient female mice show statistically significant decrease in movement measures in Zone 0 across time (two-tailed p-value=0.0230), indicated by an asterisk, as compared to wild type control mice of the same background.

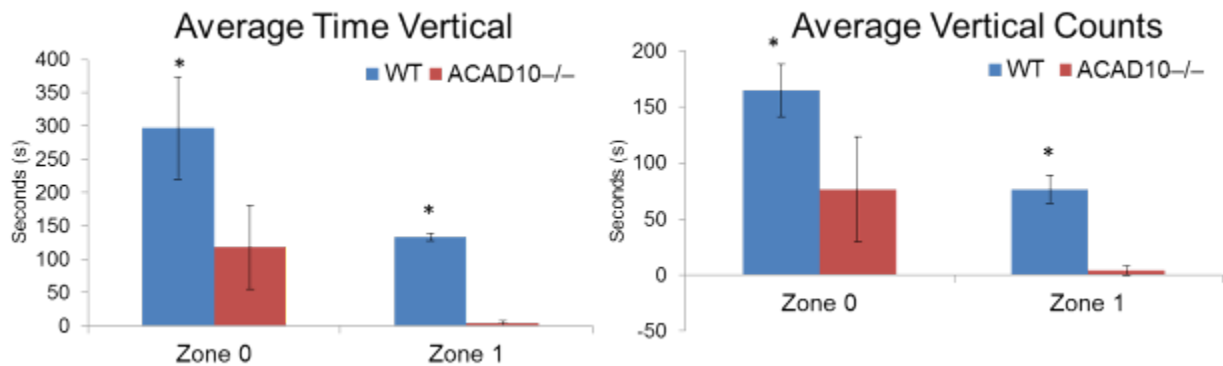


Figure 59. Open field vertical measures in female mice

Time (in seconds) spent vertical is depicted with wild type (Liu, Wang et al.) animals in blue and *Acad10*^{-/-} deficient in red. The *Acad10* deficient female mice show a statistically significant decrease in rearing in Zones 0 and

1 (two-tailed p-value= 0.0226, 0.0001 and p-value= 0.0075, <0.0001, respectively), indicated by an asterisk, as compared to wild type control mice of the same background.

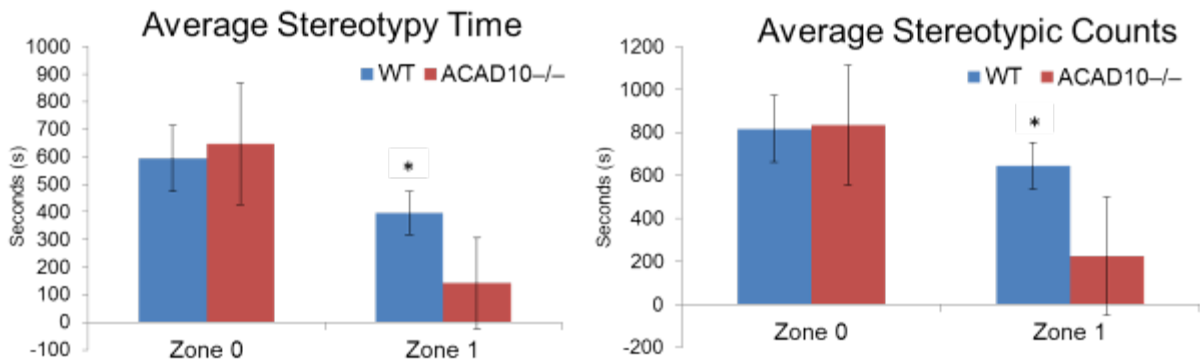


Figure 60. Open field measures of stereotypic movements in female mice

Time (in seconds) spent in each activity is depicted with wild type (Liu, Wang et al.) animals in blue and *Acad10*^{-/-} deficient in red. The *Acad10* deficient female mice show a statistically significant decrease in stereotypy in Zone 1 (two-tailed p-value= 0.0176, 0.0156, respectively), indicated by an asterisk, as compared to wild type control mice of the same background. Stereotypic behaviors are fine movements such as scratching and grooming. The animal is not moving to cover distance in the chamber, but it is breaking the infrared beams of the chamber, therefore is not motionless. Stereotypy in mice is an indicator the animal is relaxed and feels comfortable in its environment.

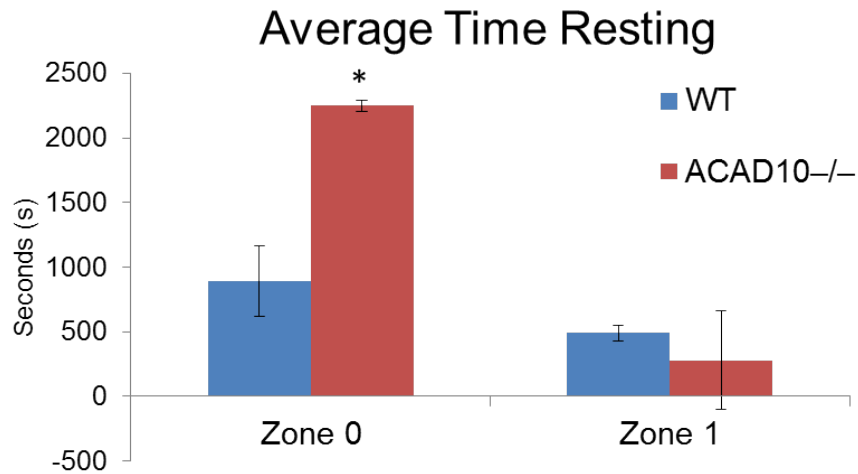


Figure 61. Open filed resting measures in female mice

Time (in seconds) spent resting in each zone is depicted with wild type (Liu, Wang et al.) animals in blue and *Acad10*^{-/-} deficient in red. The *Acad10* deficient female mice show a statistically significant increase in resting time in Zone 0 (two-tailed p-value=0.0002), indicated by an asterisk, as compared to wild type control mice of the same background.

4.6.2 Digigait Testing

DigiGait testing identified subtle changes in gait dynamics and posture in the *Acad10* deficient mouse model compared to controls. The DigiGait testing proved more sensitive than other available tests and provided detailed information on specific gait parameters. *Acad10* deficient mice showed a statistically significant decrease in percentage of brake stride and brake stance movements, while there was a statistically significant increase in the percentage of propel stride and propel stance movements in hind limbs. Correlation of these two parameters suggests that the deficient animals spend less time braking and more time in propulsion to generate movement forward, characteristic of several different neuropathologic conditions (Figure 62). The results in Figure 63 indicate that deficient animals spend more time and effort getting into motion than stopping or slowing down motion (Mouse Specifics 2010).

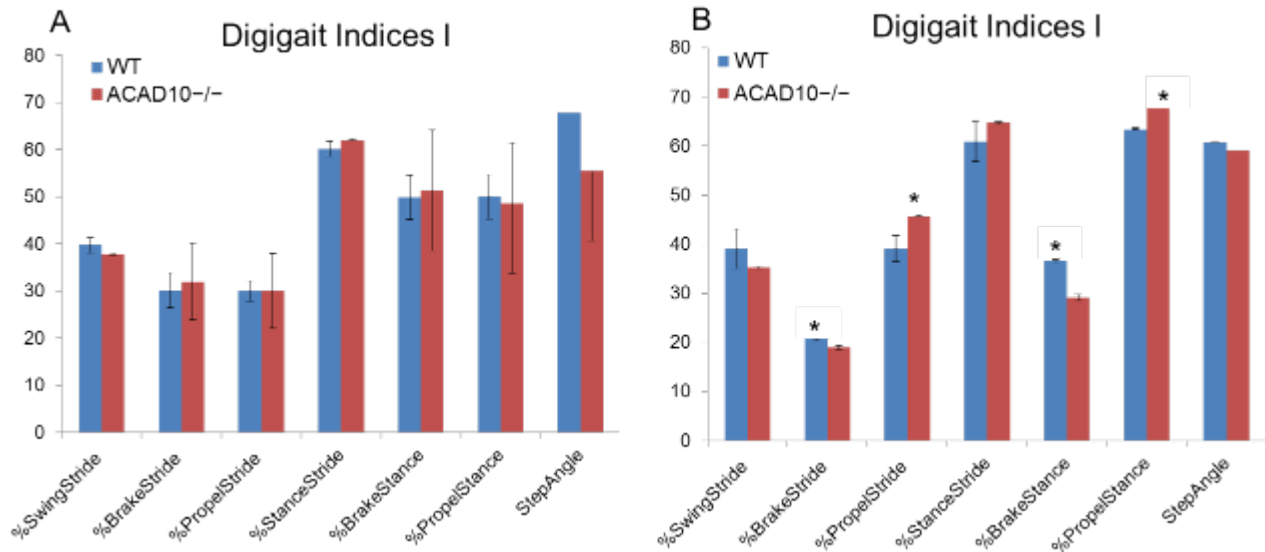


Figure 62. Digigait indices I

Percentage of each activity in (A) Forelimbs and (B) Hindlimbs is depicted with wild type (Liu, Wang et al.) animals in blue and *Acad10*^{-/-} deficient in red. The *Acad10* deficient mice show a statistically significant decrease

in %BrakeStride ($p=0.0116$) and %BrakeStance($p=0.0001$). The *Acad10* deficient mice show a statistically significant increase in %PropelStride ($p=0.0037$) and %PropelStance ($p=0.0001$).

Decreased swing and braking strides (Figure 64) confirms that the deficient animals spend less time braking and more time in propulsion to generate movement forward. *Acad10*^{-/-} deficient animals also demonstrate a decrease in paw area at peak stance in forelimbs and an increase in paw area at peak stance in hind limbs, a relative non-specific finding with multiple interpretations.

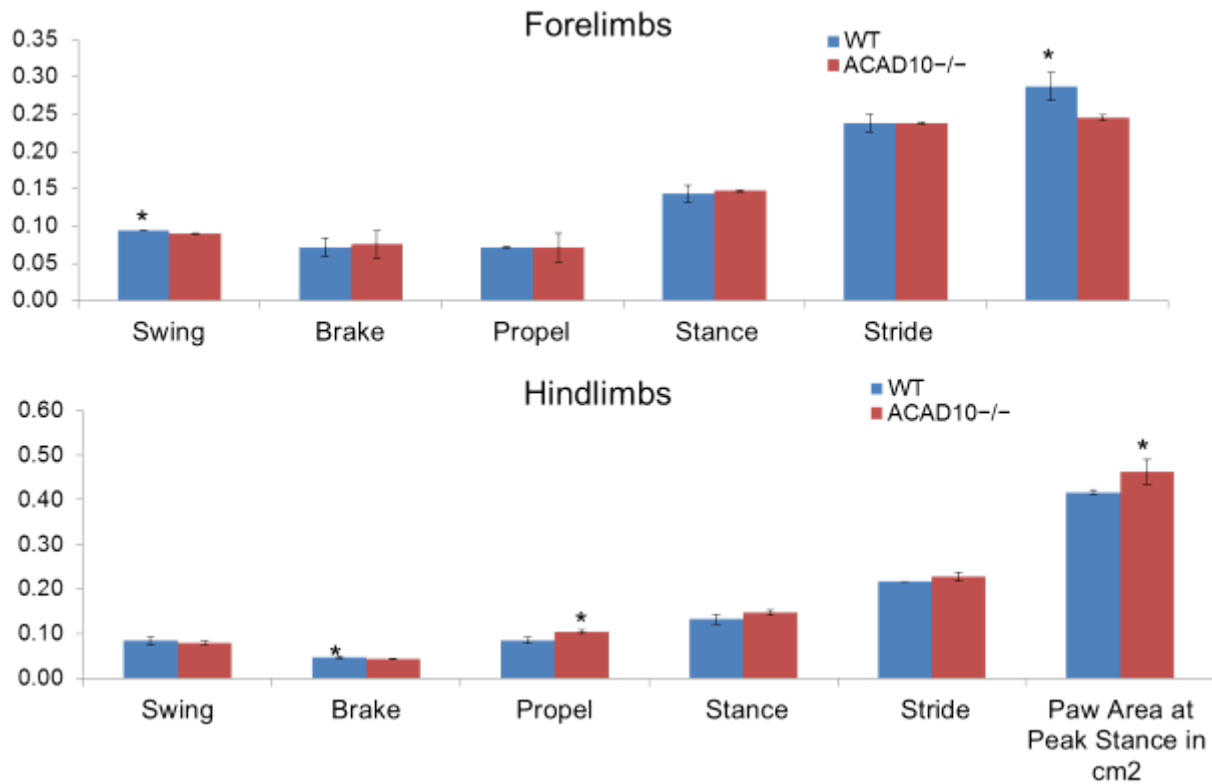


Figure 63. Digigait indices II

Measure of each activity in forelimbs and hindlimbs is depicted with wild type (Liu, Wang et al.) animals in blue and *Acad10*^{-/-} deficient in red. The *Acad10* deficient mice show a statistically significant decrease in swing ($p < 0.0001$) and paw area at peak stance in cm² ($p = 0.0065$) in the forelimbs. There is also a corresponding decrease in brake ($p = 0.0269$) and paw area at peak stance in cm² ($p = 0.0416$).

Decreased stride length variation (Figure 64) in *Acad10*^{-/-} deficient animals implies that they have good balance and stability. Thus, there does not appear to be significant motor impairment in the mutant mice.

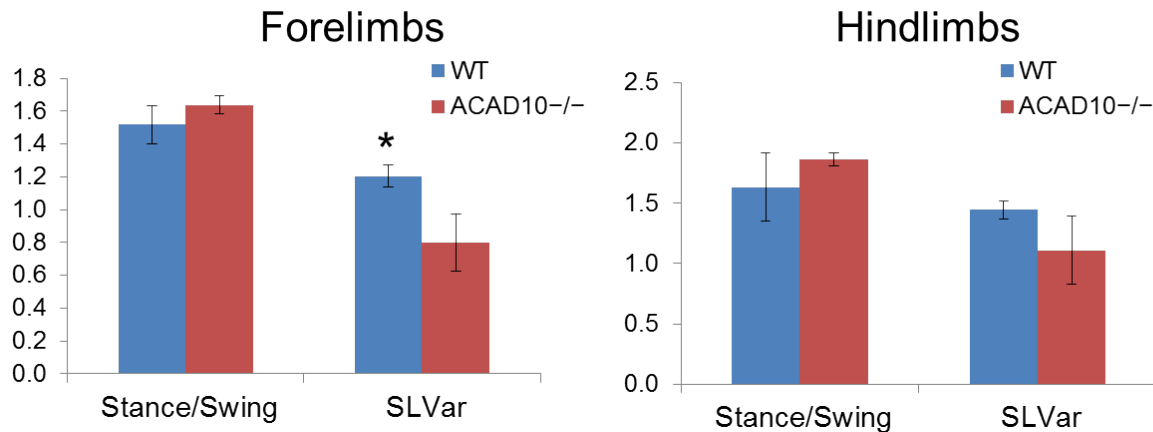


Figure 64. Digigait indices III

Measures of each activity in forelimbs and hindlimbs are depicted with wild type (Liu, Wang et al.) animals in blue and *Acad10*^{-/-} deficient in red. The *Acad10* deficient mice show a statistically significant decrease in stride length variation (SLVar) using unpaired t-test (two-tailed p-value = 0.0132).

Decreased stride length covariance (Figure 65) in *Acad10*^{-/-} deficient mice confirms the lack of variation and motor impairment. The measure MAX dA/dT is the maximal rate of change of paw area in contact with the treadmill belt during the braking phase (Mouse Specifics 2010). This parameter measures how quickly the limb is loaded with the weight of the animal to a stance position, and also how quickly the animal is capable of decelerating (Mouse Specifics 2010). MAX dA/dT is related to general muscle strength of the animal. The *Acad10*^{-/-} deficient animals show a statistically significant decrease in MAX dA/dT suggesting the presence of some muscle weakness (Figure 65). Figure 65 also shows additional parameters that were measured.

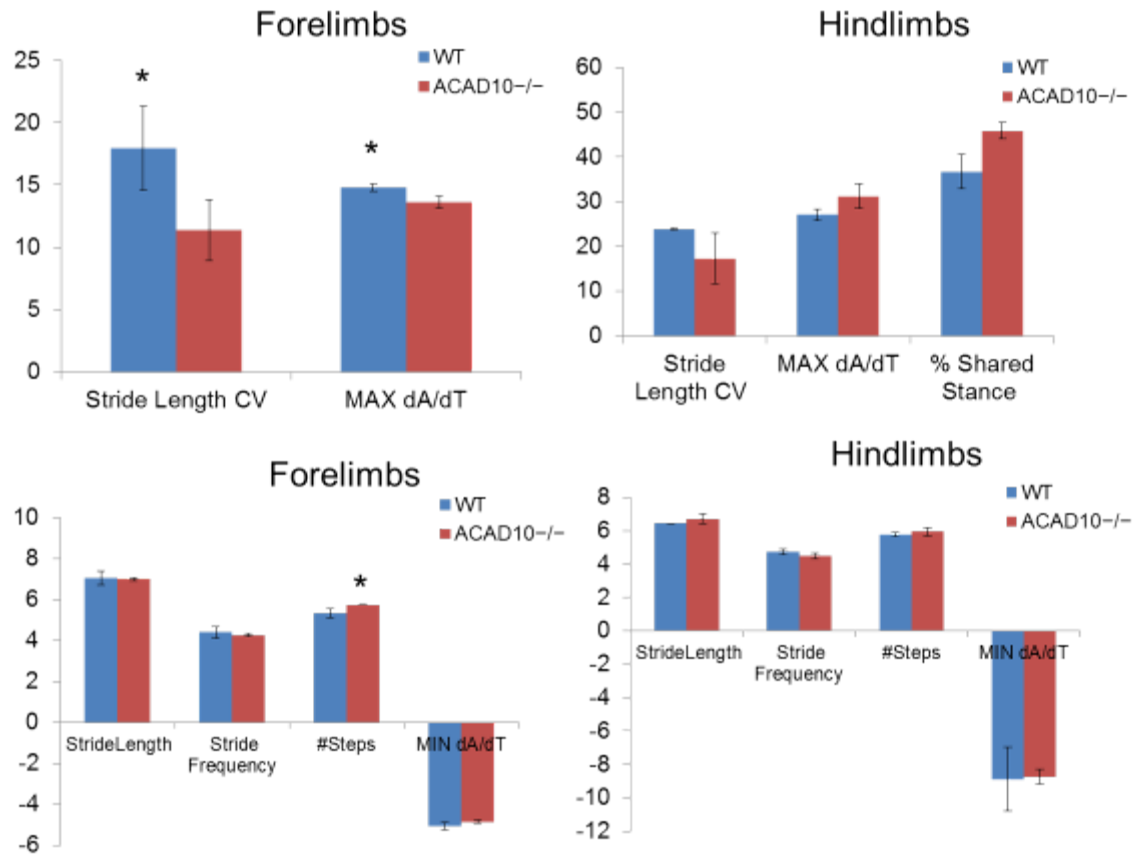


Figure 65. Digait indices IV

Measures of each activity in forelimbs and hindlimbs is depicted with wild type (Liu, Wang et al.) animals in blue and *Acad10*^{-/-} deficient in red. The *Acad10* deficient mice show a statistically significant decrease in stride length CV ($p=0.0302$) and MAX dA/dT ($p=0.0139$) in the forelimbs using unpaired t-test. The *Acad10* deficient mice show a statistically significant increase in the number of steps taken ($p=0.0152$).

4.6.3 Micro-MRI Brain

Because *Acad10*^{-/-} mice exhibited subtle abnormalities on neurobehavioral testing, brain MRI scans were performed over a period of 6 months to identify any changes in morphology. No significant abnormalities were identified as the *Acad10* deficient mice increased in age. Figure 66 shows a representative scan.

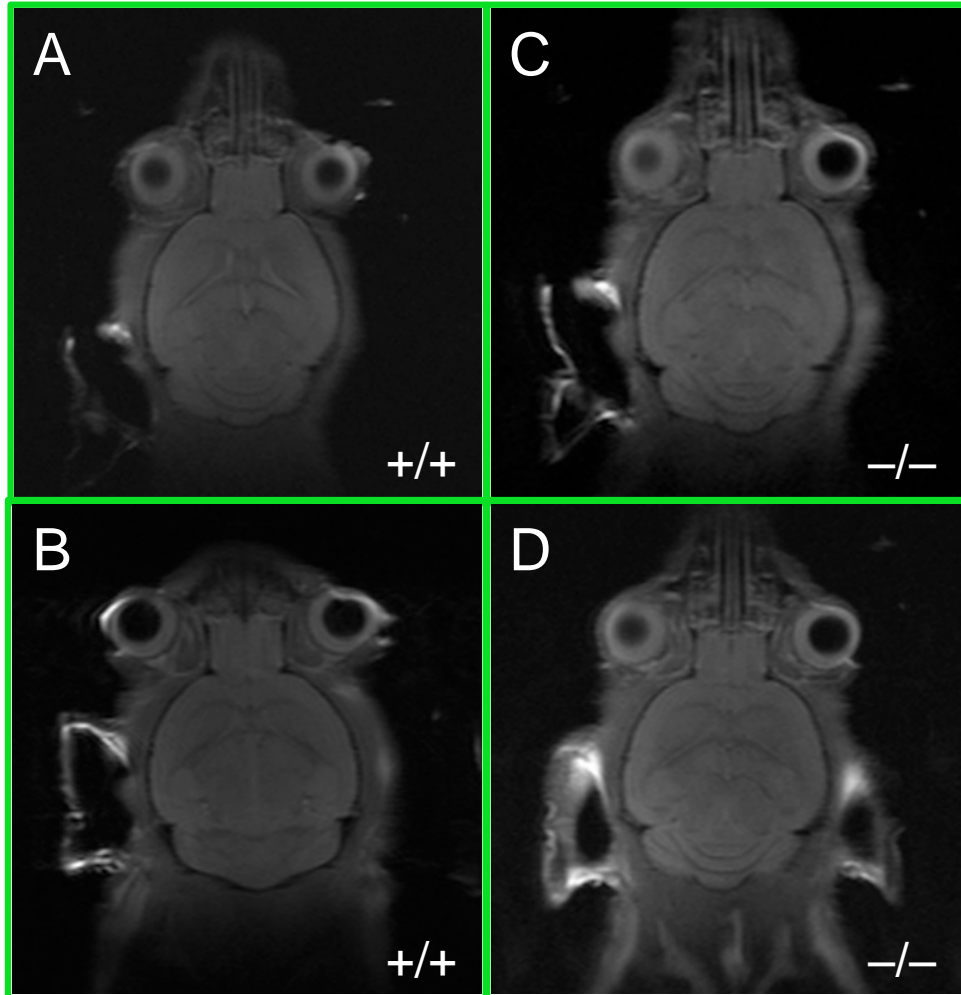


Figure 66. Micro-MRI of mouse brain

Mice were visualized using Horizontal bore 7-T MRI system, Bruker Biospin 70/30 with full vital monitoring system. (A) and (B) is the same wild type mouse at 2-3 months old and 7-8 months old, respectively, using RARE-T1 Imaging. The coronal image is whole, live, mouse brain section 11 of 15. (C) and (D) is the same *Acad10*^{-/-} mouse at 2-3 months old and 7-8 months old, respectively, using RARE-T1 Imaging. The coronal image is a representative whole, live, mouse brain section 11 of 15. The *Acad10* deficient mice do not show any significant changes in brain structure and morphology over time as compared to wild type control mice of the same background.

4.7 DISCUSSION

Over the past 20 years, 9 inborn errors of metabolism caused by deficiencies in ACADs have been described causing significant morbidity and mortality in affected individuals. Recently, two new ACADs of unknown function have been identified, raising the specter of additional unrecognized disorders related to their dysfunction. Prior research on *ACAD10* and *11* suggested a novel role in central nervous system metabolism and highlighted a possible role in the development of T2DK (Bian, Hanson et al. 2010, He 2011). The studies in this thesis were designed to determine the physiologic function of *ACAD10* and *11*. This knowledge will provide the opportunity to define clinical disorders related to deficiency of *ACAD10* and *11*, allow development of strategies for early diagnosis, and lead to rational intervention.

Disorders in fatty acid oxidation are among the most frequent of the inborn errors of metabolism and lead to a variety of phenotypes that require optimal treatment for patients to thrive (Vockley, Singh et al. 2002, Wang, Mohsen et al. 2010). Valuable progress has been made in recent years in identifying ACDs and their mutations in patients. Studies have focused initially on those enzymes most highly expressed and with easily deducible functions. More recently, the additional enzymes described in this gene family have exhibited low level expression, including *ACAD10* and *11*, and/or restricted tissue distribution, making functional studies and identification of deficient patients more difficult. Thus, additional approaches are needed to determine the roles of novel proteins such as *ACAD10*, and their possible role in disorders of mitochondrial fatty acid oxidation. Research in Dr. Vockley's lab suggests potential functions for *ACAD10* in the central nervous system, metabolism, and immunity (He 2011). *ACAD10* has also been genetically linked to type 2 diabetes, but functional studies have yet to be performed to provide feedback to these insights (Bian, Hanson et al. 2010). Results presented in this thesis

provide the first opportunity to better understand the biochemical pathways and functional interactions of ACAD10. First and foremost, animals deficient in ACAD10 develop the insulin resistance hyperglycemia characteristic of T2DM. They also exhibit the same metabolic profile in muscle previously reported by our lab in adult humans with T2DM. This pattern suggests inefficient transfer of reducing equivalents from fatty acids to the electron transport chain, likely leading to subtle energy deficiency. This finding leads to new possibilities for designing therapeutic agents to treat T2DM. Stabilization of the proteins as the interface of FAO and ETC by small molecule chaperonins could reverse the defect identifying in our mice and improve energy transfer. ACAD10 deficient mice also become obese. Characterization of the physiologic change responsible for this derangement would also be of great potential relevance to human disease. An ACAD10 polymorphism has been linked to the development of T2DM in Pima Indians. Thus, further exploration of ACAD10 sequence, expression and function may provide further insight into this devastating illness in this population.

Finally, ACAD10 deficient mice demonstrate other clinical abnormalities of potential relevance to human disease. While they do not become hypoglycemic with fasting, the classic sign seen in other mouse models of FAOD, ACAD10 mice do exhibit fasting rhabdomyolysis. This condition is a common one in humans and roughly one third of them remain without a diagnosis after extensive evaluations. Analysis of ACAD10 in these patients is warranted. ACAD10 deficient mice also develop subtle neurobehavioral abnormalities. These findings are in keeping with neurologic expression of the gene. Thus human patient may also experience neuromuscular disease. Unfortunately, my expressions studies failed to yield a stable and active ACAD10 protein for direct enzymatic studies, so an understanding of its role in mitochondrial metabolism, T2DM, obesity, and other symptoms were not possible. A number of options are

available to achieve this goal. Expressions system using mammalian cells, baculovirus, or yeast might all allow production of stable protein as they are more homologous to native processes than the prokaryotic system used. Additional exploration of the functional protein forms generated from this complex locus would also be useful.

ACAD10 and *11* share 46% homology between each other and are widely conserved across evolution (Vockley , Swigonova, Mohsen et al. 2009, He 2011). Extensive sequence analysis indicates that they are more highly conserved across evolution than the other more highly expressed ACADs, suggesting critical functions for these novel enzymes. Both genes are located within complicated loci containing multiple predicted exons and protein domains, including the ACAD domain. Database searches of transcribed sequences from these genes have identified the presence of multiple transcripts that differed mostly at either the 5' or 3' end. Acyl-CoA dehydrogenases 10 (*ACAD10*) and *11* (*ACAD11*) transcripts encoding 1059-aa (119kDa) and 780-aa (87kDa) proteins predicted to be structurally related have been identified in databases but their function is unknown. My strategy was to initially clone and express ACAD10 as recombinant protein for structural and enzyme studies and to generate antibodies to localize its presence in cells to further define its role, but I experienced difficulty in obtaining a full length clone. This difficulty may have arisen as a result of the size or amino acid composition of the ACAD10 protein and/or the possibility for alternative splicing. After the full length ACAD10 appeared to be unstable, I began to create a full length protein by cloning it into a plasmid in pieces. I was able to successfully develop a plasmid with the ACAD domain, expression and purification of this short form allowed generation of an *ACAD10* antibody. To increase stability of other *ACAD10* plasmids, I added His₆-tag to several *ACAD10* plasmid forms, including the short plasmid form that corresponded to the ACAD domain. Transcripts were expressed in *E.*

coli, but production of these proteins failed. Expression of inserts coding for ACAD10 S637-I1059 and ACAD11 S355-I780 sequences representing the ACAD domain was successful. Several of the plasmid constructs were specifically examined more extensively following protein purification. The purified proteins have absorbance spectra typical of flavoproteins but were inactive unstable.

While the only transcripts, that include a 5'-end UTR, that have been published code for 1059-aa and 1090-aa in length, recently our mRNA isolation from mouse lung has revealed the presence of a transcript missing 9 internal exons, which would code for 61.5 kDa protein. These experiments also revealed the presence of other fragments of the sizes that reflect the discrepancy in the reported genomic sequences in GenBank and Ensembl databases. In the latter, the *ACAD10* gene is reported to include an additional exon between exons 8 and 9, compared to the GenBank reported genomic sequence. Further sequence determination will resolve the various sizes and confirm the existence of more than two *ACAD10* transcripts that may possibly function in various organelles.

Despite some small successes with cloning the ACAD10 protein, we still need to learn how to isolate the native forms of this protein, especially the full length protein, which is now crucial to elucidating structure and function. By investigating the subcellular location and substrate specificities of this major protein species of this newly identified ACAD, we have just begun to determine a potential physiological function of these unique proteins, which in turn will facilitate further studies and to continue identification of ACAD10 protein function.

According to our findings, ACAD10 is detectable in both mitochondria and peroxisomes depending on tissue, while ACAD11 is largely peroxisomal. Dual localization of ACAD10 is likely related to differential splicing of the full gene transcript. For mitochondrial import to occur

a signal sequence at the N-terminus is needed, which if present is the dominant localization signal in the protein. If this signal is lost by alternative splicing, then the protein must default to another location. Cytoplasmic transport through endoplasmic reticulum generated vesicles with exocytosis is a possibility, but a peroxisomal targeting signal would interrupt this and redirect the protein to peroxisomes. A weak amino terminal peroxisomal targeting signal can be detected internal to the mitochondrial signal and may be activated by loss of the mitochondrial signal. A c-terminal peroxisomal signal is also present and may be sufficient to direct the protein to peroxisomes with loss of the mitochondrial signal. Additional subcellular fractionation and import studies will be necessary to characterize the peroxisomal variants of ACAD10 and 11. Alternative enzyme assays will also need to be employed as peroxisomes do not use ETF as an electron acceptor. Rather, oxidases take the place of dehydrogenases in peroxisomal FAO, and thus ACAD10 protein within peroxisomes may be an oxidase.

In this study, we have made significant progress towards identifying the role of ACAD10 in physiology. ACAD10 is a complex protein containing multiple domains. It appears to localize to mitochondria in muscle, lung, and kidney. It also appears to localize to the peroxisomes in lung. The deficient mouse demonstrates obesity with T2DM, subtle neurologic abnormalities, elevated short, branched chain acylcarnitines in tissues, and fasting rhabdomyolysis with abnormal muscle mitochondria. Additional study of this novel ACAD will ultimately lead to a better understanding of its role in human physiology and disease.

**APPENDIX A: TATN-1 MUTATIONS REVEAL A NOVEL ROLE FOR TYROSINE AS
A METABOLIC SIGNAL THAT INFLUENCES DEVELOPMENTAL DECISIONS AND
LONGEVITY IN CAENORHABDITIS ELEGANS**

This work has been previously published in the following location. Copyright permission was not needed to include the manuscript in this thesis dissertation.

My role in this project primarily focused on the work performed in the section *Tyrosine aminotransferase expression is controlled by diet and environment* in the following manuscript.

Ferguson AA¹, Roy S², Kormanik KN¹, Kim Y³, Dumas KJ³, Ritov VB⁴, Matern D⁵, Hu PJ⁶, Fisher AL⁷. “TATN-1 Mutations Reveal a Novel Role for Tyrosine as a Metabolic Signal That Influences Developmental Decisions and Longevity in *Caenorhabditis elegans*.” PLoS Genet. 2013 Dec;9(12):e1004020. doi: 10.1371/journal.pgen.1004020. Epub 2013 Dec 19.

Recent work has identified changes in the metabolism of the aromatic amino acid tyrosine as a risk factor for diabetes and a contributor to the development of liver cancer. While these findings could suggest a role for tyrosine as a direct regulator of the behavior of cells and tissues, evidence for this model is currently lacking. Through the use of RNAi and genetic mutants, we identify *tatn-1*, which is the worm ortholog of tyrosine aminotransferase and catalyzes the first step of the conserved tyrosine degradation pathway, as a novel regulator of the dauer decision and modulator of the *daf-2* insulin/IGF-1-like (IGFR) signaling pathway in *Caenorhabditis*

elegans. Mutations affecting *tatn-1* elevate tyrosine levels in the animal, and enhance the effects of mutations in genes that lie within the *daf-2*/insulin signaling pathway or are otherwise upstream of *daf-16*/FOXO on both dauer formation and worm longevity. These effects are mediated by elevated tyrosine levels as supplemental dietary tyrosine mimics the phenotypes produced by a *tatn-1* mutation, and the effects still occur when the enzymes needed to convert tyrosine into catecholamine neurotransmitters are missing. The effects on dauer formation and lifespan require the *aak-2*/AMPK gene, and *tatn-1* mutations increase phospho-AAK-2 levels. In contrast, the *daf-16*/FOXO transcription factor is only partially required for the effects on dauer formation and not required for increased longevity. We also find that the controlled metabolism of tyrosine by *tatn-1* may function normally in dauer formation because the expression of the TATN-1 protein is regulated both by *daf-2*/IGFR signaling and also by the same dietary and environmental cues which influence dauer formation. Our findings point to a novel role for tyrosine as a developmental regulator and modulator of longevity, and support a model where elevated tyrosine levels play a causal role in the development of diabetes and cancer in people.

A.1 INTRODUCTION

The aromatic amino acid tyrosine serves many metabolic roles including being a building block for protein synthesis, a source of energy, and a precursor for the synthesis of melanin and several neurotransmitters including dopamine and other catecholamines. Beyond these currently known functions for tyrosine, recent work has suggested that tyrosine could also play regulatory roles in both metabolism and the control of cell proliferation. Specifically, in people elevated serum tyrosine levels occur with obesity and represent a risk factor for the development of

diabetes [1]–[6]. Additionally, the enzyme tyrosine aminotransferase (TAT), which acts to normally convert tyrosine to energy, has been identified as a tumor suppressor gene which acts to promote apoptosis and prevent the development of hepatocellular carcinoma [7]. How changes in tyrosine metabolism could contribute to these disease processes is currently unknown, but it is possible that levels of this amino acid could play a direct regulatory role for the behavior of specific cells and tissues. While consistent with the available data, direct evidence for this model is currently lacking.

The nematode *Caenorhabditis elegans* normally progresses through four larval stages before developing into a reproductive adult animal. However specific cues, such as crowding, low food availability, or elevated temperature, can be sensed by the developing worm and lead to developmental arrest in a diapause state called a dauer larva [8]–[11]. Entry into dauer permits worms to delay the completion of development and the initiation of reproduction in environments which are not favorable, and instead the animals can survive as a dauer for up to several months before resuming normal development when conditions become favorable for reproductive success. This developmental decision requires a complicated interplay of sensory neurons with specific cGMP, TGF- β , and insulin-like signaling cascades controlling the choice of reproductive versus dauer development [9], [10].

In the worm, the *daf-2* insulin/IGF-1 receptor (IGFR) signaling pathway is involved in both dauer development and adult longevity [12]–[14]. Active signaling through the pathway during development enables animals to reach reproductive adulthood whereas reductions in *daf-2*/IGFR signaling due to either environmental triggers or genetic mutations lead to arrest as a dauer [9], [14]. In adult worms, *daf-2*/IGFR signaling is a major modulator of longevity and mutations impairing the pathway can result in 100% increases in lifespan [13].

At a molecular level, the *daf-2*/IGFR pathway consists of *daf-28* and other insulin-like peptides, which are thought to act as ligands for the DAF-2 insulin/IGF-1 receptor [15]–[18]. Downstream of *daf-2*/IGFR, is the *age-1* PI3 kinase and a kinase cascade consisting of the phosphoinositide-dependent kinase *pdk-1* and the protein kinase B genes *akt-1* and *akt-2* (Figure 1A) [19]–[22]. Both *akt-1* and *akt-2* normally act to phosphorylate the DAF-16 FOXO transcription factor which leads to its retention in the cytoplasm [23]–[25]. Reductions in either *daf-2*/IGFR or combined *akt-1* and *akt-2* activity result in the entry of DAF-16/FOXO into the nucleus and strong activation of DAF-16/FOXO target genes [23]–[25]. In contrast, loss of only *akt-1* activity leads to the translocation of DAF-16/FOXO into the nucleus but a lesser increase in the expression of DAF-16/FOXO target genes (Figure 1A and Table S1) [26], [27]. This finding suggested that additional pathways could be involved in controlling the transcriptional activity of DAF-16/FOXO (Figure 1A). One group of potential regulators is the *eak* (enhancer of *akt-1* null) genes, which were identified in a forward genetic screen and act in a non-cell autonomous manner to control the transcriptional activity of nuclear localized *daf-16*/FOXO (Figure 1A) [26]–[29]. The identified *eak* genes lack structural homology to one another and appear to lie in one or more poorly characterized pathways that act in parallel to *akt-1*. The identification of the *eak* genes suggests that additional novel pathways either downstream or parallel to insulin signaling may await discovery.

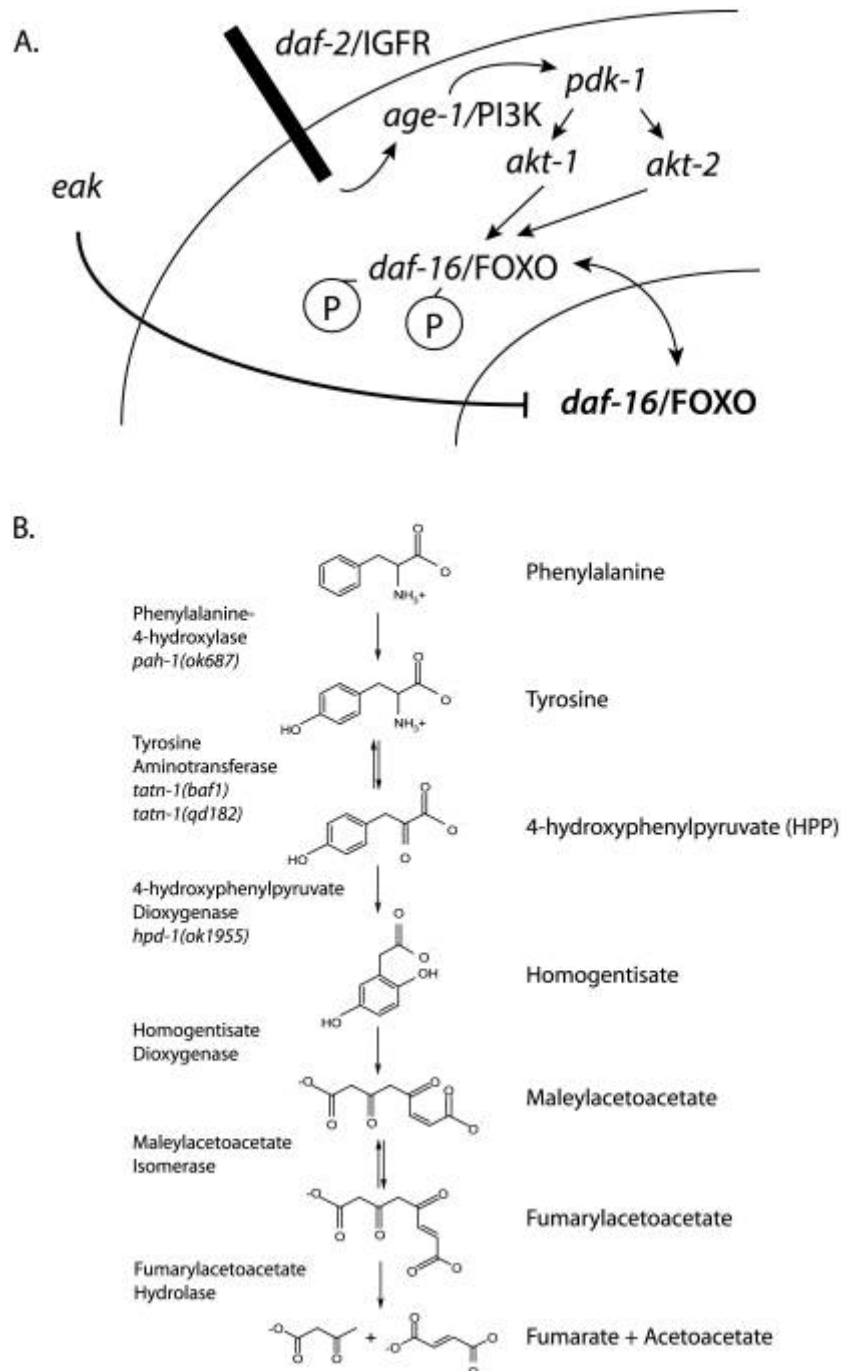


Figure 67. Diagram of *daf-2/IGFR* signaling pathway and tyrosine metabolic pathway

(A) For dauer formation in *C. elegans* the *daf-2/IGFR* receptor lies upstream of a PI_3 kinase signaling cascade consisting of *age-1/PI3* kinase, the phosphoinositide-dependent kinase *pdk-1*, and the protein kinase B family kinases *akt-1* and *akt-2*. Both AKT-1 and AKT-2 act to phosphorylate DAF-16/FOXO and prevent entry of this protein into the nucleus. Inhibition of AKT-1 leads to entry of DAF-16/FOXO into the nucleus without the activation of DAF-16 target genes. This suggested that other pathways acted to control the transcriptional activity of nuclear DAF-16/FOXO. The *eak* genes are a group of structurally unrelated genes which act in a cell non-autonomous manner to restrain the transcriptional activity of nuclear DAF-16/FOXO through an undefined molecular mechanism. (B)

Tyrosine is degraded to fumarate and acetoacetate via a five step degradation pathway. Shown are the names and structures of the intermediates as well as the names of the enzymes in the pathway that are studied in this work.

In both vertebrates and worms, there is data suggesting a link between tyrosine metabolism and insulin signaling. TAT, which catalyzes the first step in a conserved degradation pathway that converts tyrosine to fumarate and acetoacetate ([Figure 1B](#)), has been well studied as a target of regulation by insulin signaling in vertebrates with insulin effects seen at both the transcriptional and translational level [\[30\]–\[38\]](#). Further, in *C. elegans* the *hpd-1* gene, which encodes the enzyme 4-hydroxyphenylpyruvate dioxygenase and lies immediately downstream of TAT in the tyrosine degradation pathway, is a target gene for the *daf-16*/FOXO transcription factor and positively regulated by *daf-2*/IGFR signaling [\[39\]](#). The down-regulation of *hpd-1* in *daf-2*/IGFR mutants could lead to a reduction in tyrosine clearance and could, at least in part, account for the increases tyrosine levels observed in these animals [\[40\]](#). Furthermore, the inhibition of *hpd-1* by RNAi was shown to both extend lifespan and delay dauer exit through unknown mechanisms [\[39\]](#). Hence, tyrosine metabolism appears to be actively controlled by insulin signaling though the consequences of this regulation are currently unclear.

In our work, we identify *tatn-1*, which is the worm ortholog of TAT, to be a novel dauer formation regulator that is under the control of several dauer-inducing stimuli, including *daf-2*/IGFR signaling, and ultimately regulates tyrosine levels in the worm. We further find that *tatn-1* mutations enhance the dauer-formation and lifespan phenotypes of both *daf-2*/IGFR and *eak* mutants suggesting that elevated tyrosine levels have inhibitory effects on insulin signaling. These effects require the *aak-2*/AMPK gene, and *tatn-1* mutants have elevated levels of the activated phospho-AAK-2 protein consistent with activation of AAK-2 signaling in response to elevated tyrosine. The activation of AAK-2 may lead to effects on the downstream transcription factors *daf-16*/FOXO and *crh-1*/CREB. We see a partial dependence on *daf-*

16/FOXO for some *tatn-1* phenotypes and activation of *daf-16/FOXO* target genes, and the loss of *crh-1/CREB*, which is inhibited by activated *aak-2*, mimics some *tatn-1* phenotypes. Together our findings establish a novel role for tyrosine as a metabolic signal that influences insulin signaling, development, and lifespan through effects on *aak-2/AMPK* signaling. While further study is necessary, our results also suggest that the recently observed associations between tyrosine metabolism and both diabetes and cancer are due to elevated tyrosine levels playing a direct causal role in disease pathogenesis.

A.2 RESULTS

A.2.1 Reduced tyrosine aminotransferase activity promotes dauer arrest

The *eak* genes were identified in a genetic screen as enhancers of the weak dauer formation phenotype shown by *akt-1* mutants, and these genes normally act to suppress the transcriptional activity of nuclear localized *daf-16/FOXO* [26]–[29]. To identify new genes that act in parallel to *eak* genes to control dauer formation, we performed a genome-wide RNAi screen for gene inactivations that enhance the weak dauer-constitutive phenotype of the *eak-4(mg348)* mutant. Since RNAi of dauer-constitutive genes typically yields a weaker phenotype than the corresponding mutants, we constructed an *eri-3(mg408); eak-4(mg348)* double mutant to enhance the sensitivity of the *eak-4* mutant to RNAi [41], [42]. Control experiments demonstrated that RNAi inhibition of *daf-2/IGFR*, *akt-1*, or the 14-3-3 gene *ftt-2* enhance dauer arrest by the *eri-3; eak-4* mutants whereas RNAi inhibition of *daf-7*, *daf-9*, or *daf-11*, which encode components of TGF- β , dafachronic acid, and cGMP pathways, respectively, do not

(Figure 2A). These data suggested that the screen could be enriched for genes that act in the *daf-2*/IGFR pathway to control dauer arrest.

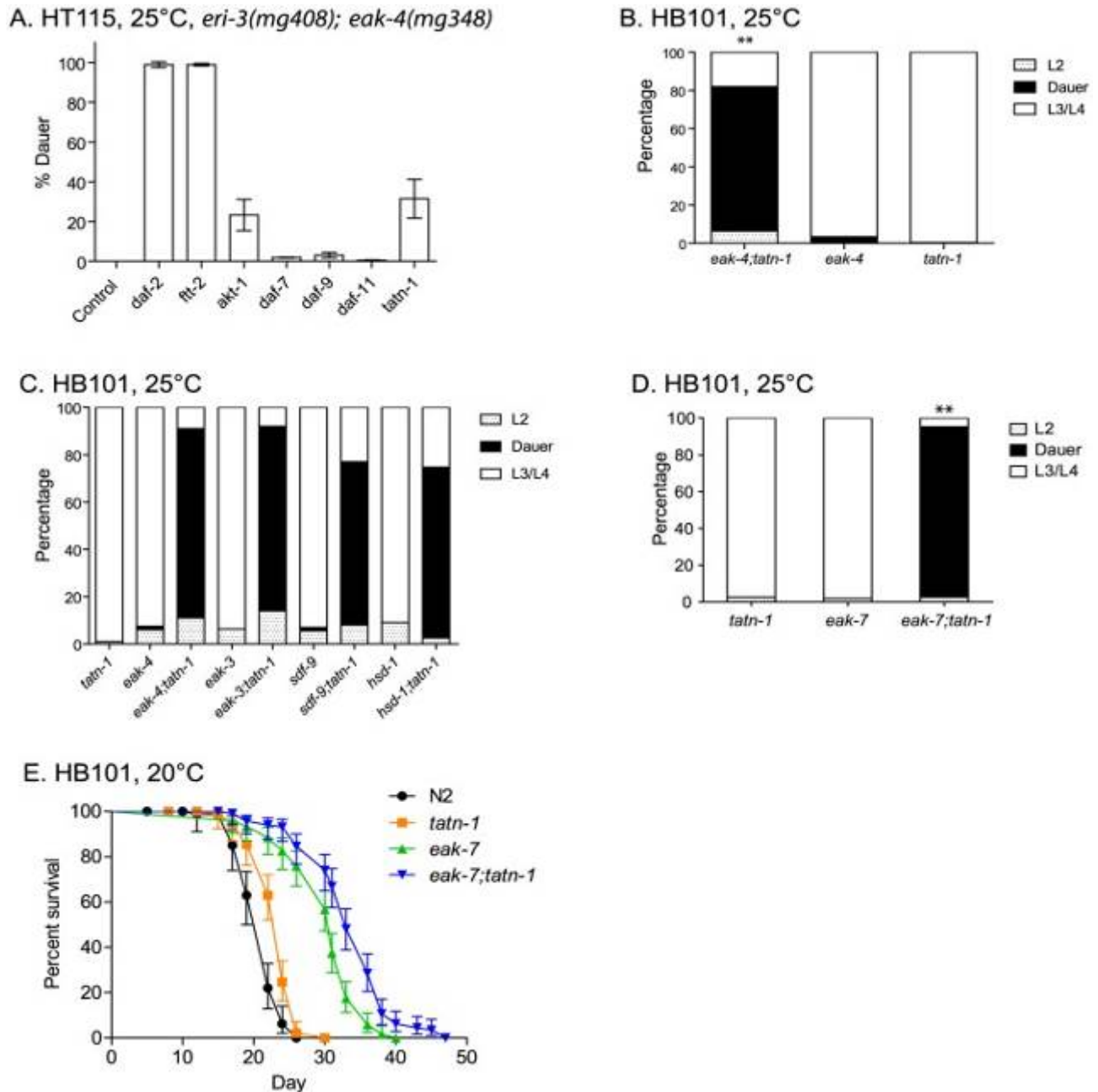


Figure 68. Tyrosine aminotransferase mutations enhance eak dauer and lifespan phenotypes

(A) Effect of treatment of *eri-3(mg408); eak-4(mg348)* mutants with RNAi clones for *daf-2*, *ftt-2*, *akt-1*, *daf-7*, *daf-9*, *daf-11*, and *tatn-1* on dauer arrest at 25°C. Bars represent mean percentage of dauers observed in two trials, and

the error bars represent standard deviation. The empty vector RNAi vector was used as a negative control. (B) Enhanced dauer formation by *eak-4(mg348)* or *tatn-1(baf1)* mutations alone. ** $p < 0.001$ for pairwise Fisher's exact test. (C) *tatn-1* mutations enhance dauer arrest by *eak-3(mg344)*, *sdf-9(mg337)*, and *hsd-1(mg337)* mutants. ** $p < 0.001$ for each double mutant compared to its respective *eak* single mutant by Fisher's exact test. (D) *tatn-1* enhances *eak-7(tm3188)* dauer arrest. ** $p < 0.001$ for comparisons between *eak-7; tatn-1* and either *tatn-1* or *eak-7* alone. (E) *tatn-1(baf1)* extends the lifespan of both wild type and *eak-7* worms. Shown are survival curves for wild type N2, *tatn-1(baf1)*, *eak-7(3188)*, and *eak-7(3188); tatn-1(baf1)*, with error bars showing the 95% confidence intervals for each point. The mean survival for N2, *tatn-1*, *eak-7*, and *eak-7; tatn-1* are 21.0, 23.0, 30.0, and 33.5 days, respectively. $P < 0.001$ for all comparisons by log-rank test.

Among the RNAi clones identified from the screen was *tatn-1*, which encodes the worm ortholog of tyrosine aminotransferase. Inhibition of *tatn-1* by RNAi enhanced dauer arrest by *eri-3; eak-4* mutants to the same extent as *akt-1* RNAi (Figure 2A)[43]. Tyrosine aminotransferase is the first enzyme in the conserved five step tyrosine degradation pathway present in worms and other eukaryotes, and this enzyme catalyzes the deamination of tyrosine to produce 4-hydroxyphenylpyruvate (Figure 1B). The subsequent steps in the degradation pathway convert 4-hydroxyphenylpyruvate into fumarate and acetoacetate which can be ultimately metabolized by the Krebs' cycle (Figure 1B).

Similarly to the effects of *tatn-1* RNAi, we also found that the *tatn-1(baf1)* mutation, which has a P224S mutation in a conserved region of the protein and is likely a partial loss of function allele [43], [44], also promoted dauer arrest by the *eak-4(mg348)* mutants (Figure 2B and Table S2). Interestingly, the interaction between *tatn-1* and *eak-4* was strongly influenced by worm diet with diets consisting of the *E. coli* K12-derived HT115 or K12-B hybrid HB101 bacterial strains showing the strongest interaction (Figure S1). Additionally, we observed that a second *tatn-1* allele, *tatn-1(qd182)*, both enhanced dauer arrest by the *eak-4* mutant and also had a weak

effect on dauer formation in isolation ([Figure S2](#)). The *tatn-1(qd182)* allele encodes a protein with a G171E mutation affecting a highly conserved glycine residue ([Figure S2](#)). Together these findings demonstrate a novel role for tyrosine aminotransferase as a regulator of the dauer development decision.

We then tested whether *tatn-1* interacted with other *eak* genes via the construction of *tatn-1; eak* mutants. We found that *tatn-1(baf1)* enhanced the dauer-constitutive phenotype of all *eak* mutants tested, including *eak-4(mg348)*, *eak-3(mg344)*, *eak-5/sdf-9(mg337)*, *eak-2/hsd-1(mg433)*, and *eak-7(tm3188)* ([Figure 2C and 2D](#)). *eak-7* showed a particularly strong interaction with *tatn-1*, with 92.4% of the population forming dauers at 25°C ([Figure 2D](#)), and we observed dauers in *eak-7; tatn-1* in cultures growing at lower temperatures or on other worm diets. These data suggest that *tatn-1* is a general enhancer of dauer formation by *eak* mutants.

In addition to enhancing dauer formation, *eak-7* mutations, but not other *eak* mutations, extend the lifespan of wild-type and *akt-1* mutant worms [[27](#)]. We tested whether a *tatn-1* mutation also enhanced the lifespan of *eak-7* mutants by conducting survival assays using wild type N2, *tatn-1(baf1)*, *eak-7(tm3188)*, and *eak-7(tm3188); tatn-1(baf1)* worm populations. We found that *tatn-1*, *eak-7*, and *eak-7; tatn-1* mutants all showed increased longevity relative to N2 (mean survivals of 21.0, 23.0, 30.0, and 33.5 days, respectively) ([Figure 2E](#) and [Table S3](#)). Specifically, *tatn-1* extends mean survival 10.4%, *eak-7* extends mean survival 43.1%, and *eak-7; tatn-1* increases survival 59.2% over wild type ([Figure 2E](#)). These findings demonstrate a novel role for *tatn-1* in modulating lifespan and also demonstrate that the effects of the *eak-7 – tatn-1* genetic interaction also influence adult longevity.

A.2.2 Tyrosine aminotransferase interacts with insulin signaling in worms

Mutations in the *eak* genes enhance the dauer formation phenotype of loss-of-function mutations affecting genes in the *daf-2*/IGFR signaling pathway, so we tested whether *tatn-1* mutations also enhanced *daf-2*/IGFR mutant phenotypes [28]. We used the *daf-2(e1368)* allele which has a strong dauer-constitutive phenotype when grown at 25°C but a weaker phenotype when grown at lower temperatures. Compared to *tatn-1(baf1)* and *daf-2(e1368)* alone, we found that *daf-2(e1368); tatn-1(baf1)* mutants showed increased levels of dauer formation when grown at 23°C (Figure 3A). Further, we found that the *tatn-1* mutation extends the adult lifespan of worms treated with *daf-2* RNAi starting at day 1 of adulthood (Figure 3B). We used RNAi treatment due to the high levels of dauer arrest that we observed with the *daf-2(e1368); tatn-1(baf1)* animals. In these RNAi experiments, the mean survival of worms were 22.0 days for N2 on control RNAi, 24.0 days for *tatn-1* on control RNAi, 30.5 days for N2 on *daf-2* RNAi, and 37.0 days for *tatn-1* on *daf-2* RNAi (Figure 3B and Table S3). Hence, while *daf-2* RNAi treatment extends the survival of wild type N2 worms by 37.4%, the inclusion of the *tatn-1* allele further extends the lifespan of *daf-2* (Mihalik, Gaborik et al.) treated worms by an additional 21%. These findings show a genetic interaction between *tatn-1* and *daf-2*/IGFR with impaired tyrosine degradation enhancing the *daf-2*/IGFR dauer formation and lifespan phenotypes.

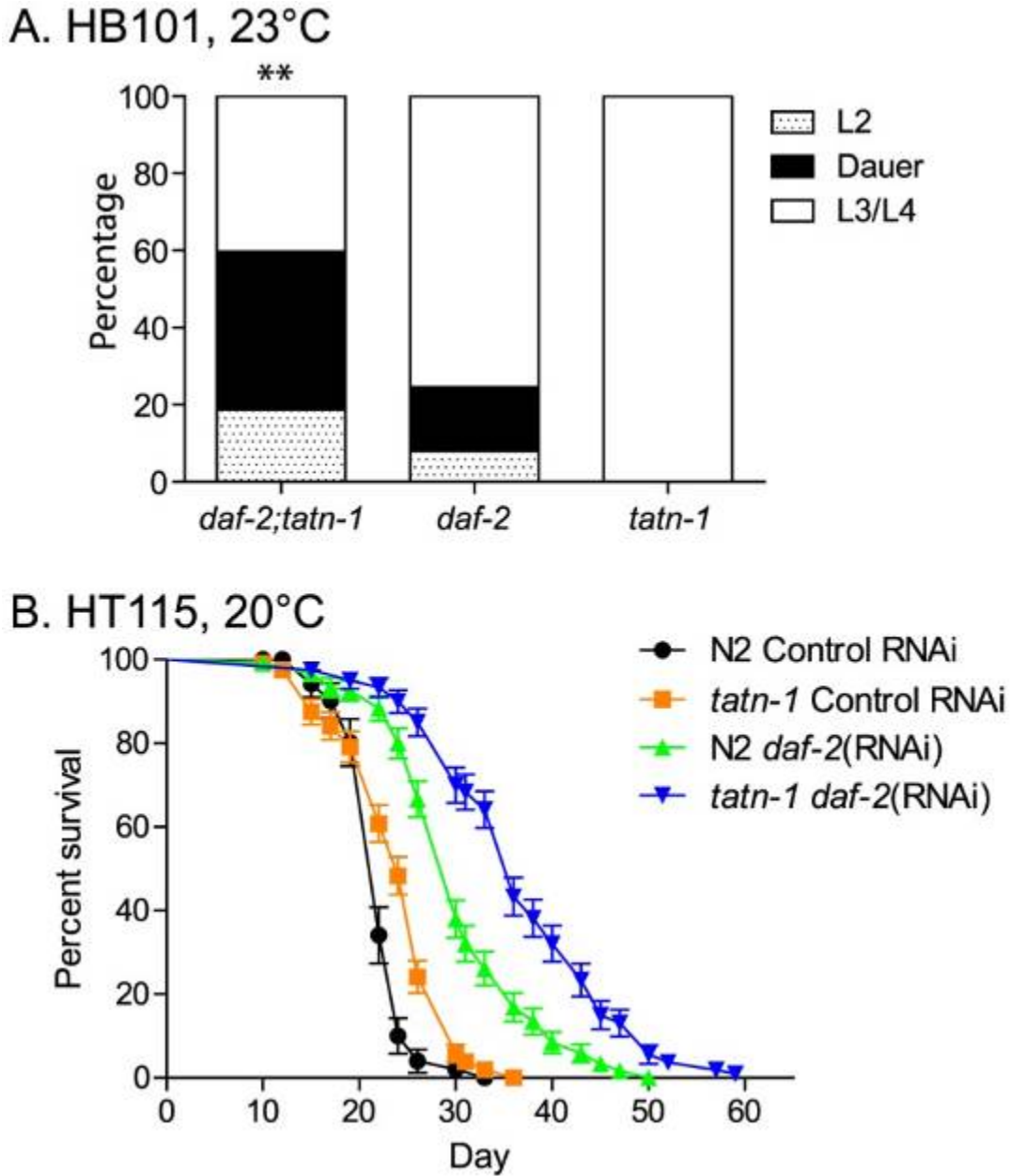


Figure 69. The *tatn-1* mutant enhances dauer formation and lifespan of worms with impaired *daf-2*/IFGR signaling

(A) Enhanced dauer formation by *daf-2(e1368); tatn-1(baf1)* compared to *daf-2(e1368)* grown at 23C for 3 days. ** $p < 0.01$ by Fisher's exact test. (B) *tatn-1* extends the lifespan of worms treated with *daf-2* RNAi from day 1 of adulthood. The mean survival for N2 control RNAi, *tatn-1(baf1)* control RNAi, N2 *daf-2*(Mihalik, Gaborik et al.), and *tatn-1(baf1) daf-2*(Mihalik, Gaborik et al.) are 22.0, 24.0, 30.5, and 37.0 days, respectively. $P < 0.001$ for N2 vs.

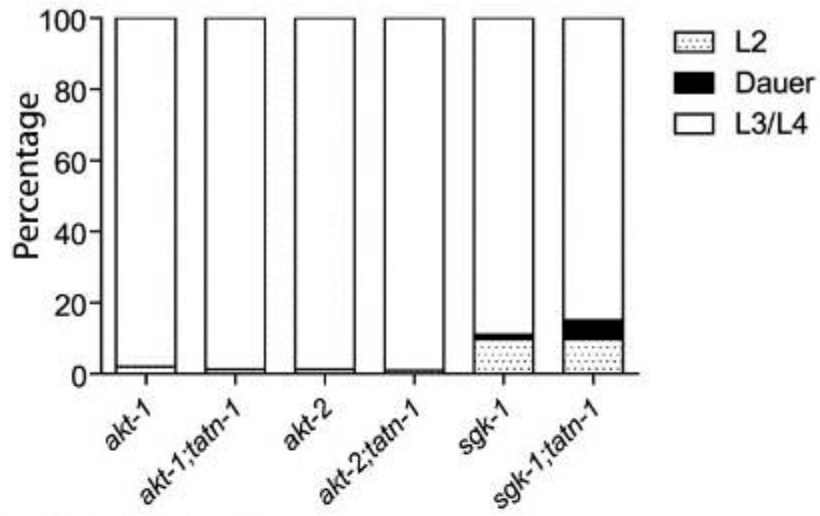
tatn-1 on control RNAi and N2 *daf-2*(Mihalik, Gaborik et al.) vs. *tatn-1 daf-2*(Mihalik, Gaborik et al.) by log-rank test.

A.2.3 *Tatn-1* likely does not alter PI3 kinase or TGF- β signaling

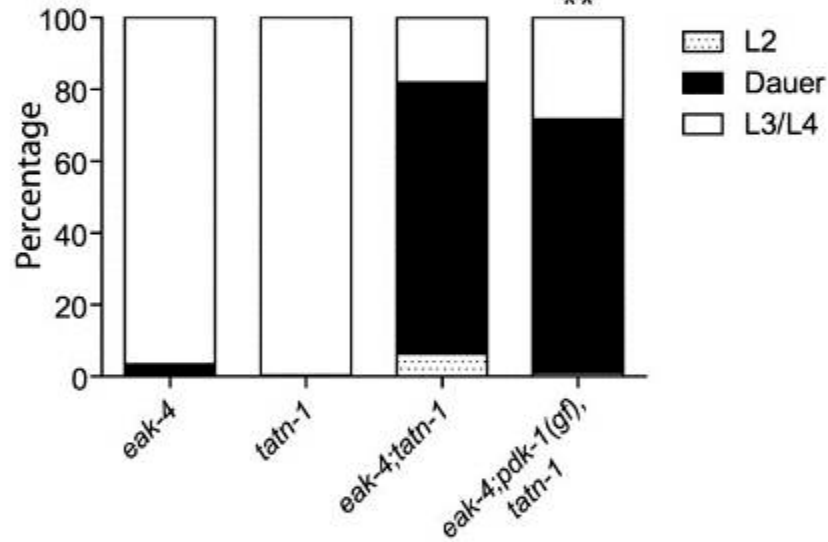
Since the *eak* mutations interact with *akt-1* mutations to enhance dauer formation, the effects of *tatn-1* mutations could be due to inhibition of the PI3 kinase signaling pathway (Figure 1A) [20]–[22], [28], [45]. To test this possibility, we looked for genetic interactions between loss-of-function and gain-of-function mutations affecting the PI3 kinase pathway with *tatn-1*. First, we constructed *tatn-1* mutants containing the loss-of-function mutations affecting the PKB genes *akt-1* and *akt-2*, and the related kinase *sgk-1*. We found that none of these genes interacts strongly with *tatn-1* mutation to enhance dauer arrest (Figure 4A). This finding suggests that *tatn-1* is not an upstream regulator of either *akt-1* or *akt-2*. To further test whether tyrosine affected the PI3 kinase signaling cascade, we tested whether the *eak-4(mg348); tatn-1(baf1)* interaction was blocked by gain-of-function mutations in either *pdk-1* or *akt-1*. These mutations were identified in genetic screens as suppressors of the dauer-constitutive phenotype of an *age-1*/PI3K null mutant [20], [21]. We constructed both *eak-4(mg348); pdk-1(mg142)*, *tatn-1(baf1)* and *eak-4(mg348); akt-1(mg144); tatn-1(baf1)* mutants and examined the effects of these mutations on dauer formation. We found that *pdk-1(mg142)*, which is a dominant gain-of-function allele of 3-phosphoinositide-dependent kinase and lies upstream of *akt-1*, *akt-2*, and *sgk-1*, had little effect on dauer formation by the *eak-4(mg348); tatn-1(baf1)* mutants (70% with *pdk-1(mg142)* versus 75% without) (Figure 4B). We further found that *akt-1(mg144)* had at

most a modest effect on dauer formation by *eak-4(mg348); tatn-1(baf1)* mutants (51% with *akt-1(mg144)* versus 77.6% without) (Figure 4C). Together these results suggest that the interaction between *eak-4* and *tatn-1* likely does not involve changes in the PI3 kinase signaling cascade.

A. HB101, 25°C



B. HB101 25°C



C. HB101, 25°C

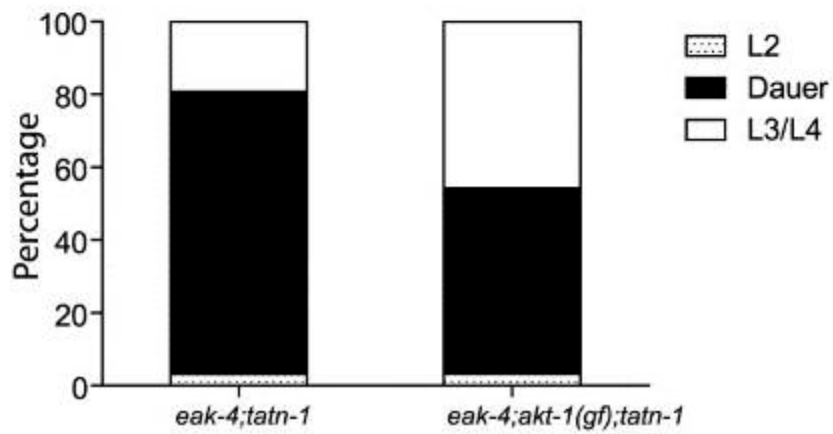


Figure 70. *tatn-1* effects on development do not require changes in PI3 kinase signaling

(A) *tatn-1(baf1)* does not augment dauer arrest by mutants with loss-of-function mutations in the protein kinase B genes *akt-1*, *akt-2*, or *sgk-1*. (B) The *pdk-1(mg142)* gain-of-function allele minimally affects dauer formation by *eak-4(mg348); tatn-1(baf1)* mutants. % dauers observed was 75.6% in *eak-4; tatn-1* and 70.7% in *eak-4; pdk-1(mg142); tatn-1*. ** p,0.001 by Fisher's exact test. (C) The *akt-1(mg144)* gain-of-function allele weakly inhibited dauer formation by *eak-4(mg348); tatn-1(baf1)* mutants. % dauers observed was 77.6% in *eak-4; tatn-1* and 51% in *eak-4; akt-1(mg144); tatn-1*.

In addition to the *daf-2*/IGFR signaling pathway, dauer formation in worms is also regulated by a TGF- β signaling pathway [9]–[11]. While traditionally these two pathways are viewed as independent, more recent work has indicated that cross-talk between the pathways may occur. Specifically, genes in one pathway, such as *sdf-9/eak-5* or *pdp-1*, have been shown to augment the dauer formation phenotypes of genes in the other pathway [46], [47]. Notably, the *pdp-1* phosphatase was identified from an RNAi screen using *daf-2*/IGFR pathway mutants as was *tatn-1*. To test whether *tatn-1* could act in the TGF- β signaling pathway, we blocked this pathway with either the *daf-3*/SMAD or *daf-5*/Sno mutations [41], [48], [49]. We found that neither mutant reduced dauer formation by the *eak-4; tatn-1* mutants (Figure S3), which is consistent with *tatn-1* acting independently of the TGF- β pathway.

A.2.4 AAK-2/AMPK is activated in *tatn-1* mutants and required for effects on dauer formation and longevity

Since *tatn-1* did not interact with *akt-1*, *akt-2*, or *sgk-1*, we looked for alternate signaling pathways that could be activated by a *tatn-1* mutation, and then interact with the *daf-2*/IGFR signaling pathway. The AMP-activated protein kinase (AMPK) ortholog AAK-2 was considered

as a candidate because *aak-2* interacts with *daf-2* signaling, plays roles in dauer development, modulates worm longevity, and acts in part through the *daf-16/FOXO* transcription factor which is part of the *daf-2/IGFR* signaling pathway [50]–[53]. To test the involvement of *aak-2/AMPK*, we compared dauer formation between *eak-4(mg348); tatn-1(baf1)* and *eak-4(mg348); tatn-1(baf1), aak-2(gt33)* mutants. We found that loss of *aak-2* strongly reduced dauer arrest from 84.7% to 10.7% (Figure 5A and Table S2). The *aak-2* mutation also reduced dauer formation by an *eak-4(mg348); tatn-1(qd182)* mutant though to a lesser degree than with the *tatn-1(baf1)* allele (Figure S4). This may be due to the *tatn-1(qd182)* allele being a stronger loss-of-function allele than *tatn-1(baf1)* as suggested by the developmental delay phenotype shown by *tatn-1(qd182)* and the higher tyrosine levels found in this mutant (Figure S4 and below). Together these findings support a necessary role for *aak-2/AMPK* for worms to respond to reductions in *tatn-1* activity, especially with weaker alleles.

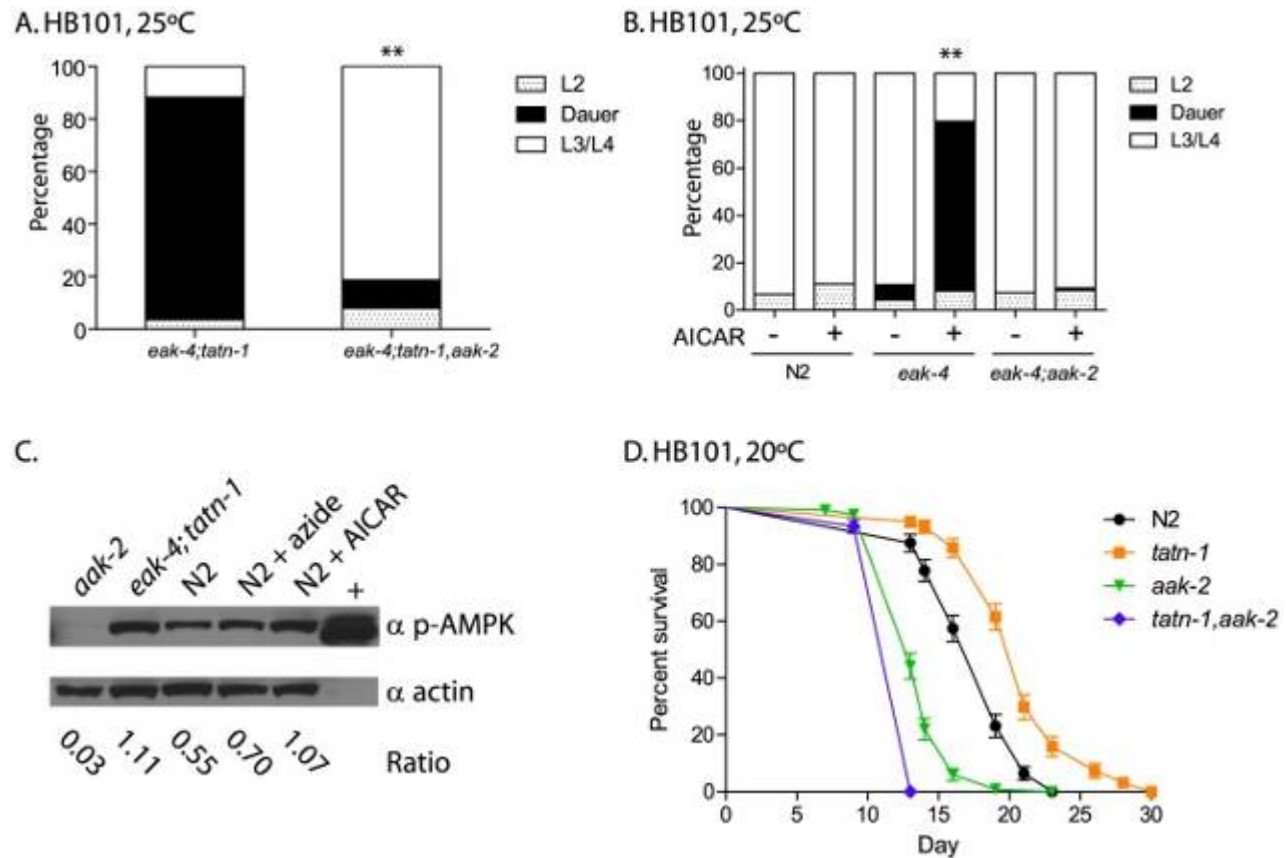


Figure 71. *aak-2* activity is necessary and sufficient for *tatn-1* effects on development and longevity

(A) The effects of *tatn-1*(*baf1*) on dauer formation require the *aak-2*/AMPK gene. ** $p < 0.001$ by Fisher's exact test. (B) Activation of *aak-2* with the AMPK agonist AICAR (0.125 mM) mimics the effects of *tatn-1* on *eak-4*(*mg348*) mutants. The effect of AICAR depends on *aak-2*/AMPK because an *eak-4*; *aak-2* mutant fails to respond to AICAR. ** $p < 0.001$ for comparison of *eak-4* with and without AICAR by Fisher's exact test. (C) Levels of phospho-AAK-2 are increased in *eak-4*(*mg348*); *tatn-1*(*baf1*) L2 larval worms or N2 L2 larval worms treated with 1 mM AICAR compared to untreated N2 L2 larval worms. Levels of phospho-AAK-2 was detected using an anti-phospho-T172 specific antibody, and actin was a loading control. The ratio represents the level of phospho-AMPK normalized for the actin level in each lane. N2 larval worms treated with 10 mM sodium azide to deplete ATP levels and the AMPK positive control extract (+) (Cell Signaling Technologies) were included as positive controls. (D) *aak-2* is required for *tatn-1* effects on lifespan. Mean survival for N2, *tatn-1*(*baf1*), *aak-2*(*gt33*), and *tatn-1*(*baf1*); *aak-2*(*gt33*) were 18.0, 21.0, 14.0, and 13.0 days, respectively. $p < 0.001$ for all pairwise curve comparisons by log-rank test.

To further explore the role of *aak-2*/AMPK in dauer formation, we treated worms with the AMPK agonist AICAR. Treatment of wild-type N2 worms with 0.125 mM AICAR had no effect on development or dauer formation, but *eak-4* mutants treated with AICAR showed a significant increase in dauer formation compared to an untreated control (Figure 5B). This effect required *aak-2*/AMPK as an *eak-4*(*mg348*); *aak-2*(*gt33*) mutant failed to respond to AICAR

([Figure 5B](#)). These findings demonstrate that *aak-2* activity is both necessary and sufficient to promote dauer formation by *eak-4* mutants.

Our findings could suggest that AAK-2 is activated in the *tatn-1* mutants. To test this possibility we used western blotting to measure levels of AAK-2 phosphorylated on the activating Thr²⁴³ residue, which is analogous to Thr¹⁷² in the vertebrate orthologs. We found that treatment of N2 wild-type animals with either sodium azide which inhibits mitochondrial function and depletes ATP levels by approximately 50% at this dose or with 1 mM AICAR leads to increases in phosphorylated AAK-2 levels compared with untreated L2 larval N2 worms grown in parallel ([Figure 5C](#)) [54]. Furthermore levels of phospho-AAK-2 were also increased in *eak-4*; *tatn1* mutant L2 larvae compared to the N2 control larvae ([Figure 5C](#)). Importantly, the phospho-AAK-2 signal was lost in *aak-2(gt33)* mutants confirming the identity of this band as AAK-2 ([Figure 5C](#)). These findings demonstrate that both *tatn-1* mutations and AICAR treatment serve to activate AMPK in *C. elegans*, and that this activation of AAK-2 is required for the effects of *tatn-1* mutations on development.

The requirement for *aak-2*/AMPK for the effects of *tatn-1* could reflect impaired tyrosine degradation leading to reduced production of the TCA cycle precursors fumarate and acetoacetate and a consequent decrease in energy production. To test this possibility we analyzed worm lysates for levels of AMP and ATP. We found that *eak-4(mg348)*; *tatn-1(baf1)* mutants had a lower AMP/ATP ratio than N2 worms grown in parallel ([Figure S5](#)). This suggests that the role of *aak-2*/AMPK does not reflect reduced energy production in the *tatn-1* mutants. Finally, we tested whether the effect of *tatn-1(baf1)* on adult lifespan requires *aak-2* activity, and we found that a *tatn-1* mutation increased wild-type lifespan by 17.8%, but decreased *aak-2(gt33)* lifespan by 8.9% compared to *aak-2(gt33)* alone (N2 mean survival 18.0 days, *tatn-*

1(baf1) 21.0 days, *aak-2(gt33)* 14.0 days, and *tatn-1(baf1), aak-2(gt33)* 13.0 days) ([Figure 5C](#) and [Table S3](#)). Hence *aak-2* is both required for the *tatn-1* lifespan increase and may even play a protective role in animals with reduced *tatn-1* activity.

A.2.5 *tatn-1* acts by *daf-16*/FOXO dependent and independent pathways

Since the effects of *eak* genes on dauer formation are dependent on both the FOXO transcription factor DAF-16 and the nuclear hormone receptor DAF-12, we tested whether these genes are required for dauer formation by *eak-4(mg348); tatn-1(baf1)* mutants through the construction of *daf-16(mgDf47); eak-4(mg348); tatn-1(baf1)* and *eak-4(mg348); tatn-1(baf1), daf-12(rh61rh411)* mutants [26]–[28]. We found that the genetic interaction is completely dependent on *daf-12* (Figure 6A). However, we identified both *daf-16* dependent and independent effects of *tatn-1*. The *tatn-1* effects on dauer formation are largely blocked by the *daf-16(mgDf47)* mutation, but a small percentage of worms still form dauers (Figure 6A). This *daf-16* independent pathway was also seen in experiments using the stronger *tatn-1(qd182)* allele (Figure S6). These findings suggest that *daf-16*/FOXO does play a vital role in the interaction between *eak* genes and *tatn-1*, but that *daf-16*/FOXO independent pathways are also involved.

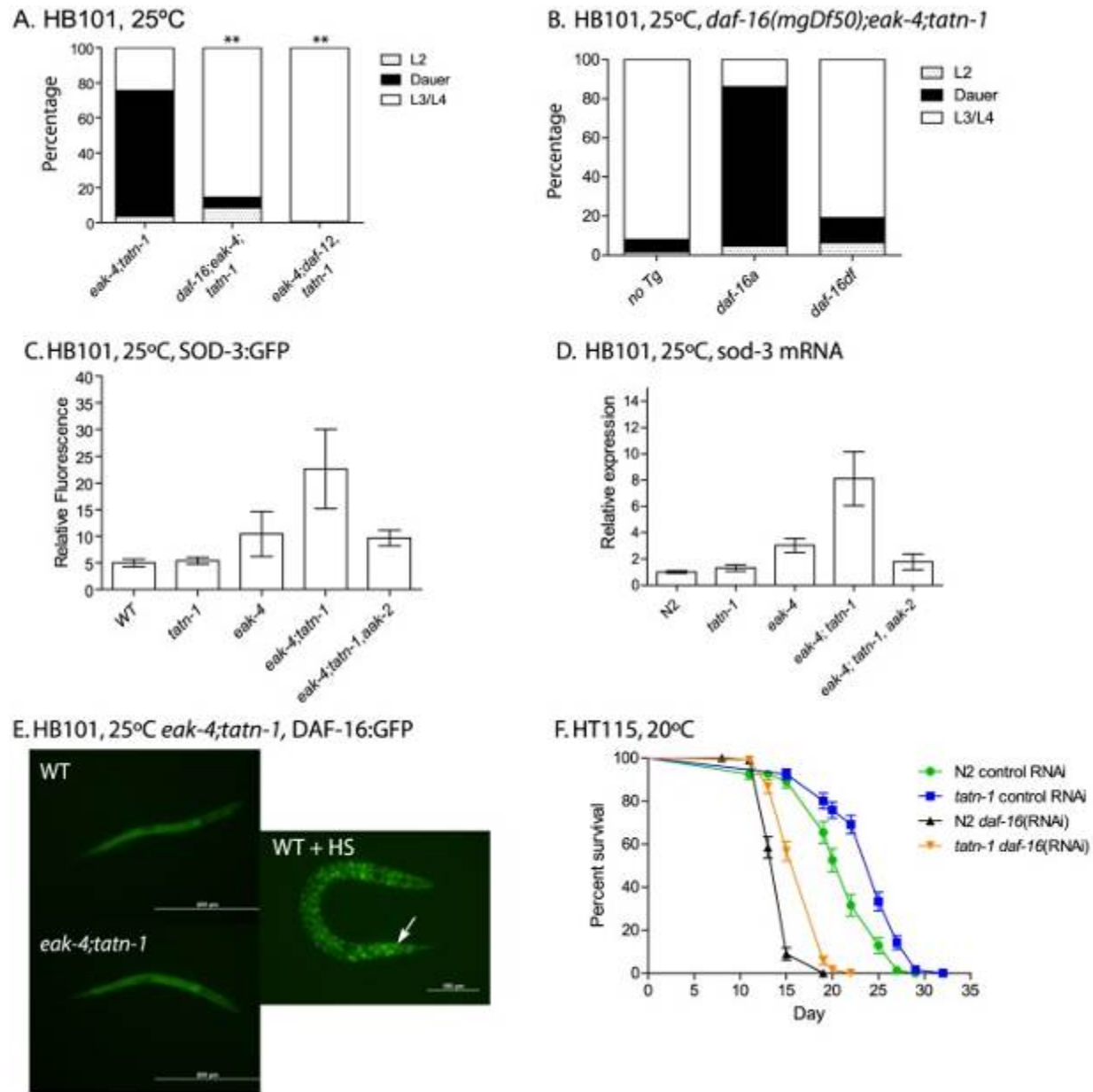


Figure 72. *tatn-1* acts by *daf-16*/FOXO dependent and independent mechanisms

(A) Mutations in *daf-16* (*daf-16(mgDf47)*) or *daf-12* (*daf-12(rh61rh411)*) inhibit dauer formation by *eak-4(mg348)*; *tatn-1(baf1)* mutant worms. ** $p < 0.001$ by Fisher's exact test. (B) The *daf-16(mgDf50)* mutation also inhibits dauer formation by *eak-4*; *tatn-1(baf1)* mutants, and a transgene expressing the DAF-16A isoform largely rescues dauer formation by *daf-16(mgDf50)*; *eak-4*; *tatn-1* mutants while a transgene expressing the DAF-16DF isoform only weakly rescues. (C) *eak-4*; *tatn-1* mutants activate expression of the *daf-16* target gene *sod-3* as indicated by expression of a *sod-3p::GFP* reporter gene in L2 larvae, and this induction requires the *aak-2/AMPK* gene. * $p < 0.05$ for t-test comparisons of *eak-4* vs. *eak-4*; *tatn-1*, and *eak-4*; *tatn-1* vs. *eak-4*; *tatn-1*; *aak-2*. (D) Induction of the endogenous *sod-3* gene in *eak-4*; *tatn-1* mutants is seen by quantitative RT-PCR, and this induction also depends on the *aak-2/AMPK* gene. (E) DAF-16A:GFP is not nuclear localized in either L2 stage WT or *eak-4*; *tatn-1* larvae, but exposure to a 1 hour 35°C heat shock produces clear nuclear localization of DAF-16A:GFP (arrow). (F) *tatn-1* effects on lifespan are *daf-16* independent. Treatment of N2 and *tatn-1* mutants with *daf-16* RNAi reduces

mean survival, but *tatn-1(baf1)* still lives longer than N2. The mean survival of N2 control RNAi, *tatn-1* control RNAi, N2 *daf-16*(Mihalik, Gaborik et al.), *tatn-1 daf-16*(Mihalik, Gaborik et al.) are 21.0, 24.0, 14.

The *daf-16/FOXO* gene encodes multiple isoforms which have been recently shown to have differential modes of regulation and have distinct effects on development and longevity [24], [55], [56]. For dauer development, three isoforms appear to be involved with DAF-16A being the predominant isoform, DAF-16DF playing a somewhat lesser role, and DAF-16B playing a modest role, at best [55]. As a result, we tested whether the developmental effects of *eak-4* and *tatn-1* are dependent on particular *daf-16* isoforms through the use of isoform-specific transgenes to rescue the dauer-constitutive phenotypes lost in *daf-16/FOXO* mutants (Figure 6B). We found that a transgene encoding a DAF-16A:mRFP fusion protein was able to strongly rescue the formation of dauers by a *daf-16(mgDf50); eak-4(mg348); tatn-1(baf1)* mutant, whereas a transgene encoding a DAF-16DF:GFP fusion protein only weakly rescued dauer formation (Figure 6B). These data suggest that the *daf-16a* isoform is most involved in the developmental effects produced by *tatn-1* mutants.

To further explore the role of *daf-16/FOXO* in *tatn-1* phenotypes, we examined the effects of *eak-4* and *tatn-1* mutations on both *daf-16/FOXO* target gene expression and DAF-16 subcellular localization. We used a *sod-3:GFP* transgene to examine the effects of *eak-4* and *tatn-1* mutations on expression of the *daf-16* target gene *sod-3*, which encodes a manganese superoxide dismutase enzyme [57], [58]. We generated combinations of *eak-4(mg348)* and *tatn-1(baf1)* with the transgene, and examined GFP expression in L2 larvae. We found that the combination of *eak-4* and *tatn-1* mutations resulted in the highest expression of *sod-3:GFP* even prior to dauer formation (Figure 6C). Furthermore, *aak-2/AMPK* was required for this enhanced activation of the *sod-3:GFP* reporter (Figure 6C). Similar effects of *tatn-1* and *eak-4* on *sod-3* expression were also seen when mRNA levels for the endogenous gene were measured by Q-PCR in L2 larvae,

and this effect on *sod-3* expression also required *aak-2*/AMPK (Figure 6D). Together these findings demonstrate that *tatn-1* and *eak-4* act in an *aak-2*/AMPK dependent manner to promote at least some aspects of *daf-16*/FOXO transcriptional activity.

Since the *eak* genes act to inhibit DAF-16/FOXO within the nucleus, a possible explanation for the enhancement of dauer formation in *eak*; *tatn-1* double mutants may be explained by the *tatn-1* allele causing increased nuclear localization of DAF-16 as do mutations affecting *akt-1* [26]. We tested for changes in DAF-16 localization via the use of transgenic animals expressing a DAF-16A:GFP fusion protein [59]. We found that *eak-4*; *tatn-1* mutants failed to show clearly visible nuclear localization of DAF-16:GFP in synchronized L2 worms grown at 25°C (Figure 6E). In contrast, exposure of animals to a 1 hour heat-shock at 35°C led to strong nuclear localization of DAF-16A:GFP (Figure 6E). Together these findings suggest that the *tatn-1* enhancement of the *eak* dauer formation phenotype could be due to an increase in *daf-16* transcriptional activity without an accompanying significant change in DAF-16 subcellular localization.

We then used *daf-16* RNAi treatment to test whether *daf-16*/FOXO is required for the lifespan extension of *tatn-1* mutants. We found that silencing of *daf-16* through RNAi results in a shortened lifespan for both *tatn-1* and wild-type N2 worms compared to control RNAi treatment (Figure 6F). However in *daf-16* RNAi treated worms, *tatn-1* still produces lifespan extension over wild type (mean survival for N2 control RNAi 21.0 days, *tatn-1*(*baf1*) control RNAi 24.0 days, N2 *daf-16*(Mihalik, Gaborik et al.) 14.5 days, and *tatn-1*(*baf1*) *daf-16*(Mihalik, Gaborik et al.) 17.0 days). Specifically, *tatn-1*(*baf1*) produced a 13.7% increase in lifespan in control RNAi treated worms, but a 17.8% increase in lifespan in *daf-16* RNAi treated worms. These data

suggest that the increased lifespan resulting from *tatn-1* is either independent of *daf-16* or occurs in a site resistant to the effects of *daf-16* RNAi.

A.2.6 *crh-1*/CREB shows overlapping gene expression and phenotypes with *tatn-1*

To explore the effects of impaired tyrosine metabolism in *C. elegans*, we performed whole transcriptome RNA sequencing (RNA-seq) to identify genes that are differentially regulated in the *tatn-1* mutants. To maximize the gene expression changes seen, we used the stronger *tatn-1*(*qd182*) allele and compared its transcriptome to that of wild-type N2 animals. Using ANOVA testing with a false-discovery rate of 5%, we identified 890 up-regulated and 3732 down-regulated genes in the *tatn-1*(*qd182*) mutant relative to N2 (Table S4).

To understand how the *tatn-1* mutants might affect the *daf-2*/IGFR pathway, we used this data set to examine whether changes in the expression of genes in pathway are seen. We found that there was no change in the expression of *daf-2*/IGFR, *daf-16*/FOXO, *aak-2*/AMPK, *eak-4*, or *akt-2* (Table S4). However we did find that levels of the *age-1* PI3-kinase are reduced almost 76% and levels of *akt-1* are reduced almost 70% compared to N2 while levels of the *daf-18*/PTEN tumor suppressor, which normally inhibits signaling through the PI3-kinase signaling pathway, is reduced almost 95% compared to wild-type animals (Table S4). Despite the observed changes in the expression of genes in the PI3-kinase signaling pathway, there is likely little net effect on the regulation of downstream targets by the pathway as we failed to observe differences in DAF-16:GFP localization, which would translocate to the nucleus if the pathway was inhibited (Figure 6E).

We then used both the DAVID program and the Panther database both to identify biologic themes within the up-regulated and down-regulated genes by testing for over-represented gene

classes based on structural and functional annotations and to visualize the gene classes seen in both groups of genes (Figure S7 and Table S5) [60], [61]. Within the up-regulated set, we found that genes involved in tyrosine metabolism and neuropeptide signaling were strongly over-represented (7–10 fold) (Table S5). Specifically, we found that every gene in the tyrosine degradation pathway is up-regulated in the *tatn-1(qd182)* mutant suggesting that the altered metabolism is detected and leads to a compensatory change in expression of the pathway (Table S4). The significance of the changes in neuropeptide signaling gene expression is currently unclear, but could suggest that impaired tyrosine metabolism or the resulting increased in AAK-2/AMPK activity produces direct changes in neuronal activity or that these changes could be the direct downstream effectors responsible for the *tatn-1* phenotypes. Graphically, we saw a greater percentage of genes which were expressed in the extracellular compartment and had catalytic or receptor activity among the up-regulated genes compared to those that were down-regulated in the *tatn-1* mutants (Figure S7). In contrast, within the down-regulated genes, we identified over-representation of a broad range of genes involved in germline development, cell cycle, DNA replication, and larval development (Table S5). Further, these genes were more likely to be expressed in the intracellular compartment and to have regulatory effects on translation or enzyme activity (Figure S7). The expression changes in genes involved in cell cycle regulation and development could perhaps account for the developmental delay observed in the *tatn-1(qd182)* mutant compared to N2 (Figure S4).

Given the requirement we found for *daf-16/FOXO* for aspects of the *tatn-1* phenotypes, we used Gene Set Association Analysis (GSAA) to test for enrichment of genes known to be regulated by *daf-16/FOXO* in the context of *daf-2/IGFR* signaling [62], [63]. Via this approach, we found

both the up-regulated and down-regulated daf-16/FOXO target genes identified by Murphy et. al. to be enriched within the tatn-1(qd182) transcriptome (Figure 7A). This suggests that the expression of a subset of daf-16/FOXO target genes is altered by changes in tyrosine metabolism.

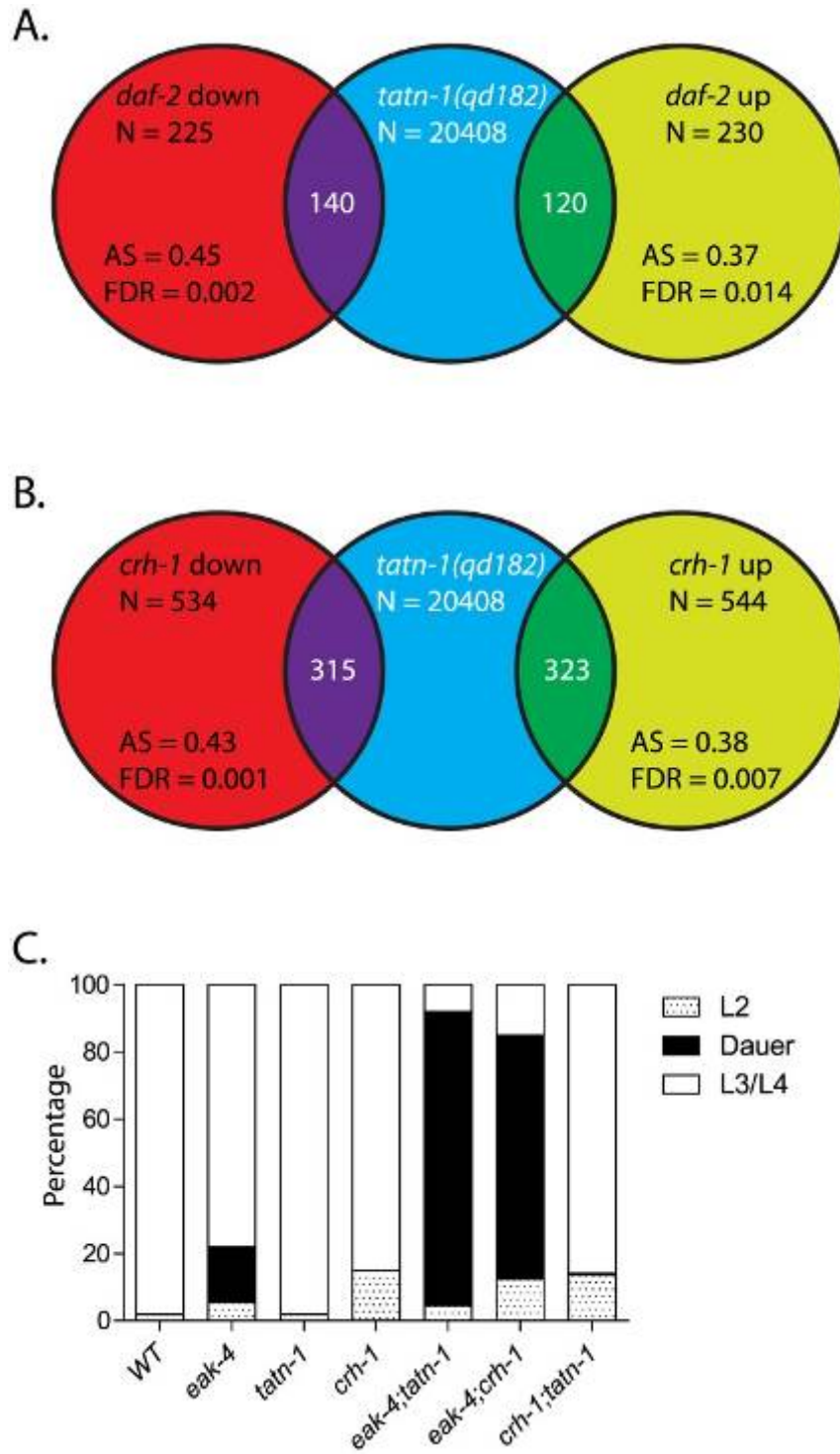


Figure 73. *tatn-1* mutants and *crh-1*/CREB mutants share gene expression profiles and effects on dauer formation

(A) Shot-gun whole transcriptome sequencing (RNA seq) was used to characterize and measure the transcriptome of N2 and *tatn-1(qd182)* mutants. From these experiments a total of 20,408 mRNA and other RNA transcripts were detected. To test for evidence of a *daf-16/FOXO* gene expression signature in the *tatn-1(qd182)* mutants Gene Set Association Analysis (GSAA) was used to determine whether the expression of *daf-16/FOXO* target genes regulated in the context of *daf-2/IGFR* signaling are associated with the *tatn-1(qd182)* mutant gene expression profile. GSAA calculates a differential expression score for each gene in the entire 20,408 gene RNA-seq dataset, and then uses a running weighted Kolmogorov-Smirnov test to examine association of an entire gene set with each phenotypic class. The strength of the association is measured by the association score (AS) where positive scores indicate association of the gene set with the phenotype, and statistical significance is measured by a false discovery rate (FDR) that is adjusted for multiple testing. From 225 genes down-regulated in *daf-2/IGFR* mutants, 140 showed association with the *tatn-1(qd182)* profile, and from 230 genes up-regulated in *daf-2/IGFR* mutants, 120 showed evidence of association by GSAA analysis. AS represents the association score with positive values indicating association, and FDR represents the false discovery rate for the association. (B) To test for evidence of a *crh-1/CREB* gene expression signature in the *tatn-1(qd182)* mutants Gene Set Association Analysis (GSAA) was used to determine whether the expression of *crh-1/CREB* target genes identified through microarray studies using wild-type and *crh-1* mutant worms associate with the *tatn-1(qd182)* expression profile. From 534 genes down-regulated in *crh-1/CREB* mutants, 315 showed evidence of association, and from 544 genes up-regulated in *crh-1/CREB* mutants, 323 showed evidence of association by GSAA analysis. AS represents the association score with positive values indicating association, and FDR represents the false discovery rate for the association. (C) *crh-1/CREB* mutants enhance dauer formation by *eak-4* mutants but not by *tatn-1* mutants.

Since our genetic studies suggested the involvement of a *daf-16*-independent pathway, we also used GSAA to test whether target genes recently identified for the CREB transcription factor *crh-1* are enriched in the *tatn-1(qd182)* mutant [53]. We chose to focus on *crh-1* because recent work has demonstrated that *crh-1/CREB* lies downstream of *aak-2/AMPK* [53]. *crh-1/CREB* and *aak-2/AMPK* are mechanistically linked because AAK-2 directly phosphorylates and inactivates the *crh-1/CREB* coactivator *crtc-1*, and as a result both *aak-2/AMPK* over-expressing and *crh-1/CREB* mutant animals are long-lived and share gene expression profiles [53]. We found that in the *tatn-1(qd182)* mutants, there is differential expression of both genes up-regulated and genes down-regulated in *crh-1/CREB* mutants (Figure 7B). This suggests that altered tyrosine metabolism could lead to changes in *crh-1* target gene expression and could suggest a role for *crh-1/CREB* in the *tatn-1* phenotypes. To test for *crh-1/CREB* involvement, we combined the *crh-1(tz2)* null allele with *tatn-1* and *eak-4* and examined the effects on dauer formation. We found that *crh-1* showed a similar interaction as *tatn-1* with *eak-4*, but did not promote dauer formation by the *tatn-1* mutant (Figure 7C). Together these findings suggest that *tatn-1* mutants share phenotypes and gene expression profiles with *crh-1/CREB* mutants and

could be consistent with *crh-1*/CREB acting as an additional downstream effector of the response to impaired tyrosine metabolism.

A.2.7 Tyrosine aminotransferase expression is controlled by diet and environment

In vertebrates, tyrosine aminotransferase has been reported to be an insulin target gene with insulin treatment leading to reduced expression [32]–[35], [38]. As a result, we asked whether *tatn-1* could also be regulated by *daf-2*/IGFR signaling in worms. To test the effects of *daf-2* signaling on *tatn-1* expression, we generated transgenic worms with an integrated transgene expressing a TATN-1:GFP fusion protein under the control of the *tatn-1* promoter. This transgene rescues the *tatn-1(baf1)* mutation and blocks dauer formation by *eak-4(mg348)*; *tatn-1(baf-1)* mutants, which demonstrates that the fusion protein is both functional and expressed in the correct anatomical locations (Figure 8A).

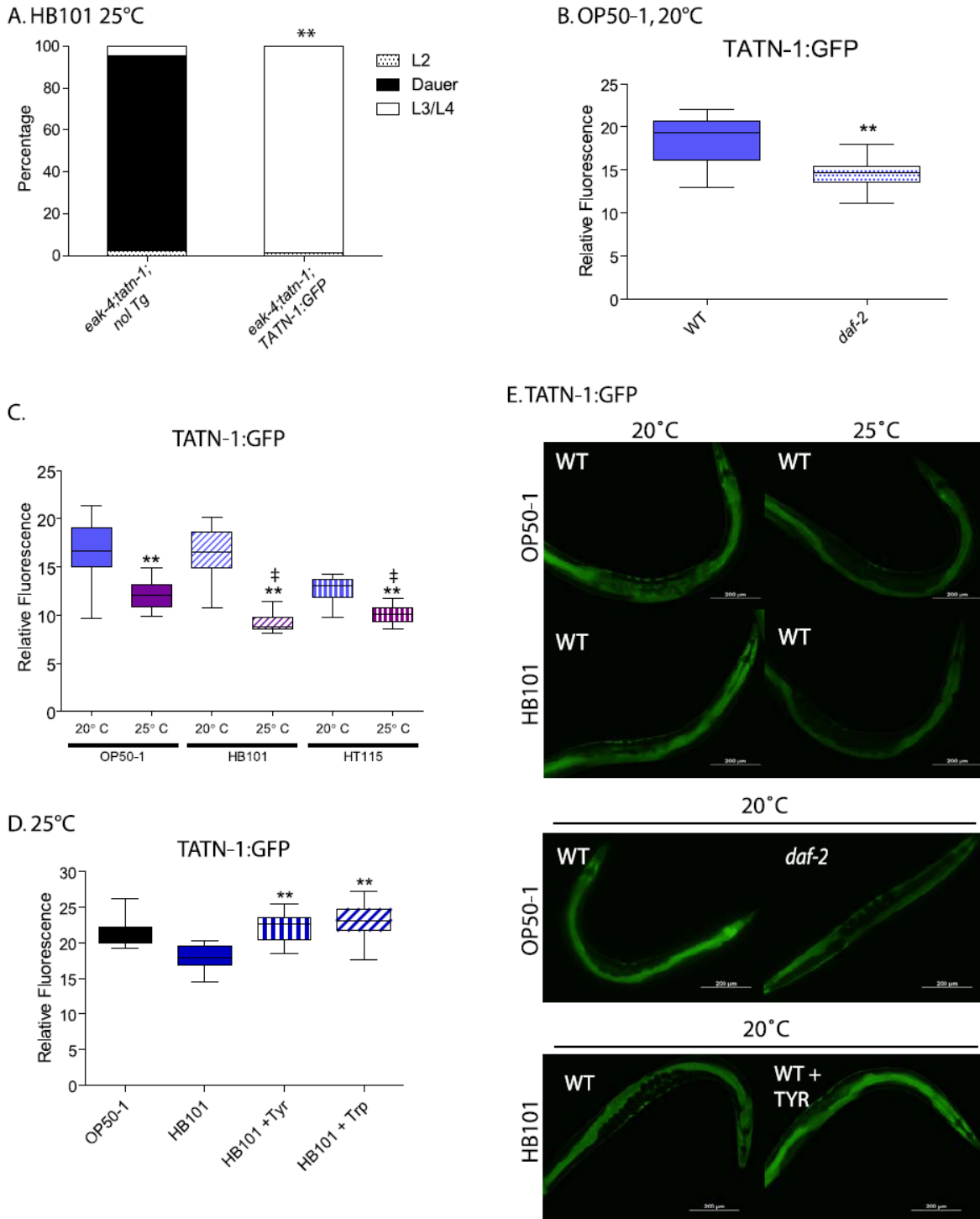


Figure 74. Control of TATN-1 protein expression by *daf-2*/IGFR signaling, diet and temperature

(A) Rescue of *tatn-1* mediated dauer arrest by a *tatn-1*:*tatn-1* cDNA:GFP transgene (*baf1s131*). (B) *daf-2* signaling positively regulates TATN-1:GFP expression. Box and whiskers plot showing comparison of GFP fluorescence between day 1 adult wild-type and *daf-2*(*e1368*) mutants expressing the TATN-1:GFP transgene and grown on OP50-1 bacteria. N\$15 worms, ** $p < 0.001$ by t-test. (C) Bacterial food source and temperature regulate TATN-

1:GFP expression. Wild-type worms expressing the TATN-1:GFP transgene were grown on the indicated bacteria until adulthood and then either kept at 20uC or shifted to 25uC overnight.

GFP fluorescence representing the TATN-1:GFP fusion protein is observed in the intestine and hypodermis of worms ([Figure 8E](#)). When we crossed the transgene into the *daf-2(e1368)* mutant, and we found that the presence of the *daf-2/IGFR* mutation led to a 20% decline in GFP expression in adult worms grown on OP50-1 at 20° ([Figure 8B](#) and [Figure 8E](#)). This is consistent with *daf-2/IGFR* signaling acting positively to promote TATN-1 expression in adult worms. Interestingly, the effect of *daf-2/IGFR* signaling on TATN-1 expression likely occurs either at the translational or protein stability level because Q-PCR experiments demonstrated almost a 50% increase in *tatn-1* mRNA expression in the *daf-2* mutant animals ([Figure S8](#)). As a result of the divergent regulation of *tatn-1* mRNA and protein levels, we focused on TATN-1:GFP expression in our subsequent experiments.

Beyond *daf-2/IGFR* signaling, we found that both diet and environmental temperature affected TATN-1 levels to a similar or even greater degree. Specifically, adult worms grown on OP50-1, HB101, or HT115 show decreases in TATN-1:GFP expression when shifted from 20°C to 25°C for 24 hours with worms grown on OP50-1 showing a 26.2% decrease, on HB101 a 44.7% decrease, and on HT115 a 24.2% decrease ([Figure 8C](#) and [Figure 8E](#)). Further, we found that the OP50-1 fed worms showed greater TATN-1:GFP expression compared to HB101 and HT115 fed worms. This difference was especially apparent in worms grown at 25°C, due to the variability of GFP intensity seen at 20°C, with HB101 and HT115 fed animals showing a 25.3% and 17.3% decrease, respectively, compared to OP50-1 fed worms ([Figure 8C](#) and [Figure 8E](#)).

The effects of diet on TATN-1:GFP expression suggests that the *E. coli* bacterial strains vary in nutrient composition in a way that can be detected by the worms. Prior work has demonstrated that protein is the primary component of these bacteria but that the overall protein levels are not

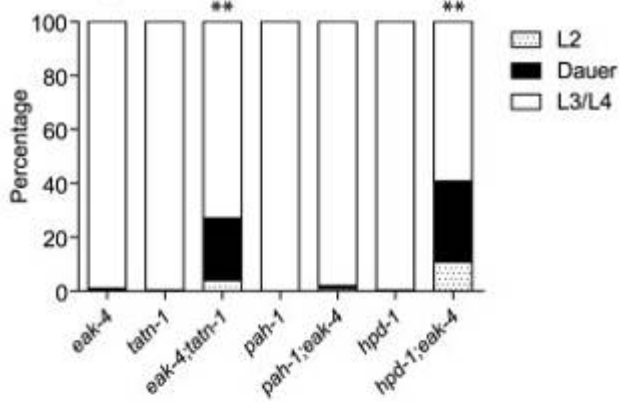
significantly different between strains [64]. However, this work also suggested that specific amino acids could vary between the strains and account for differences in fat content in worms fed each strain. Specifically, *pept-1* mutants, which lack an intestinal peptide transporter, fail to show the expected differences in fat content when fed different bacterial strains [64]. In vertebrates, tyrosine aminotransferase expression is controlled by dietary amino acid intake, most notably for tryptophan [65]–[67]. To test whether dietary amino acid intake could affect TATN-1:GFP expression, we supplemented HB101 spotted NGA plates spotted with either tyrosine or tryptophan at a final concentration of 1 mg/mL, and compared TATN-1:GFP expression to worms fed HB101 alone or OP50-1. This concentration is 8 times the level found in standard NGA media (0.125 mg/mL). We found that the addition of tyrosine or tryptophan increases the GFP expression level in HB101 fed worms up to that seen in worms grown on OP50-1 (Figure 8D and Figure 8E). Together these data demonstrate that TATN-1 levels are dynamic and under the control of both *daf-2*/IGFR signaling as well as dietary and environmental cues. Importantly many of these signals that control TATN-1 expression also influence dauer formation suggesting that *tatn-1* could be a regulated modulator of *daf-2*/IGFR signaling and developmental decisions.

A.2.8 Tyrosine mediates the effects of *tatn-1* mutations

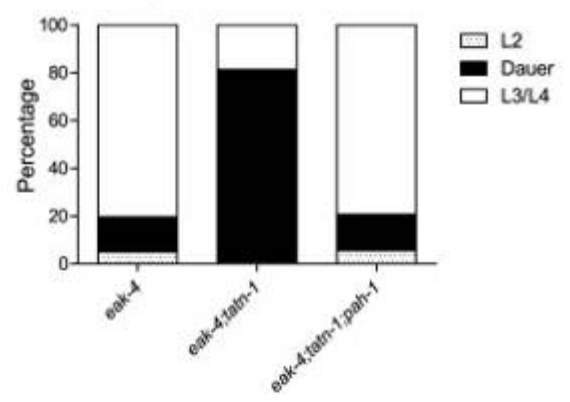
Since TATN-1 is the first enzyme in the tyrosine degradation pathway, decreased activity should both increase the levels of tyrosine and also decrease the levels of the downstream metabolites (Figure 1B). The *tatn-1* mutant phenotypes could be a direct result of changes in the level of a particular metabolite. For example, elevated fumarate levels are known promote hypoxia inducible factor (HIF) activity in certain renal cancers [68]. Alternately, *tatn-1* could have a

novel function that is independent of its metabolic activity. For example, subunits of the phenylalanine hydroxylase enzyme are known to have an additional, non-enzymatic role as a transcriptional co-activator [69]. To explore whether either of these models accounts for the *tatn-1* phenotypes, we tested for interactions between *eak-4* and mutant alleles of other enzymes in the tyrosine degradation pathway (Figure 1B) by constructing *pah-1; eak-4* and *hpd-1; eak-4* mutants. These mutants lack *pah-1*, which encodes the enzyme phenylalanine-4-hydroxylase that converts phenylalanine into tyrosine, or *hpd-1*, which encodes 4-hydroxyphenylpyruvate dioxygenase and catalyzes the step immediately downstream of *tatn-1* [39], [43], [70]. We found that *pah-1* did not enhance dauer arrest by the *eak-4* mutants (Figure 9A) whereas both *tatn-1* and *hpd-1* increased dauer formation. Lower numbers of *eak-4; tatn-1* dauers were seen because the experiment was scored after 3 days due to the slower development of the *hpd-1* mutant. Additionally, when we used the *pah-1* mutant to block the synthesis of tyrosine in a *tatn-1; eak-4* mutant, we found that this reduced dauer formation (Figure 9B). These results suggested that the effects of *tatn-1* on dauer formation were directly linked to the metabolic effects of *tatn-1*, and that the accumulation of tyrosine instead of deficiency of a downstream metabolite could be responsible for the *tatn-1* phenotype.

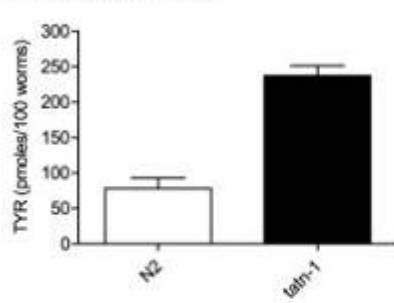
A. HB101, 25°C



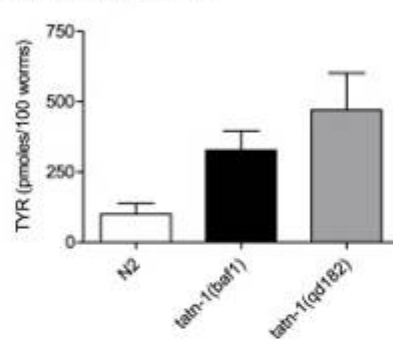
B. HB101, 25°C



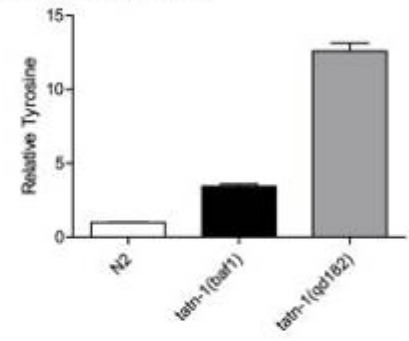
C. HB101, 25°C



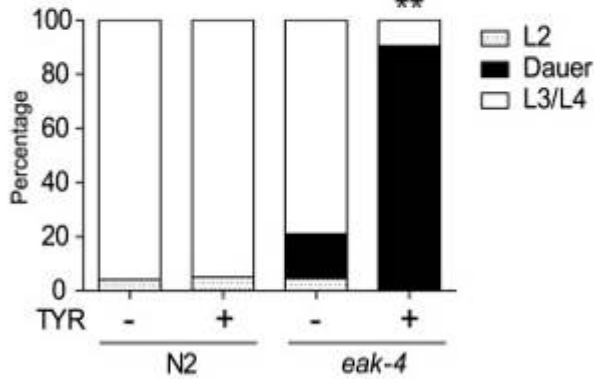
D. HB101, 25°C



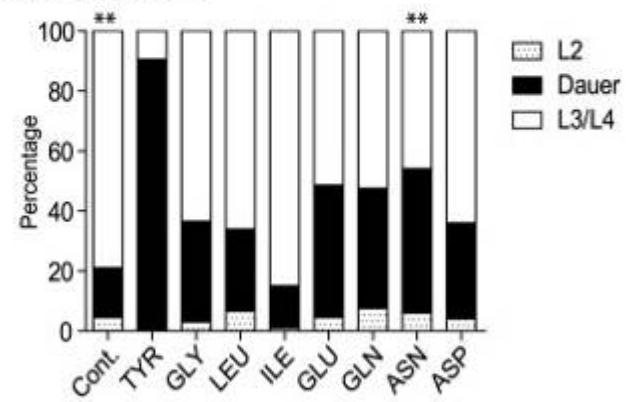
E. HB101, 25°C



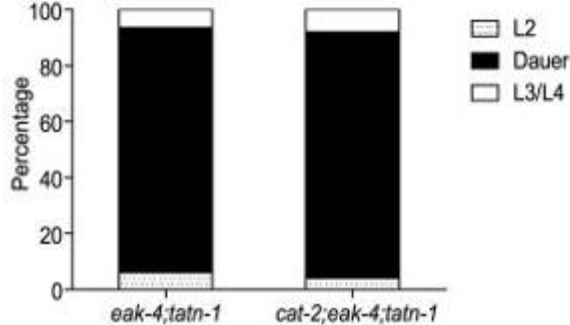
F. HB101, 25°C



G. HB101, 25°C



H. HB101, 25°C



I. HB101, 25°C

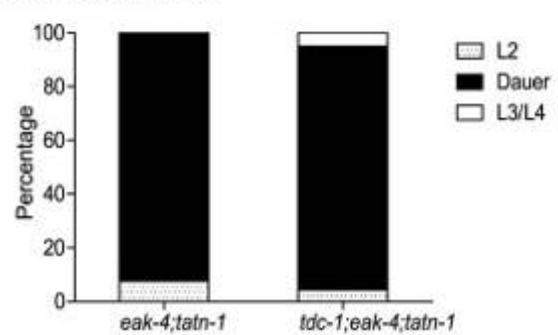


Figure 75. *tatn-1* acts by increasing tyrosine levels

(A) Both *tatn-1* and *hpd-1* mutations augment dauer arrest by *eak-4(mg348)* mutants after three days at 25°C, whereas a *pah-1* mutation does not. ** p,0.001 for comparisons between *eak-4* and *eak-4; tatn-1*, and *hpd-1; eak-4* by Fisher's exact test. (B) Inhibiting tyrosine synthesis with the *pah-1* mutation reduces dauer formation by *eak-4; tatn-1* mutants. (C) *tatn-1(baf1)* has a higher concentration of tyrosine compared to wild type N2. The bars represent the mean tyrosine concentration from four independent samples, and the error bars show the standard error of the mean. ** p,0.001 by t-test. (D) *tatn-1(qd182)* and *tatn-1(baf1)* have higher tyrosine levels compared to wild type N2. (E) *tatn-1(qd182)* has higher tyrosine levels than N2 and *tatn-1(baf1)* when the measured tyrosine levels are normalized to the levels of nonaromatic amino acids in each sample. (F) Treatment of *eak-4(mg348)* mutants but not N2 with tyrosine results in dauer arrest. ** p,0.001 for comparison of *eak-4 +* and *- tyrosine* using Fisher's exact test. (G) Tyrosine (1 mg/mL) is more potent than other amino acids in producing dauer arrest by *eak-4(mg348)* mutants. ** p,0.001 for comparison between *eak-4* vs *eak-4+tyrosine* and *eak-4+tyrosine* and *eak-4+asparagine* using Fisher's exact test. (H) Impaired dopamine synthesis in *cat-2(e1112)* mutants does not block the effect of *tatn-1* on dauer formation. (I) Impaired tyramine and octopamine synthesis in *tdc-1(ok914)* mutants does not block the effect of *tatn-1* on dauer formation.

As a result, we measured the levels of amino acids in wild-type N2, *tatn-1(baf1)*, and *tatn-1(qd182)* larval animals grown at 25°C on HB101 plates by liquid chromatography mass spectrometry (LC-MS/MS). We found that wild-type N2 worms contained an average of 78.1 pmol of tyrosine per 100 worms whereas *tatn-1(baf1)* worms contained 237.4 pmol per 100 worms (Figure 9C). Hence the *tatn-1(baf1)* mutation produced a roughly three fold increase in tyrosine levels in the mutant animals. Further to compare the effects of *tatn-1(qd182)* on tyrosine levels compared to *tatn-1(baf1)*, we measured tyrosine levels in additional samples grown and prepared in parallel. We found in these samples that wild-type N2 worms contained an average of 99.6 pmol of tyrosine per 100 worms, *tatn-1(baf1)* contained an average of 327.2 pmol per 100 worms, and *tatn-1(qd182)* contained an average of 470.2 pmol per 100 worms, which is an 43.7% increase over *tatn-1(baf1)* (Figure 9D). However, we noted that the *tatn-1(qd182)* worms were smaller than N2 or *tatn-1(baf1)* and the levels of many other amino acids measured in parallel were lower in *tatn-1(qd182)* compared to *tatn-1(baf1)*. This suggested that the *tatn-1(qd182)* samples may have contained less overall biomass, and hence our normalization to worm counts alone may underestimate the effect of the *tatn-1(qd182)* mutation on tyrosine levels. To correct for this difference, we normalized tyrosine levels to the levels of all non-aromatic amino

acids in the samples with the assumption that the net effect of these mutations on the levels of these amino acids is neutral. After normalization, we found that *tatn-1(baf1)* produced a 3.4 fold increase in tyrosine levels compared to N2 whereas *tatn-1(qd182)* produced a 12.6 fold increase compared to N2, which is also a 3.7 fold increase over *tatn-1(baf1)* levels ([Figure 9E](#)). These findings demonstrate that both *tatn-1* alleles increase tyrosine levels compared to wild-type animals, and that the stronger phenotypes of the *tatn-1(qd182)* allele are likely due to the further increases in tyrosine levels observed.

To directly test whether elevated tyrosine levels are responsible for the *tatn-1* phenotype, we treated worms with exogenous tyrosine cast into the NGA plates at 1 mg/mL. This treatment results in tyrosine levels in the worms that are elevated compared to untreated animals, but lower than those seen in the *tatn-1* mutants ([Figure S9](#)). We found that supplementation had no effect on the development of wild-type worms but lead to dauer arrest by the *eak-4* mutants ([Figure 9F](#)). These results directly demonstrate changes in tyrosine levels alter the development of *eak-4* mutant worms and are responsible for the *tatn-1* phenotype.

Amino acids are known to antagonize insulin actions in vertebrates, so our results could represent either the non-specific effects of any amino acid or a tyrosine-specific effect [[71](#)], [[72](#)]. To test these possibilities we directly compared the ability of a variety of amino acids to enhance dauer formation by *eak-4* mutants. We grew *eak-4* mutants on HB101 spotted NGA supplemented with tyrosine, glycine, leucine, isoleucine, glutamate, glutamine, asparagine, or aspartate, each at the concentration of 1 mg/mL. Since tyrosine is the largest of these amino acids, this resulted in worms being treated with higher molar equivalents of the other amino acids compared to tyrosine. We found that while other amino acids do increase the formation of dauers by *eak-4* mutants, none was as potent as tyrosine ([Figure 9G](#)). This suggests that the effect on

dauer formation shows selectivity for the presence of tyrosine. The effects of tyrosine and to a lesser extent the other amino acids is not due to a toxic effect of the amino acid supplementation as treated worms showed a similar lifespan to untreated worms ([Figure S9](#)).

Besides being a building block for proteins, tyrosine serves as a precursor for the synthesis of catecholamine neurotransmitters. In vertebrates, there is evidence that the levels of tyrosine as a precursor influences the synthesis of these neurotransmitters [\[73\]](#). Hence, one possibility is that *tatn-1* mutations raise tyrosine levels and facilitate its conversion into the neurotransmitters dopamine, octopamine, or tyramine which could produce the observed phenotypes. To test this possibility, we blocked dopamine synthesis with the *cat-2* mutation, which affects the worm tyrosine hydroxylase gene, and we blocked octopamine and tyramine synthesis with the *tdc-1* mutation, which removes the enzyme tyrosine decarboxylase [\[74\]](#), [\[75\]](#). We found that both *cat-2; eak-4; tatn-1* and *tdc-1; eak-4; tatn-1* mutants are similar to *eak-4; tatn-1* mutants with regards to the formation of dauers ([Figure 9H](#) and [Figure 9I](#)). These data demonstrate that excessive synthesis of dopamine, octopamine, or tyramine is not responsible for the *tatn-1* phenotype. Instead tyrosine is directly sensed by the worms and acts as a developmental regulator.

A.3 DISCUSSION

A.3.1 Tyrosine as a modulator of *daf-2* insulin/IGF-1 signaling effects.

Together our results identify tyrosine and tyrosine aminotransferase activity as a modifier of *daf-2*/IGFR effects in *C. elegans* ([Figure 10](#)). While the control of tyrosine aminotransferase

expression and activity has been extensively studied as a target of insulin signaling in vertebrates [30]–[34], [36], [38], a connection between tyrosine aminotransferase or tyrosine metabolism and insulin action has not been demonstrated. Prior work in *C. elegans* has suggested that the *hpd-1* gene, which encodes 4-hydroxyphenylpyruvate dioxygenase, is repressed in *daf-2* mutants and that knock-down of *hpd-1* by RNAi delayed dauer exit and extended lifespan [39]. However, the mechanism involved has been unclear. Our work shows that both *tatn-1*, and likely *hpd-1*, impact on *daf-2*/IGFR signaling through increasing tyrosine levels in the animal.

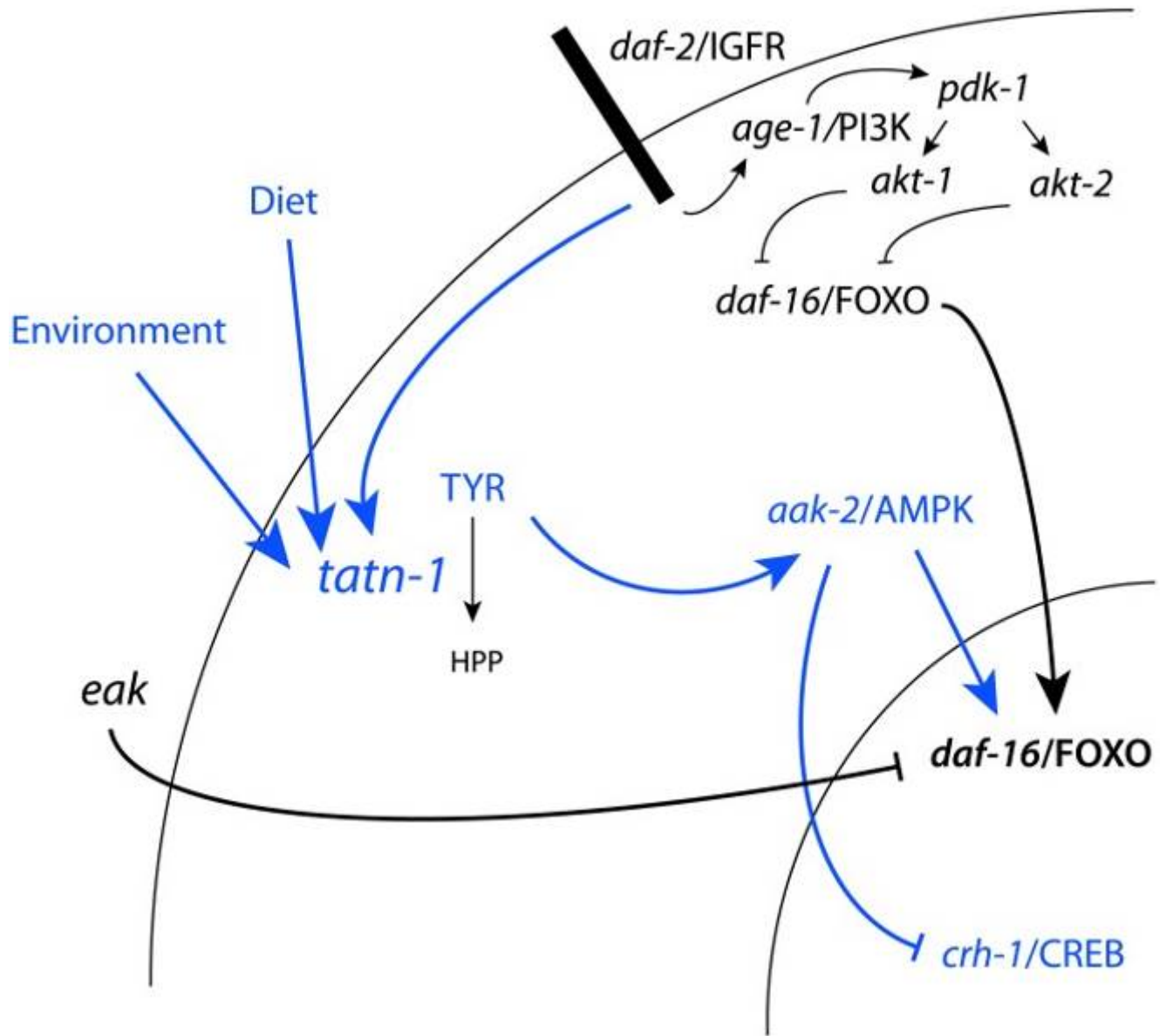


Figure 76. Model for the regulation of TATN-1 expression, tyrosine levels, and the resulting effects of tyrosine effects on cell signaling pathways

Shown is the *daf-2/IGFR* signaling pathway and *eak* genes from Figure 1A with the addition, shown in blue, of the effects of tyrosine identified in this work and the control of TATN-1 expression by *daf-2/IGFR* signaling and by dietary and environmental cues as demonstrated in Figure 8. In summary, worms sense the available diet and environmental temperature and these factors both contribute to the dauer decision and the regulation of TATN-1 protein levels. Conditions which promote the dauer decision also tend to reduce the expression of TATN-1. The reductions in TATN-1 expression lead to reduced removal of tyrosine through degradation and increase free tyrosine levels in the animal. These increases in tyrosine activate *aak-2/AMPK* and disrupt the effects of normal *daf-2/IGFR* signaling through positive effects on *daf-16/FOXO* and perhaps inhibitory effects on *crh-1/CREB*. The effects of tyrosine are particularly pronounced when the *daf-2/IGFR* pathway is compromised, such as through mutations

in the *daf-2/IGFR* gene or the *eak* genes which lie in a parallel pathway. This may be due to further reductions in *TATN-1* expression or reductions in inhibitory regulators of *daf-16/FOXO* activity.

We find the effects of tyrosine on *daf-2/IGFR* signaling to be complex with roles for both the *daf-16/FOXO* transcription factor and the *aak-2/AMPK* seen ([Figure 10](#)). One way that high tyrosine levels could interact with *daf-2/IGFR* signaling would be for tyrosine to somehow activate *aak-2/AMPK*. AMP kinases are a known regulator of both *daf-16* and the vertebrate homolog FOXO3 ([51](#)), ([76](#)). AMPK regulates FOXO transcriptional activity through the phosphorylation of up to six sites on these proteins. In our work, *aak-2/AMPK* mutations suppress the dauer promoting effects of *tatn-1* mutations, treatment of worms with the AMPK agonist AICAR is able to mimic the effects of tyrosine, and increases in the active phosphorylated form of AAK-2 are seen in the *tatn-1* mutant. These findings demonstrate that elevated tyrosine levels activate *aak-2/AMPK* which could then phosphorylate *daf-16/FOXO*. This phosphorylation event could then interfere with the inhibitory effects of an intact *daf-2/IGFR* pathway on *daf-16/FOXO* activity. Further work would be needed to test this model, and the ability of mutants lacking *aak-2/AMPK* or *daf-16/FOXO* to still respond to elevated tyrosine levels also supports the presence of alternate, currently unknown downstream pathways. These alternate pathways could either lie in parallel to *daf-16/FOXO* or could be the dominant response pathway with *daf-16/FOXO* only playing a permissive role, especially at lower tyrosine levels. One possible alternate pathway involves the CREB transcription factor *crh-1* ([Figure 10](#)). The *crtc-1* co-activator for the CREB transcription factors has been shown to be a target of regulation by *aak-2/AMPK*, and in vertebrates, CRTC co-activators are known to interact with insulin signaling in mediating the hepatic metabolic adaptation to the fed versus fasting state ([53](#)), ([77](#)), ([78](#)). We find that *tatn-1(qd182)* mutants show evidence of *crh-1/CREB*-regulated gene expression, and a *crh-1/CREB* mutant mimics the interaction of *eak-4* and *tatn-1*.

Perhaps elevated tyrosine levels lead to the activation of *aak-2*/AMPK which then results in the activation of *daf-16*/FOXO and inhibition of *crtc-1* and *crh-1*/CREB (Figure 10). The presence of paired downstream pathways could explain the partial requirement for *daf-16*/FOXO, especially at higher tyrosine levels.

Beyond effects on *daf-16*/FOXO and *crh-1*/CREB, elevated tyrosine, especially at high levels, could also have hormetic effects via changing cellular redox status, producing ER stress, or perturbing the protein folding environment [79]. These effects could account for the positive effects of increased tyrosine on longevity, and some of the genes involved in sensing hormetic stresses, such as the HSF-1 ortholog *hsf-1*, also interact with *daf-16*/FOXO and play roles in dauer formation [80]–[82]. Alternately, tyrosine could act via a novel pathway that operates independently of *daf-16*/FOXO or *crh-1*/CREB, especially at higher levels. For example, the vertebrate calcium-sensing receptor, PPAR γ nuclear receptor, and aryl hydrocarbon receptor (Agarwala, Cano et al. 2007) have all been shown to respond to aromatic amino acids, though their connection to insulin action is currently unclear [83]–[85]. The recent finding that Akt and Foxo1 are largely dispensable for the control of hepatic metabolism by insulin in vivo has suggested that FOXO-independent pathways exist and play important roles in metabolic control [86].

Our work also provides insights into the *eak* genes which are known to act via unclear mechanisms to reduce *daf-16*/FOXO transcriptional activity while not significantly affecting the subcellular localization of DAF-16/FOXO [26], [27], [29]. We find that beyond enhancing the inhibitory effects of *akt-1* on *daf-16*/FOXO activity, the *eak* genes also suppress the effects of amino acids and AMPK activity on *daf-16*/FOXO activity. Additional work will be needed to

understand if the *eak* genes normally represent a control point where the effects of these metabolic signals on insulin signaling can be enhanced or suppressed.

A.3.2 The complex control of tyrosine aminotransferase.

We find that the regulation of *tatn-1* expression in worms is complex with *daf-2* activity, diet, and environmental conditions each contributing to the expression level (Figure 10). In vertebrates, tyrosine aminotransferase has also been shown to undergo regulation at the transcriptional, translation, and degradation levels in response to hormonal and nutritional cues [66]. We find that *daf-2*/IGFR activity inhibits *tatn-1* gene transcription but raises TATN-1 protein levels. This is consistent with work in vertebrates showing that insulin shows complex effects on tyrosine aminotransferase expression with actions at both the transcriptional and translational level [30]–[34],[36], [38]. Nutritional cues appear to also be an important regulator because we find that the *E. coli* strain used as food has a powerful effect on the expression of *tatn-1* and these effects parallel the effects of the weaker *tatn-1(baf1)* allele on dauer formation. In rats, the activity of hepatic tyrosine aminotransferase varies several-fold during the day with a peak during the evening and nadir in the early morning [87]. Studies of the cyclic variation have demonstrated that dietary protein intake is a prime inducer of tyrosine aminotransferase levels [65]. Feeding animals a protein-free diet results in a constant low level of tyrosine aminotransferase, whereas feeding animals protein meals at differing times produces corresponding shifts in enzyme production. Among amino acids, some such as tryptophan are potent inducers of tyrosine aminotransferase expression [66]. The mechanisms accounting for the dietary effects of amino acids on tyrosine aminotransferase are currently unclear. This could suggest a role for additional nutrient sensitive pathways which may well be conserved as we find that both tryptophan and

tyrosine act as *tatn-1* inducers in worms. Finally, we find a novel role for environmental conditions on *tatn-1* expression as lower temperatures promote expression and higher temperatures inhibit it. How changes in temperature translate into the observed effects is unclear but perhaps hormonal changes mediated by the cytochrome P450 *daf-9* and the nuclear hormone receptor *daf-12* or changes mediated by thermosensory neurons are involved [88]. Together this suggests that the control of tyrosine aminotransferase activity, which modulates tyrosine levels, could be controlled via a complex network of internal and external cues. Our finding that changes in tyrosine levels alter both signaling pathways and gene expression patterns could suggest that carefully controlling tyrosine metabolism and ultimately tyrosine levels plays an important role in overall homeostasis (Figure 10).

A.3.3 Aromatic acids in human disease.

Recent work has suggested that levels of specific amino acids, particularly branched chain and aromatic amino acids, could influence insulin sensitivity in people and mice [1]–[6]. While the exact role of aromatic amino acids in metabolic disease is unknown, our results suggest that these could play a causal role in either insulin-resistance or the development of diabetes [89]. Given the complex nature of tyrosine aminotransferase regulation, subtle changes in hormone levels, diet, and perhaps other factors could lead to changes in hepatic tyrosine metabolism and contribute to changes in serum aromatic amino acid levels. There may also be significant changes during the day due to dietary intake or release from internal stores such as muscle. As tyrosine levels increase, it is possible that, as in worms, the increases modify responses to insulin signaling and augment pre-existing insulin resistance in a harmful way (Figure 10). The connection between insulin signaling and tyrosine metabolism could potentially even lead to a

vicious cycle of reduced insulin signaling producing elevated tyrosine levels which then lead to a further reduction in insulin signaling.

Tyrosine aminotransferase has also been found to be a tumor suppressor gene in human hepatocellular carcinoma (HCC) [7]. The human tyrosine aminotransferase gene is located on 16q, which is frequently deleted in HCC, and analysis of tumors reveals that gene deletion or silencing via hypermethylation is common [7]. Consistent with an inhibitory role in the pathogenesis of liver cancer, transfection of HCC cancer cell lines with a tyrosine aminotransferase transgene suppressed malignant behavior such as growth in soft agar and the formation of tumors in nude mice. In these cells, tyrosine aminotransferase expression also acted to inhibit tumor formation via the stimulation of apoptosis, but the exact molecular events are still unclear [7]. Our data would suggest that the activation of AMPK or the downstream effects of AMPK on FOXO transcription factors, such as FOXO3, or CREB would be attractive targets for future study. Alternately, we also saw down-regulation of genes involved in DNA repair so the elevated tyrosine levels could also promote the accumulation of additional cancer promoting mutations (Table S5). Together these findings suggest that extracellular or intracellular tyrosine levels could act as signaling molecules involved in the control of cell growth, differentiation, and physiology.

A.4 MATERIALS AND METHODS

A.4.1 *C. elegans* strains and maintenance

All *C. elegans* strains were propagated on standard nematode growth agar (NGA) plates containing streptomycin (200 µg/mL) and spotted with OP50-1, as previously described [90].

For specific experiments, worms were fed HB101, OP50, or HT115 *E. coli* strains using NGA containing streptomycin (HB101) or no antibiotics (OP50 and HT115).

The following *C. elegans* mutants were obtained from the *C. elegans* Genetics Center, which is supported in part by NIH Office of Research Infrastructure Programs (P40 OD010440): *daf-16(mgDf50)* I, *cat-2(e1112)* II, *pah-1(ok687)* II, *tdc-1(ok914)* II, *crh-1(tz2)* III, *daf-2(e1368)* III, *hpd-1(ok1955)* III, *unc-119(ed3)* III, *akt-1(mg144)* V, *akt-1(mg306)* V, *aak-2(gt33)* X, *akt-2(ok393)* X, *daf-12(rh61rh411)* X, *pdk-1(mg142)* X, *sgk-1(ok538)* X, *muIs84[pAD76(sod-3::GFP)]*, *lpIs14 [daf-16f::GFP+unc-119(+)]*, and *lpIs12 [daf-16a::RFP+unc-119(+)]*. *tatn-1(baf1)* X has been described previously, and *tatn-1(qd182)* was identified in an unrelated mutagenesis screen and is a gift from Daniel Pagano and Dennis Kim [43], [44]. *muIs109[daf-16::GFP]* X has been described previously and is a gift from Malene Hansen [59]. *daf-16(mgDf47)*, *hsd-1(mg433)* I, *eak-3(mg344)* III, *eak-4(mg348)* IV, *eak-7(tm3188)* IV, *sdf-9(mg337)* V have been described previously [26]–[28], [91]. Double and triple mutants were generated by standard genetic crosses, and the genotypes of strains were confirmed by PCR using oligos which detect gene deletions or RFLP's associated with the mutation ([Table S6](#)). Throughout this work *tatn-1* is implied to refer to the *tatn-1(baf1)* allele except specifically as noted otherwise.

A.4.2 Dauer assays

Worm embryos were isolated by sodium hypochlorite treatment, and eggs were transferred to plates, and grown at the indicated temperature in a designated incubator. The plates were scored two or three days later under a dissecting microscope for the presence of L2, dauer, and L3/L4 and older worms. We conducted control experiments to determine the robustness and reproducibility of visual scoring by having several scorers evaluate a series of still images and corresponding movies of larvae of different developmental stages. We then compared the correlation between the scorers for the entire series via the use of a kappa statistic [92]. These experiments indicated that scoring was consistent between raters within the lab with all comparisons showing “substantial” to “almost perfect” agreement (Table S7) [92].

For each assay, approximately 100 worms were scored from each of two to three plates set up in parallel for each genotype used in an experiment. This resulted in 200 to, more typically, 300 animals being scored for each genotype within an experiment. Each experiment was repeated at least once with comparable results, which resulted in between 400–600 worms being scored per genotype in total. The percentages of each stage were graphed using Prism5 software, and the graphs show pooled data from a single trial. To perform pairwise comparisons between mutant strains, a contingency table was set up using the counts for L2, dauer, and L3/L4 categories, and p-values were calculated using Fisher's exact contingency test within SAS version 9.3. To determine SDS resistance, worms were washed from plates with 1% SDS, and then incubated for 20 minutes with gentle rocking. Worms were then pelleted and washed with water. Aliquots were scored for survival as demonstrated by movement, and each experiment was repeated at least once. The percentages of living worms were graphed with Prism5.

A.4.3 Lifespan assays

Lifespan assays were conducted as previously described at 20°C using either NGA or RNAi plates containing 50 µM FUDR [93]. Lifespan assays for N2, *tatn-1(baf1)*, *eak-7(tm3188)*, and *eak-7(tm3188); tatn-1(baf1)* used NGA plates spotted with HB101, and worms were grown from eggs at 16°C to minimize larval arrest. Lifespan assays for N2, *tatn-1(baf1)*, *aak-2(gt33)*, and *tatn-1(baf1), aak-2(gt33)* used NGA plates spotted with HB101. Lifespan assays for amino acid treated N2 worms used either NGA plates or NGA plates supplemented with 1 mg./mL tyrosine, glycine, or isoleucine, and then spotted with HB101. Lifespan assays using *daf-2* and *daf-16* RNAi treatment used NGA media supplemented with carbenicillin (50 µg/mL) and isopropyl β-d-thiogalactopyranoside (IPTG, 1 mM). RNAi treatment for *daf-16* was started at egg hatching while *daf-2* RNAi treatment started on day 1 of adulthood with larval development occurring on NGA plates spotted with HB101 at 20°C.

For all lifespan assays three plates containing 40 worms each, for each genotype were set up, as well as an extra plate, with worms to replace worms that had crawled off the plate, bagged, or exploded, to reduce the number of censored events. Prism5 (Graphpad Software) was used to generate graphs and perform log-rank testing for curve comparisons. SAS was used to create lifetables and calculate mean survival.

A.4.4 Amino acid supplementation

Amino acids (Sigma-Aldrich) were dissolved as 45 mg/mL stock solutions in water, and then added to molten NGM to obtain a 1 mg/mL final concentration. These plates were dried and spotted with HB101 before use.

A.4.5 Amino acid analysis

Worms were grown on HB101 spotted NGM plates for two days at 25°C before being washed from the plates and then being rinsed twice with milliQ water. For Figure S9A, NGM plates either with or without 1 mg./mL tyrosine cast into the agar were used to grow the worm culture. To normalize the samples for worm number, a 5 µL aliquot was removed and scored for worm number. Amino acids were then extracted using aqueous methanol and crushing with a mortar and pestle as previously described [94]. The methanol solution was removed by evaporation and the residue stored frozen at -80°C. Amino acid analysis was performed via liquid chromatography tandem mass spectrometry following reconstitution of the residue in 0.1 mL water as described previously for urine [95]. Amino acid content was then either normalized to total worm number in the sample (Figure 9B, Figure 9C, and Figure S9A) or normalized to the levels of individual non-aromatic amino acids and then divided by the average normalized level observed in the wild-type N2 samples (Figure 9D).

A.4.6 AICAR treatment

Aliquots from a 250 mM AICAR solution dissolved in water (Cell Signaling Technology) were spotted onto NGA plates spotted with HB101 to give a final concentration of 0.125 mM 1 hour before eggs were added to the plates. A comparable volume of water alone was used as a negative control.

A.4.7 AMP and ATP measurements

Worms embryos were isolated by sodium hypochlorite treatment from N2 and *eak-4(mg348)*; *tatn-1(baf1)* adults, and the eggs were transferred to NGA plates spotted with HB101. The plates were incubated at 25°C for 24 hours so most of the population was L2 larvae. The worms were washed from plates with water and washed with water to remove bacteria. Nucleotides were then extracted from the worms as previously described [50]. The resulting extract was stored at -80°C until analysis. ATP, ADP, and AMP levels were measured by HPLC with UV detection of individual nucleotides.

A.4.8 Fluorescent imaging

Images of worms were obtained with a BX51 fluorescence microscope and quantified using ImageJ software as previously described [44].

A.4.9 Quantitative RT-PCR

For *sod-3* expression, worm embryos were isolated by sodium hypochlorite treatment, and eggs were transferred to NGA plates spotted with HB101 and incubated at 25°C for 24 hours. The worms were washed from plates in water, pelleted by centrifugation, washed with water, and frozen for storage. RNA extraction, reverse transcription, and quantitative PCR were performed as previously described [27], [44]. The geometric mean level of the control genes *pmp-3*, *cdc-42*, and *Y45F10D.4* were used to normalize the samples, and the relative levels of *sod-3* expression were determined using the $2^{-\Delta\Delta C_t}$ approach [96], [97].

For *tatn-1* expression, N2 and *daf-2(e1368)* embryos were isolated by sodium hypochlorite treatment, and eggs were transferred to S-basal to arrest the worms at the L1 stage. L1 larvae were added to NGA plates spotted with OP50-1 and the plates were incubated at 20°C for 3 days. Adult worms were washed from plates and RNA was isolated as described above. The geometric mean level of the control genes *pmp-3*, *cdc-42*, and Y45F10D.4 were used to normalize the samples, and the relative levels of *tatn-1* expression were determined using the $2^{-\Delta\Delta C_t}$ approach [96], [97].

The oligos used to detect *pmp-3*, *cdc-42*, and Y45F10D.4 have been previously described [98].

The expression of *sod-3* was detected using the oligos 5'-

CCAACCAGCGCTGAAATTCAATGG-3' and 5'-GGAACCGAAGTCGCGCTTAATAGT-3'

[99]. The expression of *tatn-1* was detected using 5'-CTTGATCAGAGAAGAATCAGTG-3' and

5'-GAGTGTTGATTGAAGTTGCG-3'. These oligos were designed to cross intron-exon

boundaries using the PerlPrimer program [100].

A.4.10 Whole transcriptome RNA sequencing

N2 wild-type control and *tatn-1(qd182)* mutant worms were synchronized via the use of

hypochlorite treatment and grown on HB101 spotted NGM plates at 25°C for 2 days. These

conditions and time point correspond to the conditions used for the amino acid analysis

separately performed using these strains. The worms were washed from the plates and were then

washed twice with miliQ water. The worm pellet was then suspended in QIAzol lysis reagent

(Qiagen, Valencia, CA) and frozen at -80°C. Total RNA was isolated using the Qiagen

miRNeasy mini kit and the RNA yield was measured by spectrophotometry. Total RNA was sent

to Expression Analysis (Durham, NC) for analysis including bioanalyzer electrophoresis to ensure RNA quality followed by library preparation using the Illumina TruSeq RNA sample prep kit. The resulting library was subjected to high-throughput 50 nucleotide paired end sequencing using an Illumina sequencer at a depth of 17 million reads per sample.

The resulting sequence data was clipped using internally developed software from Expression Analysis and matched to the *C. elegans* genome using RSEM [101]. The resulting transcript counts were then normalized using the upper quartile normalization approach [102].

Differentially expressed genes were then identified through the use of ANOVA testing and genes with a FDR score of 5% or lower were considered to be differentially expressed. This led to the identification of 4622 genes as being differentially expressed (890 up-regulated and 3732 down-regulated) between *tatn-1(qd182)* and wild-type N2.

Over-represented gene classes were identified in the up-regulated and down-regulated genes through the use of DAVID [60]. Analysis of the transcriptome data for *daf-16/FOXO* and *crh-1/CREB* regulated genes was performed using the Gene Set Association Analysis for RNA-seq program (available at <http://gsaa.unc.edu/login/index.html>) [63]. GSAA calculates a differential expression score for each gene in the entire RNA-seq dataset, 20408 genes in all, and then uses a running weighted Kolmogorov-Smirnov test to examine association of an entire gene set with each phenotypic class. The strength of the association is measured by the association score (AS) where positive scores indicate association of the gene set with the phenotype, and statistical significance is measured by a false discovery rate (FDR) that is adjusted for multiple testing. The *daf-16/FOXO* regulated genes were from previously published microarray data from Murphy et. al., and the *crh-1/CREB* regulated genes were from recently published microarray data from Mair et. al. [53], [62].

A.4.11 Generation of TATN-1:GFP transgenic animals

Clones for the *tatn-1* promoter and cDNA were purchased from Open Biosystems and verified by sequencing [103], [104]. A *tatn-1p:tatn-1 cDNA:GFP* transgene was generated using Gateway cloning and the vector pDEST-MB14 [104]. The resulting transgene or *punc-119cbr*, which contains the *unc-119* gene from *Caenorhabditis briggsae*, was used to bombard HT1593 (*unc-119(ed3)*) as previously described [105], [106]. From bombardment we obtained *bafIs130* from *punc-119cbr*, which carries the *unc-119* gene from *Caenorhabditis briggsae*, and *bafIs131* from the *tatn-1p:tatn-1 cDNA:GFP* transgene [106]. Both transgenes were outcrossed with N2 and then mated with *eak-4(mg348); tatn-1(baf1)* to test for rescue of the dauer formation phenotype. The *bafIs131* transgene was also crossed into a *daf-2(e1368)* mutant to generate *daf-2(e1368); bafIs131*.

A.4.12 Anti-phospho AMPK western blotting

Worm embryos were isolated by sodium hypochlorite treatment, and eggs were transferred to NGA plates spotted with HB101 and incubated at 25°C for 24 hours. For treatment with AICAR, the plate was spotted 1 hour before adding the eggs with aliquots from a 250 mM AICAR stock that was dissolved in water. As a positive control, N2 wild-type worms were grown as above, washed off in S-basal, and then exposed to 10 mM sodium azide in S-basal. This dose of S-basal has been previously shown to result in a 50% decrease in ATP concentrations in treated worms [54]. The worms were washed from plates in water, pelleted by centrifugation, washed with water, and suspended in 1× LDS loading buffer (Invitrogen) before being heated to 70°C in a

Branson sonicator waterbath (Branson) for 30–40 minutes [107]. After heating the samples were centrifuged and the supernatant retained for analysis. The protein levels were measured using the CB-X protein assay kit (G-Biosciences), and 30 µg of protein was run on a 10% Nupage SDS-PAGE gel (Invitrogen) and blotted to a nitrocellulose membrane. Phospho-AAK-2 was detected using a rabbit monoclonal antibody (Cell Signaling Technology #2535), and actin was detected using a rabbit anti-actin antibody (Cell Signaling Technology #4967) followed by detection by an anti-rabbit HRP secondary antibody and visualization using chemiluminescence (Bio-Rad). The resulting X-ray film was scanned and quantified using gel analysis tools in ImageJ [108].

A.5 SUPPORTING INFORMATION

All supporting information can be found in the published manuscript.

Ferguson AA¹, Roy S², Kormanik KN¹, Kim Y³, Dumas KJ³, Ritov VB⁴, Matern D⁵, Hu PJ⁶, Fisher AL⁷. “TATN-1 Mutations Reveal a Novel Role for Tyrosine as a Metabolic Signal That Influences Developmental Decisions and Longevity in *Caenorhabditis elegans*.” *PLoS Genet.* 2013 Dec;9(12):e1004020. doi: 10.1371/journal.pgen.1004020. Epub 2013 Dec 19.

A.5.1 Figure S1

The interaction between *tatn-1* and *eak-4* is modified by bacterial diet. Shown are the effects of HB101, HT115, OP50, or OP50-1 bacterial diets on dauer formation by *eak-4(mg408)*; *tatn-1(baf1)* mutants. These results represent one of two trials, and the shadings represent the percentages of L2, Dauer, or L3/L4 or older animals within each population. ** p,0.001 for

pairwise Fisher's exact contingency tests comparing OP50 versus HB101 or HT115 and OP50-1 versus HB101 or HT115. (EPS)

A.5.2 Figure S2 The *tatn-1(qd182)* allele enhances dauer formation by *eak-4* mutants.

(A) The point mutation in the *tatn-1(qd182)* allele produces a G to E change in a conserved residue of tyrosine aminotransferase as indicated by the arrow. This change is predicted to have an .89% chance of impairing protein function based on analysis using the coding SNP scoring tool available at the Panther database. (B) Enhanced dauer arrest by the *eak-4; tatn-1(qd182)* mutant compared to *eak-4* or *tatn-1(qd182)* alone, or the N2 wild type strain. ** p,0.001 for pairwise Fisher's exact test. (EPS)

A.5.3 Figure S3

Tatn-1 acts independently of the TGF- β signaling pathway. Inhibiting the TGF- β -like signaling pathway involved in dauer formation with mutations affecting *daf-3/SMAD* or *daf-5/Sno* genes does not block dauer formation by the *eak-4; tatn-1* mutants. (EPS)

A.5.4 Figure S4 The effects of the *tatn-1(qd182)* allele on dauer formation depend on *aak-2/AMPK*.

(A) The effects of *tatn-1(qd182)* on dauer formation also require *aak-2*. ** p,0.001 by Fisher's exact test. (B) The *tatn-1(qd182)* allele is likely stronger than *tatn-1(baf1)* because the *tatn-1(qd182)* allele shows delayed development compared to *tatn-1(baf1)* and wild type N2 worms.

The curves show the percentage of adults present at each timepoint after synchronization. (C) SDS selection, which kills animals which have not fully completed dauer development including synthesis of the dauer cuticle and cessation of pharyngeal pumping, reveals a stronger effect of *aak-2*/AMPK mutations on dauer formation by the *eak-4(mg348)*; *tatn-1(qd182)* mutants compared with scoring based on morphology. (EPS)

A.5.5 Figure S5

Tatn-1 mutations do not impair energy production and increase the AMP/ATP ratio. L2 larval wild-type N2 and *eak-4(mg348)*; *tatn-1(baf1)* worms were collected and nucleotides were extracted for measurement using HPLC with UV detection. Shown is the average AMP/ATP ratio for three separately grown worm preparations (N2 mean 0.036 and *eak-4*; *tatn-1* mean 0.029, $p = 0.73$ by t-test). (EPS)

A.5.6 Figure S6. The effects of the *tatn-1(qd182)* allele on dauer formation depend on *daf-16*/FOXO.

(A) Loss of *daf-16* in the *daf-16(mgDf47)* mutant partially inhibits dauer formation by *eak-4(mg348)*; *tatn-1(qd182)* based on morphology, but SDS selection, which kills larvae which have not fully completed dauer development (B) reveals a stronger inhibitory effect of the *daf-16(mgDf47)* mutation on dauer formation. (EPS)

A.5.7 Figure S7

Pie charts representing gene ontology categories of differentially expressed genes in the *tatn-1(qd182)* mutant compared to wild type N2. Genes as being differently expressed were divided into up-regulated and down-regulated groups and then analyzed using the tools within the Panther database. Pie charts were generated for each group using the “biologic process”, “cellular component”, and “molecular function” gene ontology perspectives. (EPS)

A.5.8 Figure S8. *daf-2*/IGFR signaling inhibits the expression of *tatn-1* mRNA.

Measurement of *tatn-1* mRNA levels in N2 and *daf-2(e1368)* mutants reveals that the *daf-2* mutants show a 40–50% increase in *tatn-1* expression compared to N2. Shown are the results of two independent trials using RNA isolated from *daf-2* and N2 adult animals. (EPS)

A.5.9 Figure S9. Tyrosine supplementation raises tyrosine levels but does not affect worm lifespan.

(A) Growth of N2 worms on NGA supplemented with 1 mg./mL tyrosine leads to an increase in tyrosine levels as shown by liquid chromatography and tandem mass spectrometry. The untreated N2 average is 74.3 mmol per 100 worms and the tyrosine treated average is 163.6 mmol per 100 worms, which is a 2.2 fold increase. (B) Lifespan assays performed with N2 worms supplemented with tyrosine, glycine, or isoleucine show no effect of tyrosine supplementation on lifespan compared to untreated N2 animals (Untreated N2 mean survival 19.5 days, tyrosine

treated 20.0 days, glycine treated 19.0 days, and isoleucine treated 21.5 days). The isoleucine treatment produces a small, but consistent effect on worm lifespan in two separate trials. (EPS)

A.5.10 Table S1. Function and human homologs for genes studied.

Table showing the function and human homolog identified using HomoloGene, or Wormbase if not hits were identified, for each of the genes studied. (DOCX)

A.5.11 Table S2. Effects of *tatn-1* on dauer formation.

Excel spreadsheet showing the genetic and dauer formation assay data used to create each panel. (ZIP)

A.5.12 Table S3. Effects of *tatn-1* on longevity.

Excel spreadsheet showing the lifetable analysis for lifespan experiments shown in Figure 2, 3, 5, and 6. (ZIP)

A.5.13 Table S4. Genes differentially expressed between tatn-1(qd182) mutants and N2 worms.

Excel spreadsheet showing genes identified as up-regulated or down-regulated at a 5% false discovery rate through RNA-seq experiments with three tatn-1(qd182) and three wild-type N2 RNA samples. (ZIP)

A.5.14 Table S5

Gene classes identified as enriched via use of the DAVID program. The lists of up-regulated and down-regulated genes were searched for evidence of enriched functional or structure gene classes via use of the DAVID computer program. Shown is an Excel spreadsheet showing the DAVID output for each gene list. (ZIP)

A.5.15 Table S6. List of oligos and enzymes used to genotype progeny of crosses.

Excel spreadsheet containing the oligo sequences and when needed restriction enzymes used to genotype the progeny of crosses involving the listed mutations. For all experiments, multiple rounds of self-fertilization and PCR genotyping were used to identify progeny homozygous for all mutations. (ZIP)

A.5.16 Table S7

Correlation between raters for a set of control images depicting worm larval stages. A group of raters independently viewed a series of 60 images and accompanying movies of larval worms of differing developmental stages in random order. Raters scored each animal as L2 or below, dauer, or L3 or above. Correlation between the raters was determined via the kappa statistic. Note that one rater had never previously worked with *C.elegans* and learned to perform scoring via a brief tutorial prior to scoring the image set. (DOCX)

A.6 ACKNOWLEDGEMENTS

We thank Dennis Kim and Daniel Pagano for sharing the *tatn-1(qd182)* mutant worms, sharing unpublished data, and for discussion of our results and draft manuscripts. We thank Qing Xiong for help with getting started with the GSAA program. We also thank Gordon Lithgow and Arjumand Ghazi for discussions and critical comments, and thank Malene Hansen for her gift of the *muIs109* strain.

A.7 AUTHOR CONTRIBUTIONS

Conceived and designed the experiments: AAF SR YK VBR DM PJH ALF. Performed the experiments: AAF SR KNK YK KJD VBR ALF. Analyzed the data: AAF SR YK KJD VBR DM PJH ALF. Contributed reagents/materials/analysis tools: VBR DM. Wrote the paper: AAF SR DM PJH ALF.

A.8 REFERENCES

1. Newgard CB, An J, Bain JR, Muehlbauer MJ, Stevens RD, et al. (2009) A branchedchain amino acid-related metabolic signature that differentiates obese and lean humans and contributes to insulin resistance. *Cell Metab* 9: 311-326.
2. Wurtz P, Tiainen M, Makinen VP, Kangas AJ, Soininen P, et al. (2012) Circulating Metabolite Predictors of Glycemia in Middle-Aged Men and Women. *Diabetes Care*.
3. Wang TJ, Larson MG, Vasani RS, Cheng S, Rhee EP, et al. (2011) Metabolite profiles and the risk of developing diabetes. *Nat Med* 17: 448-453.
4. Stancakova A, Civelek M, Saleem NK, Soininen P, Kangas AJ, et al. (2012) Hyperglycemia and a Common Variant of GCKR Are Associated With the Levels of Eight Amino Acids in 9,369 Finnish Men. *Diabetes*.
5. Cheng S, Rhee EP, Larson MG, Lewis GD, McCabe EL, et al. (2012) Metabolite profiling identifies pathways associated with metabolic risk in humans. *Circulation* 125: 2222-2231.
6. Wurtz P, Makinen VP, Soininen P, Kangas AJ, Tukiainen T, et al. (2012) Metabolic signatures of insulin resistance in 7,098 young adults. *Diabetes* 61: 1372-1380.
7. Fu L, Dong SS, Xie YW, Tai LS, Chen L, et al. (2010) Down-regulation of tyrosineaminotransferase at a frequently deleted region 16q22 contributes to the pathogenesis of hepatocellular carcinoma. *Hepatology* 51: 1624-1634.
8. Cassada RC, Russell RL (1975) The dauerlarva, a post-embryonic developmental variant of the nematode *Caenorhabditis elegans*. *Dev Biol* 46: 326-342.

9. Riddle DL, Albert PS, Riddle DL, Blumenthal T, Meyer BJ, et al. (1997) Genetic and environmental regulation of dauer larva formation. *C elegans II*. Cold Spring Harbor, NY: Cold Spring Harbor Laboratory Press. pp. 739–768.
10. Hu PJ (2007) Dauer. *WormBook*: 1–19.
11. Fielenbach N, Antebi A (2008) *C. elegans* dauer formation and the molecular basis of plasticity. *Genes Dev* 22: 2149–2165.
12. Riddle DL, Swanson MM, Albert PS (1981) Interacting genes in nematode dauer larva formation. *Nature* 290: 668–671.
13. Kenyon C, Chang J, Gensch E, Rudner A, Tabtiang R (1993) A *C. elegans* mutant that lives twice as long as wild type. *Nature* 366: 461–464.
14. Kimura KD, Tissenbaum HA, Liu Y, Ruvkun G (1997) *daf-2*, an insulin receptor-like gene that regulates longevity and diapause in *Caenorhabditis elegans*. *Science* 277: 942–946.
15. Pierce SB, Costa M, Wisotzkey R, Devadhar S, Homburger SA, et al. (2001) Regulation of DAF-2 receptor signaling by human insulin and *ins-1*, a member of the unusually large and diverse *C. elegans* insulin gene family. *Genes and Development* 15: 672–686.
16. Li W, Kennedy SG, Ruvkun G (2003) *daf-28* encodes a *C. elegans* insulin superfamily member that is regulated by environmental cues and acts in the DAF-2 signaling pathway. *Genes Dev* 17: 844–858.
17. Michaelson D, Korta DZ, Capua Y, Hubbard EJ (2010) Insulin signaling promotes germline proliferation in *C. elegans*. *Development* 137: 671–680.
18. Cornils A, Gloeck M, Chen Z, Zhang Y, Alcedo J (2011) Specific insulin-like peptides encode sensory information to regulate distinct developmental processes. *Development* 138: 1183–1193.
19. Malone EA, Inoue T, Thomas JH (1996) Genetic analysis of the roles of *daf-28* and *age-1* in regulating *Caenorhabditis elegans* dauer formation. *Genetics* 143: 1193–1205.
20. Paradis S, Ruvkun G (1998) *Caenorhabditis elegans* Akt/PKB transduces insulin receptor-like signals from AGE-1 PI3 kinase to the DAF-16 transcription factor. *Genes and Development* 12: 2488–2498.
21. Paradis S, Ailion M, Toker A, Thomas JH, Ruvkun G (1999) A PDK1 homolog is necessary and sufficient to transduce AGE-1 PI3 kinase signals that regulate diapause in *Caenorhabditis elegans*. *Genes and Development* 13: 1438–1452.
22. Morris JZ, Tissenbaum HA, Ruvkun G (1996) A phosphatidylinositol-3-OH kinase family member regulating longevity and diapause in *Caenorhabditis elegans*. *Nature* 382: 536–539.

23. Lin K, Hsin H, Libina N, Kenyon C (2001) Regulation of the *Caenorhabditis elegans* longevity protein DAF-16 by insulin/IGF-1 and germline signaling. *NatGenet* 28: 139–145.
24. Lee RY, Hench J, Ruvkun G (2001) Regulation of *C. elegans* DAF-16 and its human ortholog FKHL1 by the *daf-2* insulin-like signaling pathway. *CurrBiol* 11: 1950–1957.
25. Henderson ST, Johnson TE (2001) *daf-16* integrates developmental and environmental inputs to mediate aging in the nematode *Caenorhabditis elegans*. *CurrBiol* 11: 1975–1980.
26. Zhang Y, Xu J, Puscau C, Kim Y, Wang X, et al. (2008) *Caenorhabditis elegans* EAK-3 inhibits dauer arrest via nonautonomous regulation of nuclear DAF-16/FoxO activity. *Dev Biol* 315: 290-302.
27. Alam H, Williams TW, Dumas KJ, Guo C, Yoshina S, et al. (2010) EAK-7 controls development and life span by regulating nuclear DAF-16/FoxO activity. *Cell Metab* 12: 30-41.
28. Hu PJ, Xu J, Ruvkun G (2006) Two membrane-associated tyrosine phosphatase homologs potentiate *C. elegans* AKT-1/PKB signaling. *PLoS Genet* 2: e99.
29. Dumas KJ, Guo C, Wang X, Burkhart KB, Adams EJ, et al. (2010) Functional divergence of dafachronic acid pathways in the control of *C. elegans* development and lifespan. *Dev Biol* 340: 605-612.
30. Spencer CJ, Heaton JH, Gelehrter TD, Richardson KI, Garwin JL (1978) Insulin selectively slows the degradation rate of tyrosine aminotransferase. *J Biol Chem* 253: 7677-7682.
31. Reshef L, Greengard O (1969) The effect of amino acid mixtures, insulin, epinephrine and glucagon in vivo on the levels of rat liver tyrosine aminotransferase. *Enzymol Biol Clin (Basel)* 10: 113-121.
32. Nitsch D, Boshart M, Schutz G (1993) Activation of the tyrosine aminotransferase gene is dependent on synergy between liver-specific and hormone-responsive elements. *Proc Natl Acad Sci U S A* 90: 5479-5483.
33. Moore PS, Koontz JW (1989) Insulin-mediated regulation of tyrosine aminotransferase in rat hepatoma cells: inhibition of transcription and inhibition of enzyme degradation. *Arch Biochem Biophys* 275: 486-495.
34. Messina JL, Chatterjee AK, Strapko HT, Weinstock RS (1992) Short- and long-term effects of insulin on tyrosine aminotransferase gene expression. *Arch Biochem Biophys* 298: 56-62.
35. Lee KL, Isham KR, Johnson A, Kenney FT (1986) Insulin enhances transcription of the tyrosine aminotransferase gene in rat liver. *Arch Biochem Biophys* 248: 597- 603.

36. Gelehrter TD, Tomkins GM (1970) Posttranscriptional control of tyrosine aminotransferase synthesis by insulin. *Proc Natl Acad Sci U S A* 66: 390-397.
37. Gelehrter TD, Emanuel JR, Spencer CJ (1972) Induction of tyrosine aminotransferase by dexamethasone, insulin, and serum. Characterization of the induced enzyme. *J Biol Chem* 247: 6197-6203.
38. Crettaz M, Muller-Wieland D, Kahn CR (1988) Transcriptional and posttranscriptional regulation of tyrosine aminotransferase by insulin in rat hepatoma cells. *Biochemistry* 27: 495-500.
39. Lee SS, Kennedy S, Tolonen AC, Ruvkun G (2003) DAF-16 target genes that control *C. elegans* life-span and metabolism. *Science* 300: 644-647.
40. Fuchs S, Bundy JG, Davies SK, Viney JM, Swire JS, et al. (2010) A metabolic signature of long life in *Caenorhabditis elegans*. *BMC Biol* 8: 14.
41. Tewari M, Hu PJ, Ahn JS, yivi-Guedehoussou N, Vidalain PO, et al. (2004) Systematic interactome mapping and genetic perturbation analysis of a *C. elegans* TGF-beta signaling network. *MolCell* 13: 469-482.
42. Duchaine TF, Wohlschlegel JA, Kennedy S, Bei Y, Conte D, Jr., et al. (2006) Functional proteomics reveals the biochemical niche of *C. elegans* DCR-1 in multiple small-RNA-mediated pathways. *Cell* 124: 343-354.
43. Fisher AL, Page KE, Lithgow GJ, Nash L (2008) The *Caenorhabditis elegans* K10C2.4 Gene Encodes a Member of the Fumarylacetoacetate Hydrolase Family: A CAENORHABDITIS ELEGANS MODEL OF TYPE I TYROSINEMIA. *J BiolChem* 283: 9127-9135.
44. Ferguson AA, Springer MG, Fisher AL (2010) *skn-1*-Dependent and -independent regulation of *aip-1* expression following metabolic stress in *Caenorhabditis elegans*. *Mol Cell Biol* 30: 2651-2667.
45. Hertweck M, Gobel C, Baumeister R (2004) *C. elegans* SGK-1 is the critical component in the Akt/PKB kinase complex to control stress response and lifespan. *Dev Cell* 6: 577-588.
46. Jensen VL, Albert PS, Riddle DL (2007) *Caenorhabditis elegans* SDF-9 enhances insulin/insulin-like signaling through interaction with DAF-2. *Genetics* 177: 661-666.
47. Narasimhan SD, Yen K, Bansal A, Kwon ES, Padmanabhan S, et al. (2011) PDP-1 links the TGF-beta and IIS pathways to regulate longevity, development, and metabolism. *PLoS Genet* 7: e1001377.
48. Patterson GI, Koweeck A, Wong A, Liu Y, Ruvkun G (1997) The DAF-3 Smad protein antagonizes TGF-beta-related receptor signaling in the *Caenorhabditis elegans* dauer pathway. *Genes Dev* 11: 2679-2690.

49. da Graca LS, Zimmerman KK, Mitchell MC, Kozhan-Gorodetska M, Sekiewicz K, et al. (2004) DAF-5 is a Ski oncoprotein homolog that functions in a neuronal TGF beta pathway to regulate *C. elegans* dauer development. *Development* 131: 435-446.
50. Apfeld J, O'Connor G, McDonagh T, DiStefano PS, Curtis R (2004) The AMPactivated protein kinase AAK-2 links energy levels and insulin-like signals to lifespan in *C. elegans*. *Genes Dev* 18: 3004-3009.
51. Greer EL, Dowlatshahi D, Banko MR, Villen J, Hoang K, et al. (2007) An AMPKFOXO pathway mediates longevity induced by a novel method of dietary restriction in *C. elegans*. *Curr Biol* 17: 1646-1656.
52. Narbonne P, Roy R (2009) *Caenorhabditis elegans* dauers need LKB1/AMPK to ration lipid reserves and ensure long-term survival. *Nature* 457: 210-214.
53. Mair W, Morante I, Rodrigues AP, Manning G, Montminy M, et al. (2011) Lifespan extension induced by AMPK and calcineurin is mediated by CRTC-1 and CREB. *Nature* 470: 404-408.
54. Lagido C, Pettitt J, Flett A, Glover LA (2008) Bridging the phenotypic gap: real-time assessment of mitochondrial function and metabolism of the nematode *Caenorhabditis elegans*. *BMC Physiol* 8: 7.
55. Kwon ES, Narasimhan SD, Yen K, Tissenbaum HA (2010) A new DAF-16 isoform regulates longevity. *Nature* 466: 498-502.
56. Robida-Stubbs S, Glover-Cutter K, Lamming DW, Mizunuma M, Narasimhan SD, et al. (2012) TOR signaling and rapamycin influence longevity by regulating SKN-1/Nrf and DAF-16/FoxO. *Cell Metab* 15: 713-724.
57. Honda Y, Honda S (1999) The *daf-2* gene network for longevity regulates oxidative stress resistance and Mn-superoxide dismutase gene expression in *Caenorhabditis elegans*. *FASEB J* 13: 1385-1393.
58. Libina N, Berman JR, Kenyon C (2003) Tissue-specific activities of *C. elegans* DAF-16 in the regulation of lifespan. *Cell* 115: 489-502.
59. Berman JR, Kenyon C (2006) Germ-cell loss extends *C. elegans* life span through regulation of DAF-16 by *kri-1* and lipophilic-hormone signaling. *Cell* 124: 1055-1068.
60. Huang da W, Sherman BT, Lempicki RA (2009) Systematic and integrative analysis of large gene lists using DAVID bioinformatics resources. *Nat Protoc* 4: 44-57.
61. Mi H, Muruganujan A, Thomas PD (2013) PANTHER in 2013: modeling the evolution of gene function, and other gene attributes, in the context of phylogenetic trees. *Nucleic Acids Res* 41: D377-386.

62. Murphy CT, McCarroll SA, Bargmann CI, Fraser A, Kamath RS, et al. (2003) Genes that act downstream of DAF-16 to influence the lifespan of *Caenorhabditis elegans*. *Nature* 424: 277-283.
63. Xiong Q, Ancona N, Hauser ER, Mukherjee S, Furey TS (2012) Integrating genetic and gene expression evidence into genome-wide association analysis of gene sets. *Genome Res* 22: 386-397.
64. Brooks KK, Liang B, Watts JL (2009) The influence of bacterial diet on fat storage in *C. elegans*. *PLoS ONE* 4: e7545.
65. Zigmond MJ, Shoemaker WJ, Larin F, Wurtman RJ (1969) Hepatic tyrosine transaminase rhythm: interaction of environmental lighting, food consumption and dietary protein content. *J Nutr* 98: 71-75.
66. Wurtman RJ (1974) Daily rhythms in tyrosine transaminase and other hepatic enzymes that metabolize amino acids: mechanisms and possible consequences. *Life Sci* 15: 827-847.
67. Ross DS, Fernstrom JD, Wurtman RJ (1973) The role of dietary protein in generating daily rhythms in rat liver tryptophan pyrrolase and tyrosine transaminase. *Metabolism* 22: 1175-1184.
68. Isaacs JS, Jung YJ, Mole DR, Lee S, Torres-Cabala C, et al. (2005) HIF overexpression correlates with biallelic loss of fumarate hydratase in renal cancer: novel role of fumarate in regulation of HIF stability. *Cancer Cell* 8: 143-153.
69. Citron BA, Davis MD, Milstien S, Gutierrez J, Mendel DB, et al. (1992) Identity of 4a-carbinolamine dehydratase, a component of the phenylalanine hydroxylation system, and DCoH, a transregulator of homeodomain proteins. *Proc Natl Acad Sci USA* 89: 11891-11894.
70. Calvo AC, Pey AL, Ying M, Loer CM, Martinez A (2008) Anabolic function of phenylalanine hydroxylase in *Caenorhabditis elegans*. *FASEB J* 22: 3046-3058.
71. Tremblay F, Lavigne C, Jacques H, Marette A (2007) Role of dietary proteins and amino acids in the pathogenesis of insulin resistance. *Annu Rev Nutr* 27: 293-310.
72. Tremblay F, Marette A (2001) Amino acid and insulin signaling via the mTOR/p70 S6 kinase pathway. A negative feedback mechanism leading to insulin resistance in skeletal muscle cells. *J Biol Chem* 276: 38052-38060.
73. Wurtman RJ, Larin F, Mostafapour S, Fernstrom JD (1974) Brain catechol synthesis: control by brain tyrosine concentration. *Science* 185: 183-184.
74. Lints R, Emmons SW (1999) Patterning of dopaminergic neurotransmitter identity among *Caenorhabditis elegans* ray sensory neurons by a TGFbeta family signaling pathway and a Hox gene. *Development* 126: 5819-5831.

75. Alkema MJ, Hunter-Ensor M, Ringstad N, Horvitz HR (2005) Tyramine Functions independently of octopamine in the *Caenorhabditis elegans* nervous system. *Neuron* 46: 247-260.
76. Greer EL, Oskoui PR, Banko MR, Maniar JM, Gygi MP, et al. (2007) The energy sensor AMP-activated protein kinase directly regulates the mammalian FOXO3 transcription factor. *J Biol Chem* 282: 30107-30119.
77. Koo SH, Flechner L, Qi L, Zhang X, Sreaton RA, et al. (2005) The CREB coactivator TORC2 is a key regulator of fasting glucose metabolism. *Nature* 437:1109-1111.
78. Dentin R, Liu Y, Koo SH, Hedrick S, Vargas T, et al. (2007) Insulin modulates gluconeogenesis by inhibition of the coactivator TORC2. *Nature* 449: 366-369.
79. Cypser JR, Johnson TE (2002) Multiple stressors in *Caenorhabditis elegans* induce stress hormesis and extended longevity. *J Gerontol A Biol Sci Med Sci* 57: B109-114.
80. Walker GA, Thompson FJ, Brawley A, Scanlon T, Devaney E (2003) Heat shock factor functions at the convergence of the stress response and developmental pathways in *Caenorhabditis elegans*. *FASEB J* 17: 1960-1962.
81. Morley JF, Morimoto RI (2004) Regulation of longevity in *Caenorhabditis elegans* by heat shock factor and molecular chaperones. *Mol Biol Cell* 15: 657-664.
82. Hsu AL, Murphy CT, Kenyon C (2003) Regulation of aging and age-related disease by DAF-16 and heat-shock factor. *Science* 300: 1142-1145.
83. Conigrave AD, Quinn SJ, Brown EM (2000) L-amino acid sensing by the extracellular Ca²⁺-sensing receptor. *Proc Natl Acad Sci U S A* 97: 4814-4819.
84. Bittinger MA, Nguyen LP, Bradfield CA (2003) Aspartate aminotransferase generates proagonists of the aryl hydrocarbon receptor. *Mol Pharmacol* 64: 550-556.
85. Schumacher U, Lukacs Z, Kaltschmidt C, Freudlsperger C, Schulz D, et al. (2008) High concentrations of phenylalanine stimulate peroxisome proliferator-activated receptor gamma: implications for the pathophysiology of phenylketonuria. *Neurobiol Dis* 32: 385-390.
86. Lu M, Wan M, Leavens KF, Chu Q, Monks BR, et al. (2012) Insulin regulates liver metabolism in vivo in the absence of hepatic Akt and Foxo1. *Nat Med* 18: 388-395.
87. Wurtman RJ, Axelrod J (1967) Daily rhythmic changes in tyrosine transaminase activity of the rat liver. *Proc Natl Acad Sci U S A* 57: 1594-1598.
88. Lee SJ, Kenyon C (2009) Regulation of the longevity response to temperature by thermosensory neurons in *Caenorhabditis elegans*. *Curr Biol* 19: 715-722.

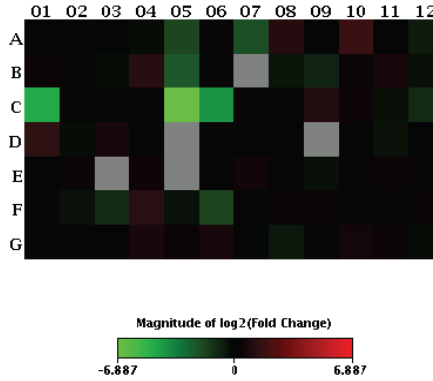
89. Langenberg C, Savage DB (2011) An amino acid profile to predict diabetes? *NatMed* 17: 418-420.
90. Sulston JE, Horvitz HR (1988) Methods. In: Wood WB, editor. *The nematode, Caenorhabditis elegans*. Cold Spring Harbor, NY: Cold Spring Harbor Laboratory Press. pp. 587-606.
91. Patel DS, Fang LL, Svy DK, Ruvkun G, Li W (2008) Genetic identification of HSD-1, a conserved steroidogenic enzyme that directs larval development in *Caenorhabditis elegans*. *Development* 135: 2239-2249.
92. Landis JR, Koch GG (1977) The measurement of observer agreement for categorical data. *Biometrics* 33: 159-174.
93. Powolny AA, Singh SV, Melov S, Hubbard A, Fisher AL (2011) The garlic constituent diallyl trisulfide increases the lifespan of *C. elegans* via *skn-1* activation. *Exp Gerontol*.
94. Geier FM, Want EJ, Leroi AM, Bundy JG (2011) Cross-platform comparison of *Caenorhabditis elegans* tissue extraction strategies for comprehensive metabolome coverage. *Anal Chem* 83: 3730-3736.
95. Held PK, White L, Pasquali M (2011) Quantitative urine amino acid analysis using liquid chromatography tandem mass spectrometry and aTRAQ reagents. *J Chromatogr B Analyt Technol Biomed Life Sci* 879: 2695-2703.
96. Livak KJ, Schmittgen TD (2001) Analysis of relative gene expression data using real-time quantitative PCR and the $2^{-\Delta\Delta C(T)}$ Method. *Methods* 25: 402-408.
97. Hoogewijs D, Houthoofd K, Matthijssens F, Vandesompele J, Vanfleteren JR (2008) Selection and validation of a set of reliable reference genes for quantitative sod gene expression analysis in *C. elegans*. *BMC Mol Biol* 9: 9.
98. Hochbaum D, Zhang Y, Stuckenholtz C, Labhart P, Alexiadis V, et al. (2011) DAF-12 regulates a connected network of genes to ensure robust developmental decisions. *PLoS Genet* 7: e1002179.
99. Li J, Ebata A, Dong Y, Rizki G, Iwata T, et al. (2008) *Caenorhabditis elegans* HCF-1 functions in longevity maintenance as a DAF-16 regulator. *PLoS Biol* 6: e233.
100. Marshall OJ (2004) PerlPrimer: cross-platform, graphical primer design for standard, bisulphite and real-time PCR. *Bioinformatics* 20: 2471-2472.
101. Li B, Dewey CN (2011) RSEM: accurate transcript quantification from RNA-Seq data with or without a reference genome. *BMC Bioinformatics* 12: 323.
102. Bullard JH, Purdom E, Hansen KD, Dudoit S (2010) Evaluation of statistical methods for normalization and differential expression in mRNA-Seq experiments. *BMC Bioinformatics* 11: 94.

103. Lamesch P, Milstein S, Hao T, Rosenberg J, Li N, et al. (2004) C. elegans ORFeome version 3.1: increasing the coverage of ORFeome resources with improved gene predictions. *Genome Res* 14: 2064-2069.
104. Dupuy D, Li QR, Deplancke B, Boxem M, Hao T, et al. (2004) A first version of the *Caenorhabditis elegans* Promoterome. *Genome Res* 14: 2169-2175.
105. Hochbaum D, Ferguson AA, Fisher AL (2010) Generation of transgenic *C. elegans* by biolistic transformation. *J Vis Exp*.
106. Ferguson AA, Cai L, Kashyap L, Fisher AL (2013) Improved Vectors for Selection of Transgenic *Caenorhabditis elegans*. *Methods Mol Biol* 940: 87-102.
107. Zanin E, Dumont J, Gassmann R, Cheeseman I, Maddox P, et al. (2011) Affinity purification of protein complexes in *C. elegans*. *Methods Cell Biol* 106: 289-322.
108. Abramoff MDM, P.J.; Ram, S.J. (2004) Image Processing with ImageJ. *Biophotonics International* 11: 36-42.

APPENDIX B: QUANTITATIVE PCR

Treated Group: Control Group:
 Log2 transform fold change

Visualization of log₂(Fold Change)



Layout	01	02	03	04	05	06	07	08	09	10	11	12
A	Ace -1.00 OKAY	Acly -1.20 OKAY	Adra1a -1.03 OKAY	Adrb3 -1.29 OKAY	Agt -3.73 OKAY	Akt2 -1.17 OKAY	Aqp2 -4.45 OKAY	Ccl5 2.02 OKAY	Ccr2 -1.03 OKAY	Cd28 3.36 OKAY	Ceacam1 1.09 OKAY	Cebpa -1.60 OKAY
	B	Ctla4 1.22 OKAY	Dpp4 -1.22 OKAY	Dusp4 -1.30 OKAY	Enpp1 2.20 OKAY	Fbp1 -5.14 OKAY	Foxc2 -1.14 OKAY	Foxg1 -1.08 C	Foxp3 -1.50 OKAY	G6pc -1.80 A	G6pd2 1.15 OKAY	Gcg 1.56 B
C	Glp1r -29.01 A	Gpd1 1.02 OKAY	Gsk3b -1.12 OKAY	Hmox1 1.11 OKAY	Hnf1b -118.33 A	Hnf4a -17.98 OKAY	Icam1 1.13 OKAY	Ide 1.13 OKAY	Ifng 1.97 OKAY	Igfbp5 1.26 OKAY	Ikbkb -1.34 OKAY	Il10 -2.18 OKAY
	D	Il12b 2.60 OKAY	Il4ra -1.28 OKAY	Il6 1.56 OKAY	Inpp1 -1.14 OKAY	Ins1 -1.08 C	Irs1 1.12 OKAY	Mapk14 -1.07 OKAY	Mapk8 1.02 OKAY	Neurod1 -1.08 C	Nfkb1 1.07 OKAY	Nos3 -1.39 OKAY
E	Nsf 1.04 OKAY	Parp1 1.14 OKAY	Pax4 -1.08 C	Pck1 1.28 OKAY	Pdx1 -1.08 C	Pfkfb3 -1.14 OKAY	Pik3cd 1.40 OKAY	Pik3r1 1.03 OKAY	Ppara -1.34 OKAY	Pparg 1.08 OKAY	Ppargc1a 1.17 OKAY	Ptpn1 1.13 OKAY
	F	Pygl -1.13 OKAY	Rab4a -1.39 OKAY	Retn -2.17 OKAY	Sell 2.32 OKAY	Serpine1 -1.42 OKAY	Slc14a2 -3.69 A	Slc2a4 -1.03 OKAY	Snap23 1.23 OKAY	Snap25 1.22 B	Sod2 1.10 OKAY	Srebfb1 -1.03 OKAY
G	Stxbp1 -1.10 OKAY	Stxbp4 -1.12 OKAY	Tgfb1 1.02 OKAY	Tnf 1.56 OKAY	Tnfrsf1a 1.21 OKAY	Tnfrsf1b 1.54 OKAY	Trib3 -1.05 OKAY	Ucp2 -1.56 OKAY	Vamp2 1.09 OKAY	Vamp3 1.45 OKAY	Vapa 1.22 OKAY	Vegfa -1.32 OKAY

A: This gene's average threshold cycle is relatively high (> 30) in either the control or the test sample, and is reasonably low in the other sample (< 30).

These data mean that the gene's expression is relatively low in one sample and reasonably detected in the other sample suggesting that the actual fold-change value is at least as large as the calculated and reported fold-change result.

This fold-change result may also have greater variations; therefore, it is important to have a sufficient number of biological replicates to validate the result for this gene.

B: This gene's average threshold cycle is relatively high (> 30), meaning that its relative expression level is low, in both control and test samples, and the p-value for the fold-change is either unavailable or relatively high (p > 0.05).

This fold-change result may also have greater variations; therefore, it is important to have a sufficient number of biological replicates to validate the result for this gene.

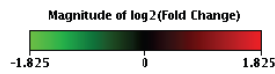
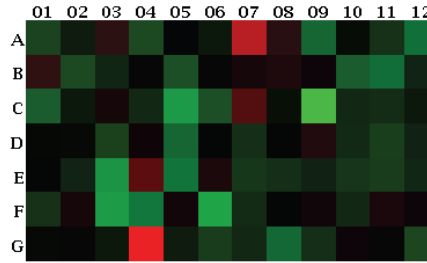
C: This gene's average threshold cycle is either not determined or greater than the defined cut-off value (default 35), in both samples meaning that its expression was undetected, making this fold-change result erroneous and un-interpretable.

Cells in the heat map corresponding to genes with erroneous fold changes are colored gray.

Figure 77. qPCR raw data for ACAD10 deficient mouse fat tissue

Treated Group: Control Group:
 Log2 transform fold change

Visualization of log₂(Fold Change)



Layout	01	02	03	04	05	06	07	08	09	10	11	12
A	Ace	Acly	Adra1a	Adrb3	Agt	Akt2	Aqp2	Ccl5	Ccr2	Cd28	Ceacam1	Cebpa
	-1.40 OKAY	-1.14 OKAY	1.26 OKAY	-1.44 OKAY	-1.00 OKAY	-1.13 OKAY	2.65 B	1.25 OKAY	-1.67 OKAY	-1.07 OKAY	-1.28 OKAY	-1.75 OKAY
B	Ctla4	Dpp4	Dusp4	Enpp1	Fbp1	Foxc2	Foxg1	Foxp3	G6pc	G6pd2	Gcg	Gcgr
	1.30 B	-1.45 OKAY	-1.18 OKAY	-1.03 OKAY	-1.48 A	-1.04 OKAY	1.12 B	1.17 B	1.06 B	-1.59 OKAY	-1.74 B	-1.17 B
C	Glp1r	Gpd1	Gsk3b	Hmox1	Hnf1b	Hnf4a	Icam1	Ide	Ifng	Igfbp5	Ikkbb	Il10
	-1.59 B	-1.13 OKAY	1.12 OKAY	-1.21 OKAY	-2.21 B	-1.49 B	1.55 OKAY	-1.08 OKAY	-2.95 B	-1.21 OKAY	-1.25 OKAY	-1.13 B
D	Il12b	Il4ra	Il6	Inpp1	Ins1	Irs1	Mapk14	Mapk8	Neurod1	Nfkb1	Nos3	Nrf1
	-1.05 B	-1.06 OKAY	-1.37 B	1.07 OKAY	-1.68 B	-1.02 OKAY	-1.25 OKAY	-1.02 OKAY	1.20 B	-1.22 OKAY	-1.36 OKAY	-1.16 OKAY
E	Nsf	Parp1	Pax4	Pck1	Pdx1	Pfkfb3	Pik3cd	Pik3r1	Ppara	Pparg	Ppargc1a	Ptpn1
	-1.01 OKAY	-1.17 OKAY	-2.15 B	1.61 OKAY	-1.81 OKAY	1.15 OKAY	-1.32 OKAY	-1.25 OKAY	-1.16 OKAY	-1.31 OKAY	-1.35 OKAY	-1.20 OKAY
F	Pygl	Rab4a	Retn	Sell	Serpine1	Slc14a2	Slc2a4	Snap23	Snap25	Sod2	Srebf1	Stx4a
	-1.28 OKAY	1.11 OKAY	-2.23 B	-1.83 OKAY	1.10 OKAY	-2.34 B	-1.23 OKAY	-1.02 OKAY	1.08 B	-1.20 OKAY	1.14 OKAY	1.06 OKAY
G	Stxbp1	Stxbp4	Tgfb1	Tnf	Tnfrsf1a	Tnfrsf1b	Trib3	Ucp2	Vamp2	Vamp3	Vapa	Vegfa
	-1.06 OKAY	-1.03 OKAY	-1.13 OKAY	3.54 A	-1.14 OKAY	-1.35 OKAY	-1.21 OKAY	-1.69 OKAY	-1.26 OKAY	1.06 OKAY	-1.04 OKAY	-1.41 OKAY

A: This gene's average threshold cycle is relatively high (> 30) in either the control or the test sample, and is reasonably low in the other sample (< 30).

These data mean that the gene's expression is relatively low in one sample and reasonably detected in the other sample suggesting that the actual fold-change value is at least as large as the calculated and reported fold-change result.

This fold-change result may also have greater variations; therefore, it is important to have a sufficient number of biological replicates to validate the result for this gene.

B: This gene's average threshold cycle is relatively high (> 30), meaning that its relative expression level is low, in both control and test samples, and the p-value for the fold-change is either unavailable or relatively high ($p > 0.05$).

This fold-change result may also have greater variations; therefore, it is important to have a sufficient number of biological replicates to validate the result for this gene.

C: This gene's average threshold cycle is either not determined or greater than the defined cut-off value (default 35), in both samples meaning that its expression was undetected, making this fold-change result erroneous and un-interpretable.

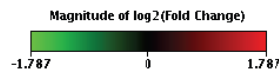
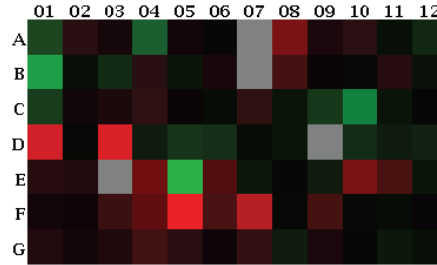
Cells in the heat map corresponding to genes with erroneous fold changes are colored gray.

Figure 78. qPCR raw data for ACAD10 deficient mouse muscle tissue

Treated Group:
 Log2 transform fold change

Control Group:

Visualization of log₂(Fold Change)



Layout	01	02	03	04	05	06	07	08	09	10	11	12
A	Ace	Acly	Adra1a	Adrb3	Agt	Akt2	Aqp2	Ccl5	Ccr2	Cd28	Ceacam1	Cebpa
	-1.40 OKAY	1.24 OKAY	1.12 OKAY	-1.60 OKAY	1.09 OKAY	-1.03 OKAY	-1.17 C	1.87 OKAY	1.13 OKAY	1.25 OKAY	-1.08 OKAY	-1.21 OKAY
B	Ctla4	Dpp4	Dusp4	Enpp1	Fbp1	Foxc2	Foxg1	Foxp3	G6pc	G6pd2	Gcg	Gcgr
	-2.25 B	-1.08 OKAY	-1.23 OKAY	1.24 OKAY	-1.11 OKAY	1.12 A	-1.17 C	1.44 B	1.05 OKAY	-1.06 OKAY	1.21 B	-1.09 OKAY
C	Glp1r	Gpd1	Gsk3b	Hmox1	Hnf1b	Hnf4a	Icam1	Ide	Ifng	Igfbp5	Ikbkb	Il10
	-1.33 B	1.08 OKAY	1.14 OKAY	1.28 OKAY	1.04 OKAY	-1.07 OKAY	1.28 OKAY	-1.10 OKAY	-1.31 B	-1.91 OKAY	-1.10 OKAY	1.02 B
D	Il12b	Il4ra	Il6	Inpp1	Ins1	Irs1	Mapk14	Mapk8	Neurod1	Nfkb1	Nos3	Nrf1
	2.95 B	-1.06 OKAY	3.07 OKAY	-1.14 OKAY	-1.29 OKAY	-1.25 OKAY	-1.07 OKAY	-1.10 OKAY	-1.17 C	-1.24 OKAY	-1.14 OKAY	-1.16 OKAY
E	Nsf	Parp1	Pax4	Pck1	Pdx1	Pfkfb3	Pik3cd	Pik3r1	Ppara	Pparg	Ppargc1a	Ptpn1
	1.20 OKAY	1.19 OKAY	-1.17 C	1.76 OKAY	-2.48 B	1.53 A	-1.12 OKAY	-1.04 OKAY	-1.14 OKAY	1.89 OKAY	1.48 OKAY	-1.11 OKAY
F	Pygl	Rab4a	Retn	Sell	Serpine1	Slc14a2	Slc2a4	Snap23	Snap25	Sod2	Srebfl	Stx4a
	1.09 OKAY	1.07 OKAY	1.36 B	1.63 OKAY	3.45 A	1.46 B	2.56 A	-1.06 OKAY	1.44 B	-1.06 OKAY	-1.07 OKAY	1.03 OKAY
G	Stxbp1	Stxbp4	Tgfb1	Tnf	Tnfrsf1a	Tnfrsf1b	Trib3	Ucp2	Vamp2	Vamp3	Vapa	Vegfa
	1.19 OKAY	1.10 OKAY	1.17 OKAY	1.42 A	1.23 OKAY	1.06 OKAY	1.32 OKAY	-1.13 OKAY	1.13 OKAY	1.03 OKAY	-1.12 OKAY	-1.08 OKAY

A: This gene's average threshold cycle is relatively high (> 30) in either the control or the test sample, and is reasonably low in the other sample (< 30).

These data mean that the gene's expression is relatively low in one sample and reasonably detected in the other sample suggesting that the actual fold-change value is at least as large as the calculated and reported fold-change result.

This fold-change result may also have greater variations; therefore, it is important to have a sufficient number of biological replicates to validate the result for this gene.

B: This gene's average threshold cycle is relatively high (> 30), meaning that its relative expression level is low, in both control and test samples, and the p-value for the fold-change is either unavailable or relatively high ($p > 0.05$).

This fold-change result may also have greater variations; therefore, it is important to have a sufficient number of biological replicates to validate the result for this gene.

C: This gene's average threshold cycle is either not determined or greater than the defined cut-off value (default 35), in both samples meaning that its expression was undetected, making this fold-change result erroneous and un-interpretable.

Cells in the heat map corresponding to genes with erroneous fold changes are colored gray.

Figure 79. qPCR raw data for ACAD10 deficient mouse liver tissue

APPENDIX C: DIGIGAIT IMAGING SYSTEMS - INDICES

DIGIGAIT IMAGING SYSTEM - INDICES

MOUSE SPECIFICS, INC.

DigiGait™ Imaging System - Indices



The DigiGait™ Imaging System generates numerous indices of gait dynamics and posture, most of which are summarized below. DigiGait™ simplifies kinematic observations and analyses by imaging the animals from below a transparent treadmill. Proprietary software, including many artificial intelligence algorithms, quantifies the characteristics of gait, including step sequence patterns, stride length, cadence, and paw placement. The output from the DigiGait™ system also includes swing and stance durations, as well as braking and propulsion durations. Indices computed by DigiGait™ convey information about sensory and motor inputs modulating gait and gait variability. Reflective markers are not required, as DigiGait™ imaging software interprets the color of the underside of subjects' paws. Only one camera is needed, eliminating the need to synchronize multiple cameras to characterize the dynamics of each of the subjects' limbs. DigiGait™ is non-invasive, robust, and quantitative, providing investigators with physiological gait signals from which numerous studies of locomotive ability and capacity become possible.

Index	Meaning	Units	Definition	Example, Application, or Reference
Swing Duration	Swing duration	ms	Time duration of the swing phase (no paw contact with belt)	Swing duration decreases with increasing speed, and there is a limit on how brief swing duration can be. Arthritic animals may have increased swing duration because of loss of mobility of the joints. Swing duration increases with pain (Vrinten and Hamers, <i>Pain</i> 102:203-209, 2003). Longer swing in the forelimbs might provide mice with ample opportunity for limb placement prior to weight bearing (Clarke and Still, <i>Behav Res Methods</i> , 33:422-426, 2001, Budsberg et al. <i>Am J Vet Res</i> 48:915-918, 1987).
% Swing	% of Stride in swing	%	% of the total stride duration that the paw is in the air.	If total stride duration is 100%, then X% is paw contact (stance) and Y% is no paw contact (swing). $X\% \text{ stance} + Y\% \text{ swing} = 100\% \text{ stride}$. % swing is typically around 35%; this value will typically increase with increasing speed.
Braking Duration	Braking duration	ms	Time duration of the braking phase (initial paw contact to maximum paw contact, commencing after the swing phase)	Time required for decelerating the motion and controlling the initiation of the stance phase. Could be longer or shorter depending on the pathology. A longer duration might indicate more precise control and distribution of loading

"...better data from every mouse."

DigiGait™ Indices – January 2010



% Braking	% of stride in braking	%	% of the total stride duration that the paw is in the braking phase	during stance and reduced peak load. If total stance duration is 100%, then B% is paw deceleration (braking) and P% is paw acceleration (propulsion). $B\%braking+P\%propulsion=100\%stance.$
% Brake of Stance	% braking of the stance phase	%	% of the stance phase (paw contact) that the paw is in the braking phase.	Braking constitutes about 50% of stance, is different in forelimbs compared to hind limbs, and changes with speed and pathology.
Propulsion Duration	Propulsion duration	ms	Time duration of the propulsion phase (maximum paw contact to just before the swing phase)	Time required for accelerating the motion and continuing forward motion of the animal. This could be briefer or delayed depending on the phenotype. A shorter duration might indicate greater strength and better control.
% Propulsion	% of stride in propulsion	%	% of the total stride duration that the paw is in the propulsion phase	If total stance duration is 100%, then B% is paw deceleration (braking) and P% is paw acceleration (propulsion). $B\%braking+P\%propulsion=100\%stance.$
% Propel of Stance	% propulsion of the stance phase	ms	% of the stance phase (paw contact) that the paw is in the propulsion phase (paw coming off of belt)	Propulsion constitutes about 50% of stance, is different in forelimbs compared to hind limbs, and changes with pathology.
Stance Duration	Stance duration	ms	Time duration of the stance duration (paw contact with belt). Stance duration is equal to the sum of braking duration and propulsion duration).	Stance duration will decrease with increased speed. Moreover, with increased speed, stance duration will decrease to a greater extent than swing duration.
% Stance	% of stride in stance	%	% of the total stride duration that the paw is in any contact with the belt.	As speed changes, the % of stride spent in stance changes more significantly than the % of stride spent in swing.
Stride Duration	Stride duration	ms	Time duration of one complete stride for one paw. Equal to the sum of stance duration and swing duration.	The predominate step pattern in mice at normal walking speed is alternate (forelimb contralateral hindlimb, in sequence). Stride duration is dependent on speed of motion and on stride frequency. Stride duration for all limbs are



Swing – to – Stance Ratio	Ratio of swing phase time to stance phase time	Real #	Ratio of swing phase time to stance phase time	usually approximately equivalent (Clarke and Still, <i>Physiol & Behav</i> 66:723-729, 1999). An indicator of the temporal structure of gait at a given cadence. The ratio changes with stride frequency, and is approximately the same for both hind limbs and both forelimbs. In humans, at the point when walking changes over to running, the ratio is equal to one (Drillis, <i>Ann New York Acad. Sci.</i> 74: 86,1958). In disease conditions, the ratio for each limb may be different and represents a structural asymmetry of performance.
Stride Frequency	Stride frequency, or “cadence”	Strides per second	The number of times each second that a paw takes a complete stride.	Stride frequency in mice ranges from ~2.5 Hz to ~8 Hz (Clarke and Still, <i>Physiol & Behav</i> 66:723-729, 1999; James RS et al. <i>J Exp Biol</i> 198:491-02, 1995). This is likely strain dependent and phenotype dependent.
Stride Length	Stride length	cm	The spatial length that a paw traverses through a given stride.	Distance between successive strides of the same paw. This number should normally be nearly equivalent among the 4 paws of a given animal (Hannigan and Riley, <i>Alcohol</i> , 5:451-454, 1989). Prenatal and neonatal ethanol exposure results in significantly shorter stride length. As rodents increase walking speed, stride length increases and stance duration decreases (Hruska RE et al. <i>Life Sciences</i> 25:171-180, 1979). Mice with arthritis also have shorter stride length (Williams et al., <i>J Bone Joint Surg</i> 11:172-180, 1993).
Paw Angle	Paw placement angle	deg	The angle that the paw makes with the long axis of the direction of motion of the animal.	Otherwise known as “degree of external rotation”, “thigh-foot angle” (in people), “toe in/out angle” (in people), or “splay angle”. This value may decrease with walking speed (extent of which seems strain dependent). Normally, this value is ~5 deg in fore paws and ~10 deg in



Stance Width	Width between both forelimbs or both hind limbs	cm	The perpendicular distance between the centroids of either set of axial paws during peak stance	hind paws. More open angles of the hind paws are associated with ataxia, spinal cord injury, and demyelinating disease (<i>Powell et al. Physiol Behav</i> 67:819-21, 1999). Normally, the stance width of the forelimbs is less than the hind limbs. These distances are size-dependent. Larger or smaller values may indicate postural adjustments for stability. Humans avoid narrow step widths because they are less stable (Donelan et al. <i>J Biomech</i> 37:827-35, 2004). It is sometimes referred to as the “base of support”. Barron and Irvine (<i>Neurotoxicol Teratol</i> 16:89-94, 1994) showed that prenatal cocaine narrowed stance width in developing rats. Recent unpublished observations indicate a narrow stance width in young SOD1 G93A mice, a mouse model of amyotrophic lateral sclerosis, dependent on the treadmill walking conditions [speed and incline].
Step Angle	Step angle	deg	The angle made between left and right hind paws as a function of stride length and stance width.	Step angle increases with decreasing stride length and/or increasing stance width. Increased step angle reflects dysfunctional ataxia (Hannigan and Riley, <i>Alcohol</i> 5:451-454, 1989. Prenatal ethanol exposure increases the step angle in rats.) Although it is reported for the forelimbs and the hind limbs, the Hannigan and Riley approach applied to the hind limbs only. Another study described effects of prenatal cocaine exposure on step angle and stance width [Barron and Irvine, <i>Neurotoxicol Teratol</i> 16:89-94, 1994].
Stride Length Variability	Step-to-step variability in stride length	cm	The standard deviation of the stride length for the set of strides recorded (reflecting the dispersion	Stride length variability is higher in patients with Parkinson’s disease, Huntington’s disease, and ALS (Hausdorff et al. <i>J Appl Physiol</i> 88: 2045-



Stance Width Variability	Step-to-step variability in stance width	cm	<p>about the average value).</p> <p>The standard deviation of the stance width for the set of strides recorded (reflecting the dispersion about the average value).</p>	<p>2053, 2000). In mice, stride length variability is increased after ethanol intoxication (Kale et al. <i>Alcohol Clin Exp Res</i> 28: 1839-48, 2004), MPTP-treatment, and 3-nitropropionic acid-treatment (Amende et al. <i>J NeuroEngineer & Rehabil</i> July 25; 2:20, 2005).</p> <p>Step width variability is higher in older than younger adults. Higher variability is associated with falls. It is increased in the forelimbs of 3-nitropropionic acid (Amende et al. <i>J NeuroEngineer & Rehabil</i> July 25; 2:20, 2005) and in a mouse model of HD (Lin et al., <i>Hum Mol Genet</i> 10:137-144, 2001).</p>
Step Angle Variability	Step-to-step variability in step angle	deg	The SD of step angle for the set of strides recorded.	Step angle factors both stance width and stride length. Therefore step angle variability may or may not provide a useful indicator.
Stride Length CV	Coefficient of variation of stride length	%	CV was calculated from the equation: $100 \times \text{standard deviation}/\text{mean value}$ (the variability normalized to the mean)	Since variation in stride length may scale with the stride length, the CV can account for this. In humans, stride length CV is ~3-6%. In mice, it is normally ~7-12%. It is higher in the forelimbs of mice than in the hind limbs (Amende et al. <i>J NeuroEngineer & Rehabil</i> July 25; 2:20, 2005).
Stance Width CV	Coefficient of variation of stance width	%	See above	The normal range for stance width CV is similar in humans and mice (~15-20%).
Step Angle CV	Coefficient of variation of step angle	%	See above	Step angle factors both stance width and stride length. Therefore the step angle CV may or may not provide a useful indicator.
Paw Area	Paw area	cm ²	The area seen by the camera, and reported at the time corresponding to peak stance (e.g., maximal paw area)	The paw area may indicate the extent of plantar placement as a function of nerve injury, ability to load the limb, and pain. Rats with chronic pain, for example, were shown to have alterations in fore and hind paw area (Coulthard et al. <i>J Neurosci Methods</i> 116:197-213, 2002).



Paw Area Variability	Paw area variability	cm ²	The standard deviation of the paw area for the set of strides recorded (reflecting the dispersion about the average value).	Hind limb paw area is smaller in a Huntington's transgenic model (unpublished), but unchanged in a Down syndrome model (Hampton et al. <i>Physiol Behav</i> 82:381-389, 2004). The area of the underside of a paw exposed to the walking surface is fairly regular step-to-step in a healthy subject. Injury to a nerve and motor neuron disease can cause an increase in paw area variability. This metric should be increased in animals recovering from spinal cord injury with dorsal and plantar-stepping.
Hind Limb Shared Stance	Time both hind paws contact belt	ms	Also known as "dual stance" and "double support".	Shard stance time increases with stride time. (Clarke and Steadman, <i>Neuropeptides</i> , 14:65-70, 1989), and had been found to decrease with administration of thyrotropin-releasing hormone (Ibid), and increase with carrageenan induced rodent paw inflammation (Coulthard et al. <i>J Neurosci Methods</i> 125:95-102, 2003). Patients with peripheral arterial disease spent more time in double support (Gardner et al., <i>Vasc Med</i> 6:31-34, 2001). Wang et al. recently reported changes to double support time in rats following experimental stroke (<i>Journal of Cerebral Blood Flow & Metabolism</i> 28:1936-1950, 2008). Changes in double stance duration in collagenase-treated rats were reversed by buprenorphine, suggesting that the detected gait changes were associated with pain (<i>J Neurosci Methods</i> ;179:309-18, 2009).
Stance Factor	Ratio of left and right rear stance durations	Real #	As reported is the ratio of left forelimb stance duration to right forelimb stance, and left hind limb stance to right hind limb stance duration.	Obese children display asymmetry in stance factor (Hills and Parker, <i>Child Care Health Dev</i> 18:29-34, 1992). Stance factor was found to be an accurate and consistent means of evaluating peripheral nerve function after nerve injury and repair (Varejao et al. <i>Microsurgery</i> 21:383-388,



Gait Symmetry	Ratio of forelimb stepping frequency to hind limb stepping frequency	Real #	[Right forelimb step frequency + left forelimb step frequency] / [Right hind limb step frequency + left hind limb step frequency]	2001). In a healthy subject walking fluidly, the gait symmetry will be ~ unity. In animals recovering from spinal cord injury, the hind limbs often step more frequently to compensate for hind limb failure, in which case Gait symmetry > 1.0. Gait symmetry declined with age; treadmill training counteracted the decline of gait symmetry (Dorner et al., <i>Gerontology</i> 42:7-13, 1996).
MAX dA/dt	Maximal rate of change of paw area in contact with the treadmill belt during the braking phase	cm ² /s	How quickly the limb is loaded during the initial period of stance; how rapidly does the animal decelerate.	It remains to be determined to what extent this metric reflects alterations in muscle strength. Unpublished data suggest that forelimb loading is accelerated in mice with Huntington's disease.
MIN dA/dt	Maximal rate of change of paw area in contact with the treadmill belt during the propulsion phase	cm ² /s	How quickly the limb is unloaded during the later period of stance. How rapidly is the animal able to propel itself into the next step.	It remains to be determined to what extent this metric reflects alterations in muscle strength. Unpublished data suggest that there is a decrease in the rate of force development in the hind limbs of SOD1 G93A mice, a model of amyotrophic lateral sclerosis.
Total Number of Strides	Total number of strides	integer	The numbers of strides used to calculate the above gait indices, as imaged with the DigiGait recorder.	Aim to record 6+ sequential strides. In most instances this is straightforward, but may be difficult in severely affected animals. We usually obtain 3+ seconds of video images, representing ~ 10 strides.
Tau Propulsion	Time constant	ms	The time constant of decay of the gait signal during the propulsion	Applies to hind limb gait signals only. This number assumes that the propulsion period of stance, in part, can be described as an



Paw Overlap	Overlap extent of ipsilateral fore and hind paws	cm	<p>phase of stance.</p> <p>Were paws to have been painted and paw prints made, ipsilateral fore and hind paws can become somewhat superimposed ["footprints in the sand"].</p>	<p>exponential decay, where Tau is determined from an exponential curve fit according to the equation $A=A_0e^{-t/Tau}$, where A represents paw at time instance t, and A_0 is the paw area just after peak stance. The assumption regarding exponential decay is more robust at faster walking speeds and may not apply at slower walking speeds. This metric has not yet been published, but is believed to be affected by muscle strength. Further work in neonatal mice and animals with muscular dystrophy should provide more insight into the usefulness of Tau. Paw Overlap is the average overlap distance between 2 same sided fore and hind paws measured across successive steps. Starting with a fore paw, the ipsilateral subsequent hind paw position is determined and then the overlap distance is measured between the centroids of these 2 paws. The overlap could be negative if the paws do not overlap.</p> <p>The indices for each side are repeated [LF & LR, RF & RR] in case one wishes to compare left side to right side and/or forelimb to hind limb metrics.</p> <p>Bear in mind that, unlike paw inking, or "footprints in the sand", the treadmill paradigm does not provide the same phenomenon, and this metric is quantified in a different, dynamic, manner than one expects from the physical creation of static paw prints.</p>
Forelimb Weight	Strength	Real#	Calculated by adding the width of each fore paw to	We developed this metric based on observations in spinal injured animals, and on



Support			the average stance width of the front paws of the animal, and dividing the sum by the average width of the entire animal (measure across the widest part of the body perpendicular to the central axis passing through the body joining the tail base and nose.	simulations of attempted ambulation in humans with loss of hind limb functionality. Postural adjustments to the splay of the digits and to the forelimb stance width appear to be invoked in order to propel such subjects forward. It is thought that differences in the Forelimb Weight Support metric may reflect these types of postural adjustments.
Ataxia Coefficient	Gait variability metric	Real #	Calculated as [(MAX Stride Length – MIN Stride Length) / MEAN Stride Length] for each limb	An index of step-to-step variability, which is known to increase in Parkinson's disease and Huntington's disease.
SFI	Sciatic Functional Index	Real #	The SFI is calculated from an equation based on a multiple linear regression analysis of factors derived from measurements of walking tracks in rats with defined nerve injuries. The equation includes the paw width and paw length for each hind limb. The equation as published also requires an input for the distance between the 2 nd and 4 th toes, which is approximated as 2 mm for both hind paws, which makes this factor = 0..	The Sciatic Functional Index (SFI) is widely used to evaluate functional recovery after sciatic nerve injury, primarily in the rat, and more recently shown useful in the mouse. This quantitative, non-invasive method allows tracking of regeneration capability, visible in the gait of the animal. [see Monte-Raso VV et al. <i>J Neurosci Methods</i> 2008 170:255-61]. The equations used to generate the SFI are based on reports from rats walking overground.



TFI	Tibial Functional Index	Real #	See above, similar derivation for TFI.	The tibial functional index (TFI) and peroneal functional index (PFI) are based on multiple linear regression analysis of factors derived from measurements of walking tracks in rats with either tibial or peroneal nerve injury. The factors that contributed to these formulas were print-length factor (PLF), toe-spread factor (TSF), and intermediary toe-spread factor (ITF). It was shown that animals with selective nerve injuries gave walking tracks that were consistent, predictable, and based on known neuromuscular deficits. The sciatic functional index, tibial functional index, and peroneal functional index offer the peripheral nerve investigator a noninvasive quantitative assessment of hind limb motor function in the rat with selective hind limb nerve injury. See Bain JR, Mackinnon SE, Hunter DA. <i>Plast Reconstr Surg</i> 1989 83:129-38.
PFI	Peroneal Functional Index	Real #	See above, similar derivation for PFI.	Please see above
Phase Dispersion	Phase Dispersion	%	Phase dispersion are designed to describe interlimb coordination during quadrupedal walking. The equations used to generate the phase dispersion values for come from overground walking at unknown walking speeds; DigiGait is the first to apply them to treadmill walking at a range of walking speeds.	Locomotor and sensory recovery after graded contusive SCI with various cord displacements were examined for 6 weeks in Sprague-Dawley rats. Seven SCI gradations resulted in three locomotor performance levels measured with BBB. Analysis of interlimb coordination using new phase dispersion (PD) techniques delineated three recovery patterns: synchronous, concordant, or disengaged depending on the severity of the injury. See Kloos AD et al. <i>Exp Neurol</i> 2005 191:251-65.



Animal Length	Length	cm	Distance between the beginning of the snout to the base of the tail as seen ventrally.	Both length and width are normalized for the animal twisting and turning while running on the belt, and the average is taken from all the frames of the video. The number can be used to normalize gait metrics according to animal length. It is recommended, however, to size-match animals for study, rather than age- or weight-match.
Animal Width	Width	cm	Widest part of the body perpendicular to the central axis passing through the body joining the tail base and nose as seen ventrally.	Both length and width are normalized for the animal twisting and turning while running on the belt, and the average is taken from all the frames of the video. The number can be used to normalize gait metrics according to animal length. Stance width, for example, could be normalized to animal width as larger animals may have a wider stance independent of postural or motor defects. It is recommended, moreover, to size-match animals for study, rather than age- or weight-match.

Additional notes: Laboratory mice typically ambulate at velocities ranging from ~10 to ~45 cm/s, with an average of ~25 cm/s (Clarke and Still, *Physiol & Behav* 66:723-729, 1999). These estimates are from Swiss mice, so that variation in the “normal” walking speed for mice is probably strain dependent. In order to increase speed, mice decrease stride time primarily (~70%) and stride length modestly (~30%) to double their speed from 20 cm/s to 40 cm/s (Clarke and Still, *Physiol & Behav* 66:723-729; 1999). In the DigiGait™ system, this range of velocities is performed well by most mice we have examined. The DigiGait™ system empowers the investigator to pre-set the speed, which eliminates speed as a variable that significantly affects the gait indices).

To acclimatize the animals to the environment of the treadmill, the mice may be introduced to the belt with the motor speed set to zero prior to the recordings. A few short bouts of walking on the motorized belt usually familiarize the mice to the environment such that most mice walk and run during the imaging session.



Treadmill walking may result in changes in spatial and temporal gait parameters in humans compared to over ground walking at the same speed (Stolze et al. *Electro Clin Neur* 105:490-497; 1997), and the same could apply to mice. Gait parameters of mice running across a walkway were not affected by texturing the surface (Walter, R.M. *J Ex. Biol* 206:1739-1749; 2003).

Fast walking and running speeds, in which paw contact phases can be as short as 25 ms, should be imaged with fast frame capture rates to obtain the best temporal resolution. DigiGait images up to 150 frames per second (fps) for gait analysis in mice, and up to 100 fps for gait analysis in rats and guinea pigs. This temporal resolution will provide the opportunity for development of additional gait indices related to specific components of the braking and propulsion phases of gait.



Figure 1. A. Plotting the areas (in pixels) of each digital paw print (Paw Contact Area) provides a dynamic gait signal, representing the temporal history of paw placement through sequential strides. The signals are comprised of a stride interval, which includes the stance duration when the paw is in contact with the walking surface, plus the swing duration when the paw is not in contact with the surface. The stance phase is comprised of braking and propulsion phases. B. Gait signals for the right fore paw and left hind paw of a mouse walking at a speed of 18 cm/s. The paw contact area was normalized to the maximum area. The gait signals of the fore and hind paws of a mouse are qualitatively and quantitatively different.

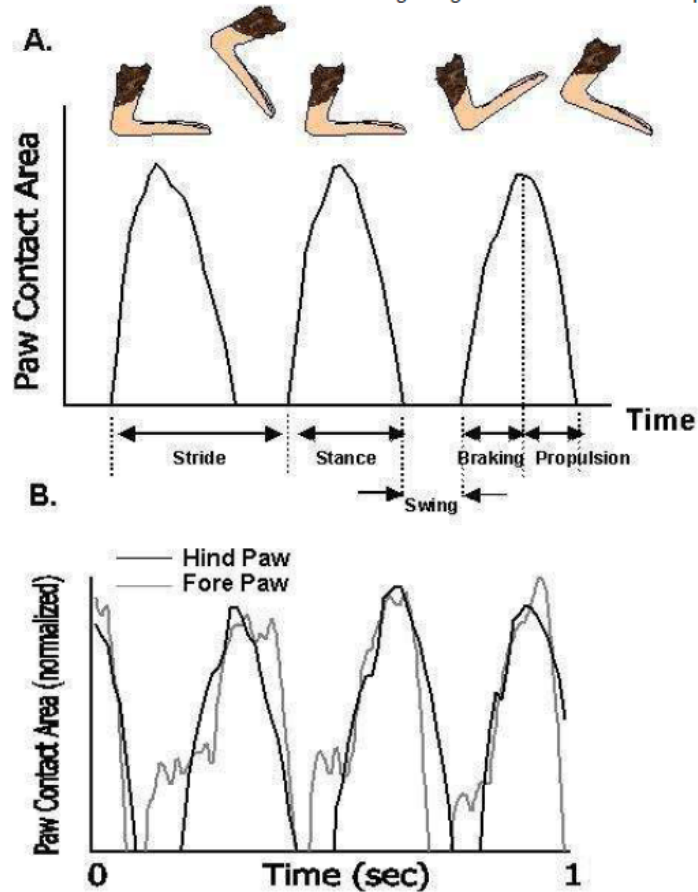
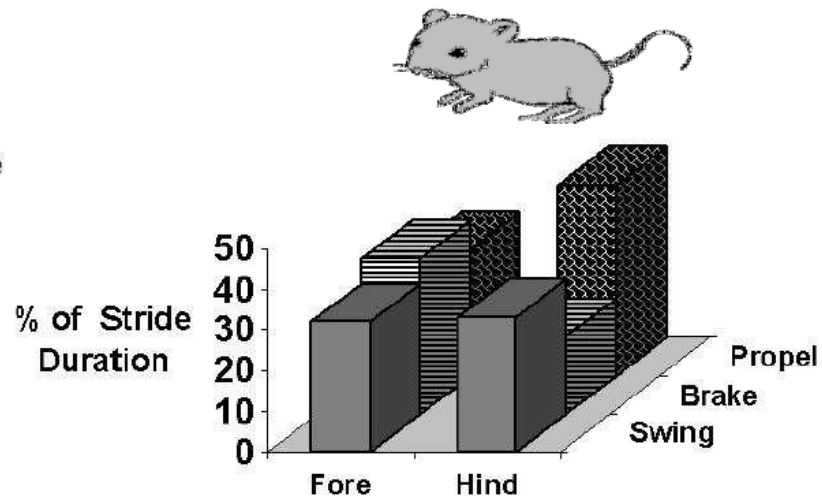


Figure 2. The relative contributions of swing, braking, and propulsion to the stride duration of forelimbs and hind limbs in a mouse walking at 18 cm/s.



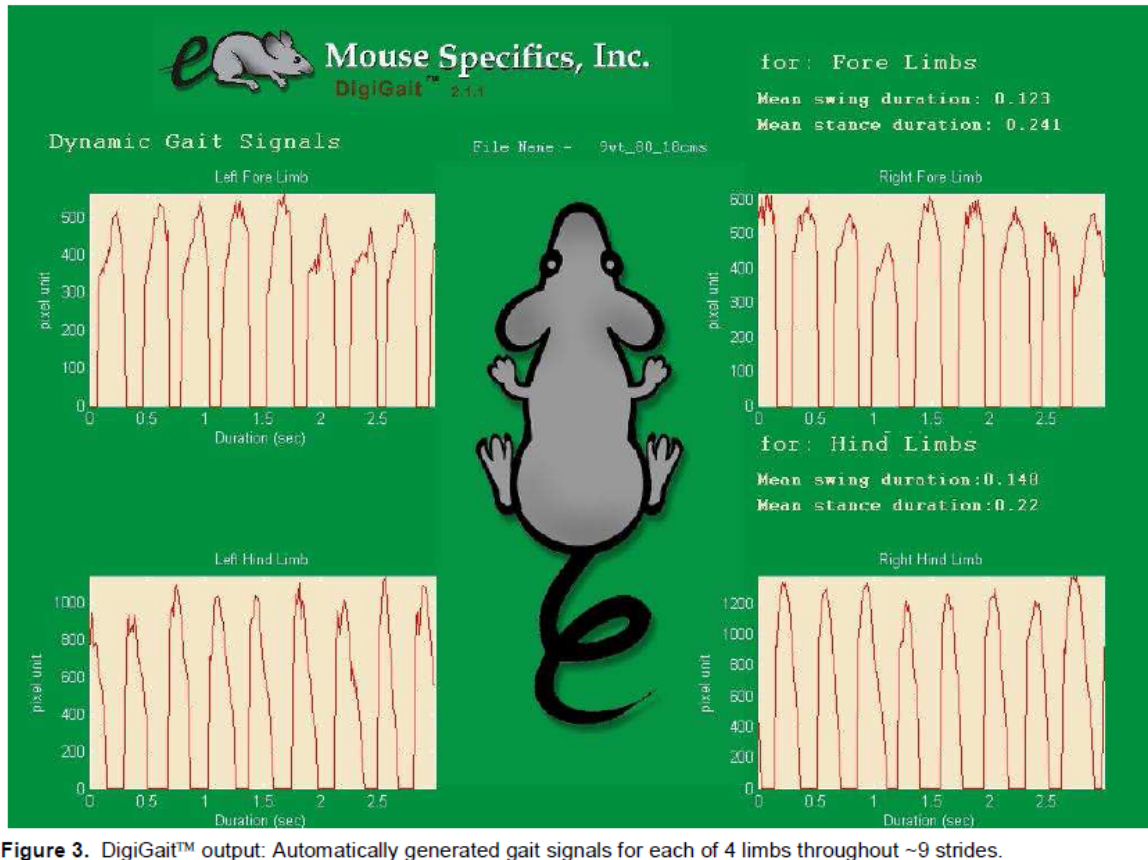




Figure 4. Example DigiGait™ output opened in an Excel spreadsheet.

	A	B	C	D	E	F	G	H	I	J	K	L	M	N	O	P	Q
1	File Name	PAW	Swing (ms)	% Swing (%)	Braking (ms)	% Brake (%)	Propulsion (ms)	% Propel (%)	Stance (ms)	% Stance (%)	Stride (ms)	Stance/Swing (real)	Stride Length (cm)	Frequency (steps/s)	Paw Angle (deg)	SL Var (cm)	SW Va (cm)
3	Rat e5 treated	LF	0.102	20.8	0.212	43.4	0.175	35.8	0.388	79.2	0.489	3.8	12.2	2.1	17.5	1.3	0.32
4	Rat e5 treated	RF	0.127	24	0.142	26.8	0.26	49.2	0.402	76	0.529	3.2	13.2	1.9	9.1	2.7	
5	Rat e5 treated	LR	0.14	26.8	0.069	13.2	0.313	60	0.381	73.2	0.521	2.7	13	2	25.4	0.9	0.14
6	Rat e5 treated	RR	0.098	19.9	0.054	11	0.34	69.1	0.394	80.1	0.492	4	12.3	2.2	23.2	0.61	
7																	
8																	
9																	
10																	
11																	
12																	
13																	
14																	
15																	
16																	
17																	

**APPENDIX D: ACYLCARNITINE MS/MS SPECTRA FOR MOUSE WHOLE BLOOD
AND HEART SAMPLES**

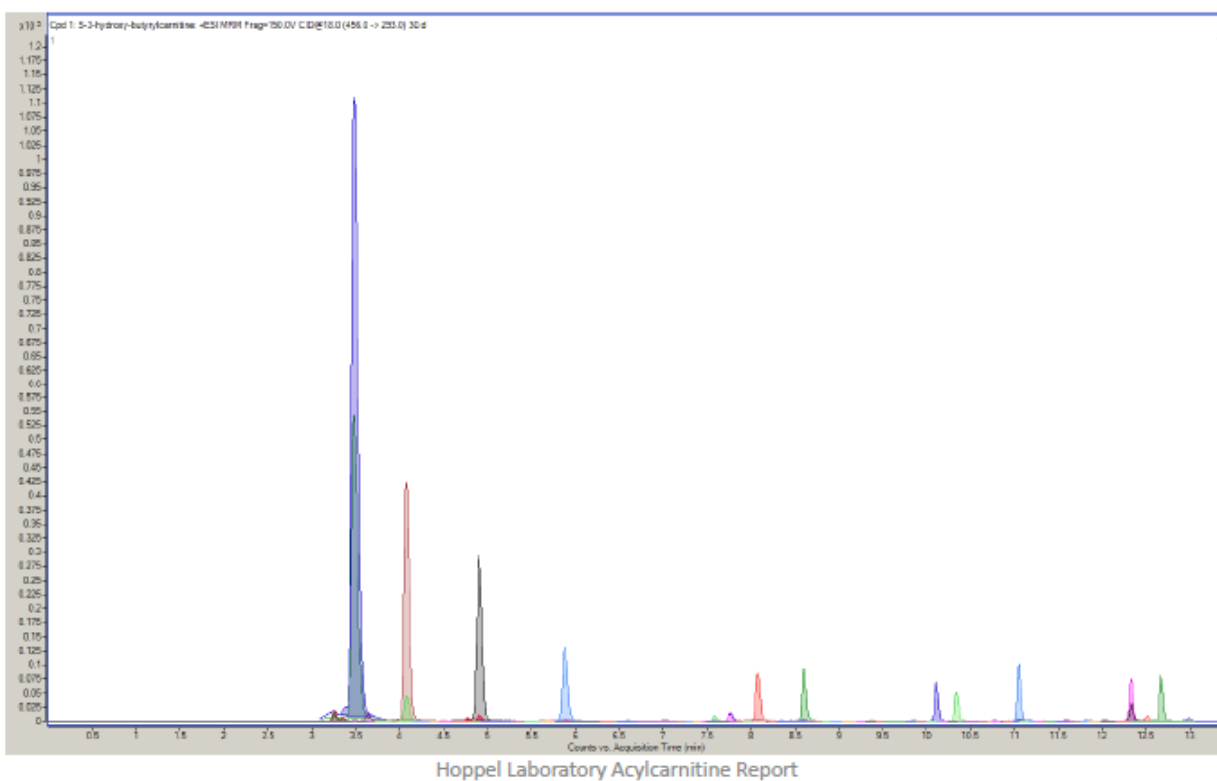


Figure 80. Wild type Mouse Whole Blood Acylcarnitine Chromatogram I

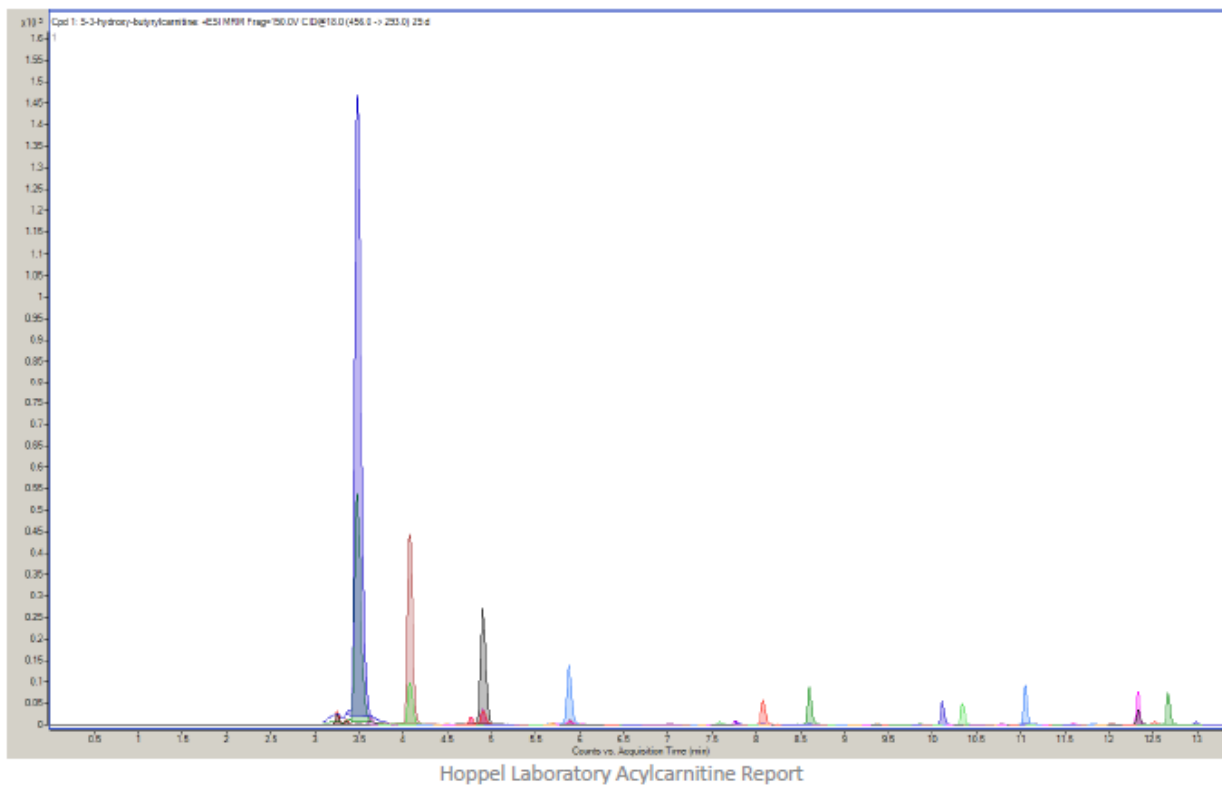
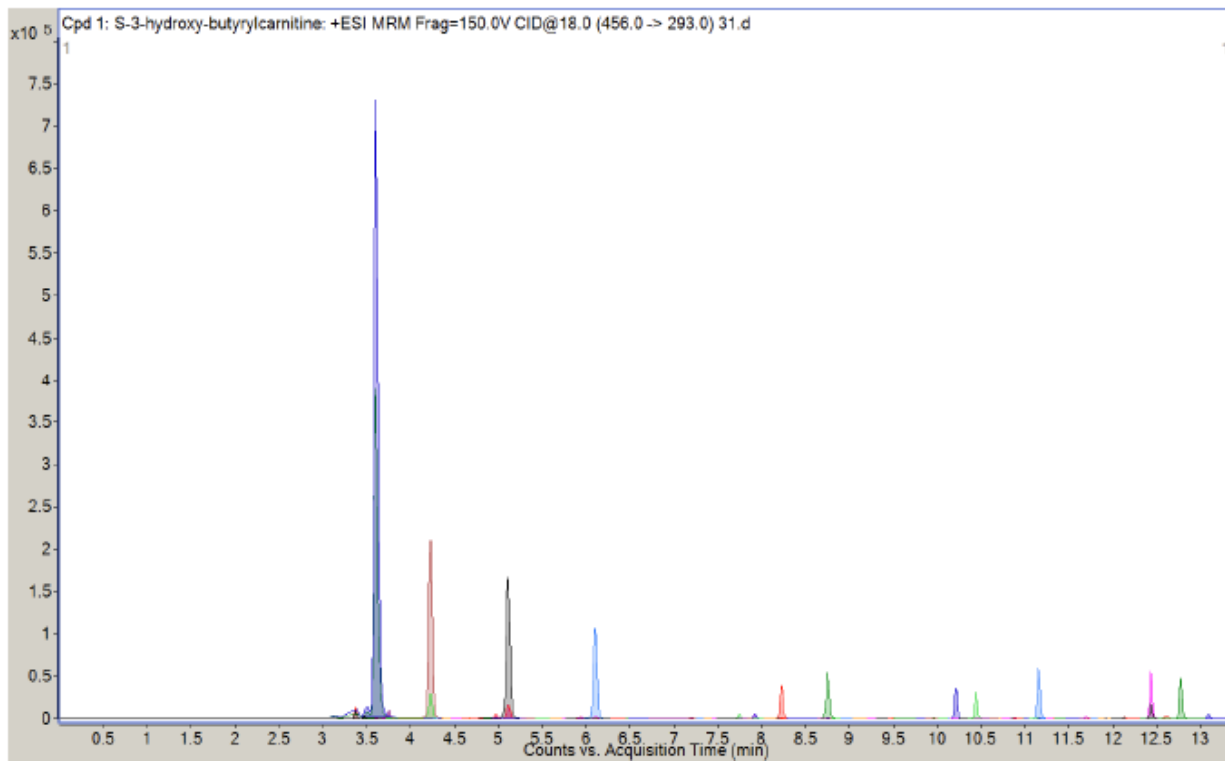
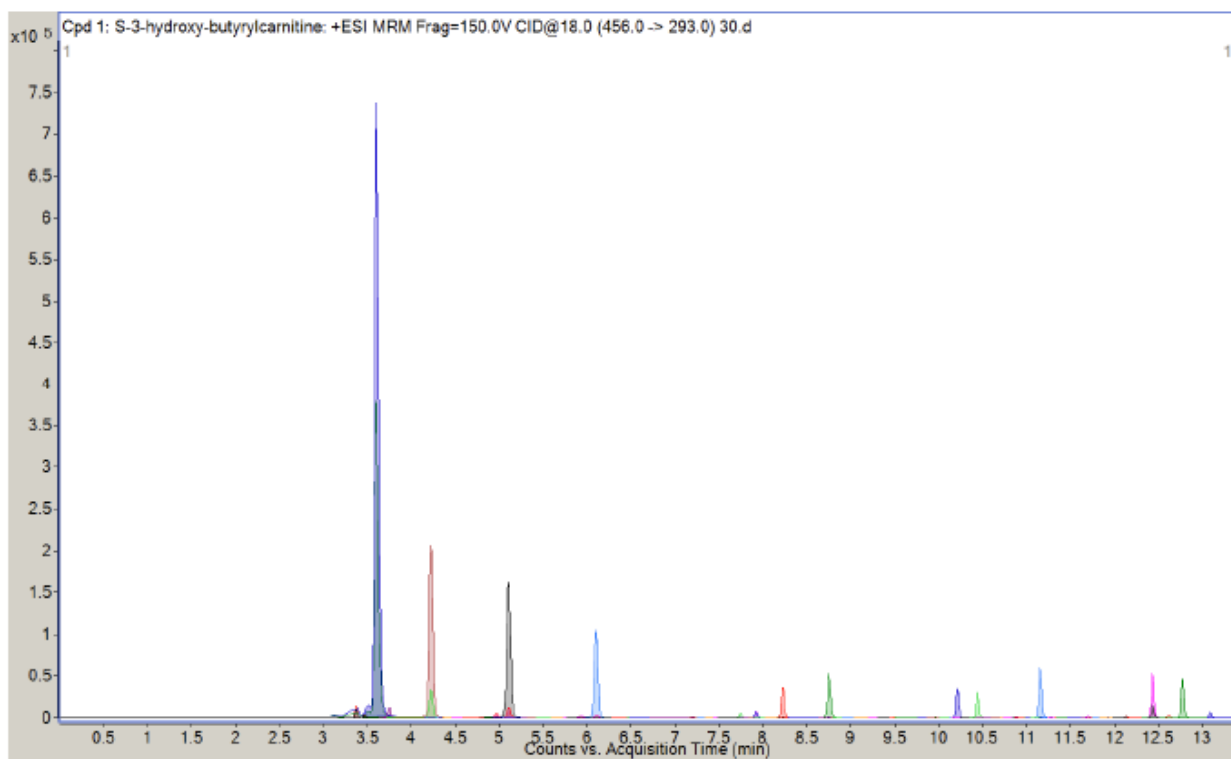


Figure 81. Acad10^{-/-} Mouse Whole Blood Acylcarnitine Chromatogram I



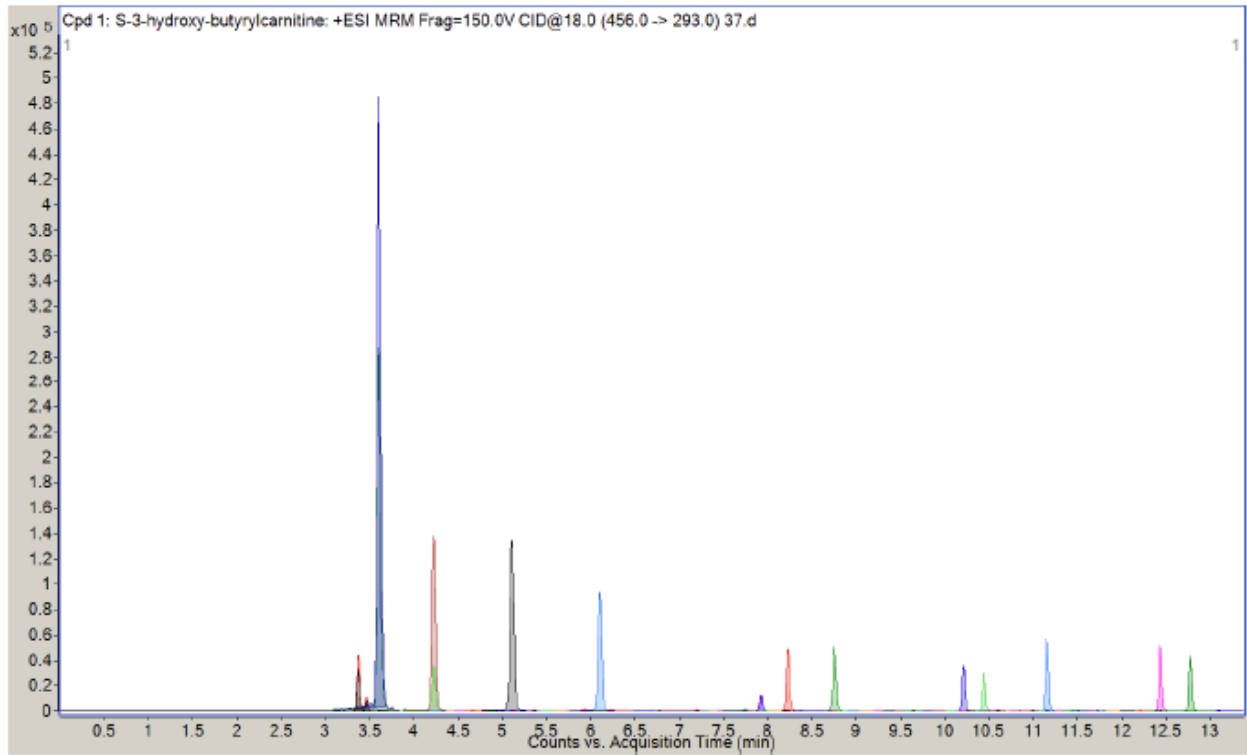
Hoppel Laboratory Acylcarnitine Report

Figure 82. Wild type Mouse Whole Blood Acylcarnitine Chromatogram II



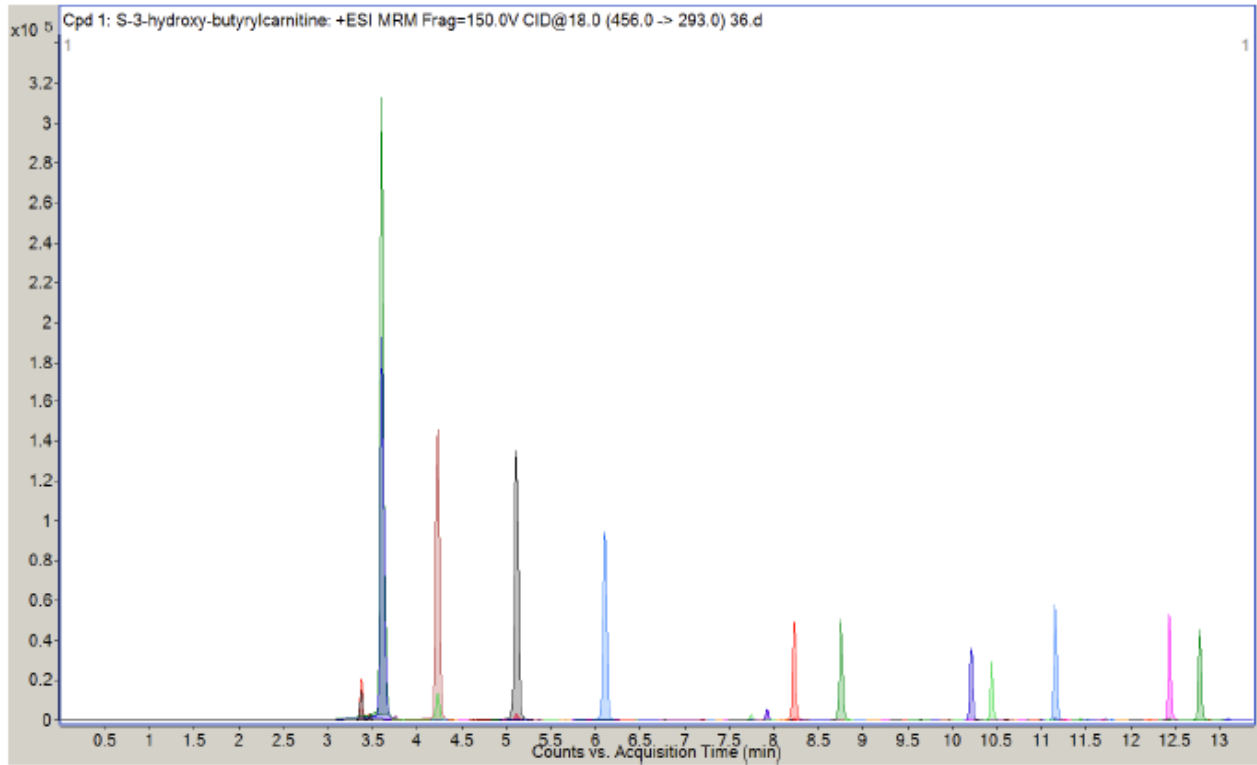
Hoppel Laboratory Acylcarnitine Report

Figure 83. *Acad10*^{-/-} Mouse Whole Blood Acylcarnitine Chromatogram II



Hoppel Laboratory Acylcarnitine Report

Figure 84. Wild type Mouse Heart Acylcarnitine Chromatogram I



Hoppel Laboratory Acylcarnitine Report

Figure 85. Acad10^{-/-} Mouse Heart Acylcarnitine Chromatogram I

APPENDIX E: COMPLETE ACYLCARNITINE RAW DATA

Sample	CompoundName	Sample Prep I	Sample Prep II	Sample Prep III
ACD 10 KO Urine	acetylcarnitine	20.73	16.01	21.216
ACD 10 KO Urine	propionylcarnitine	0.37	0.50	0.528
ACD 10 KO Urine	butyrylcarnitine	0.52	0.75	0.442
ACD 10 KO Urine	isobutyrylcarnitine	0.22	0.19	0.292
ACD 10 KO Urine	R-3-hydroxy-butyrylcarnitine	0.02	0.09	0.003
ACD 10 KO Urine	S-3-hydroxy-butyrylcarnitine	0.02	0.06	0.000
ACD 10 KO Urine	valerylcarnitine	0.01	0.02	0.011
ACD 10 KO Urine	isovalerylcarnitine	0.07	0.07	0.032
ACD 10 KO Urine	3-hydroxy-isovalerylcarnitine	0.67	0.62	0.684
ACD 10 KO Urine	2-methyl-butyrylcarnitine	0.07	0.07	0.089
ACD 10 KO Urine	tigloylcarnitine	0.03	0.03	0.026
ACD 10 KO Urine	3-methyl-crotonylcarnitine	0.00	0.00	0.001
ACD 10 KO Urine	hexanoylcarnitine	0.08	0.06	0.024
ACD 10 KO Urine	R-3-hydroxy-hexanoylcarnitine	0.02	0.02	0.009
ACD 10 KO Urine	S-3-hydroxy-hexanoylcarnitine	0.03	0.02	0.017
ACD 10 KO Urine	phenylacetylcarnitine	0.01	0.00	0.001

ACD 10 KO Urine	phenylpropionylcarnitine	0.01	0.01	
ACD 10 KO Urine	4-phenyl-butyrylcarnitine	0.01	0.00	
ACD 10 KO Urine	benzoylcarnitine	0.08	0.30	0.214
ACD 10 KO Urine	4-methyl-hexanoylcarnitine	0.01	0.01	0.002
ACD 10 KO Urine	octanoylcarnitine	0.03	0.03	0.005
ACD 10 KO Urine	R-3-hydroxy-octanoylcarnitine	0.00	0.02	0.003
ACD 10 KO Urine	S-3-hydroxy-octanoylcarnitine	0.01	0.02	0.006
ACD 10 KO Urine	branched-chain C8	0.01	0.01	0.000
ACD 10 KO Urine	cis-3,4-methylene-heptanoylcarnitine	0.03	0.02	0.011
ACD 10 KO Urine	4-methyl-octanoylcarnitine	0.01	0.02	0.003
ACD 10 KO Urine	2,6-dimethyl-heptanoylcarnitine	0.02	0.02	0.001
ACD 10 KO Urine	decanoylcarnitine	0.01	0.00	0.005
ACD 10 KO Urine	cis-4-decenoylcarnitine	0.01	0.01	0.009
ACD 10 KO Urine	cis-3,4-methylene-nonanoylcarnitine	0.04	0.04	0.034
ACD 10 KO Urine	R-3-hydroxy-decanoylcarnitine	0.00	0.01	0.002
ACD 10 KO Urine	S-3-hydroxy-decanoylcarnitine	0.02	0.02	0.002
ACD 10 KO Urine	5-decynoylcarnitine	0.02	0.01	0.009
ACD 10 KO Urine	lauroylcarnitine	0.01	0.01	
ACD 10 KO Urine	trans-2-dodecenoylcarnitine	0.00	0.01	
ACD 10 KO Urine	R-3-hydroxy-lauroylcarnitine	0.01	0.00	
ACD 10 KO Urine	S-3-hydroxy-lauroylcarnitine	0.00	0.01	
ACD 10 KO Urine	myristoylcarnitine	0.00	0.01	
ACD 10 KO Urine	myristoleoylcarnitine	0.02	0.02	
ACD 10 KO Urine	cis-5-tetradecenoylcarnitine	0.00	0.01	
ACD 10 KO Urine	trans-2-tetradecenoylcarnitine	0.00	0.02	

ACD 10 KO Urine	cis,cis-5,8-tetradecadienoylcarnitine	0.01	0.02	
ACD 10 KO Urine	R-3-hydroxy-myristoylcarnitine	0.00	0.01	
ACD 10 KO Urine	S-3-hydroxy-myristoylcarnitine	0.01	0.00	
ACD 10 KO Urine	hydroxy-C14:1	0.00	0.01	
ACD 10 KO Urine	palmitoylcarnitine	0.01	0.02	
ACD 10 KO Urine	palmitoleoylcarnitine	0.00	0.01	
ACD 10 KO Urine	trans-2-hexadecenoylcarnitine	0.00	0.02	
ACD 10 KO Urine	R-3-hydroxy-palmitoylcarnitine	0.02	0.02	
ACD 10 KO Urine	S-3-hydroxy-palmitoylcarnitine	0.00	0.01	
ACD 10 KO Urine	hydroxy-C16:1	0.00	0.01	
ACD 10 KO Urine	stearoylcarnitine	0.05	0.01	
ACD 10 KO Urine	oleoylcarnitine	0.00	0.00	
ACD 10 KO Urine	linoleoylcarnitine	0.02	0.03	
ACD 10 KO Urine	alpha-linolenoylcarnitine	0.00	0.01	
ACD 10 KO Urine	gamma-linolenoylcarnitine	0.00	0.02	
ACD 10 KO Urine	R-3-hydroxy-stearoylcarnitine	0.01	0.02	
ACD 10 KO Urine	S-3-hydroxy-stearoylcarnitine	0.01	0.01	
ACD 10 KO Urine	hydroxy-C18:1	0.01	0.01	
ACD 10 KO Urine	hydroxy-C18:2	0.01	0.01	
ACD 10 KO Urine	hydroxy-C18:3	0.01	0.01	
ACD 10 KO Urine	malonylcarnitine	2.14	2.95	2.252
ACD 10 KO Urine	succinylcarnitine	1.83	2.57	2.435
ACD 10 KO Urine	methyl-malonylcarnitine	0.74	1.34	1.347
ACD 10 KO Urine	ethyl-malonylcarnitine	0.03	0.02	0.005
ACD 10 KO Urine	glutaroylcarnitine	2.12	3.05	2.096
ACD 10 KO Urine	adipoylcarnitine	2.65	2.37	2.008

ACD 10 KO Urine	3-methyl-glutaroylcarnitine	0.23	0.31	0.240
ACD 10 KO Urine	suberoylcarnitine	1.05	0.88	1.135
ACD 10 KO Urine	sebacoylcarnitine	0.26	0.31	0.351
WT Urine	acetylcarnitine	42.63	21.40	8.690
WT Urine	propionylcarnitine	0.83	0.83	0.320
WT Urine	butyrylcarnitine	1.39	0.88	0.237
WT Urine	isobutyrylcarnitine	0.37	0.30	0.281
WT Urine	R-3-hydroxy-butyrylcarnitine	0.04	0.13	0.002
WT Urine	S-3-hydroxy-butyrylcarnitine	0.04	0.08	0.000
WT Urine	valerylcarnitine	0.05	0.01	0.011
WT Urine	isovalerylcarnitine	0.22	0.04	0.053
WT Urine	3-hydroxy-isovalerylcarnitine	1.42	0.73	0.372
WT Urine	2-methyl-butyrylcarnitine	0.19	0.07	0.042
WT Urine	tigloylcarnitine	0.06	0.03	0.020
WT Urine	3-methyl-crotonylcarnitine	0.00	0.00	0.001
WT Urine	hexanoylcarnitine	0.23	0.04	0.020
WT Urine	R-3-hydroxy-hexanoylcarnitine	0.16	0.01	0.009
WT Urine	S-3-hydroxy-hexanoylcarnitine	0.03	0.02	0.007
WT Urine	phenylacetylcarnitine	0.01	0.00	0.002
WT Urine	phenylpropionylcarnitine	0.01	0.01	
WT Urine	4-phenyl-butyrylcarnitine	0.01	0.00	
WT Urine	benzoylcarnitine	0.12	0.43	0.002
WT Urine	4-methyl-hexanoylcarnitine	0.01	0.01	0.001
WT Urine	octanoylcarnitine	0.20	0.02	0.000
WT Urine	R-3-hydroxy-octanoylcarnitine	0.05	0.01	0.002
WT Urine	S-3-hydroxy-octanoylcarnitine	0.07	0.02	0.002
WT Urine	branched-chain C8	0.01	0.01	0.000

WT Urine	cis-3,4-methylene-heptanoylcarnitine	0.10	0.03	0.006
WT Urine	4-methyl-octanoylcarnitine	0.05	0.02	0.001
WT Urine	2,6-dimethyl-heptanoylcarnitine	0.06	0.02	0.002
WT Urine	decanoylcarnitine	0.08	0.00	0.005
WT Urine	cis-4-decenoylcarnitine	0.18	0.00	0.008
WT Urine	cis-3,4-methylene-nonanoylcarnitine	0.17	0.03	0.028
WT Urine	R-3-hydroxy-decanoylcarnitine	0.03	0.01	0.001
WT Urine	S-3-hydroxy-decanoylcarnitine	0.04	0.02	0.001
WT Urine	5-decynoylcarnitine	0.03	0.02	0.007
WT Urine	lauroylcarnitine	0.03	0.01	
WT Urine	trans-2-dodecenoylcarnitine	0.00	0.01	
WT Urine	R-3-hydroxy-lauroylcarnitine	0.01	0.00	
WT Urine	S-3-hydroxy-lauroylcarnitine	0.01	0.01	
WT Urine	myristoylcarnitine	0.02	0.01	
WT Urine	myristoleoylcarnitine	0.06	0.02	
WT Urine	cis-5-tetradecenoylcarnitine	0.04	0.01	
WT Urine	trans-2-tetradecenoylcarnitine	0.04	0.02	
WT Urine	cis,cis-5,8-tetradecadienoylcarnitine	0.02	0.02	
WT Urine	R-3-hydroxy-myristoylcarnitine	0.00	0.01	
WT Urine	S-3-hydroxy-myristoylcarnitine	0.01	0.00	
WT Urine	hydroxy-C14:1	0.01	0.01	
WT Urine	palmitoylcarnitine	0.08	0.02	
WT Urine	palmitoleoylcarnitine	0.02	0.01	
WT Urine	trans-2-hexadecenoylcarnitine	0.05	0.01	

WT Urine	R-3-hydroxy-palmitoylcarnitine	0.02	0.02	
WT Urine	S-3-hydroxy-palmitoylcarnitine	0.00	0.01	
WT Urine	hydroxy-C16:1	0.00	0.01	
WT Urine	stearoylcarnitine	0.08	0.01	
WT Urine	oleoylcarnitine	0.01	0.00	
WT Urine	linoleoylcarnitine	0.03	0.02	
WT Urine	alpha-linolenoylcarnitine	0.02	0.01	
WT Urine	gamma-linolenoylcarnitine	0.01	0.01	
WT Urine	R-3-hydroxy-stearoylcarnitine	0.01	0.02	
WT Urine	S-3-hydroxy-stearoylcarnitine	0.01	0.01	
WT Urine	hydroxy-C18:1	0.01	0.01	
WT Urine	hydroxy-C18:2	0.02	0.01	
WT Urine	hydroxy-C18:3	0.01	0.01	
WT Urine	malonylcarnitine	8.73	1.47	1.718
WT Urine	succinylcarnitine	5.80	1.52	1.513
WT Urine	methyl-malonylcarnitine	4.29	0.57	0.789
WT Urine	ethyl-malonylcarnitine	0.00	0.01	0.001
WT Urine	glutaroylcarnitine	5.91	1.66	2.220
WT Urine	adipoylcarnitine	7.45	1.56	2.539
WT Urine	3-methyl-glutaroylcarnitine	0.94	0.29	0.201
WT Urine	suberoylcarnitine	2.59	0.85	0.812
WT Urine	sebacoylcarnitine	0.68	0.13	0.250
ACD 10 KO Plasma	acetylcarnitine	22.65	15.03	20.850
ACD 10 KO Plasma	propionylcarnitine	0.92	0.63	0.548
ACD 10 KO Plasma	butyrylcarnitine	0.68	0.39	0.726
ACD 10 KO Plasma	isobutyrylcarnitine	0.20	0.10	0.109
ACD 10 KO Plasma	R-3-hydroxy-butyrylcarnitine	0.06	0.05	0.022

ACD 10 KO Plasma	S-3-hydroxy-butyrylcarnitine	0.16	0.08	0.066
ACD 10 KO Plasma	valerylcarnitine	0.03	0.01	0.008
ACD 10 KO Plasma	isovalerylcarnitine	0.20	0.09	0.100
ACD 10 KO Plasma	3-hydroxy-isovalerylcarnitine	0.11	0.08	0.033
ACD 10 KO Plasma	2-methyl-butyrylcarnitine	0.09	0.08	0.102
ACD 10 KO Plasma	tigloylcarnitine	0.01	0.01	0.005
ACD 10 KO Plasma	3-methyl-crotonylcarnitine	0.00	0.00	0.000
ACD 10 KO Plasma	hexanoylcarnitine	0.06	0.04	0.038
ACD 10 KO Plasma	R-3-hydroxy-hexanoylcarnitine	0.00	0.00	0.003
ACD 10 KO Plasma	S-3-hydroxy-hexanoylcarnitine	0.01	0.00	0.005
ACD 10 KO Plasma	phenylacetylcarnitine	0.01	0.00	0.000
ACD 10 KO Plasma	phenylpropionylcarnitine	0.03	0.01	
ACD 10 KO Plasma	4-phenyl-butyrylcarnitine	0.01	0.00	
ACD 10 KO Plasma	benzoylcarnitine	0.00	0.00	0.004
ACD 10 KO Plasma	4-methyl-hexanoylcarnitine	0.01	0.01	0.000
ACD 10 KO Plasma	octanoylcarnitine	0.02	0.02	0.000
ACD 10 KO Plasma	R-3-hydroxy-octanoylcarnitine	0.01	0.01	0.003
ACD 10 KO Plasma	S-3-hydroxy-octanoylcarnitine	0.02	0.02	0.009
ACD 10 KO Plasma	branched-chain C8	0.01	0.01	0.000
ACD 10 KO Plasma	cis-3,4-methylene-heptanoylcarnitine	0.01	0.01	0.001
ACD 10 KO Plasma	4-methyl-octanoylcarnitine	0.01	0.02	0.000
ACD 10 KO Plasma	2,6-dimethyl-heptanoylcarnitine	0.02	0.01	0.000
ACD 10 KO Plasma	decanoylcarnitine	0.02	0.00	0.011
ACD 10 KO Plasma	cis-4-decenoylcarnitine	0.02	0.00	0.006
ACD 10 KO Plasma	cis-3,4-methylene-nonanoylcarnitine	0.01	0.00	0.002

ACD 10 KO Plasma	R-3-hydroxy-decanoylcarnitine	0.01	0.01	0.003
ACD 10 KO Plasma	S-3-hydroxy-decanoylcarnitine	0.02	0.02	0.008
ACD 10 KO Plasma	5-decynoylcarnitine	0.01	0.00	0.000
ACD 10 KO Plasma	lauroylcarnitine	0.03	0.02	0.007
ACD 10 KO Plasma	trans-2-dodecenoylcarnitine	0.00	0.01	0.001
ACD 10 KO Plasma	R-3-hydroxy-lauroylcarnitine	0.01	0.00	0.001
ACD 10 KO Plasma	S-3-hydroxy-lauroylcarnitine	0.00	0.01	0.002
ACD 10 KO Plasma	myristoylcarnitine	0.03	0.03	0.032
ACD 10 KO Plasma	myristoleoylcarnitine	0.02	0.02	0.017
ACD 10 KO Plasma	cis-5-tetradecenoylcarnitine	0.01	0.03	0.018
ACD 10 KO Plasma	trans-2-tetradecenoylcarnitine	0.00	0.02	0.001
ACD 10 KO Plasma	cis,cis-5,8-tetradecadienoylcarnitine	0.01	0.03	0.011
ACD 10 KO Plasma	R-3-hydroxy-myristoylcarnitine	0.01	0.01	0.000
ACD 10 KO Plasma	S-3-hydroxy-myristoylcarnitine	0.02	0.00	0.002
ACD 10 KO Plasma	hydroxy-C14:1	0.01	0.01	0.005
ACD 10 KO Plasma	palmitoylcarnitine	0.12	0.08	0.132
ACD 10 KO Plasma	palmitoleoylcarnitine	0.00	0.02	0.038
ACD 10 KO Plasma	trans-2-hexadecenoylcarnitine	0.00	0.01	0.002
ACD 10 KO Plasma	R-3-hydroxy-palmitoylcarnitine	0.02	0.02	0.000
ACD 10 KO Plasma	S-3-hydroxy-palmitoylcarnitine	0.00	0.01	0.004
ACD 10 KO Plasma	hydroxy-C16:1	0.00	0.01	0.003
ACD 10 KO Plasma	stearoylcarnitine	0.08	0.03	0.032
ACD 10 KO Plasma	oleoylcarnitine	0.06	0.06	0.122
ACD 10 KO Plasma	linoleoylcarnitine	0.04	0.06	0.057
ACD 10 KO Plasma	alpha-linolenoylcarnitine	0.01	0.01	0.006
ACD 10 KO Plasma	gamma-linolenoylcarnitine	0.00	0.02	0.002

ACD 10 KO Plasma	R-3-hydroxy-stearoylcarnitine	0.01	0.02	0.006
ACD 10 KO Plasma	S-3-hydroxy-stearoylcarnitine	0.01	0.01	0.001
ACD 10 KO Plasma	hydroxy-C18:1	0.01	0.01	0.008
ACD 10 KO Plasma	hydroxy-C18:2	0.01	0.01	0.004
ACD 10 KO Plasma	hydroxy-C18:3	0.01	0.01	0.002
ACD 10 KO Plasma	malonylcarnitine	0.03	0.01	0.008
ACD 10 KO Plasma	succinylcarnitine	0.05	0.03	0.016
ACD 10 KO Plasma	methyl-malonylcarnitine	0.02	0.02	0.005
ACD 10 KO Plasma	ethyl-malonylcarnitine	0.01	0.00	0.000
ACD 10 KO Plasma	glutaroylcarnitine	0.03	0.02	0.009
ACD 10 KO Plasma	adipoylcarnitine	0.03	0.02	0.010
ACD 10 KO Plasma	3-methyl-glutaroylcarnitine	0.00	0.01	0.000
ACD 10 KO Plasma	suberoylcarnitine	0.01	0.02	0.010
ACD 10 KO Plasma	sebacoylcarnitine	0.01	0.01	0.002
WT Plasma	acetylcarnitine	16.85	17.79	26.232
WT Plasma	propionylcarnitine	0.41	0.53	1.489
WT Plasma	butyrylcarnitine	0.23	0.74	0.774
WT Plasma	isobutyrylcarnitine	0.08	0.10	0.191
WT Plasma	R-3-hydroxy-butyrylcarnitine	0.04	0.06	0.040
WT Plasma	S-3-hydroxy-butyrylcarnitine	0.08	0.08	0.048
WT Plasma	valerylcarnitine	0.00	0.01	0.013
WT Plasma	isovalerylcarnitine	0.07	0.07	0.181
WT Plasma	3-hydroxy-isovalerylcarnitine	0.09	0.07	0.080
WT Plasma	2-methyl-butyrylcarnitine	0.06	0.07	0.124
WT Plasma	tigloylcarnitine	0.01	0.01	0.008
WT Plasma	3-methyl-crotonylcarnitine	0.00	0.00	0.000
WT Plasma	hexanoylcarnitine	0.05	0.04	0.020

WT Plasma	R-3-hydroxy-hexanoylcarnitine	0.00	0.00	0.002
WT Plasma	S-3-hydroxy-hexanoylcarnitine	0.00	0.00	0.004
WT Plasma	phenylacetylcarnitine	0.01	0.00	0.002
WT Plasma	phenylpropionylcarnitine	0.01	0.01	
WT Plasma	4-phenyl-butyrylcarnitine	0.01	0.00	
WT Plasma	benzoylcarnitine	0.00	0.01	0.000
WT Plasma	4-methyl-hexanoylcarnitine	0.01	0.01	0.000
WT Plasma	octanoylcarnitine	0.02	0.02	0.000
WT Plasma	R-3-hydroxy-octanoylcarnitine	0.01	0.01	0.002
WT Plasma	S-3-hydroxy-octanoylcarnitine	0.02	0.02	0.007
WT Plasma	branched-chain C8	0.01	0.01	0.000
WT Plasma	cis-3,4-methylene-heptanoylcarnitine	0.01	0.01	0.000
WT Plasma	4-methyl-octanoylcarnitine	0.01	0.02	0.000
WT Plasma	2,6-dimethyl-heptanoylcarnitine	0.02	0.01	0.000
WT Plasma	decanoylcarnitine	0.02	0.00	0.007
WT Plasma	cis-4-decenoylcarnitine	0.02	0.00	0.005
WT Plasma	cis-3,4-methylene-nonanoylcarnitine	0.01	0.00	0.000
WT Plasma	R-3-hydroxy-decanoylcarnitine	0.01	0.01	0.002
WT Plasma	S-3-hydroxy-decanoylcarnitine	0.04	0.03	0.005
WT Plasma	5-decynoylcarnitine	0.01	0.00	0.000
WT Plasma	lauroylcarnitine	0.03	0.02	0.008
WT Plasma	trans-2-dodecenoylcarnitine	0.01	0.01	0.000
WT Plasma	R-3-hydroxy-lauroylcarnitine	0.01	0.00	0.001
WT Plasma	S-3-hydroxy-lauroylcarnitine	0.00	0.01	0.000
WT Plasma	myristoylcarnitine	0.04	0.04	0.029

WT Plasma	myristoleoylcarnitine	0.02	0.03	0.003
WT Plasma	cis-5-tetradecenoylcarnitine	0.03	0.03	0.001
WT Plasma	trans-2-tetradecenoylcarnitine	0.00	0.01	0.001
WT Plasma	cis,cis-5,8-tetradecadienoylcarnitine	0.02	0.03	0.009
WT Plasma	R-3-hydroxy-myristoylcarnitine	0.00	0.01	0.000
WT Plasma	S-3-hydroxy-myristoylcarnitine	0.01	0.00	0.002
WT Plasma	hydroxy-C14:1	0.01	0.01	0.004
WT Plasma	palmitoylcarnitine	0.15	0.11	0.117
WT Plasma	palmitoleoylcarnitine	0.02	0.02	0.007
WT Plasma	trans-2-hexadecenoylcarnitine	0.00	0.01	0.001
WT Plasma	R-3-hydroxy-palmitoylcarnitine	0.02	0.02	0.001
WT Plasma	S-3-hydroxy-palmitoylcarnitine	0.00	0.01	0.004
WT Plasma	hydroxy-C16:1	0.00	0.02	0.001
WT Plasma	stearoylcarnitine	0.08	0.04	0.036
WT Plasma	oleoylcarnitine	0.11	0.09	0.047
WT Plasma	linoleoylcarnitine	0.06	0.06	0.034
WT Plasma	alpha-linolenoylcarnitine	0.01	0.01	0.003
WT Plasma	gamma-linolenoylcarnitine	0.00	0.01	0.002
WT Plasma	R-3-hydroxy-stearoylcarnitine	0.02	0.03	0.005
WT Plasma	S-3-hydroxy-stearoylcarnitine	0.01	0.01	0.001
WT Plasma	hydroxy-C18:1	0.01	0.01	0.003
WT Plasma	hydroxy-C18:2	0.01	0.01	0.004
WT Plasma	hydroxy-C18:3	0.01	0.01	0.002
WT Plasma	malonylcarnitine	0.04	0.02	0.026
WT Plasma	succinylcarnitine	0.04	0.02	0.013
WT Plasma	methyl-malonylcarnitine	0.03	0.01	0.004

WT Plasma	ethyl-malonylcarnitine	0.01	0.00	0.000
WT Plasma	glutaroylcarnitine	0.00	0.01	0.015
WT Plasma	adipoylcarnitine	0.03	0.02	0.017
WT Plasma	3-methyl-glutaroylcarnitine	0.01	0.01	0.000
WT Plasma	suberoylcarnitine	0.01	0.03	0.012
WT Plasma	sebacoylcarnitine	0.01	0.01	0.002
ACD 10 KO Whole Blood	acetylcarnitine	32.15	22.37	
ACD 10 KO Whole Blood	propionylcarnitine	0.82	0.57	
ACD 10 KO Whole Blood	butyrylcarnitine	0.47	0.27	
ACD 10 KO Whole Blood	isobutyrylcarnitine	0.19	0.09	
ACD 10 KO Whole Blood	R-3-hydroxy-butyrylcarnitine	0.10	0.08	
ACD 10 KO Whole Blood	S-3-hydroxy-butyrylcarnitine	0.24	0.16	
ACD 10 KO Whole Blood	valerylcarnitine	0.02	0.01	
ACD 10 KO Whole Blood	isovalerylcarnitine	0.20	0.09	
ACD 10 KO Whole Blood	3-hydroxy-isovalerylcarnitine	0.16	0.14	
ACD 10 KO Whole Blood	2-methyl-butyrylcarnitine	0.08	0.07	
ACD 10 KO Whole Blood	tigloylcarnitine	0.01	0.01	
ACD 10 KO Whole Blood	3-methyl-crotonylcarnitine	0.00	0.00	
ACD 10 KO Whole Blood	hexanoylcarnitine	0.04	0.03	
ACD 10 KO Whole Blood	R-3-hydroxy-hexanoylcarnitine	0.00	0.01	
ACD 10 KO Whole Blood	S-3-hydroxy-hexanoylcarnitine	0.01	0.01	
ACD 10 KO Whole Blood	phenylacetylcarnitine	0.01	0.00	
ACD 10 KO Whole Blood	phenylpropionylcarnitine	0.02	0.01	
ACD 10 KO Whole Blood	4-phenyl-butyrylcarnitine	0.01	0.00	
ACD 10 KO Whole Blood	benzoylcarnitine	0.00	0.00	
ACD 10 KO Whole Blood	4-methyl-hexanoylcarnitine	0.01	0.01	
ACD 10 KO Whole Blood	octanoylcarnitine	0.04	0.04	

ACD 10 KO Whole Blood	R-3-hydroxy-octanoylcarnitine	0.00	0.01	
ACD 10 KO Whole Blood	S-3-hydroxy-octanoylcarnitine	0.02	0.02	
ACD 10 KO Whole Blood	branched-chain C8	0.01	0.01	
ACD 10 KO Whole Blood	cis-3,4-methylene-heptanoylcarnitine	0.01	0.01	
ACD 10 KO Whole Blood	4-methyl-octanoylcarnitine	0.01	0.02	
ACD 10 KO Whole Blood	2,6-dimethyl-heptanoylcarnitine	0.02	0.01	
ACD 10 KO Whole Blood	decanoylcarnitine	0.03	0.01	
ACD 10 KO Whole Blood	cis-4-decenoylcarnitine	0.03	0.01	
ACD 10 KO Whole Blood	cis-3,4-methylene-nonanoylcarnitine	0.00	0.00	
ACD 10 KO Whole Blood	R-3-hydroxy-decanoylcarnitine	0.01	0.01	
ACD 10 KO Whole Blood	S-3-hydroxy-decanoylcarnitine	0.03	0.03	
ACD 10 KO Whole Blood	5-decynoylcarnitine	0.01	0.00	
ACD 10 KO Whole Blood	lauroylcarnitine	0.03	0.04	
ACD 10 KO Whole Blood	trans-2-dodecenoylcarnitine	0.00	0.01	
ACD 10 KO Whole Blood	R-3-hydroxy-lauroylcarnitine	0.01	0.01	
ACD 10 KO Whole Blood	S-3-hydroxy-lauroylcarnitine	0.01	0.01	
ACD 10 KO Whole Blood	myristoylcarnitine	0.08	0.10	
ACD 10 KO Whole Blood	myristoleoylcarnitine	0.03	0.02	
ACD 10 KO Whole Blood	cis-5-tetradecenoylcarnitine	0.03	0.03	
ACD 10 KO Whole Blood	trans-2-tetradecenoylcarnitine	0.01	0.02	
ACD 10 KO Whole Blood	cis,cis-5,8-tetradecadienoylcarnitine	0.01	0.03	
ACD 10 KO Whole Blood	R-3-hydroxy-myristoylcarnitine	0.01	0.01	
ACD 10 KO Whole Blood	S-3-hydroxy-myristoylcarnitine	0.01	0.01	
ACD 10 KO Whole Blood	hydroxy-C14:1	0.01	0.01	

ACD 10 KO Whole Blood	palmitoylcarnitine	1.06	0.86	
ACD 10 KO Whole Blood	palmitoleoylcarnitine	0.02	0.03	
ACD 10 KO Whole Blood	trans-2-hexadecenoylcarnitine	0.00	0.02	
ACD 10 KO Whole Blood	R-3-hydroxy-palmitoylcarnitine	0.02	0.02	
ACD 10 KO Whole Blood	S-3-hydroxy-palmitoylcarnitine	0.00	0.02	
ACD 10 KO Whole Blood	hydroxy-C16:1	0.00	0.01	
ACD 10 KO Whole Blood	stearoylcarnitine	0.27	0.35	
ACD 10 KO Whole Blood	oleoylcarnitine	0.36	0.31	
ACD 10 KO Whole Blood	linoleoylcarnitine	0.14	0.14	
ACD 10 KO Whole Blood	alpha-linolenoylcarnitine	0.03	0.04	
ACD 10 KO Whole Blood	gamma-linolenoylcarnitine	0.00	0.02	
ACD 10 KO Whole Blood	R-3-hydroxy-stearoylcarnitine	0.02	0.03	
ACD 10 KO Whole Blood	S-3-hydroxy-stearoylcarnitine	0.01	0.01	
ACD 10 KO Whole Blood	hydroxy-C18:1	0.02	0.01	
ACD 10 KO Whole Blood	hydroxy-C18:2	0.01	0.01	
ACD 10 KO Whole Blood	hydroxy-C18:3	0.01	0.01	
ACD 10 KO Whole Blood	malonylcarnitine	0.13	0.08	
ACD 10 KO Whole Blood	succinylcarnitine	0.41	0.39	
ACD 10 KO Whole Blood	methyl-malonylcarnitine	0.11	0.07	
ACD 10 KO Whole Blood	ethyl-malonylcarnitine	0.02	0.00	
ACD 10 KO Whole Blood	glutaroylcarnitine	0.01	0.01	
ACD 10 KO Whole Blood	adipoylcarnitine	0.04	0.01	
ACD 10 KO Whole Blood	3-methyl-glutaroylcarnitine	0.01	0.01	
ACD 10 KO Whole Blood	suberoylcarnitine	0.02	0.02	
ACD 10 KO Whole Blood	sebacoylcarnitine	0.01	0.01	
WT Whole Blood	acetylcarnitine	24.14	21.97	
WT Whole Blood	propionylcarnitine	0.42	0.50	

WT Whole Blood	butyrylcarnitine	0.13	0.37
WT Whole Blood	isobutyrylcarnitine	0.07	0.08
WT Whole Blood	R-3-hydroxy-butyrylcarnitine	0.06	0.07
WT Whole Blood	S-3-hydroxy-butyrylcarnitine	0.16	0.14
WT Whole Blood	valerylcarnitine	0.00	0.01
WT Whole Blood	isovalerylcarnitine	0.06	0.06
WT Whole Blood	3-hydroxy-isovalerylcarnitine	0.13	0.12
WT Whole Blood	2-methyl-butyrylcarnitine	0.05	0.06
WT Whole Blood	tigloylcarnitine	0.01	0.01
WT Whole Blood	3-methyl-crotonylcarnitine	0.00	0.00
WT Whole Blood	hexanoylcarnitine	0.03	0.03
WT Whole Blood	R-3-hydroxy-hexanoylcarnitine	0.00	0.01
WT Whole Blood	S-3-hydroxy-hexanoylcarnitine	0.01	0.01
WT Whole Blood	phenylacetylcarnitine	0.01	0.00
WT Whole Blood	phenylpropionylcarnitine	0.01	0.01
WT Whole Blood	4-phenyl-butyrylcarnitine	0.01	0.00
WT Whole Blood	benzoylcarnitine	0.00	0.00
WT Whole Blood	4-methyl-hexanoylcarnitine	0.01	0.01
WT Whole Blood	octanoylcarnitine	0.04	0.04
WT Whole Blood	R-3-hydroxy-octanoylcarnitine	0.00	0.01
WT Whole Blood	S-3-hydroxy-octanoylcarnitine	0.02	0.02
WT Whole Blood	branched-chain C8	0.01	0.01
WT Whole Blood	cis-3,4-methylene- heptanoylcarnitine	0.01	0.01
WT Whole Blood	4-methyl-octanoylcarnitine	0.00	0.02
WT Whole Blood	2,6-dimethyl-heptanoylcarnitine	0.02	0.01
WT Whole Blood	decanoylcarnitine	0.02	0.01

WT Whole Blood	cis-4-decenoylcarnitine	0.02	0.01
WT Whole Blood	cis-3,4-methylene- nonanoylcarnitine	0.01	0.00
WT Whole Blood	R-3-hydroxy-decanoylcarnitine	0.01	0.01
WT Whole Blood	S-3-hydroxy-decanoylcarnitine	0.03	0.03
WT Whole Blood	5-decynoylcarnitine	0.01	0.00
WT Whole Blood	lauroylcarnitine	0.03	0.03
WT Whole Blood	trans-2-dodecenoylcarnitine	0.00	0.01
WT Whole Blood	R-3-hydroxy-lauroylcarnitine	0.01	0.01
WT Whole Blood	S-3-hydroxy-lauroylcarnitine	0.01	0.01
WT Whole Blood	myristoylcarnitine	0.07	0.09
WT Whole Blood	myristoleoylcarnitine	0.01	0.03
WT Whole Blood	cis-5-tetradecenoylcarnitine	0.03	0.03
WT Whole Blood	trans-2-tetradecenoylcarnitine	0.01	0.02
WT Whole Blood	cis,cis-5,8- tetradecadienoylcarnitine	0.01	0.03
WT Whole Blood	R-3-hydroxy-myristoylcarnitine	0.00	0.01
WT Whole Blood	S-3-hydroxy-myristoylcarnitine	0.02	0.01
WT Whole Blood	hydroxy-C14:1	0.01	0.02
WT Whole Blood	palmitoylcarnitine	0.94	0.99
WT Whole Blood	palmitoleoylcarnitine	0.03	0.05
WT Whole Blood	trans-2-hexadecenoylcarnitine	0.00	0.02
WT Whole Blood	R-3-hydroxy-palmitoylcarnitine	0.02	0.02
WT Whole Blood	S-3-hydroxy-palmitoylcarnitine	0.00	0.02
WT Whole Blood	hydroxy-C16:1	0.00	0.02
WT Whole Blood	stearoylcarnitine	0.20	0.30
WT Whole Blood	oleoylcarnitine	0.40	0.39

WT Whole Blood	linoleoylcarnitine	0.16	0.12	
WT Whole Blood	alpha-linolenoylcarnitine	0.03	0.03	
WT Whole Blood	gamma-linolenoylcarnitine	0.00	0.01	
WT Whole Blood	R-3-hydroxy-stearoylcarnitine	0.02	0.03	
WT Whole Blood	S-3-hydroxy-stearoylcarnitine	0.01	0.01	
WT Whole Blood	hydroxy-C18:1	0.02	0.01	
WT Whole Blood	hydroxy-C18:2	0.01	0.01	
WT Whole Blood	hydroxy-C18:3	0.01	0.01	
WT Whole Blood	malonylcarnitine	0.12	0.06	
WT Whole Blood	succinylcarnitine	0.42	0.29	
WT Whole Blood	methyl-malonylcarnitine	0.06	0.06	
WT Whole Blood	ethyl-malonylcarnitine	0.00	0.00	
WT Whole Blood	glutaroylcarnitine	0.01	0.01	
WT Whole Blood	adipoylcarnitine	0.02	0.02	
WT Whole Blood	3-methyl-glutaroylcarnitine	0.01	0.01	
WT Whole Blood	suberoylcarnitine	0.01	0.02	
WT Whole Blood	sebacoylcarnitine	0.01	0.01	
ACD 10 KO Muscle	acetylcarnitine	147.79	135.75	67.982
ACD 10 KO Muscle	propionylcarnitine	2.96	2.89	0.549
ACD 10 KO Muscle	butyrylcarnitine	3.10	3.00	1.705
ACD 10 KO Muscle	isobutyrylcarnitine	0.35	0.44	0.715
ACD 10 KO Muscle	R-3-hydroxy-butyrylcarnitine	1.20	1.56	0.191
ACD 10 KO Muscle	S-3-hydroxy-butyrylcarnitine	5.16	6.13	1.310
ACD 10 KO Muscle	valerylcarnitine	0.27	0.16	0.036
ACD 10 KO Muscle	isovalerylcarnitine	1.33	0.43	2.266
ACD 10 KO Muscle	3-hydroxy-isovalerylcarnitine	1.44	1.76	0.716
ACD 10 KO Muscle	2-methyl-butyrylcarnitine	0.84	0.79	0.556

ACD 10 KO Muscle	tigloylcarnitine	0.41	0.25	0.132
ACD 10 KO Muscle	3-methyl-crotonylcarnitine	0.14	0.04	0.005
ACD 10 KO Muscle	hexanoylcarnitine	0.57	0.47	0.321
ACD 10 KO Muscle	R-3-hydroxy-hexanoylcarnitine	0.06	0.14	0.019
ACD 10 KO Muscle	S-3-hydroxy-hexanoylcarnitine	0.40	0.15	0.057
ACD 10 KO Muscle	phenylacetylcarnitine	0.24	0.04	0.000
ACD 10 KO Muscle	phenylpropionylcarnitine	0.23	0.34	
ACD 10 KO Muscle	4-phenyl-butyrylcarnitine	0.28	0.09	
ACD 10 KO Muscle	benzoylcarnitine	0.03	0.04	0.004
ACD 10 KO Muscle	4-methyl-hexanoylcarnitine	0.24	0.24	0.003
ACD 10 KO Muscle	octanoylcarnitine	0.41	0.46	0.000
ACD 10 KO Muscle	R-3-hydroxy-octanoylcarnitine	0.46	0.34	0.031
ACD 10 KO Muscle	S-3-hydroxy-octanoylcarnitine	0.57	0.47	0.112
ACD 10 KO Muscle	branched-chain C8	0.20	0.17	0.000
ACD 10 KO Muscle	cis-3,4-methylene-heptanoylcarnitine	0.32	0.32	0.007
ACD 10 KO Muscle	4-methyl-octanoylcarnitine	0.21	0.48	0.000
ACD 10 KO Muscle	2,6-dimethyl-heptanoylcarnitine	0.57	0.39	0.000
ACD 10 KO Muscle	decanoylcarnitine	0.26	0.00	0.122
ACD 10 KO Muscle	cis-4-decenoylcarnitine	0.23	0.00	0.006
ACD 10 KO Muscle	cis-3,4-methylene-nonanoylcarnitine	0.13	0.00	0.000
ACD 10 KO Muscle	R-3-hydroxy-decanoylcarnitine	0.09	0.29	0.022
ACD 10 KO Muscle	S-3-hydroxy-decanoylcarnitine	0.65	0.71	0.037
ACD 10 KO Muscle	5-decynoylcarnitine	0.16	0.11	0.000
ACD 10 KO Muscle	lauroylcarnitine	0.31	0.38	0.003
ACD 10 KO Muscle	trans-2-dodecenoylcarnitine	0.05	0.31	0.000

ACD 10 KO Muscle	R-3-hydroxy-lauroylcarnitine	0.34	0.16	0.002
ACD 10 KO Muscle	S-3-hydroxy-lauroylcarnitine	0.48	0.26	0.018
ACD 10 KO Muscle	myristoylcarnitine	0.23	0.60	0.325
ACD 10 KO Muscle	myristoleoylcarnitine	0.68	0.53	0.098
ACD 10 KO Muscle	cis-5-tetradecenoylcarnitine	0.00	0.31	0.000
ACD 10 KO Muscle	trans-2-tetradecenoylcarnitine	0.30	0.51	0.000
ACD 10 KO Muscle	cis,cis-5,8-tetradecadienoylcarnitine	0.13	0.58	0.055
ACD 10 KO Muscle	R-3-hydroxy-myristoylcarnitine	0.08	0.29	0.000
ACD 10 KO Muscle	S-3-hydroxy-myristoylcarnitine	0.20	0.11	0.013
ACD 10 KO Muscle	hydroxy-C14:1	0.00	0.25	0.022
ACD 10 KO Muscle	palmitoylcarnitine	1.45	1.84	1.817
ACD 10 KO Muscle	palmitoleoylcarnitine	0.00	0.43	0.107
ACD 10 KO Muscle	trans-2-hexadecenoylcarnitine	0.20	0.48	0.009
ACD 10 KO Muscle	R-3-hydroxy-palmitoylcarnitine	0.45	0.59	0.000
ACD 10 KO Muscle	S-3-hydroxy-palmitoylcarnitine	0.00	0.55	0.069
ACD 10 KO Muscle	hydroxy-C16:1	0.00	0.42	0.019
ACD 10 KO Muscle	stearoylcarnitine	2.04	1.05	0.646
ACD 10 KO Muscle	oleoylcarnitine	0.51	1.44	1.712
ACD 10 KO Muscle	linoleoylcarnitine	0.75	1.65	1.430
ACD 10 KO Muscle	alpha-linolenoylcarnitine	0.31	0.34	0.107
ACD 10 KO Muscle	gamma-linolenoylcarnitine	0.01	0.41	0.014
ACD 10 KO Muscle	R-3-hydroxy-stearoylcarnitine	0.29	0.58	0.003
ACD 10 KO Muscle	S-3-hydroxy-stearoylcarnitine	0.21	0.34	0.023
ACD 10 KO Muscle	hydroxy-C18:1	0.32	0.40	0.174
ACD 10 KO Muscle	hydroxy-C18:2	0.22	0.46	0.070
ACD 10 KO Muscle	hydroxy-C18:3	0.20	0.27	0.051

ACD 10 KO Muscle	malonylcarnitine	1.02	0.40	0.360
ACD 10 KO Muscle	succinylcarnitine	0.89	0.76	0.293
ACD 10 KO Muscle	methyl-malonylcarnitine	0.14	0.42	0.078
ACD 10 KO Muscle	ethyl-malonylcarnitine	0.14	0.10	0.000
ACD 10 KO Muscle	glutaroylcarnitine	0.08	0.19	0.078
ACD 10 KO Muscle	adipoylcarnitine	0.22	0.27	0.016
ACD 10 KO Muscle	3-methyl-glutaroylcarnitine	0.00	0.33	0.000
ACD 10 KO Muscle	suberoylcarnitine	0.08	0.36	0.000
ACD 10 KO Muscle	sebacoylcarnitine	0.14	0.23	0.000
WT Muscle	acetylcarnitine	113.43	127.63	137.438
WT Muscle	propionylcarnitine	2.90	2.77	2.263
WT Muscle	butyrylcarnitine	1.72	3.56	1.562
WT Muscle	isobutyrylcarnitine	0.44	0.43	0.150
WT Muscle	R-3-hydroxy-butyrylcarnitine	1.19	1.70	0.369
WT Muscle	S-3-hydroxy-butyrylcarnitine	3.26	6.51	2.297
WT Muscle	valerylcarnitine	0.32	0.15	0.062
WT Muscle	isovalerylcarnitine	0.58	0.38	0.000
WT Muscle	3-hydroxy-isovalerylcarnitine	1.54	1.67	1.020
WT Muscle	2-methyl-butyrylcarnitine	0.81	0.76	0.217
WT Muscle	tigloylcarnitine	0.32	0.26	0.061
WT Muscle	3-methyl-crotonylcarnitine	0.05	0.05	0.003
WT Muscle	hexanoylcarnitine	0.73	0.55	0.177
WT Muscle	R-3-hydroxy-hexanoylcarnitine	0.04	0.16	0.033
WT Muscle	S-3-hydroxy-hexanoylcarnitine	0.32	0.15	0.078
WT Muscle	phenylacetylcarnitine	0.25	0.05	0.000
WT Muscle	phenylpropionylcarnitine	0.23	0.37	
WT Muscle	4-phenyl-butyrylcarnitine	0.30	0.09	

WT Muscle	benzoylcarnitine	0.07	0.04	0.013
WT Muscle	4-methyl-hexanoylcarnitine	0.25	0.25	0.001
WT Muscle	octanoylcarnitine	0.55	0.47	0.000
WT Muscle	R-3-hydroxy-octanoylcarnitine	0.45	0.33	0.032
WT Muscle	S-3-hydroxy-octanoylcarnitine	0.68	0.51	0.087
WT Muscle	branched-chain C8	0.20	0.18	0.000
WT Muscle	cis-3,4-methylene- heptanoylcarnitine	0.33	0.36	0.009
WT Muscle	4-methyl-octanoylcarnitine	0.12	0.52	0.006
WT Muscle	2,6-dimethyl-heptanoylcarnitine	0.42	0.43	0.000
WT Muscle	decanoylcarnitine	0.23	0.00	0.151
WT Muscle	cis-4-decenoylcarnitine	0.24	0.00	0.005
WT Muscle	cis-3,4-methylene- nonanoylcarnitine	0.16	0.00	0.000
WT Muscle	R-3-hydroxy-decanoylcarnitine	0.15	0.32	0.020
WT Muscle	S-3-hydroxy-decanoylcarnitine	0.72	0.75	0.048
WT Muscle	5-decynoylcarnitine	0.15	0.13	0.000
WT Muscle	lauroylcarnitine	0.27	0.44	0.018
WT Muscle	trans-2-dodecenoylcarnitine	0.08	0.30	0.000
WT Muscle	R-3-hydroxy-lauroylcarnitine	0.34	0.17	0.002
WT Muscle	S-3-hydroxy-lauroylcarnitine	0.00	0.28	0.016
WT Muscle	myristoylcarnitine	0.51	0.57	0.288
WT Muscle	myristoleoylcarnitine	0.83	0.61	0.105
WT Muscle	cis-5-tetradecenoylcarnitine	0.00	0.29	0.000
WT Muscle	trans-2-tetradecenoylcarnitine	0.19	0.49	0.019
WT Muscle	cis,cis-5,8- tetradecadienoylcarnitine	0.23	0.58	0.023

WT Muscle	R-3-hydroxy-myristoylcarnitine	0.11	0.32	0.000
WT Muscle	S-3-hydroxy-myristoylcarnitine	0.31	0.15	0.029
WT Muscle	hydroxy-C14:1	0.00	0.26	0.015
WT Muscle	palmitoylcarnitine	2.23	2.11	1.620
WT Muscle	palmitoleoylcarnitine	0.00	0.60	0.204
WT Muscle	trans-2-hexadecenoylcarnitine	0.10	0.58	0.015
WT Muscle	R-3-hydroxy-palmitoylcarnitine	0.46	0.66	0.020
WT Muscle	S-3-hydroxy-palmitoylcarnitine	0.00	0.57	0.154
WT Muscle	hydroxy-C16:1	0.00	0.46	0.055
WT Muscle	stearoylcarnitine	1.96	1.18	0.687
WT Muscle	oleoylcarnitine	1.73	1.85	1.183
WT Muscle	linoleoylcarnitine	1.35	1.39	0.907
WT Muscle	alpha-linolenoylcarnitine	0.32	0.38	0.076
WT Muscle	gamma-linolenoylcarnitine	0.02	0.45	0.027
WT Muscle	R-3-hydroxy-stearoylcarnitine	0.31	0.64	0.017
WT Muscle	S-3-hydroxy-stearoylcarnitine	0.23	0.37	0.084
WT Muscle	hydroxy-C18:1	0.35	0.49	0.225
WT Muscle	hydroxy-C18:2	0.31	0.39	0.104
WT Muscle	hydroxy-C18:3	0.30	0.25	0.024
WT Muscle	malonylcarnitine	0.96	0.48	0.689
WT Muscle	succinylcarnitine	0.84	0.68	1.024
WT Muscle	methyl-malonylcarnitine	0.07	0.49	0.153
WT Muscle	ethyl-malonylcarnitine	0.04	0.13	0.000
WT Muscle	glutaroylcarnitine	0.03	0.12	0.000
WT Muscle	adipoylcarnitine	0.34	0.29	0.021
WT Muscle	3-methyl-glutaroylcarnitine	0.00	0.36	0.000
WT Muscle	suberoylcarnitine	0.08	0.41	0.000

WT Muscle	sebacoylcarnitine	0.20	0.24	0.000
ACD 10 KO Liver	acetylcarnitine	68.17	90.74	77.053
ACD 10 KO Liver	propionylcarnitine	5.70	9.11	13.448
ACD 10 KO Liver	butyrylcarnitine	0.97	1.81	3.709
ACD 10 KO Liver	isobutyrylcarnitine	0.84	1.55	0.559
ACD 10 KO Liver	R-3-hydroxy-butyrylcarnitine	2.77	3.11	0.978
ACD 10 KO Liver	S-3-hydroxy-butyrylcarnitine	1.67	2.68	0.676
ACD 10 KO Liver	valerylcarnitine	0.19	0.12	1.426
ACD 10 KO Liver	isovalerylcarnitine	0.88	0.53	0.503
ACD 10 KO Liver	3-hydroxy-isovalerylcarnitine	0.90	1.48	0.448
ACD 10 KO Liver	2-methyl-butyrylcarnitine	0.69	1.06	0.704
ACD 10 KO Liver	tigloylcarnitine	0.25	0.22	0.016
ACD 10 KO Liver	3-methyl-crotonylcarnitine	0.04	0.06	0.003
ACD 10 KO Liver	hexanoylcarnitine	0.28	0.15	0.498
ACD 10 KO Liver	R-3-hydroxy-hexanoylcarnitine	0.04	0.21	0.047
ACD 10 KO Liver	S-3-hydroxy-hexanoylcarnitine	0.32	0.29	0.085
ACD 10 KO Liver	phenylacetylcarnitine	0.22	0.04	0.002
ACD 10 KO Liver	phenylpropionylcarnitine	0.33	0.75	
ACD 10 KO Liver	4-phenyl-butyrylcarnitine	0.24	0.09	
ACD 10 KO Liver	benzoylcarnitine	0.03	0.03	0.004
ACD 10 KO Liver	4-methyl-hexanoylcarnitine	0.21	0.26	0.041
ACD 10 KO Liver	octanoylcarnitine	0.31	0.43	0.000
ACD 10 KO Liver	R-3-hydroxy-octanoylcarnitine	0.38	0.38	0.035
ACD 10 KO Liver	S-3-hydroxy-octanoylcarnitine	0.50	0.55	0.048
ACD 10 KO Liver	branched-chain C8	0.17	0.19	0.000
ACD 10 KO Liver	cis-3,4-methylene-heptanoylcarnitine	0.29	0.39	0.009

ACD 10 KO Liver	4-methyl-octanoylcarnitine	0.07	0.54	0.000
ACD 10 KO Liver	2,6-dimethyl-heptanoylcarnitine	0.35	0.47	0.000
ACD 10 KO Liver	decanoylcarnitine	0.15	0.00	0.030
ACD 10 KO Liver	cis-4-decenoylcarnitine	0.15	0.00	0.001
ACD 10 KO Liver	cis-3,4-methylene- nonanoylcarnitine	0.19	0.00	0.004
ACD 10 KO Liver	R-3-hydroxy-decanoylcarnitine	0.05	0.36	0.008
ACD 10 KO Liver	S-3-hydroxy-decanoylcarnitine	0.56	0.80	0.000
ACD 10 KO Liver	5-decynoylcarnitine	0.16	0.11	0.000
ACD 10 KO Liver	lauroylcarnitine	0.19	0.35	0.000
ACD 10 KO Liver	trans-2-dodecenoylcarnitine	0.05	0.26	0.000
ACD 10 KO Liver	R-3-hydroxy-lauroylcarnitine	0.29	0.16	0.001
ACD 10 KO Liver	S-3-hydroxy-lauroylcarnitine	0.44	0.26	0.000
ACD 10 KO Liver	myristoylcarnitine	0.02	0.24	0.000
ACD 10 KO Liver	myristoleoylcarnitine	0.65	0.53	0.006
ACD 10 KO Liver	cis-5-tetradecenoylcarnitine	0.00	0.32	0.000
ACD 10 KO Liver	trans-2-tetradecenoylcarnitine	0.13	0.51	0.018
ACD 10 KO Liver	cis,cis-5,8- tetradecadienoylcarnitine	0.09	0.54	0.000
ACD 10 KO Liver	R-3-hydroxy-myristoylcarnitine	0.07	0.32	0.000
ACD 10 KO Liver	S-3-hydroxy-myristoylcarnitine	0.20	0.05	0.000
ACD 10 KO Liver	hydroxy-C14:1	0.00	0.25	0.020
ACD 10 KO Liver	palmitoylcarnitine	0.33	0.56	0.297
ACD 10 KO Liver	palmitoleoylcarnitine	0.00	0.32	0.000
ACD 10 KO Liver	trans-2-hexadecenoylcarnitine	0.12	0.52	0.000
ACD 10 KO Liver	R-3-hydroxy-palmitoylcarnitine	0.39	0.64	0.000
ACD 10 KO Liver	S-3-hydroxy-palmitoylcarnitine	0.00	0.39	0.012

ACD 10 KO Liver	hydroxy-C16:1	0.00	0.45	0.015
ACD 10 KO Liver	stearoylcarnitine	1.36	0.40	0.407
ACD 10 KO Liver	oleoylcarnitine	0.00	0.00	0.000
ACD 10 KO Liver	linoleoylcarnitine	0.28	0.78	0.297
ACD 10 KO Liver	alpha-linolenoylcarnitine	0.00	0.26	0.000
ACD 10 KO Liver	gamma-linolenoylcarnitine	0.00	0.36	0.000
ACD 10 KO Liver	R-3-hydroxy-stearoylcarnitine	0.26	0.65	0.006
ACD 10 KO Liver	S-3-hydroxy-stearoylcarnitine	0.24	0.32	0.033
ACD 10 KO Liver	hydroxy-C18:1	0.24	0.30	0.063
ACD 10 KO Liver	hydroxy-C18:2	0.20	0.27	0.018
ACD 10 KO Liver	hydroxy-C18:3	0.18	0.25	0.000
ACD 10 KO Liver	malonylcarnitine	2.29	2.21	1.625
ACD 10 KO Liver	succinylcarnitine	0.74	0.65	0.465
ACD 10 KO Liver	methyl-malonylcarnitine	0.05	0.53	0.073
ACD 10 KO Liver	ethyl-malonylcarnitine	0.20	0.13	0.000
ACD 10 KO Liver	glutaroylcarnitine	2.26	4.27	3.456
ACD 10 KO Liver	adipoylcarnitine	1.70	2.97	2.081
ACD 10 KO Liver	3-methyl-glutaroylcarnitine	0.14	0.46	0.011
ACD 10 KO Liver	suberoylcarnitine	0.07	0.62	0.064
ACD 10 KO Liver	sebacoylcarnitine	0.18	0.34	0.044
WT Liver	acetylcarnitine	106.78	107.49	76.101
WT Liver	propionylcarnitine	8.94	13.02	6.053
WT Liver	butyrylcarnitine	0.57	0.93	5.906
WT Liver	isobutyrylcarnitine	1.25	1.31	0.768
WT Liver	R-3-hydroxy-butyrylcarnitine	4.20	3.90	2.816
WT Liver	S-3-hydroxy-butyrylcarnitine	2.18	2.63	1.192
WT Liver	valerylcarnitine	0.20	0.12	0.610

WT Liver	isovalerylcarnitine	0.57	0.57	0.139
WT Liver	3-hydroxy-isovalerylcarnitine	1.18	1.25	0.471
WT Liver	2-methyl-butyrylcarnitine	0.92	1.46	0.615
WT Liver	tigloylcarnitine	0.31	0.22	0.008
WT Liver	3-methyl-crotonylcarnitine	0.07	0.09	0.000
WT Liver	hexanoylcarnitine	0.27	0.13	0.877
WT Liver	R-3-hydroxy-hexanoylcarnitine	0.09	0.20	0.047
WT Liver	S-3-hydroxy-hexanoylcarnitine	0.36	0.28	0.101
WT Liver	phenylacetylcarnitine	0.20	0.05	0.002
WT Liver	phenylpropionylcarnitine	0.28	0.54	
WT Liver	4-phenyl-butyrylcarnitine	0.25	0.10	
WT Liver	benzoylcarnitine	0.04	0.06	0.012
WT Liver	4-methyl-hexanoylcarnitine	0.22	0.24	0.029
WT Liver	octanoylcarnitine	0.33	0.36	0.000
WT Liver	R-3-hydroxy-octanoylcarnitine	0.29	0.34	0.035
WT Liver	S-3-hydroxy-octanoylcarnitine	0.53	0.45	0.071
WT Liver	branched-chain C8	0.17	0.16	
WT Liver	cis-3,4-methylene-heptanoylcarnitine	0.28	0.33	0.000
WT Liver	4-methyl-octanoylcarnitine	0.19	0.49	0.007
WT Liver	2,6-dimethyl-heptanoylcarnitine	0.48	0.37	0.006
WT Liver	decanoylcarnitine	0.16	0.00	0.082
WT Liver	cis-4-decenoylcarnitine	0.21	0.00	0.000
WT Liver	cis-3,4-methylene-nonanoylcarnitine	0.12	0.00	0.000
WT Liver	R-3-hydroxy-decanoylcarnitine	0.07	0.29	0.030
WT Liver	S-3-hydroxy-decanoylcarnitine	0.55	0.64	0.038

WT Liver	5-decynoylcarnitine	0.13	0.12	0.000
WT Liver	lauroylcarnitine	0.19	0.32	0.000
WT Liver	trans-2-dodecenoylcarnitine	0.05	0.26	0.000
WT Liver	R-3-hydroxy-lauroylcarnitine	0.29	0.16	0.005
WT Liver	S-3-hydroxy-lauroylcarnitine	0.00	0.23	0.028
WT Liver	myristoylcarnitine	0.00	0.21	0.161
WT Liver	myristoleoylcarnitine	0.46	0.43	0.019
WT Liver	cis-5-tetradecenoylcarnitine	0.00	0.15	0.000
WT Liver	trans-2-tetradecenoylcarnitine	0.15	0.44	0.000
WT Liver	cis,cis-5,8-tetradecadienoylcarnitine	0.08	0.47	0.005
WT Liver	R-3-hydroxy-myristoylcarnitine	0.07	0.28	0.000
WT Liver	S-3-hydroxy-myristoylcarnitine	0.16	0.07	0.029
WT Liver	hydroxy-C14:1	0.00	0.20	0.031
WT Liver	palmitoylcarnitine	0.22	0.44	1.330
WT Liver	palmitoleoylcarnitine	0.00	0.30	0.121
WT Liver	trans-2-hexadecenoylcarnitine	0.13	0.47	0.004
WT Liver	R-3-hydroxy-palmitoylcarnitine	0.41	0.55	0.003
WT Liver	S-3-hydroxy-palmitoylcarnitine	0.00	0.33	0.097
WT Liver	hydroxy-C16:1	0.00	0.34	0.010
WT Liver	stearoylcarnitine	1.52	0.29	0.895
WT Liver	oleoylcarnitine	0.00	0.00	0.993
WT Liver	linoleoylcarnitine	0.29	0.65	0.576
WT Liver	alpha-linolenoylcarnitine	0.00	0.22	0.048
WT Liver	gamma-linolenoylcarnitine	0.00	0.35	0.000
WT Liver	R-3-hydroxy-stearoylcarnitine	0.31	0.54	0.023
WT Liver	S-3-hydroxy-stearoylcarnitine	0.25	0.26	0.036

WT Liver	hydroxy-C18:1	0.35	0.23	0.149
WT Liver	hydroxy-C18:2	0.27	0.24	0.136
WT Liver	hydroxy-C18:3	0.26	0.20	0.020
WT Liver	malonylcarnitine	1.84	1.70	1.212
WT Liver	succinylcarnitine	0.76	0.79	0.516
WT Liver	methyl-malonylcarnitine	0.05	0.45	0.032
WT Liver	ethyl-malonylcarnitine	0.23	0.11	0.000
WT Liver	glutaroylcarnitine	3.09	4.27	2.640
WT Liver	adipoylcarnitine	2.84	2.43	2.165
WT Liver	3-methyl-glutaroylcarnitine	0.00	0.41	0.000
WT Liver	suberoylcarnitine	0.16	0.45	0.059
WT Liver	sebacoylcarnitine	0.18	0.26	0.058
ACD 10 KO Whole Brain	acetylcarnitine	49.38	58.09	30.024
ACD 10 KO Whole Brain	propionylcarnitine	3.09	3.35	1.221
ACD 10 KO Whole Brain	butyrylcarnitine	1.33	1.59	1.048
ACD 10 KO Whole Brain	isobutyrylcarnitine	0.37	0.50	0.167
ACD 10 KO Whole Brain	R-3-hydroxy-butyrylcarnitine	0.74	1.07	0.088
ACD 10 KO Whole Brain	S-3-hydroxy-butyrylcarnitine	1.11	1.50	0.312
ACD 10 KO Whole Brain	valerylcarnitine	0.33	0.12	0.040
ACD 10 KO Whole Brain	isovalerylcarnitine	1.41	0.78	0.176
ACD 10 KO Whole Brain	3-hydroxy-isovalerylcarnitine	1.04	1.25	0.415
ACD 10 KO Whole Brain	2-methyl-butyrylcarnitine	0.71	0.63	0.263
ACD 10 KO Whole Brain	tigloylcarnitine	0.26	0.14	0.012
ACD 10 KO Whole Brain	3-methyl-crotonylcarnitine	0.03	0.02	0.001
ACD 10 KO Whole Brain	hexanoylcarnitine	0.36	0.18	0.069
ACD 10 KO Whole Brain	R-3-hydroxy-hexanoylcarnitine	0.08	0.10	0.025
ACD 10 KO Whole Brain	S-3-hydroxy-hexanoylcarnitine	0.28	0.07	0.026

ACD 10 KO Whole Brain	phenylacetylcarnitine	0.23	0.01	0.000
ACD 10 KO Whole Brain	phenylpropionylcarnitine	0.19	0.29	
ACD 10 KO Whole Brain	4-phenyl-butyrylcarnitine	0.25	0.06	
ACD 10 KO Whole Brain	benzoylcarnitine	0.03	0.01	0.002
ACD 10 KO Whole Brain	4-methyl-hexanoylcarnitine	0.22	0.20	0.000
ACD 10 KO Whole Brain	octanoylcarnitine	0.33	0.33	0.000
ACD 10 KO Whole Brain	R-3-hydroxy-octanoylcarnitine	0.33	0.28	0.002
ACD 10 KO Whole Brain	S-3-hydroxy-octanoylcarnitine	0.50	0.35	0.006
ACD 10 KO Whole Brain	branched-chain C8	0.17	0.16	0.000
ACD 10 KO Whole Brain	cis-3,4-methylene-heptanoylcarnitine	0.30	0.29	0.001
ACD 10 KO Whole Brain	4-methyl-octanoylcarnitine	0.22	0.43	0.008
ACD 10 KO Whole Brain	2,6-dimethyl-heptanoylcarnitine	0.52	0.34	0.000
ACD 10 KO Whole Brain	decanoylcarnitine	0.19	0.00	0.050
ACD 10 KO Whole Brain	cis-4-decenoylcarnitine	0.23	0.00	0.011
ACD 10 KO Whole Brain	cis-3,4-methylene-nonanoylcarnitine	0.12	0.00	0.000
ACD 10 KO Whole Brain	R-3-hydroxy-decanoylcarnitine	0.05	0.24	0.010
ACD 10 KO Whole Brain	S-3-hydroxy-decanoylcarnitine	0.57	0.57	0.002
ACD 10 KO Whole Brain	5-decynoylcarnitine	0.15	0.08	0.000
ACD 10 KO Whole Brain	lauroylcarnitine	0.24	0.33	0.060
ACD 10 KO Whole Brain	trans-2-dodecenoylcarnitine	0.07	0.21	0.003
ACD 10 KO Whole Brain	R-3-hydroxy-lauroylcarnitine	0.31	0.12	0.000
ACD 10 KO Whole Brain	S-3-hydroxy-lauroylcarnitine	0.03	0.19	0.003
ACD 10 KO Whole Brain	myristoylcarnitine	0.84	1.07	0.842
ACD 10 KO Whole Brain	myristoleoylcarnitine	0.57	0.46	0.136
ACD 10 KO Whole Brain	cis-5-tetradecenoylcarnitine	0.00	0.19	0.000

ACD 10 KO Whole Brain	trans-2-tetradecenoylcarnitine	0.23	0.46	0.000
ACD 10 KO Whole Brain	cis,cis-5,8-tetradecadienoylcarnitine	0.08	0.43	0.000
ACD 10 KO Whole Brain	R-3-hydroxy-myristoylcarnitine	0.10	0.24	0.000
ACD 10 KO Whole Brain	S-3-hydroxy-myristoylcarnitine	0.26	0.02	0.000
ACD 10 KO Whole Brain	hydroxy-C14:1	0.00	0.20	0.015
ACD 10 KO Whole Brain	palmitoylcarnitine	1.95	2.38	3.335
ACD 10 KO Whole Brain	palmitoleoylcarnitine	0.00	0.57	0.349
ACD 10 KO Whole Brain	trans-2-hexadecenoylcarnitine	0.15	0.47	0.000
ACD 10 KO Whole Brain	R-3-hydroxy-palmitoylcarnitine	0.38	0.52	0.000
ACD 10 KO Whole Brain	S-3-hydroxy-palmitoylcarnitine	0.00	0.32	0.000
ACD 10 KO Whole Brain	hydroxy-C16:1	0.00	0.35	0.004
ACD 10 KO Whole Brain	stearoylcarnitine	2.33	0.81	0.840
ACD 10 KO Whole Brain	oleoylcarnitine	1.20	1.52	2.988
ACD 10 KO Whole Brain	linoleoylcarnitine	0.32	0.79	0.080
ACD 10 KO Whole Brain	alpha-linolenoylcarnitine	0.00	0.26	0.000
ACD 10 KO Whole Brain	gamma-linolenoylcarnitine	0.00	0.36	0.000
ACD 10 KO Whole Brain	R-3-hydroxy-stearoylcarnitine	0.26	0.52	0.008
ACD 10 KO Whole Brain	S-3-hydroxy-stearoylcarnitine	0.18	0.21	0.000
ACD 10 KO Whole Brain	hydroxy-C18:1	0.28	0.24	0.057
ACD 10 KO Whole Brain	hydroxy-C18:2	0.19	0.21	0.006
ACD 10 KO Whole Brain	hydroxy-C18:3	0.17	0.22	0.000
ACD 10 KO Whole Brain	malonylcarnitine	0.55	0.40	0.280
ACD 10 KO Whole Brain	succinylcarnitine	0.31	0.32	0.267
ACD 10 KO Whole Brain	methyl-malonylcarnitine	0.01	0.34	0.100
ACD 10 KO Whole Brain	ethyl-malonylcarnitine	0.15	0.09	0.000
ACD 10 KO Whole Brain	glutaroylcarnitine	0.29	0.50	0.068

ACD 10 KO Whole Brain	adipoylcarnitine	0.28	0.24	0.008
ACD 10 KO Whole Brain	3-methyl-glutaroylcarnitine	0.00	0.31	0.000
ACD 10 KO Whole Brain	suberoylcarnitine	0.06	0.31	0.000
ACD 10 KO Whole Brain	sebacoylcarnitine	0.18	0.20	0.000
WT Whole Brain	acetylcarnitine	60.42	60.95	49.166
WT Whole Brain	propionylcarnitine	3.64	3.90	1.643
WT Whole Brain	butyrylcarnitine	1.18	1.55	1.252
WT Whole Brain	isobutyrylcarnitine	0.44	0.52	0.355
WT Whole Brain	R-3-hydroxy-butyrylcarnitine	0.83	1.18	0.147
WT Whole Brain	S-3-hydroxy-butyrylcarnitine	1.33	1.59	0.308
WT Whole Brain	valerylcarnitine	0.27	0.13	0.044
WT Whole Brain	isovalerylcarnitine	0.88	0.60	0.453
WT Whole Brain	3-hydroxy-isovalerylcarnitine	1.10	1.36	0.376
WT Whole Brain	2-methyl-butyrylcarnitine	0.66	0.71	0.340
WT Whole Brain	tigloylcarnitine	0.28	0.15	0.017
WT Whole Brain	3-methyl-crotonylcarnitine	0.05	0.02	0.001
WT Whole Brain	hexanoylcarnitine	0.35	0.19	0.088
WT Whole Brain	R-3-hydroxy-hexanoylcarnitine	0.12	0.11	0.019
WT Whole Brain	S-3-hydroxy-hexanoylcarnitine	0.25	0.08	0.017
WT Whole Brain	phenylacetylcarnitine	0.20	0.01	0.000
WT Whole Brain	phenylpropionylcarnitine	0.19	0.33	
WT Whole Brain	4-phenyl-butyrylcarnitine	0.25	0.07	
WT Whole Brain	benzoylcarnitine	0.03	0.01	0.000
WT Whole Brain	4-methyl-hexanoylcarnitine	0.20	0.22	0.000
WT Whole Brain	octanoylcarnitine	0.30	0.40	0.000
WT Whole Brain	R-3-hydroxy-octanoylcarnitine	0.19	0.28	0.004
WT Whole Brain	S-3-hydroxy-octanoylcarnitine	0.33	0.38	0.020

WT Whole Brain	branched-chain C8	0.17	0.18	0.000
WT Whole Brain	cis-3,4-methylene-heptanoylcarnitine	0.27	0.32	0.003
WT Whole Brain	4-methyl-octanoylcarnitine	0.25	0.46	0.000
WT Whole Brain	2,6-dimethyl-heptanoylcarnitine	0.46	0.39	0.003
WT Whole Brain	decanoylcarnitine	0.20	0.00	0.065
WT Whole Brain	cis-4-decenoylcarnitine	0.09	0.00	0.017
WT Whole Brain	cis-3,4-methylene-nonanoylcarnitine	0.05	0.00	0.009
WT Whole Brain	R-3-hydroxy-decanoylcarnitine	0.04	0.29	0.015
WT Whole Brain	S-3-hydroxy-decanoylcarnitine	0.60	0.66	0.001
WT Whole Brain	5-decynoylcarnitine	0.16	0.09	0.000
WT Whole Brain	lauroylcarnitine	0.32	0.42	0.167
WT Whole Brain	trans-2-dodecenoylcarnitine	0.04	0.24	0.000
WT Whole Brain	R-3-hydroxy-lauroylcarnitine	0.29	0.13	0.000
WT Whole Brain	S-3-hydroxy-lauroylcarnitine	0.43	0.21	0.001
WT Whole Brain	myristoylcarnitine	0.81	1.77	1.519
WT Whole Brain	myristoleoylcarnitine	0.44	0.55	0.220
WT Whole Brain	cis-5-tetradecenoylcarnitine	0.00	0.26	0.000
WT Whole Brain	trans-2-tetradecenoylcarnitine	0.06	0.53	0.007
WT Whole Brain	cis,cis-5,8-tetradecadienoylcarnitine	0.07	0.50	0.005
WT Whole Brain	R-3-hydroxy-myristoylcarnitine	0.09	0.27	0.000
WT Whole Brain	S-3-hydroxy-myristoylcarnitine	0.23	0.02	0.000
WT Whole Brain	hydroxy-C14:1	0.00	0.22	0.012
WT Whole Brain	palmitoylcarnitine	2.26	3.65	3.712
WT Whole Brain	palmitoleoylcarnitine	0.00	0.77	0.550

WT Whole Brain	trans-2-hexadecenoylcarnitine	0.09	0.42	0.005
WT Whole Brain	R-3-hydroxy-palmitoylcarnitine	0.37	0.57	0.000
WT Whole Brain	S-3-hydroxy-palmitoylcarnitine	0.00	0.35	0.008
WT Whole Brain	hydroxy-C16:1	0.00	0.35	0.028
WT Whole Brain	stearoylcarnitine	2.08	0.74	0.567
WT Whole Brain	oleoylcarnitine	1.33	2.56	2.678
WT Whole Brain	linoleoylcarnitine	0.54	0.86	0.174
WT Whole Brain	alpha-linolenoylcarnitine	0.25	0.22	0.000
WT Whole Brain	gamma-linolenoylcarnitine	0.00	0.32	0.022
WT Whole Brain	R-3-hydroxy-stearoylcarnitine	0.28	0.59	0.031
WT Whole Brain	S-3-hydroxy-stearoylcarnitine	0.18	0.25	0.001
WT Whole Brain	hydroxy-C18:1	0.22	0.26	0.028
WT Whole Brain	hydroxy-C18:2	0.15	0.23	0.004
WT Whole Brain	hydroxy-C18:3	0.16	0.23	0.022
WT Whole Brain	malonylcarnitine	0.07	0.81	0.147
WT Whole Brain	succinylcarnitine	0.33	0.38	0.138
WT Whole Brain	methyl-malonylcarnitine	0.02	0.40	0.047
WT Whole Brain	ethyl-malonylcarnitine	0.13	0.11	0.000
WT Whole Brain	glutaroylcarnitine	0.69	0.48	0.248
WT Whole Brain	adipoylcarnitine	0.34	0.28	0.020
WT Whole Brain	3-methyl-glutaroylcarnitine	0.01	0.35	0.000
WT Whole Brain	suberoylcarnitine	0.07	0.35	0.000
WT Whole Brain	sebacoylcarnitine	0.14	0.22	0.000
KO Heart	total_carnitine		1183.29	507.785
KO Heart	free_carnitine		731.44	310.147
KO Heart	butyrobetaine		19.03	7.532
KO Heart	acetylcarnitine		308.83	153.214

KO Heart	propionylcarnitine		14.66	2.146
KO Heart	butyrylcarnitine		4.14	4.757
KO Heart	isobutyrylcarnitine		0.47	0.418
KO Heart	R-3-hydroxy-butyrylcarnitine		3.40	1.551
KO Heart	S-3-hydroxy-butyrylcarnitine		12.72	4.532
KO Heart	valerylcarnitine		0.59	0.152
KO Heart	isovalerylcarnitine		0.42	0.240
KO Heart	3-hydroxy-isovalerylcarnitine		2.75	1.295
KO Heart	2-methyl-butyrylcarnitine		1.14	0.364
KO Heart	tigloylcarnitine		0.35	0.169
KO Heart	3-methyl-crotonylcarnitine		0.04	0.002
KO Heart	hexanoylcarnitine		0.70	0.476
KO Heart	R-3-hydroxy-hexanoylcarnitine		0.22	0.059
KO Heart	S-3-hydroxy-hexanoylcarnitine		0.37	0.208
KO Heart	phenylacetylcarnitine		0.02	0.000
KO Heart	phenylpropionylcarnitine		0.48	
KO Heart	4-phenyl-butyrylcarnitine		0.10	
KO Heart	benzoylcarnitine		0.09	0.015
KO Heart	4-methyl-hexanoylcarnitine		0.33	0.000
KO Heart	octanoylcarnitine		0.67	0.000
KO Heart	R-3-hydroxy-octanoylcarnitine		0.55	0.057
KO Heart	S-3-hydroxy-octanoylcarnitine		1.02	0.157
KO Heart	branched-chain C8		0.24	0.000
KO Heart	cis-3,4-methylene- heptanoylcarnitine		0.47	0.018
KO Heart	4-methyl-octanoylcarnitine		0.69	0.007
KO Heart	2,6-dimethyl-heptanoylcarnitine		0.56	0.000

KO Heart	decanoylcarnitine		0.00	0.189
KO Heart	cis-4-decenoylcarnitine		0.00	0.005
KO Heart	cis-3,4-methylene- nonanoylcarnitine		0.00	0.000
KO Heart	R-3-hydroxy-decanoylcarnitine		0.64	0.048
KO Heart	S-3-hydroxy-decanoylcarnitine		1.99	0.128
KO Heart	5-decynoylcarnitine		0.14	0.004
KO Heart	lauroylcarnitine		0.60	0.137
KO Heart	trans-2-dodecenoylcarnitine		0.39	0.001
KO Heart	R-3-hydroxy-lauroylcarnitine		0.32	0.000
KO Heart	S-3-hydroxy-lauroylcarnitine		1.14	0.052
KO Heart	myristoylcarnitine		0.73	0.948
KO Heart	myristoleoylcarnitine		0.63	0.195
KO Heart	cis-5-tetradecenoylcarnitine		0.43	0.000
KO Heart	trans-2-tetradecenoylcarnitine		0.74	0.019
KO Heart	cis,cis-5,8- tetradecadienoylcarnitine		0.73	0.163
KO Heart	R-3-hydroxy-myristoylcarnitine		0.79	0.000
KO Heart	S-3-hydroxy-myristoylcarnitine		1.77	0.095
KO Heart	hydroxy-C14:1		1.21	0.081
KO Heart	palmitoylcarnitine		1.87	2.118
KO Heart	palmitoleoylcarnitine		0.44	0.047
KO Heart	trans-2-hexadecenoylcarnitine		1.00	0.042
KO Heart	R-3-hydroxy-palmitoylcarnitine		1.33	0.046
KO Heart	S-3-hydroxy-palmitoylcarnitine		3.10	0.285
KO Heart	hydroxy-C16:1		2.33	0.076
KO Heart	stearoylcarnitine		1.65	2.969

KO Heart	oleoylcarnitine		0.14	1.579
KO Heart	linoleoylcarnitine		1.13	1.697
KO Heart	alpha-linolenoylcarnitine		0.42	0.094
KO Heart	gamma-linolenoylcarnitine		0.53	0.040
KO Heart	R-3-hydroxy-stearoylcarnitine		1.08	0.031
KO Heart	S-3-hydroxy-stearoylcarnitine		1.56	0.267
KO Heart	hydroxy-C18:1		3.04	0.591
KO Heart	hydroxy-C18:2		2.42	0.343
KO Heart	hydroxy-C18:3		0.71	0.031
KO Heart	malonylcarnitine		5.24	2.067
KO Heart	succinylcarnitine		8.98	4.625
KO Heart	methyl-malonylcarnitine		1.65	0.747
KO Heart	ethyl-malonylcarnitine		0.15	0.000
KO Heart	glutaroylcarnitine		0.00	0.000
KO Heart	adipoylcarnitine		0.36	0.015
KO Heart	3-methyl-glutaroylcarnitine		0.39	0.000
KO Heart	suberoylcarnitine		0.52	0.000
KO Heart	sebacoylcarnitine		0.31	0.000
WT Heart	total_carnitine		1271.39	936.466
WT Heart	free_carnitine		699.31	568.849
WT Heart	butyrobetaine		17.85	15.851
WT Heart	acetylcarnitine		510.14	244.638
WT Heart	propionylcarnitine		22.55	22.953
WT Heart	butyrylcarnitine		0.89	11.295
WT Heart	isobutyrylcarnitine		0.27	0.246
WT Heart	R-3-hydroxy-butyrylcarnitine		4.93	2.299
WT Heart	S-3-hydroxy-butyrylcarnitine		16.76	7.270

WT Heart	valerylcarnitine		0.74	1.871
WT Heart	isovalerylcarnitine		0.25	0.131
WT Heart	3-hydroxy-isovalerylcarnitine		1.88	3.114
WT Heart	2-methyl-butyrylcarnitine		1.27	1.474
WT Heart	tigloylcarnitine		0.46	0.407
WT Heart	3-methyl-crotonylcarnitine		0.04	0.013
WT Heart	hexanoylcarnitine		0.73	1.115
WT Heart	R-3-hydroxy-hexanoylcarnitine		0.24	0.157
WT Heart	S-3-hydroxy-hexanoylcarnitine		0.67	0.484
WT Heart	phenylacetylcarnitine		0.03	0.000
WT Heart	phenylpropionylcarnitine		0.31	
WT Heart	4-phenyl-butyrylcarnitine		0.07	
WT Heart	benzoylcarnitine		0.12	0.073
WT Heart	4-methyl-hexanoylcarnitine		0.22	0.004
WT Heart	octanoylcarnitine		0.41	0.000
WT Heart	R-3-hydroxy-octanoylcarnitine		0.38	0.063
WT Heart	S-3-hydroxy-octanoylcarnitine		0.74	0.152
WT Heart	branched-chain C8		0.16	0.000
WT Heart	cis-3,4-methylene-heptanoylcarnitine		0.30	0.012
WT Heart	4-methyl-octanoylcarnitine		0.44	0.009
WT Heart	2,6-dimethyl-heptanoylcarnitine		0.36	0.006
WT Heart	decanoylcarnitine		0.00	0.216
WT Heart	cis-4-decenoylcarnitine		0.00	0.000
WT Heart	cis-3,4-methylene-nonanoylcarnitine		0.00	0.000
WT Heart	R-3-hydroxy-decanoylcarnitine		0.55	0.007

WT Heart	S-3-hydroxy-decanoylcarnitine		1.62	0.068
WT Heart	5-decynoylcarnitine		0.09	0.000
WT Heart	lauroylcarnitine		0.36	0.000
WT Heart	trans-2-dodecenoylcarnitine		0.26	0.000
WT Heart	R-3-hydroxy-lauroylcarnitine		0.30	0.000
WT Heart	S-3-hydroxy-lauroylcarnitine		0.98	0.042
WT Heart	myristoylcarnitine		0.27	0.217
WT Heart	myristoleoylcarnitine		0.46	0.055
WT Heart	cis-5-tetradecenoylcarnitine		0.08	0.000
WT Heart	trans-2-tetradecenoylcarnitine		0.50	0.031
WT Heart	cis,cis-5,8-tetradecadienoylcarnitine		0.43	0.044
WT Heart	R-3-hydroxy-myristoylcarnitine		0.67	0.000
WT Heart	S-3-hydroxy-myristoylcarnitine		1.40	0.019
WT Heart	hydroxy-C14:1		1.05	0.042
WT Heart	palmitoylcarnitine		0.71	1.151
WT Heart	palmitoleoylcarnitine		0.27	0.003
WT Heart	trans-2-hexadecenoylcarnitine		0.66	0.001
WT Heart	R-3-hydroxy-palmitoylcarnitine		1.03	0.001
WT Heart	S-3-hydroxy-palmitoylcarnitine		1.44	0.106
WT Heart	hydroxy-C16:1		1.94	0.059
WT Heart	stearoylcarnitine		0.44	1.419
WT Heart	oleoylcarnitine		0.03	0.409
WT Heart	linoleoylcarnitine		0.67	0.777
WT Heart	alpha-linolenoylcarnitine		0.27	0.039
WT Heart	gamma-linolenoylcarnitine		0.35	0.037
WT Heart	R-3-hydroxy-stearoylcarnitine		0.77	0.045

WT Heart	S-3-hydroxy-stearoylcarnitine		0.97	0.089
WT Heart	hydroxy-C18:1		1.60	0.251
WT Heart	hydroxy-C18:2		0.65	0.191
WT Heart	hydroxy-C18:3		0.28	0.051
WT Heart	malonylcarnitine		6.71	3.143
WT Heart	succinylcarnitine		12.99	16.055
WT Heart	methyl-malonylcarnitine		1.52	1.056
WT Heart	ethyl-malonylcarnitine		0.11	0.000
WT Heart	glutaroylcarnitine		0.15	0.000
WT Heart	adipoylcarnitine		0.26	0.031
WT Heart	3-methyl-glutaroylcarnitine		0.29	0.000
WT Heart	suberoylcarnitine		0.33	0.000
WT Heart	sebacoylcarnitine		0.21	0.000

SampleID	WT/KO	SpecimenType	CompoundName	Value
15	KO	Mouse Blood (Whole)	total_carnitine	60.895
15	KO	Mouse Blood (Whole)	free_carnitine	30.995
15	KO	Mouse Blood (Whole)	calculated_acylcarnitines	29.900
15	KO	Mouse Blood (Whole)	acyl/free	0.965
15	KO	Mouse Blood (Whole)	butyrobetaine	2.466
15	KO	Mouse Blood (Whole)	acetylcarnitine	29.135
15	KO	Mouse Blood (Whole)	propionylcarnitine	0.484
15	KO	Mouse Blood (Whole)	butyrylcarnitine	0.338
15	KO	Mouse Blood (Whole)	isobutyrylcarnitine	0.069
15	KO	Mouse Blood (Whole)	R-3-hydroxy-butyrylcarnitine	0.006
15	KO	Mouse Blood (Whole)	S-3-hydroxy-butyrylcarnitine	0.024
15	KO	Mouse Blood (Whole)	valerylcarnitine	0.003
15	KO	Mouse Blood (Whole)	isovalerylcarnitine	0.146

15	KO	Mouse Blood (Whole)	3-hydroxy-isovalerylcarnitine	0.068
15	KO	Mouse Blood (Whole)	2-methyl-butrylcarnitine	0.085
15	KO	Mouse Blood (Whole)	pivaloylcarnitine	0.000
15	KO	Mouse Blood (Whole)	tigloylcarnitine	0.002
15	KO	Mouse Blood (Whole)	3-methyl-crotonylcarnitine	0.000
15	KO	Mouse Blood (Whole)	hexanoylcarnitine	0.019
15	KO	Mouse Blood (Whole)	R-3-hydroxy-hexanoylcarnitine	0.003
15	KO	Mouse Blood (Whole)	S-3-hydroxy-hexanoylcarnitine	0.003
15	KO	Mouse Blood (Whole)	phenylacetylcarnitine	0.000
15	KO	Mouse Blood (Whole)	phenylpropionylcarnitine	0.000
15	KO	Mouse Blood (Whole)	4-phenyl-butyrylcarnitine	0.000
15	KO	Mouse Blood (Whole)	benzoylcarnitine	0.001
15	KO	Mouse Blood (Whole)	4-methyl-hexanoylcarnitine	0.000
15	KO	Mouse Blood (Whole)	octanoylcarnitine	0.024
15	KO	Mouse Blood (Whole)	R-3-hydroxy-octanoylcarnitine	0.001
15	KO	Mouse Blood (Whole)	S-3-hydroxy-octanoylcarnitine	0.005
15	KO	Mouse Blood (Whole)	valproylcarnitine	0.000
15	KO	Mouse Blood (Whole)	branched-chain C8	0.000
15	KO	Mouse Blood (Whole)	cis-3,4-methylene-heptanoylcarnitine	0.001
15	KO	Mouse Blood (Whole)	4-methyl-octanoylcarnitine	0.000
15	KO	Mouse Blood (Whole)	2,6-dimethyl-heptanoylcarnitine	0.000
15	KO	Mouse Blood (Whole)	decanoylcarnitine	0.022
15	KO	Mouse Blood (Whole)	cis-4-decenoylcarnitine	0.022
15	KO	Mouse Blood (Whole)	cis-3,4-methylene-nonanoylcarnitine	0.002
15	KO	Mouse Blood (Whole)	R-3-hydroxy-decanoylcarnitine	0.004

15	KO	Mouse Blood (Whole)	S-3-hydroxy-decanoylcarnitine	0.010
15	KO	Mouse Blood (Whole)	5-decynoylcarnitine	0.000
15	KO	Mouse Blood (Whole)	lauroylcarnitine	0.018
15	KO	Mouse Blood (Whole)	trans-2-dodecenoylcarnitine	0.003
15	KO	Mouse Blood (Whole)	R-3-hydroxy-lauroylcarnitine	0.001
15	KO	Mouse Blood (Whole)	S-3-hydroxy-lauroylcarnitine	0.004
15	KO	Mouse Blood (Whole)	myristoylcarnitine	0.070
15	KO	Mouse Blood (Whole)	myristoleoylcarnitine	0.023
15	KO	Mouse Blood (Whole)	cis-5-tetradecenoylcarnitine	0.026
15	KO	Mouse Blood (Whole)	trans-2-tetradecenoylcarnitine	0.005
15	KO	Mouse Blood (Whole)	cis,cis-5,8-tetradecadienoylcarnitine	0.013
15	KO	Mouse Blood (Whole)	R-3-hydroxy-myristoylcarnitine	0.002
15	KO	Mouse Blood (Whole)	S-3-hydroxy-myristoylcarnitine	0.005
15	KO	Mouse Blood (Whole)	hydroxy-C14:1	0.005
15	KO	Mouse Blood (Whole)	palmitoylcarnitine	0.597
15	KO	Mouse Blood (Whole)	palmitoleoylcarnitine	0.046
15	KO	Mouse Blood (Whole)	trans-2-hexadecenoylcarnitine	0.003
15	KO	Mouse Blood (Whole)	R-3-hydroxy-palmitoylcarnitine	0.002
15	KO	Mouse Blood (Whole)	S-3-hydroxy-palmitoylcarnitine	0.007
15	KO	Mouse Blood (Whole)	hydroxy-C16:1	0.001
15	KO	Mouse Blood (Whole)	stearoylcarnitine	0.199
15	KO	Mouse Blood (Whole)	oleoylcarnitine	0.465
15	KO	Mouse Blood (Whole)	linoleoylcarnitine	0.140
15	KO	Mouse Blood (Whole)	alpha-linolenoylcarnitine	0.025
15	KO	Mouse Blood (Whole)	gamma-linolenoylcarnitine	0.004
15	KO	Mouse Blood (Whole)	R-3-hydroxy-stearoylcarnitine	0.008

15	KO	Mouse Blood (Whole)	S-3-hydroxy-stearoylcarnitine	0.003
15	KO	Mouse Blood (Whole)	hydroxy-C18:1	0.010
15	KO	Mouse Blood (Whole)	hydroxy-C18:2	0.001
15	KO	Mouse Blood (Whole)	hydroxy-C18:3	0.002
15	KO	Mouse Blood (Whole)	malonylcarnitine	0.088
15	KO	Mouse Blood (Whole)	succinylcarnitine	0.458
15	KO	Mouse Blood (Whole)	methyl-malonylcarnitine	0.052
15	KO	Mouse Blood (Whole)	ethyl-malonylcarnitine	0.001
15	KO	Mouse Blood (Whole)	glutaroylcarnitine	0.003
15	KO	Mouse Blood (Whole)	adipoylcarnitine	0.006
15	KO	Mouse Blood (Whole)	3-methyl-glutaroylcarnitine	0.001
15	KO	Mouse Blood (Whole)	suberoylcarnitine	0.011
15	KO	Mouse Blood (Whole)	sebacoylcarnitine	0.001
15	KO	Mouse Blood (Whole)	sum_of_individual_acylcarnitines	32.791
15	KO	Mouse Blood (Whole)	ratio:_sum/calculated	1.097
43	KO	Mouse Blood (Whole)	total_carnitine	42.126
43	KO	Mouse Blood (Whole)	free_carnitine	23.120
43	KO	Mouse Blood (Whole)	calculated_acylcarnitines	19.007
43	KO	Mouse Blood (Whole)	acyl/free	0.822
43	KO	Mouse Blood (Whole)	butyrobetaine	2.064
43	KO	Mouse Blood (Whole)	acetylcarnitine	17.998
43	KO	Mouse Blood (Whole)	propionylcarnitine	0.340
43	KO	Mouse Blood (Whole)	butyrylcarnitine	0.225
43	KO	Mouse Blood (Whole)	isobutyrylcarnitine	0.042
43	KO	Mouse Blood (Whole)	R-3-hydroxy-butyrylcarnitine	0.003
43	KO	Mouse Blood (Whole)	S-3-hydroxy-butyrylcarnitine	0.010
43	KO	Mouse Blood (Whole)	valerylcarnitine	0.001

43	KO	Mouse Blood (Whole)	isovalerylcarnitine	0.069
43	KO	Mouse Blood (Whole)	3-hydroxy-isovalerylcarnitine	0.042
43	KO	Mouse Blood (Whole)	2-methyl-butyrylcarnitine	0.043
43	KO	Mouse Blood (Whole)	pivaloylcarnitine	0.000
43	KO	Mouse Blood (Whole)	tigloylcarnitine	0.001
43	KO	Mouse Blood (Whole)	3-methyl-crotonylcarnitine	0.000
43	KO	Mouse Blood (Whole)	hexanoylcarnitine	0.009
43	KO	Mouse Blood (Whole)	R-3-hydroxy-hexanoylcarnitine	0.001
43	KO	Mouse Blood (Whole)	S-3-hydroxy-hexanoylcarnitine	0.001
43	KO	Mouse Blood (Whole)	phenylacetylcarnitine	0.001
43	KO	Mouse Blood (Whole)	phenylpropionylcarnitine	0.000
43	KO	Mouse Blood (Whole)	4-phenyl-butyrylcarnitine	0.000
43	KO	Mouse Blood (Whole)	benzoylcarnitine	0.002
43	KO	Mouse Blood (Whole)	4-methyl-hexanoylcarnitine	0.000
43	KO	Mouse Blood (Whole)	octanoylcarnitine	0.019
43	KO	Mouse Blood (Whole)	R-3-hydroxy-octanoylcarnitine	0.001
43	KO	Mouse Blood (Whole)	S-3-hydroxy-octanoylcarnitine	0.002
43	KO	Mouse Blood (Whole)	valproylcarnitine	0.000
43	KO	Mouse Blood (Whole)	branched-chain C8	0.000
43	KO	Mouse Blood (Whole)	cis-3,4-methylene-heptanoylcarnitine	0.000
43	KO	Mouse Blood (Whole)	4-methyl-octanoylcarnitine	0.000
43	KO	Mouse Blood (Whole)	2,6-dimethyl-heptanoylcarnitine	0.000
43	KO	Mouse Blood (Whole)	decanoylcarnitine	0.016
43	KO	Mouse Blood (Whole)	cis-4-decenoylcarnitine	0.016
43	KO	Mouse Blood (Whole)	cis-3,4-methylene-nonanoylcarnitine	0.000

43	KO	Mouse Blood (Whole)	R-3-hydroxy-decanoylcarnitine	0.002
43	KO	Mouse Blood (Whole)	S-3-hydroxy-decanoylcarnitine	0.003
43	KO	Mouse Blood (Whole)	5-decynoylcarnitine	0.000
43	KO	Mouse Blood (Whole)	lauroylcarnitine	0.010
43	KO	Mouse Blood (Whole)	trans-2-dodecenoylcarnitine	0.000
43	KO	Mouse Blood (Whole)	R-3-hydroxy-lauroylcarnitine	0.001
43	KO	Mouse Blood (Whole)	S-3-hydroxy-lauroylcarnitine	0.002
43	KO	Mouse Blood (Whole)	myristoylcarnitine	0.048
43	KO	Mouse Blood (Whole)	myristoleoylcarnitine	0.011
43	KO	Mouse Blood (Whole)	cis-5-tetradecenoylcarnitine	0.006
43	KO	Mouse Blood (Whole)	trans-2-tetradecenoylcarnitine	0.001
43	KO	Mouse Blood (Whole)	cis,cis-5,8-tetradecadienoylcarnitine	0.006
43	KO	Mouse Blood (Whole)	R-3-hydroxy-myristoylcarnitine	0.000
43	KO	Mouse Blood (Whole)	S-3-hydroxy-myristoylcarnitine	0.002
43	KO	Mouse Blood (Whole)	hydroxy-C14:1	0.003
43	KO	Mouse Blood (Whole)	palmitoylcarnitine	0.641
43	KO	Mouse Blood (Whole)	palmitoleoylcarnitine	0.028
43	KO	Mouse Blood (Whole)	trans-2-hexadecenoylcarnitine	0.003
43	KO	Mouse Blood (Whole)	R-3-hydroxy-palmitoylcarnitine	0.003
43	KO	Mouse Blood (Whole)	S-3-hydroxy-palmitoylcarnitine	0.002
43	KO	Mouse Blood (Whole)	hydroxy-C16:1	0.000
43	KO	Mouse Blood (Whole)	stearoylcarnitine	0.265
43	KO	Mouse Blood (Whole)	oleoylcarnitine	0.389
43	KO	Mouse Blood (Whole)	linoleoylcarnitine	0.100
43	KO	Mouse Blood (Whole)	alpha-linolenoylcarnitine	0.013
43	KO	Mouse Blood (Whole)	gamma-linolenoylcarnitine	0.003

43	KO	Mouse Blood (Whole)	R-3-hydroxy-stearoylcarnitine	0.007
43	KO	Mouse Blood (Whole)	S-3-hydroxy-stearoylcarnitine	0.002
43	KO	Mouse Blood (Whole)	hydroxy-C18:1	0.005
43	KO	Mouse Blood (Whole)	hydroxy-C18:2	0.002
43	KO	Mouse Blood (Whole)	hydroxy-C18:3	0.002
43	KO	Mouse Blood (Whole)	malonylcarnitine	0.060
43	KO	Mouse Blood (Whole)	succinylcarnitine	0.228
43	KO	Mouse Blood (Whole)	methyl-malonylcarnitine	0.044
43	KO	Mouse Blood (Whole)	ethyl-malonylcarnitine	0.001
43	KO	Mouse Blood (Whole)	glutaroylcarnitine	0.006
43	KO	Mouse Blood (Whole)	adipoylcarnitine	0.004
43	KO	Mouse Blood (Whole)	3-methyl-glutaroylcarnitine	0.001
43	KO	Mouse Blood (Whole)	suberoylcarnitine	0.006
43	KO	Mouse Blood (Whole)	sebacoylcarnitine	0.001
43	KO	Mouse Blood (Whole)	sum_of_individual_acylcarnitines	20.753
43	KO	Mouse Blood (Whole)	ratio:_sum/calculated	1.092
70	KO	Mouse Blood (Whole)	total_carnitine	76.024
70	KO	Mouse Blood (Whole)	free_carnitine	34.427
70	KO	Mouse Blood (Whole)	calculated_acylcarnitines	41.597
70	KO	Mouse Blood (Whole)	acyl/free	1.208
70	KO	Mouse Blood (Whole)	butyrobetaine	3.129
70	KO	Mouse Blood (Whole)	acetylcarnitine	39.835
70	KO	Mouse Blood (Whole)	propionylcarnitine	1.346
70	KO	Mouse Blood (Whole)	butyrylcarnitine	0.755
70	KO	Mouse Blood (Whole)	isobutyrylcarnitine	0.194
70	KO	Mouse Blood (Whole)	R-3-hydroxy-butyrylcarnitine	0.007
70	KO	Mouse Blood (Whole)	S-3-hydroxy-butyrylcarnitine	0.046

70	KO	Mouse Blood (Whole)	valerylcarnitine	0.016
70	KO	Mouse Blood (Whole)	isovalerylcarnitine	0.261
70	KO	Mouse Blood (Whole)	3-hydroxy-isovalerylcarnitine	0.136
70	KO	Mouse Blood (Whole)	2-methyl-butyrylcarnitine	0.146
70	KO	Mouse Blood (Whole)	pivaloylcarnitine	0.000
70	KO	Mouse Blood (Whole)	tigloylcarnitine	0.005
70	KO	Mouse Blood (Whole)	3-methyl-crotonylcarnitine	0.000
70	KO	Mouse Blood (Whole)	hexanoylcarnitine	0.018
70	KO	Mouse Blood (Whole)	R-3-hydroxy-hexanoylcarnitine	0.002
70	KO	Mouse Blood (Whole)	S-3-hydroxy-hexanoylcarnitine	0.001
70	KO	Mouse Blood (Whole)	phenylacetylcarnitine	0.005
70	KO	Mouse Blood (Whole)	phenylpropionylcarnitine	0.001
70	KO	Mouse Blood (Whole)	4-phenyl-butyrylcarnitine	0.000
70	KO	Mouse Blood (Whole)	benzoylcarnitine	0.008
70	KO	Mouse Blood (Whole)	4-methyl-hexanoylcarnitine	0.001
70	KO	Mouse Blood (Whole)	octanoylcarnitine	0.017
70	KO	Mouse Blood (Whole)	R-3-hydroxy-octanoylcarnitine	0.001
70	KO	Mouse Blood (Whole)	S-3-hydroxy-octanoylcarnitine	0.003
70	KO	Mouse Blood (Whole)	valproylcarnitine	0.000
70	KO	Mouse Blood (Whole)	branched-chain C8	0.000
70	KO	Mouse Blood (Whole)	cis-3,4-methylene-heptanoylcarnitine	0.000
70	KO	Mouse Blood (Whole)	4-methyl-octanoylcarnitine	0.000
70	KO	Mouse Blood (Whole)	2,6-dimethyl-heptanoylcarnitine	0.000
70	KO	Mouse Blood (Whole)	decanoylcarnitine	0.015
70	KO	Mouse Blood (Whole)	cis-4-decenoylcarnitine	0.010
70	KO	Mouse Blood (Whole)	cis-3,4-methylene-	0.000

			nonanoylcarnitine	
70	KO	Mouse Blood (Whole)	R-3-hydroxy-decanoylcarnitine	0.002
70	KO	Mouse Blood (Whole)	S-3-hydroxy-decanoylcarnitine	0.005
70	KO	Mouse Blood (Whole)	5-decynoylcarnitine	0.000
70	KO	Mouse Blood (Whole)	lauroylcarnitine	0.012
70	KO	Mouse Blood (Whole)	trans-2-dodecenoylcarnitine	0.001
70	KO	Mouse Blood (Whole)	R-3-hydroxy-lauroylcarnitine	0.002
70	KO	Mouse Blood (Whole)	S-3-hydroxy-lauroylcarnitine	0.003
70	KO	Mouse Blood (Whole)	myristoylcarnitine	0.053
70	KO	Mouse Blood (Whole)	myristoleoylcarnitine	0.011
70	KO	Mouse Blood (Whole)	cis-5-tetradecenoylcarnitine	0.010
70	KO	Mouse Blood (Whole)	trans-2-tetradecenoylcarnitine	0.003
70	KO	Mouse Blood (Whole)	cis,cis-5,8-tetradecadienoylcarnitine	0.013
70	KO	Mouse Blood (Whole)	R-3-hydroxy-myristoylcarnitine	0.000
70	KO	Mouse Blood (Whole)	S-3-hydroxy-myristoylcarnitine	0.004
70	KO	Mouse Blood (Whole)	hydroxy-C14:1	0.003
70	KO	Mouse Blood (Whole)	palmitoylcarnitine	0.768
70	KO	Mouse Blood (Whole)	palmitoleoylcarnitine	0.034
70	KO	Mouse Blood (Whole)	trans-2-hexadecenoylcarnitine	0.002
70	KO	Mouse Blood (Whole)	R-3-hydroxy-palmitoylcarnitine	0.001
70	KO	Mouse Blood (Whole)	S-3-hydroxy-palmitoylcarnitine	0.004
70	KO	Mouse Blood (Whole)	hydroxy-C16:1	0.001
70	KO	Mouse Blood (Whole)	stearoylcarnitine	0.225
70	KO	Mouse Blood (Whole)	oleoylcarnitine	0.325
70	KO	Mouse Blood (Whole)	linoleoylcarnitine	0.114
70	KO	Mouse Blood (Whole)	alpha-linolenoylcarnitine	0.021

70	KO	Mouse Blood (Whole)	gamma-linolenoylcarnitine	0.001
70	KO	Mouse Blood (Whole)	R-3-hydroxy-stearoylcarnitine	0.008
70	KO	Mouse Blood (Whole)	S-3-hydroxy-stearoylcarnitine	0.001
70	KO	Mouse Blood (Whole)	hydroxy-C18:1	0.008
70	KO	Mouse Blood (Whole)	hydroxy-C18:2	0.002
70	KO	Mouse Blood (Whole)	hydroxy-C18:3	0.002
70	KO	Mouse Blood (Whole)	malonylcarnitine	0.097
70	KO	Mouse Blood (Whole)	succinylcarnitine	0.348
70	KO	Mouse Blood (Whole)	methyl-malonylcarnitine	0.074
70	KO	Mouse Blood (Whole)	ethyl-malonylcarnitine	0.000
70	KO	Mouse Blood (Whole)	glutaroylcarnitine	0.004
70	KO	Mouse Blood (Whole)	adipoylcarnitine	0.006
70	KO	Mouse Blood (Whole)	3-methyl-glutaroylcarnitine	0.000
70	KO	Mouse Blood (Whole)	suberoylcarnitine	0.009
70	KO	Mouse Blood (Whole)	sebacoylcarnitine	0.001
70	KO	Mouse Blood (Whole)	sum_of_individual_acylcarnitines	45.006
70	KO	Mouse Blood (Whole)	ratio:_sum/calculated	1.082
96	WT	Mouse Blood (Whole)	total_carnitine	44.086
96	WT	Mouse Blood (Whole)	free_carnitine	22.989
96	WT	Mouse Blood (Whole)	calculated_acylcarnitines	21.097
96	WT	Mouse Blood (Whole)	acyl/free	0.918
96	WT	Mouse Blood (Whole)	butyrobetaine	2.263
96	WT	Mouse Blood (Whole)	acetylcarnitine	20.862
96	WT	Mouse Blood (Whole)	propionylcarnitine	0.438
96	WT	Mouse Blood (Whole)	butyrylcarnitine	0.228
96	WT	Mouse Blood (Whole)	isobutyrylcarnitine	0.068
96	WT	Mouse Blood (Whole)	R-3-hydroxy-butyrylcarnitine	0.006

96	WT	Mouse Blood (Whole)	S-3-hydroxy-butrylcarnitine	0.019
96	WT	Mouse Blood (Whole)	valerylcarnitine	0.001
96	WT	Mouse Blood (Whole)	isovalerylcarnitine	0.056
96	WT	Mouse Blood (Whole)	3-hydroxy-isovalerylcarnitine	0.063
96	WT	Mouse Blood (Whole)	2-methyl-butrylcarnitine	0.072
96	WT	Mouse Blood (Whole)	pivaloylcarnitine	0.000
96	WT	Mouse Blood (Whole)	tigloylcarnitine	0.002
96	WT	Mouse Blood (Whole)	3-methyl-crotonylcarnitine	0.000
96	WT	Mouse Blood (Whole)	hexanoylcarnitine	0.016
96	WT	Mouse Blood (Whole)	R-3-hydroxy-hexanoylcarnitine	0.002
96	WT	Mouse Blood (Whole)	S-3-hydroxy-hexanoylcarnitine	0.002
96	WT	Mouse Blood (Whole)	phenylacetylcarnitine	0.001
96	WT	Mouse Blood (Whole)	phenylpropionylcarnitine	0.000
96	WT	Mouse Blood (Whole)	4-phenyl-butrylcarnitine	0.000
96	WT	Mouse Blood (Whole)	benzoylcarnitine	0.002
96	WT	Mouse Blood (Whole)	4-methyl-hexanoylcarnitine	0.000
96	WT	Mouse Blood (Whole)	octanoylcarnitine	0.030
96	WT	Mouse Blood (Whole)	R-3-hydroxy-octanoylcarnitine	0.001
96	WT	Mouse Blood (Whole)	S-3-hydroxy-octanoylcarnitine	0.004
96	WT	Mouse Blood (Whole)	valproylcarnitine	0.000
96	WT	Mouse Blood (Whole)	branched-chain C8	0.000
96	WT	Mouse Blood (Whole)	cis-3,4-methylene-heptanoylcarnitine	0.000
96	WT	Mouse Blood (Whole)	4-methyl-octanoylcarnitine	0.000
96	WT	Mouse Blood (Whole)	2,6-dimethyl-heptanoylcarnitine	0.000
96	WT	Mouse Blood (Whole)	decanoylcarnitine	0.019
96	WT	Mouse Blood (Whole)	cis-4-decenoylcarnitine	0.022

96	WT	Mouse Blood (Whole)	cis-3,4-methylene- nonanoylcarnitine	0.001
96	WT	Mouse Blood (Whole)	R-3-hydroxy-decanoylcarnitine	0.003
96	WT	Mouse Blood (Whole)	S-3-hydroxy-decanoylcarnitine	0.005
96	WT	Mouse Blood (Whole)	5-decynoylcarnitine	0.000
96	WT	Mouse Blood (Whole)	lauroylcarnitine	0.014
96	WT	Mouse Blood (Whole)	trans-2-dodecenoylcarnitine	0.001
96	WT	Mouse Blood (Whole)	R-3-hydroxy-lauroylcarnitine	0.001
96	WT	Mouse Blood (Whole)	S-3-hydroxy-lauroylcarnitine	0.003
96	WT	Mouse Blood (Whole)	myristoylcarnitine	0.060
96	WT	Mouse Blood (Whole)	myristoleoylcarnitine	0.015
96	WT	Mouse Blood (Whole)	cis-5-tetradecenoylcarnitine	0.011
96	WT	Mouse Blood (Whole)	trans-2-tetradecenoylcarnitine	0.002
96	WT	Mouse Blood (Whole)	cis,cis-5,8- tetradecadienoylcarnitine	0.009
96	WT	Mouse Blood (Whole)	R-3-hydroxy-myristoylcarnitine	0.000
96	WT	Mouse Blood (Whole)	S-3-hydroxy-myristoylcarnitine	0.004
96	WT	Mouse Blood (Whole)	hydroxy-C14:1	0.002
96	WT	Mouse Blood (Whole)	palmitoylcarnitine	0.612
96	WT	Mouse Blood (Whole)	palmitoleoylcarnitine	0.029
96	WT	Mouse Blood (Whole)	trans-2-hexadecenoylcarnitine	0.002
96	WT	Mouse Blood (Whole)	R-3-hydroxy-palmitoylcarnitine	0.001
96	WT	Mouse Blood (Whole)	S-3-hydroxy-palmitoylcarnitine	0.006
96	WT	Mouse Blood (Whole)	hydroxy-C16:1	0.001
96	WT	Mouse Blood (Whole)	stearoylcarnitine	0.238
96	WT	Mouse Blood (Whole)	oleoylcarnitine	0.325
96	WT	Mouse Blood (Whole)	linoleoylcarnitine	0.101

96	WT	Mouse Blood (Whole)	alpha-linolenoylcarnitine	0.027
96	WT	Mouse Blood (Whole)	gamma-linolenoylcarnitine	0.001
96	WT	Mouse Blood (Whole)	R-3-hydroxy-stearoylcarnitine	0.006
96	WT	Mouse Blood (Whole)	S-3-hydroxy-stearoylcarnitine	0.001
96	WT	Mouse Blood (Whole)	hydroxy-C18:1	0.007
96	WT	Mouse Blood (Whole)	hydroxy-C18:2	0.001
96	WT	Mouse Blood (Whole)	hydroxy-C18:3	0.002
96	WT	Mouse Blood (Whole)	malonylcarnitine	0.054
96	WT	Mouse Blood (Whole)	succinylcarnitine	0.303
96	WT	Mouse Blood (Whole)	methyl-malonylcarnitine	0.059
96	WT	Mouse Blood (Whole)	ethyl-malonylcarnitine	0.001
96	WT	Mouse Blood (Whole)	glutaroylcarnitine	0.004
96	WT	Mouse Blood (Whole)	adipoylcarnitine	0.005
96	WT	Mouse Blood (Whole)	3-methyl-glutaroylcarnitine	0.001
96	WT	Mouse Blood (Whole)	suberoylcarnitine	0.007
96	WT	Mouse Blood (Whole)	sebacoylcarnitine	0.001
96	WT	Mouse Blood (Whole)	sum_of_individual_acylcarnitines	23.839
96	WT	Mouse Blood (Whole)	ratio:_sum/calculated	1.130
97	WT	Mouse Blood (Whole)	total_carnitine	66.228
97	WT	Mouse Blood (Whole)	free_carnitine	34.389
97	WT	Mouse Blood (Whole)	calculated_acylcarnitines	31.839
97	WT	Mouse Blood (Whole)	acyl/free	0.926
97	WT	Mouse Blood (Whole)	butyrobetaine	2.273
97	WT	Mouse Blood (Whole)	acetylcarnitine	28.050
97	WT	Mouse Blood (Whole)	propionylcarnitine	0.928
97	WT	Mouse Blood (Whole)	butyrylcarnitine	1.067
97	WT	Mouse Blood (Whole)	isobutyrylcarnitine	0.197

97	WT	Mouse Blood (Whole)	R-3-hydroxy-butyrylcarnitine	0.010
97	WT	Mouse Blood (Whole)	S-3-hydroxy-butyrylcarnitine	0.045
97	WT	Mouse Blood (Whole)	valerylcarnitine	0.009
97	WT	Mouse Blood (Whole)	isovalerylcarnitine	0.083
97	WT	Mouse Blood (Whole)	3-hydroxy-isovalerylcarnitine	0.077
97	WT	Mouse Blood (Whole)	2-methyl-butyrylcarnitine	0.099
97	WT	Mouse Blood (Whole)	pivaloylcarnitine	0.000
97	WT	Mouse Blood (Whole)	tigloylcarnitine	0.004
97	WT	Mouse Blood (Whole)	3-methyl-crotonylcarnitine	0.000
97	WT	Mouse Blood (Whole)	hexanoylcarnitine	0.034
97	WT	Mouse Blood (Whole)	R-3-hydroxy-hexanoylcarnitine	0.003
97	WT	Mouse Blood (Whole)	S-3-hydroxy-hexanoylcarnitine	0.003
97	WT	Mouse Blood (Whole)	phenylacetylcarnitine	0.004
97	WT	Mouse Blood (Whole)	phenylpropionylcarnitine	0.004
97	WT	Mouse Blood (Whole)	4-phenyl-butyrylcarnitine	0.000
97	WT	Mouse Blood (Whole)	benzoylcarnitine	0.003
97	WT	Mouse Blood (Whole)	4-methyl-hexanoylcarnitine	0.001
97	WT	Mouse Blood (Whole)	octanoylcarnitine	0.027
97	WT	Mouse Blood (Whole)	R-3-hydroxy-octanoylcarnitine	0.001
97	WT	Mouse Blood (Whole)	S-3-hydroxy-octanoylcarnitine	0.005
97	WT	Mouse Blood (Whole)	valproylcarnitine	0.000
97	WT	Mouse Blood (Whole)	branched-chain C8	0.000
97	WT	Mouse Blood (Whole)	cis-3,4-methylene-heptanoylcarnitine	0.001
97	WT	Mouse Blood (Whole)	4-methyl-octanoylcarnitine	0.000
97	WT	Mouse Blood (Whole)	2,6-dimethyl-heptanoylcarnitine	0.000
97	WT	Mouse Blood (Whole)	decanoylcarnitine	0.022

97	WT	Mouse Blood (Whole)	cis-4-decenoylcarnitine	0.018
97	WT	Mouse Blood (Whole)	cis-3,4-methylene- nonanoylcarnitine	0.000
97	WT	Mouse Blood (Whole)	R-3-hydroxy-decanoylcarnitine	0.006
97	WT	Mouse Blood (Whole)	S-3-hydroxy-decanoylcarnitine	0.011
97	WT	Mouse Blood (Whole)	5-decynoylcarnitine	0.000
97	WT	Mouse Blood (Whole)	lauroylcarnitine	0.018
97	WT	Mouse Blood (Whole)	trans-2-dodecenoylcarnitine	0.002
97	WT	Mouse Blood (Whole)	R-3-hydroxy-lauroylcarnitine	0.002
97	WT	Mouse Blood (Whole)	S-3-hydroxy-lauroylcarnitine	0.005
97	WT	Mouse Blood (Whole)	myristoylcarnitine	0.069
97	WT	Mouse Blood (Whole)	myristoleoylcarnitine	0.023
97	WT	Mouse Blood (Whole)	cis-5-tetradecenoylcarnitine	0.020
97	WT	Mouse Blood (Whole)	trans-2-tetradecenoylcarnitine	0.002
97	WT	Mouse Blood (Whole)	cis,cis-5,8- tetradecadienoylcarnitine	0.009
97	WT	Mouse Blood (Whole)	R-3-hydroxy-myristoylcarnitine	0.002
97	WT	Mouse Blood (Whole)	S-3-hydroxy-myristoylcarnitine	0.007
97	WT	Mouse Blood (Whole)	hydroxy-C14:1	0.005
97	WT	Mouse Blood (Whole)	palmitoylcarnitine	0.760
97	WT	Mouse Blood (Whole)	palmitoleoylcarnitine	0.041
97	WT	Mouse Blood (Whole)	trans-2-hexadecenoylcarnitine	0.003
97	WT	Mouse Blood (Whole)	R-3-hydroxy-palmitoylcarnitine	0.002
97	WT	Mouse Blood (Whole)	S-3-hydroxy-palmitoylcarnitine	0.006
97	WT	Mouse Blood (Whole)	hydroxy-C16:1	0.000
97	WT	Mouse Blood (Whole)	stearoylcarnitine	0.229
97	WT	Mouse Blood (Whole)	oleoylcarnitine	0.399

97	WT	Mouse Blood (Whole)	linoleoylcarnitine	0.121
97	WT	Mouse Blood (Whole)	alpha-linolenoylcarnitine	0.018
97	WT	Mouse Blood (Whole)	gamma-linolenoylcarnitine	0.001
97	WT	Mouse Blood (Whole)	R-3-hydroxy-stearoylcarnitine	0.006
97	WT	Mouse Blood (Whole)	S-3-hydroxy-stearoylcarnitine	0.003
97	WT	Mouse Blood (Whole)	hydroxy-C18:1	0.011
97	WT	Mouse Blood (Whole)	hydroxy-C18:2	0.002
97	WT	Mouse Blood (Whole)	hydroxy-C18:3	0.002
97	WT	Mouse Blood (Whole)	malonylcarnitine	0.063
97	WT	Mouse Blood (Whole)	succinylcarnitine	0.356
97	WT	Mouse Blood (Whole)	methyl-malonylcarnitine	0.056
97	WT	Mouse Blood (Whole)	ethyl-malonylcarnitine	0.000
97	WT	Mouse Blood (Whole)	glutaroylcarnitine	0.003
97	WT	Mouse Blood (Whole)	adipoylcarnitine	0.005
97	WT	Mouse Blood (Whole)	3-methyl-glutaroylcarnitine	0.001
97	WT	Mouse Blood (Whole)	suberoylcarnitine	0.009
97	WT	Mouse Blood (Whole)	sebacylcarnitine	0.001
97	WT	Mouse Blood (Whole)	sum_of_individual_acylcarnitines	32.975
97	WT	Mouse Blood (Whole)	ratio:_sum/calculated	1.036
98	WT	Mouse Blood (Whole)	total_carnitine	50.582
98	WT	Mouse Blood (Whole)	free_carnitine	27.491
98	WT	Mouse Blood (Whole)	calculated_acylcarnitines	23.091
98	WT	Mouse Blood (Whole)	acyl/free	0.840
98	WT	Mouse Blood (Whole)	butyrobetaine	2.276
98	WT	Mouse Blood (Whole)	acetylcarnitine	22.528
98	WT	Mouse Blood (Whole)	propionylcarnitine	0.531
98	WT	Mouse Blood (Whole)	butyrylcarnitine	0.341

98	WT	Mouse Blood (Whole)	isobutyrylcarnitine	0.105
98	WT	Mouse Blood (Whole)	R-3-hydroxy-butyrylcarnitine	0.005
98	WT	Mouse Blood (Whole)	S-3-hydroxy-butyrylcarnitine	0.017
98	WT	Mouse Blood (Whole)	valerylcarnitine	0.002
98	WT	Mouse Blood (Whole)	isovalerylcarnitine	0.072
98	WT	Mouse Blood (Whole)	3-hydroxy-isovalerylcarnitine	0.067
98	WT	Mouse Blood (Whole)	2-methyl-butyrylcarnitine	0.060
98	WT	Mouse Blood (Whole)	pivaloylcarnitine	0.000
98	WT	Mouse Blood (Whole)	tigloylcarnitine	0.002
98	WT	Mouse Blood (Whole)	3-methyl-crotonylcarnitine	0.000
98	WT	Mouse Blood (Whole)	hexanoylcarnitine	0.015
98	WT	Mouse Blood (Whole)	R-3-hydroxy-hexanoylcarnitine	0.002
98	WT	Mouse Blood (Whole)	S-3-hydroxy-hexanoylcarnitine	0.002
98	WT	Mouse Blood (Whole)	phenylacetylcarnitine	0.000
98	WT	Mouse Blood (Whole)	phenylpropionylcarnitine	0.001
98	WT	Mouse Blood (Whole)	4-phenyl-butyrylcarnitine	0.000
98	WT	Mouse Blood (Whole)	benzoylcarnitine	0.003
98	WT	Mouse Blood (Whole)	4-methyl-hexanoylcarnitine	0.000
98	WT	Mouse Blood (Whole)	octanoylcarnitine	0.023
98	WT	Mouse Blood (Whole)	R-3-hydroxy-octanoylcarnitine	0.001
98	WT	Mouse Blood (Whole)	S-3-hydroxy-octanoylcarnitine	0.004
98	WT	Mouse Blood (Whole)	valproylcarnitine	0.000
98	WT	Mouse Blood (Whole)	branched-chain C8	0.000
98	WT	Mouse Blood (Whole)	cis-3,4-methylene-heptanoylcarnitine	0.001
98	WT	Mouse Blood (Whole)	4-methyl-octanoylcarnitine	0.000
98	WT	Mouse Blood (Whole)	2,6-dimethyl-heptanoylcarnitine	0.000

98	WT	Mouse Blood (Whole)	decanoylcarnitine	0.017
98	WT	Mouse Blood (Whole)	cis-4-decenoylcarnitine	0.019
98	WT	Mouse Blood (Whole)	cis-3,4-methylene- nonanoylcarnitine	0.002
98	WT	Mouse Blood (Whole)	R-3-hydroxy-decanoylcarnitine	0.002
98	WT	Mouse Blood (Whole)	S-3-hydroxy-decanoylcarnitine	0.005
98	WT	Mouse Blood (Whole)	5-decynoylcarnitine	0.000
98	WT	Mouse Blood (Whole)	lauroylcarnitine	0.016
98	WT	Mouse Blood (Whole)	trans-2-dodecenoylcarnitine	0.001
98	WT	Mouse Blood (Whole)	R-3-hydroxy-lauroylcarnitine	0.001
98	WT	Mouse Blood (Whole)	S-3-hydroxy-lauroylcarnitine	0.003
98	WT	Mouse Blood (Whole)	myristoylcarnitine	0.062
98	WT	Mouse Blood (Whole)	myristoleoylcarnitine	0.011
98	WT	Mouse Blood (Whole)	cis-5-tetradecenoylcarnitine	0.011
98	WT	Mouse Blood (Whole)	trans-2-tetradecenoylcarnitine	0.004
98	WT	Mouse Blood (Whole)	cis,cis-5,8- tetradecadienoylcarnitine	0.012
98	WT	Mouse Blood (Whole)	R-3-hydroxy-myristoylcarnitine	0.000
98	WT	Mouse Blood (Whole)	S-3-hydroxy-myristoylcarnitine	0.001
98	WT	Mouse Blood (Whole)	hydroxy-C14:1	0.002
98	WT	Mouse Blood (Whole)	palmitoylcarnitine	0.715
98	WT	Mouse Blood (Whole)	palmitoleoylcarnitine	0.034
98	WT	Mouse Blood (Whole)	trans-2-hexadecenoylcarnitine	0.002
98	WT	Mouse Blood (Whole)	R-3-hydroxy-palmitoylcarnitine	0.002
98	WT	Mouse Blood (Whole)	S-3-hydroxy-palmitoylcarnitine	0.004
98	WT	Mouse Blood (Whole)	hydroxy-C16:1	0.000
98	WT	Mouse Blood (Whole)	stearoylcarnitine	0.276

98	WT	Mouse Blood (Whole)	oleoylcarnitine	0.359
98	WT	Mouse Blood (Whole)	linoleoylcarnitine	0.116
98	WT	Mouse Blood (Whole)	alpha-linolenoylcarnitine	0.020
98	WT	Mouse Blood (Whole)	gamma-linolenoylcarnitine	0.000
98	WT	Mouse Blood (Whole)	R-3-hydroxy-stearoylcarnitine	0.007
98	WT	Mouse Blood (Whole)	S-3-hydroxy-stearoylcarnitine	0.001
98	WT	Mouse Blood (Whole)	hydroxy-C18:1	0.003
98	WT	Mouse Blood (Whole)	hydroxy-C18:2	0.001
98	WT	Mouse Blood (Whole)	hydroxy-C18:3	0.002
98	WT	Mouse Blood (Whole)	malonylcarnitine	0.066
98	WT	Mouse Blood (Whole)	succinylcarnitine	0.324
98	WT	Mouse Blood (Whole)	methyl-malonylcarnitine	0.047
98	WT	Mouse Blood (Whole)	ethyl-malonylcarnitine	0.001
98	WT	Mouse Blood (Whole)	glutaroylcarnitine	0.003
98	WT	Mouse Blood (Whole)	adipoylcarnitine	0.005
98	WT	Mouse Blood (Whole)	3-methyl-glutaroylcarnitine	0.001
98	WT	Mouse Blood (Whole)	suberoylcarnitine	0.005
98	WT	Mouse Blood (Whole)	sebacoylcarnitine	0.001
98	WT	Mouse Blood (Whole)	sum_of_individual_acylcarnitines	25.943
98	WT	Mouse Blood (Whole)	ratio:_sum/calculated	1.124
15	KO	Mouse Plasma	total_carnitine	86.203
15	KO	Mouse Plasma	free_carnitine	52.836
15	KO	Mouse Plasma	calculated_acylcarnitines	33.368
15	KO	Mouse Plasma	acyl/free	0.632
15	KO	Mouse Plasma	butyrobetaine	1.413
15	KO	Mouse Plasma	acetylcarnitine	31.858
15	KO	Mouse Plasma	propionylcarnitine	0.633

15	KO	Mouse Plasma	butyrylcarnitine	0.682
15	KO	Mouse Plasma	isobutyrylcarnitine	0.124
15	KO	Mouse Plasma	R-3-hydroxy-butyrylcarnitine	0.056
15	KO	Mouse Plasma	S-3-hydroxy-butyrylcarnitine	0.121
15	KO	Mouse Plasma	valerylcarnitine	0.012
15	KO	Mouse Plasma	isovalerylcarnitine	0.246
15	KO	Mouse Plasma	3-hydroxy-isovalerylcarnitine	0.070
15	KO	Mouse Plasma	2-methyl-butyrylcarnitine	0.156
15	KO	Mouse Plasma	pivaloylcarnitine	0.000
15	KO	Mouse Plasma	tigloylcarnitine	0.004
15	KO	Mouse Plasma	3-methyl-crotonylcarnitine	0.000
15	KO	Mouse Plasma	hexanoylcarnitine	0.048
15	KO	Mouse Plasma	R-3-hydroxy-hexanoylcarnitine	0.004
15	KO	Mouse Plasma	S-3-hydroxy-hexanoylcarnitine	0.006
15	KO	Mouse Plasma	phenylacetylcarnitine	0.001
15	KO	Mouse Plasma	phenylpropionylcarnitine	0.001
15	KO	Mouse Plasma	4-phenyl-butyrylcarnitine	0.000
15	KO	Mouse Plasma	benzoylcarnitine	0.005
15	KO	Mouse Plasma	4-methyl-hexanoylcarnitine	0.000
15	KO	Mouse Plasma	octanoylcarnitine	0.015
15	KO	Mouse Plasma	R-3-hydroxy-octanoylcarnitine	0.004
15	KO	Mouse Plasma	S-3-hydroxy-octanoylcarnitine	0.011
15	KO	Mouse Plasma	valproylcarnitine	0.000
15	KO	Mouse Plasma	branched-chain C8	0.000
15	KO	Mouse Plasma	cis-3,4-methylene-heptanoylcarnitine	0.000
15	KO	Mouse Plasma	4-methyl-octanoylcarnitine	0.000

15	KO	Mouse Plasma	2,6-dimethyl-heptanoylcarnitine	0.000
15	KO	Mouse Plasma	decanoylcarnitine	0.021
15	KO	Mouse Plasma	cis-4-decenoylcarnitine	0.017
15	KO	Mouse Plasma	cis-3,4-methylene- nonanoylcarnitine	0.002
15	KO	Mouse Plasma	R-3-hydroxy-decanoylcarnitine	0.005
15	KO	Mouse Plasma	S-3-hydroxy-decanoylcarnitine	0.016
15	KO	Mouse Plasma	5-decynoylcarnitine	0.000
15	KO	Mouse Plasma	lauroylcarnitine	0.023
15	KO	Mouse Plasma	trans-2-dodecenoylcarnitine	0.002
15	KO	Mouse Plasma	R-3-hydroxy-lauroylcarnitine	0.002
15	KO	Mouse Plasma	S-3-hydroxy-lauroylcarnitine	0.005
15	KO	Mouse Plasma	myristoylcarnitine	0.062
15	KO	Mouse Plasma	myristoleoylcarnitine	0.027
15	KO	Mouse Plasma	cis-5-tetradecenoylcarnitine	0.070
15	KO	Mouse Plasma	trans-2-tetradecenoylcarnitine	0.012
15	KO	Mouse Plasma	cis,cis-5,8- tetradecadienoylcarnitine	0.031
15	KO	Mouse Plasma	R-3-hydroxy-myristoylcarnitine	0.005
15	KO	Mouse Plasma	S-3-hydroxy-myristoylcarnitine	0.006
15	KO	Mouse Plasma	hydroxy-C14:1	0.013
15	KO	Mouse Plasma	palmitoylcarnitine	0.182
15	KO	Mouse Plasma	palmitoleoylcarnitine	0.049
15	KO	Mouse Plasma	trans-2-hexadecenoylcarnitine	0.003
15	KO	Mouse Plasma	R-3-hydroxy-palmitoylcarnitine	0.005
15	KO	Mouse Plasma	S-3-hydroxy-palmitoylcarnitine	0.009
15	KO	Mouse Plasma	hydroxy-C16:1	0.002

15	KO	Mouse Plasma	stearoylcarnitine	0.048
15	KO	Mouse Plasma	oleoylcarnitine	0.283
15	KO	Mouse Plasma	linoleoylcarnitine	0.117
15	KO	Mouse Plasma	alpha-linolenoylcarnitine	0.011
15	KO	Mouse Plasma	gamma-linolenoylcarnitine	0.002
15	KO	Mouse Plasma	R-3-hydroxy-stearoylcarnitine	0.007
15	KO	Mouse Plasma	S-3-hydroxy-stearoylcarnitine	0.001
15	KO	Mouse Plasma	hydroxy-C18:1	0.016
15	KO	Mouse Plasma	hydroxy-C18:2	0.002
15	KO	Mouse Plasma	hydroxy-C18:3	0.003
15	KO	Mouse Plasma	malonylcarnitine	0.027
15	KO	Mouse Plasma	succinylcarnitine	0.026
15	KO	Mouse Plasma	methyl-malonylcarnitine	0.005
15	KO	Mouse Plasma	ethyl-malonylcarnitine	0.000
15	KO	Mouse Plasma	glutaroylcarnitine	0.001
15	KO	Mouse Plasma	adipoylcarnitine	0.012
15	KO	Mouse Plasma	3-methyl-glutaroylcarnitine	0.002
15	KO	Mouse Plasma	suberoylcarnitine	0.017
15	KO	Mouse Plasma	sebacylcarnitine	0.002
15	KO	Mouse Plasma	sum_of_individual_acylcarnitines	35.211
15	KO	Mouse Plasma	ratio:_sum/calculated	1.055
43	KO	Mouse Plasma	total_carnitine	62.694
43	KO	Mouse Plasma	free_carnitine	41.110
43	KO	Mouse Plasma	calculated_acylcarnitines	21.584
43	KO	Mouse Plasma	acyl/free	0.525
43	KO	Mouse Plasma	butyrobetaine	1.204
43	KO	Mouse Plasma	acetylcarnitine	19.670

43	KO	Mouse Plasma	propionylcarnitine	0.451
43	KO	Mouse Plasma	butyrylcarnitine	0.455
43	KO	Mouse Plasma	isobutyrylcarnitine	0.053
43	KO	Mouse Plasma	R-3-hydroxy-butyrylcarnitine	0.020
43	KO	Mouse Plasma	S-3-hydroxy-butyrylcarnitine	0.024
43	KO	Mouse Plasma	valerylcarnitine	0.004
43	KO	Mouse Plasma	isovalerylcarnitine	0.093
43	KO	Mouse Plasma	3-hydroxy-isovalerylcarnitine	0.037
43	KO	Mouse Plasma	2-methyl-butyrylcarnitine	0.060
43	KO	Mouse Plasma	pivaloylcarnitine	0.000
43	KO	Mouse Plasma	tigloylcarnitine	0.003
43	KO	Mouse Plasma	3-methyl-crotonylcarnitine	0.000
43	KO	Mouse Plasma	hexanoylcarnitine	0.015
43	KO	Mouse Plasma	R-3-hydroxy-hexanoylcarnitine	0.001
43	KO	Mouse Plasma	S-3-hydroxy-hexanoylcarnitine	0.003
43	KO	Mouse Plasma	phenylacetylcarnitine	0.001
43	KO	Mouse Plasma	phenylpropionylcarnitine	0.001
43	KO	Mouse Plasma	4-phenyl-butyrylcarnitine	0.000
43	KO	Mouse Plasma	benzoylcarnitine	0.005
43	KO	Mouse Plasma	4-methyl-hexanoylcarnitine	0.000
43	KO	Mouse Plasma	octanoylcarnitine	0.005
43	KO	Mouse Plasma	R-3-hydroxy-octanoylcarnitine	0.002
43	KO	Mouse Plasma	S-3-hydroxy-octanoylcarnitine	0.004
43	KO	Mouse Plasma	valproylcarnitine	0.000
43	KO	Mouse Plasma	branched-chain C8	0.000
43	KO	Mouse Plasma	cis-3,4-methylene-heptanoylcarnitine	0.000

43	KO	Mouse Plasma	4-methyl-octanoylcarnitine	0.000
43	KO	Mouse Plasma	2,6-dimethyl-heptanoylcarnitine	0.000
43	KO	Mouse Plasma	decanoylcarnitine	0.007
43	KO	Mouse Plasma	cis-4-decenoylcarnitine	0.006
43	KO	Mouse Plasma	cis-3,4-methylene- nonanoylcarnitine	0.000
43	KO	Mouse Plasma	R-3-hydroxy-decanoylcarnitine	0.002
43	KO	Mouse Plasma	S-3-hydroxy-decanoylcarnitine	0.004
43	KO	Mouse Plasma	5-decynoylcarnitine	0.000
43	KO	Mouse Plasma	lauroylcarnitine	0.005
43	KO	Mouse Plasma	trans-2-dodecenoylcarnitine	0.000
43	KO	Mouse Plasma	R-3-hydroxy-lauroylcarnitine	0.000
43	KO	Mouse Plasma	S-3-hydroxy-lauroylcarnitine	0.001
43	KO	Mouse Plasma	myristoylcarnitine	0.024
43	KO	Mouse Plasma	myristoleoylcarnitine	0.015
43	KO	Mouse Plasma	cis-5-tetradecenoylcarnitine	0.008
43	KO	Mouse Plasma	trans-2-tetradecenoylcarnitine	0.001
43	KO	Mouse Plasma	cis,cis-5,8- tetradecadienoylcarnitine	0.010
43	KO	Mouse Plasma	R-3-hydroxy-myristoylcarnitine	0.000
43	KO	Mouse Plasma	S-3-hydroxy-myristoylcarnitine	0.003
43	KO	Mouse Plasma	hydroxy-C14:1	0.003
43	KO	Mouse Plasma	palmitoylcarnitine	0.122
43	KO	Mouse Plasma	palmitoleoylcarnitine	0.014
43	KO	Mouse Plasma	trans-2-hexadecenoylcarnitine	0.002
43	KO	Mouse Plasma	R-3-hydroxy-palmitoylcarnitine	0.001
43	KO	Mouse Plasma	S-3-hydroxy-palmitoylcarnitine	0.003

43	KO	Mouse Plasma	hydroxy-C16:1	0.001
43	KO	Mouse Plasma	stearoylcarnitine	0.052
43	KO	Mouse Plasma	oleoylcarnitine	0.138
43	KO	Mouse Plasma	linoleoylcarnitine	0.059
43	KO	Mouse Plasma	alpha-linolenoylcarnitine	0.002
43	KO	Mouse Plasma	gamma-linolenoylcarnitine	0.001
43	KO	Mouse Plasma	R-3-hydroxy-stearoylcarnitine	0.006
43	KO	Mouse Plasma	S-3-hydroxy-stearoylcarnitine	0.001
43	KO	Mouse Plasma	hydroxy-C18:1	0.008
43	KO	Mouse Plasma	hydroxy-C18:2	0.001
43	KO	Mouse Plasma	hydroxy-C18:3	0.001
43	KO	Mouse Plasma	malonylcarnitine	0.013
43	KO	Mouse Plasma	succinylcarnitine	0.009
43	KO	Mouse Plasma	methyl-malonylcarnitine	0.003
43	KO	Mouse Plasma	ethyl-malonylcarnitine	0.000
43	KO	Mouse Plasma	glutaroylcarnitine	0.001
43	KO	Mouse Plasma	adipoylecarnitine	0.009
43	KO	Mouse Plasma	3-methyl-glutaroylcarnitine	0.000
43	KO	Mouse Plasma	suberoylcarnitine	0.008
43	KO	Mouse Plasma	sebacoylcarnitine	0.001
43	KO	Mouse Plasma	sum_of_individual_acylcarnitines	21.455
43	KO	Mouse Plasma	ratio:_sum/calculated	0.994
70	KO	Mouse Plasma	total_carnitine	115.697
70	KO	Mouse Plasma	free_carnitine	33.199
70	KO	Mouse Plasma	calculated_acylcarnitines	82.498
70	KO	Mouse Plasma	acyl/free	2.485
70	KO	Mouse Plasma	butyrobetaine	0.395

70	KO	Mouse Plasma	acetylcarnitine	47.872
70	KO	Mouse Plasma	propionylcarnitine	2.576
70	KO	Mouse Plasma	butyrylcarnitine	1.501
70	KO	Mouse Plasma	isobutyrylcarnitine	0.313
70	KO	Mouse Plasma	R-3-hydroxy-butyrylcarnitine	0.060
70	KO	Mouse Plasma	S-3-hydroxy-butyrylcarnitine	0.256
70	KO	Mouse Plasma	valerylcarnitine	0.049
70	KO	Mouse Plasma	isovalerylcarnitine	0.509
70	KO	Mouse Plasma	3-hydroxy-isovalerylcarnitine	0.187
70	KO	Mouse Plasma	2-methyl-butyrylcarnitine	0.272
70	KO	Mouse Plasma	pivaloylcarnitine	0.000
70	KO	Mouse Plasma	tigloylcarnitine	0.011
70	KO	Mouse Plasma	3-methyl-crotonylcarnitine	0.001
70	KO	Mouse Plasma	hexanoylcarnitine	0.061
70	KO	Mouse Plasma	R-3-hydroxy-hexanoylcarnitine	0.003
70	KO	Mouse Plasma	S-3-hydroxy-hexanoylcarnitine	0.004
70	KO	Mouse Plasma	phenylacetylcarnitine	0.012
70	KO	Mouse Plasma	phenylpropionylcarnitine	0.004
70	KO	Mouse Plasma	4-phenyl-butyrylcarnitine	0.000
70	KO	Mouse Plasma	benzoylcarnitine	0.026
70	KO	Mouse Plasma	4-methyl-hexanoylcarnitine	0.001
70	KO	Mouse Plasma	octanoylcarnitine	0.016
70	KO	Mouse Plasma	R-3-hydroxy-octanoylcarnitine	0.003
70	KO	Mouse Plasma	S-3-hydroxy-octanoylcarnitine	0.008
70	KO	Mouse Plasma	valproylcarnitine	0.000
70	KO	Mouse Plasma	branched-chain C8	0.000
70	KO	Mouse Plasma	cis-3,4-methylene-	0.001

			heptanoylcarnitine	
70	KO	Mouse Plasma	4-methyl-octanoylcarnitine	0.000
70	KO	Mouse Plasma	2,6-dimethyl-heptanoylcarnitine	0.000
70	KO	Mouse Plasma	decanoylcarnitine	0.018
70	KO	Mouse Plasma	cis-4-decenoylcarnitine	0.010
70	KO	Mouse Plasma	cis-3,4-methylene- nonanoylcarnitine	0.001
70	KO	Mouse Plasma	R-3-hydroxy-decanoylcarnitine	0.003
70	KO	Mouse Plasma	S-3-hydroxy-decanoylcarnitine	0.010
70	KO	Mouse Plasma	5-decynoylcarnitine	0.000
70	KO	Mouse Plasma	lauroylcarnitine	0.025
70	KO	Mouse Plasma	trans-2-dodecenoylcarnitine	0.003
70	KO	Mouse Plasma	R-3-hydroxy-lauroylcarnitine	0.001
70	KO	Mouse Plasma	S-3-hydroxy-lauroylcarnitine	0.004
70	KO	Mouse Plasma	myristoylcarnitine	0.048
70	KO	Mouse Plasma	myristoleoylcarnitine	0.020
70	KO	Mouse Plasma	cis-5-tetradecenoylcarnitine	0.030
70	KO	Mouse Plasma	trans-2-tetradecenoylcarnitine	0.006
70	KO	Mouse Plasma	cis,cis-5,8- tetradecadienoylcarnitine	0.025
70	KO	Mouse Plasma	R-3-hydroxy-myristoylcarnitine	0.002
70	KO	Mouse Plasma	S-3-hydroxy-myristoylcarnitine	0.008
70	KO	Mouse Plasma	hydroxy-C14:1	0.007
70	KO	Mouse Plasma	palmitoylcarnitine	0.158
70	KO	Mouse Plasma	palmitoleoylcarnitine	0.027
70	KO	Mouse Plasma	trans-2-hexadecenoylcarnitine	0.002
70	KO	Mouse Plasma	R-3-hydroxy-palmitoylcarnitine	0.001

70	KO	Mouse Plasma	S-3-hydroxy-palmitoylcarnitine	0.005
70	KO	Mouse Plasma	hydroxy-C16:1	0.001
70	KO	Mouse Plasma	stearoylcarnitine	0.032
70	KO	Mouse Plasma	oleoylcarnitine	0.125
70	KO	Mouse Plasma	linoleoylcarnitine	0.091
70	KO	Mouse Plasma	alpha-linolenoylcarnitine	0.009
70	KO	Mouse Plasma	gamma-linolenoylcarnitine	0.001
70	KO	Mouse Plasma	R-3-hydroxy-stearoylcarnitine	0.006
70	KO	Mouse Plasma	S-3-hydroxy-stearoylcarnitine	0.001
70	KO	Mouse Plasma	hydroxy-C18:1	0.007
70	KO	Mouse Plasma	hydroxy-C18:2	0.001
70	KO	Mouse Plasma	hydroxy-C18:3	0.002
70	KO	Mouse Plasma	malonylcarnitine	0.035
70	KO	Mouse Plasma	succinylcarnitine	0.024
70	KO	Mouse Plasma	methyl-malonylcarnitine	0.005
70	KO	Mouse Plasma	ethyl-malonylcarnitine	0.000
70	KO	Mouse Plasma	glutaroylcarnitine	0.012
70	KO	Mouse Plasma	adipoylcarnitine	0.019
70	KO	Mouse Plasma	3-methyl-glutaroylcarnitine	0.003
70	KO	Mouse Plasma	suberoylcarnitine	0.021
70	KO	Mouse Plasma	sebacoylcarnitine	0.003
70	KO	Mouse Plasma	sum_of_individual_acylcarnitines	54.557
70	KO	Mouse Plasma	ratio:_sum/calculated	0.661
96	WT	Mouse Plasma	total_carnitine	65.675
96	WT	Mouse Plasma	free_carnitine	47.432
96	WT	Mouse Plasma	calculated_acylcarnitines	18.243
96	WT	Mouse Plasma	acyl/free	0.385

96	WT	Mouse Plasma	butyrobetaine	0.829
96	WT	Mouse Plasma	acetylcarnitine	23.878
96	WT	Mouse Plasma	propionylcarnitine	0.779
96	WT	Mouse Plasma	butyrylcarnitine	0.649
96	WT	Mouse Plasma	isobutyrylcarnitine	0.107
96	WT	Mouse Plasma	R-3-hydroxy-butyrylcarnitine	0.047
96	WT	Mouse Plasma	S-3-hydroxy-butyrylcarnitine	0.077
96	WT	Mouse Plasma	valerylcarnitine	0.007
96	WT	Mouse Plasma	isovalerylcarnitine	0.091
96	WT	Mouse Plasma	3-hydroxy-isovalerylcarnitine	0.059
96	WT	Mouse Plasma	2-methyl-butyrylcarnitine	0.107
96	WT	Mouse Plasma	pivaloylcarnitine	0.000
96	WT	Mouse Plasma	tigloylcarnitine	0.006
96	WT	Mouse Plasma	3-methyl-crotonylcarnitine	0.000
96	WT	Mouse Plasma	hexanoylcarnitine	0.032
96	WT	Mouse Plasma	R-3-hydroxy-hexanoylcarnitine	0.002
96	WT	Mouse Plasma	S-3-hydroxy-hexanoylcarnitine	0.004
96	WT	Mouse Plasma	phenylacetylcarnitine	0.002
96	WT	Mouse Plasma	phenylpropionylcarnitine	0.003
96	WT	Mouse Plasma	4-phenyl-butyrylcarnitine	0.000
96	WT	Mouse Plasma	benzoylcarnitine	0.008
96	WT	Mouse Plasma	4-methyl-hexanoylcarnitine	0.000
96	WT	Mouse Plasma	octanoylcarnitine	0.010
96	WT	Mouse Plasma	R-3-hydroxy-octanoylcarnitine	0.003
96	WT	Mouse Plasma	S-3-hydroxy-octanoylcarnitine	0.008
96	WT	Mouse Plasma	valproylcarnitine	0.000
96	WT	Mouse Plasma	branched-chain C8	0.000

96	WT	Mouse Plasma	cis-3,4-methylene-heptanoylcarnitine	0.001
96	WT	Mouse Plasma	4-methyl-octanoylcarnitine	0.000
96	WT	Mouse Plasma	2,6-dimethyl-heptanoylcarnitine	0.000
96	WT	Mouse Plasma	decanoylcarnitine	0.015
96	WT	Mouse Plasma	cis-4-decenoylcarnitine	0.010
96	WT	Mouse Plasma	cis-3,4-methylene-nonanoylcarnitine	0.000
96	WT	Mouse Plasma	R-3-hydroxy-decanoylcarnitine	0.002
96	WT	Mouse Plasma	S-3-hydroxy-decanoylcarnitine	0.010
96	WT	Mouse Plasma	5-decynoylcarnitine	0.000
96	WT	Mouse Plasma	lauroylcarnitine	0.019
96	WT	Mouse Plasma	trans-2-dodecenoylcarnitine	0.001
96	WT	Mouse Plasma	R-3-hydroxy-lauroylcarnitine	0.001
96	WT	Mouse Plasma	S-3-hydroxy-lauroylcarnitine	0.003
96	WT	Mouse Plasma	myristoylcarnitine	0.042
96	WT	Mouse Plasma	myristoleoylcarnitine	0.021
96	WT	Mouse Plasma	cis-5-tetradecenoylcarnitine	0.035
96	WT	Mouse Plasma	trans-2-tetradecenoylcarnitine	0.009
96	WT	Mouse Plasma	cis,cis-5,8-tetradecadienoylcarnitine	0.025
96	WT	Mouse Plasma	R-3-hydroxy-myristoylcarnitine	0.002
96	WT	Mouse Plasma	S-3-hydroxy-myristoylcarnitine	0.011
96	WT	Mouse Plasma	hydroxy-C14:1	0.005
96	WT	Mouse Plasma	palmitoylcarnitine	0.160
96	WT	Mouse Plasma	palmitoleoylcarnitine	0.026
96	WT	Mouse Plasma	trans-2-hexadecenoylcarnitine	0.003

96	WT	Mouse Plasma	R-3-hydroxy-palmitoylcarnitine	0.003
96	WT	Mouse Plasma	S-3-hydroxy-palmitoylcarnitine	0.006
96	WT	Mouse Plasma	hydroxy-C16:1	0.001
96	WT	Mouse Plasma	stearoylcarnitine	0.045
96	WT	Mouse Plasma	oleoylcarnitine	0.182
96	WT	Mouse Plasma	linoleoylcarnitine	0.086
96	WT	Mouse Plasma	alpha-linolenoylcarnitine	0.007
96	WT	Mouse Plasma	gamma-linolenoylcarnitine	0.001
96	WT	Mouse Plasma	R-3-hydroxy-stearoylcarnitine	0.007
96	WT	Mouse Plasma	S-3-hydroxy-stearoylcarnitine	0.001
96	WT	Mouse Plasma	hydroxy-C18:1	0.007
96	WT	Mouse Plasma	hydroxy-C18:2	0.001
96	WT	Mouse Plasma	hydroxy-C18:3	0.002
96	WT	Mouse Plasma	malonylcarnitine	0.018
96	WT	Mouse Plasma	succinylcarnitine	0.022
96	WT	Mouse Plasma	methyl-malonylcarnitine	0.005
96	WT	Mouse Plasma	ethyl-malonylcarnitine	0.000
96	WT	Mouse Plasma	glutaroylcarnitine	0.010
96	WT	Mouse Plasma	adipoylcarnitine	0.013
96	WT	Mouse Plasma	3-methyl-glutaroylcarnitine	0.001
96	WT	Mouse Plasma	suberoylcarnitine	0.013
96	WT	Mouse Plasma	sebacoylcarnitine	0.002
96	WT	Mouse Plasma	sum_of_individual_acylcarnitines	26.717
96	WT	Mouse Plasma	ratio:_sum/calculated	1.464
97	WT	Mouse Plasma	total_carnitine	92.469
97	WT	Mouse Plasma	free_carnitine	55.174
97	WT	Mouse Plasma	calculated_acylcarnitines	37.296

97	WT	Mouse Plasma	acyl/free	0.676
97	WT	Mouse Plasma	butyrobetaine	1.440
97	WT	Mouse Plasma	acetylcarnitine	33.390
97	WT	Mouse Plasma	propionylcarnitine	1.601
97	WT	Mouse Plasma	butyrylcarnitine	2.621
97	WT	Mouse Plasma	isobutyrylcarnitine	0.277
97	WT	Mouse Plasma	R-3-hydroxy-butyrylcarnitine	0.078
97	WT	Mouse Plasma	S-3-hydroxy-butyrylcarnitine	0.159
97	WT	Mouse Plasma	valerylcarnitine	0.046
97	WT	Mouse Plasma	isovalerylcarnitine	0.150
97	WT	Mouse Plasma	3-hydroxy-isovalerylcarnitine	0.080
97	WT	Mouse Plasma	2-methyl-butyrylcarnitine	0.150
97	WT	Mouse Plasma	pivaloylcarnitine	0.000
97	WT	Mouse Plasma	tigloylcarnitine	0.008
97	WT	Mouse Plasma	3-methyl-crotonylcarnitine	0.001
97	WT	Mouse Plasma	hexanoylcarnitine	0.121
97	WT	Mouse Plasma	R-3-hydroxy-hexanoylcarnitine	0.003
97	WT	Mouse Plasma	S-3-hydroxy-hexanoylcarnitine	0.007
97	WT	Mouse Plasma	phenylacetylcarnitine	0.010
97	WT	Mouse Plasma	phenylpropionylcarnitine	0.022
97	WT	Mouse Plasma	4-phenyl-butyrylcarnitine	0.000
97	WT	Mouse Plasma	benzoylcarnitine	0.009
97	WT	Mouse Plasma	4-methyl-hexanoylcarnitine	0.001
97	WT	Mouse Plasma	octanoylcarnitine	0.015
97	WT	Mouse Plasma	R-3-hydroxy-octanoylcarnitine	0.004
97	WT	Mouse Plasma	S-3-hydroxy-octanoylcarnitine	0.010
97	WT	Mouse Plasma	valproylcarnitine	0.000

97	WT	Mouse Plasma	branched-chain C8	0.000
97	WT	Mouse Plasma	cis-3,4-methylene-heptanoylcarnitine	0.000
97	WT	Mouse Plasma	4-methyl-octanoylcarnitine	0.000
97	WT	Mouse Plasma	2,6-dimethyl-heptanoylcarnitine	0.000
97	WT	Mouse Plasma	decanoylcarnitine	0.014
97	WT	Mouse Plasma	cis-4-decenoylcarnitine	0.009
97	WT	Mouse Plasma	cis-3,4-methylene-nonanoylcarnitine	0.000
97	WT	Mouse Plasma	R-3-hydroxy-decanoylcarnitine	0.004
97	WT	Mouse Plasma	S-3-hydroxy-decanoylcarnitine	0.014
97	WT	Mouse Plasma	5-decynoylcarnitine	0.000
97	WT	Mouse Plasma	lauroylcarnitine	0.014
97	WT	Mouse Plasma	trans-2-dodecenoylcarnitine	0.002
97	WT	Mouse Plasma	R-3-hydroxy-lauroylcarnitine	0.001
97	WT	Mouse Plasma	S-3-hydroxy-lauroylcarnitine	0.004
97	WT	Mouse Plasma	myristoylcarnitine	0.041
97	WT	Mouse Plasma	myristoleoylcarnitine	0.022
97	WT	Mouse Plasma	cis-5-tetradecenoylcarnitine	0.025
97	WT	Mouse Plasma	trans-2-tetradecenoylcarnitine	0.002
97	WT	Mouse Plasma	cis,cis-5,8-tetradecadienoylcarnitine	0.015
97	WT	Mouse Plasma	R-3-hydroxy-myristoylcarnitine	0.004
97	WT	Mouse Plasma	S-3-hydroxy-myristoylcarnitine	0.007
97	WT	Mouse Plasma	hydroxy-C14:1	0.008
97	WT	Mouse Plasma	palmitoylcarnitine	0.134
97	WT	Mouse Plasma	palmitoleoylcarnitine	0.029

97	WT	Mouse Plasma	trans-2-hexadecenoylcarnitine	0.002
97	WT	Mouse Plasma	R-3-hydroxy-palmitoylcarnitine	0.003
97	WT	Mouse Plasma	S-3-hydroxy-palmitoylcarnitine	0.005
97	WT	Mouse Plasma	hydroxy-C16:1	0.002
97	WT	Mouse Plasma	stearoylcarnitine	0.029
97	WT	Mouse Plasma	oleoylcarnitine	0.125
97	WT	Mouse Plasma	linoleoylcarnitine	0.054
97	WT	Mouse Plasma	alpha-linolenoylcarnitine	0.003
97	WT	Mouse Plasma	gamma-linolenoylcarnitine	0.002
97	WT	Mouse Plasma	R-3-hydroxy-stearoylcarnitine	0.006
97	WT	Mouse Plasma	S-3-hydroxy-stearoylcarnitine	0.001
97	WT	Mouse Plasma	hydroxy-C18:1	0.008
97	WT	Mouse Plasma	hydroxy-C18:2	0.003
97	WT	Mouse Plasma	hydroxy-C18:3	0.003
97	WT	Mouse Plasma	malonylcarnitine	0.041
97	WT	Mouse Plasma	succinylcarnitine	0.027
97	WT	Mouse Plasma	methyl-malonylcarnitine	0.004
97	WT	Mouse Plasma	ethyl-malonylcarnitine	0.000
97	WT	Mouse Plasma	glutaroylcarnitine	0.007
97	WT	Mouse Plasma	adipoylcarnitine	0.015
97	WT	Mouse Plasma	3-methyl-glutaroylcarnitine	0.001
97	WT	Mouse Plasma	suberoylcarnitine	0.019
97	WT	Mouse Plasma	sebacoylcarnitine	0.003
97	WT	Mouse Plasma	sum_of_individual_acylcarnitines	39.471
97	WT	Mouse Plasma	ratio:_sum/calculated	1.058
98	WT	Mouse Plasma	total_carnitine	81.297
98	WT	Mouse Plasma	free_carnitine	49.917

98	WT	Mouse Plasma	calculated_acylcarnitines	31.381
98	WT	Mouse Plasma	acyl/free	0.629
98	WT	Mouse Plasma	butyrobetaine	1.603
98	WT	Mouse Plasma	acetylcarnitine	28.897
98	WT	Mouse Plasma	propionylcarnitine	0.842
98	WT	Mouse Plasma	butyrylcarnitine	0.731
98	WT	Mouse Plasma	isobutyrylcarnitine	0.154
98	WT	Mouse Plasma	R-3-hydroxy-butyrylcarnitine	0.065
98	WT	Mouse Plasma	S-3-hydroxy-butyrylcarnitine	0.141
98	WT	Mouse Plasma	valerylcarnitine	0.013
98	WT	Mouse Plasma	isovalerylcarnitine	0.100
98	WT	Mouse Plasma	3-hydroxy-isovalerylcarnitine	0.077
98	WT	Mouse Plasma	2-methyl-butyrylcarnitine	0.092
98	WT	Mouse Plasma	pivaloylcarnitine	0.000
98	WT	Mouse Plasma	tigloylcarnitine	0.005
98	WT	Mouse Plasma	3-methyl-crotonylcarnitine	0.000
98	WT	Mouse Plasma	hexanoylcarnitine	0.046
98	WT	Mouse Plasma	R-3-hydroxy-hexanoylcarnitine	0.003
98	WT	Mouse Plasma	S-3-hydroxy-hexanoylcarnitine	0.006
98	WT	Mouse Plasma	phenylacetylcarnitine	0.001
98	WT	Mouse Plasma	phenylpropionylcarnitine	0.003
98	WT	Mouse Plasma	4-phenyl-butyrylcarnitine	0.000
98	WT	Mouse Plasma	benzoylcarnitine	0.007
98	WT	Mouse Plasma	4-methyl-hexanoylcarnitine	0.001
98	WT	Mouse Plasma	octanoylcarnitine	0.013
98	WT	Mouse Plasma	R-3-hydroxy-octanoylcarnitine	0.002
98	WT	Mouse Plasma	S-3-hydroxy-octanoylcarnitine	0.008

98	WT	Mouse Plasma	valproylcarnitine	0.000
98	WT	Mouse Plasma	branched-chain C8	0.000
98	WT	Mouse Plasma	cis-3,4-methylene-heptanoylcarnitine	0.000
98	WT	Mouse Plasma	4-methyl-octanoylcarnitine	0.000
98	WT	Mouse Plasma	2,6-dimethyl-heptanoylcarnitine	0.000
98	WT	Mouse Plasma	decanoylcarnitine	0.019
98	WT	Mouse Plasma	cis-4-decenoylcarnitine	0.011
98	WT	Mouse Plasma	cis-3,4-methylene-nonanoylcarnitine	0.000
98	WT	Mouse Plasma	R-3-hydroxy-decanoylcarnitine	0.002
98	WT	Mouse Plasma	S-3-hydroxy-decanoylcarnitine	0.010
98	WT	Mouse Plasma	5-decynoylcarnitine	0.000
98	WT	Mouse Plasma	lauroylcarnitine	0.024
98	WT	Mouse Plasma	trans-2-dodecenoylcarnitine	0.002
98	WT	Mouse Plasma	R-3-hydroxy-lauroylcarnitine	0.001
98	WT	Mouse Plasma	S-3-hydroxy-lauroylcarnitine	0.004
98	WT	Mouse Plasma	myristoylcarnitine	0.076
98	WT	Mouse Plasma	myristoleoylcarnitine	0.021
98	WT	Mouse Plasma	cis-5-tetradecenoylcarnitine	0.045
98	WT	Mouse Plasma	trans-2-tetradecenoylcarnitine	0.008
98	WT	Mouse Plasma	cis,cis-5,8-tetradecadienoylcarnitine	0.021
98	WT	Mouse Plasma	R-3-hydroxy-myristoylcarnitine	0.003
98	WT	Mouse Plasma	S-3-hydroxy-myristoylcarnitine	0.008
98	WT	Mouse Plasma	hydroxy-C14:1	0.008
98	WT	Mouse Plasma	palmitoylcarnitine	0.177

98	WT	Mouse Plasma	palmitoleoylcarnitine	0.047
98	WT	Mouse Plasma	trans-2-hexadecenoylcarnitine	0.003
98	WT	Mouse Plasma	R-3-hydroxy-palmitoylcarnitine	0.003
98	WT	Mouse Plasma	S-3-hydroxy-palmitoylcarnitine	0.006
98	WT	Mouse Plasma	hydroxy-C16:1	0.001
98	WT	Mouse Plasma	stearoylcarnitine	0.044
98	WT	Mouse Plasma	oleoylcarnitine	0.192
98	WT	Mouse Plasma	linoleoylcarnitine	0.092
98	WT	Mouse Plasma	alpha-linolenoylcarnitine	0.007
98	WT	Mouse Plasma	gamma-linolenoylcarnitine	0.003
98	WT	Mouse Plasma	R-3-hydroxy-stearoylcarnitine	0.006
98	WT	Mouse Plasma	S-3-hydroxy-stearoylcarnitine	0.001
98	WT	Mouse Plasma	hydroxy-C18:1	0.012
98	WT	Mouse Plasma	hydroxy-C18:2	0.004
98	WT	Mouse Plasma	hydroxy-C18:3	0.001
98	WT	Mouse Plasma	malonylcarnitine	0.048
98	WT	Mouse Plasma	succinylcarnitine	0.067
98	WT	Mouse Plasma	methyl-malonylcarnitine	0.009
98	WT	Mouse Plasma	ethyl-malonylcarnitine	0.000
98	WT	Mouse Plasma	glutaroylcarnitine	0.009
98	WT	Mouse Plasma	adipoylcarnitine	0.013
98	WT	Mouse Plasma	3-methyl-glutaroylcarnitine	0.001
98	WT	Mouse Plasma	suberoylcarnitine	0.012
98	WT	Mouse Plasma	sebacoylcarnitine	0.001
98	WT	Mouse Plasma	sum_of_individual_acylcarnitines	32.231
98	WT	Mouse Plasma	ratio:_sum/calculated	1.027
15	KO	Mouse Urine	total_carnitine	737.740

15	KO	Mouse Urine	free_carnitine	598.817
15	KO	Mouse Urine	calculated_acylcarnitines	138.923
15	KO	Mouse Urine	acyl/free	0.232
15	KO	Mouse Urine	butyrobetaine	24.060
15	KO	Mouse Urine	acetylcarnitine	36.318
15	KO	Mouse Urine	propionylcarnitine	0.626
15	KO	Mouse Urine	butyrylcarnitine	0.806
15	KO	Mouse Urine	isobutyrylcarnitine	0.124
15	KO	Mouse Urine	R-3-hydroxy-butyrylcarnitine	0.012
15	KO	Mouse Urine	S-3-hydroxy-butyrylcarnitine	0.064
15	KO	Mouse Urine	valerylcarnitine	0.012
15	KO	Mouse Urine	isovalerylcarnitine	0.160
15	KO	Mouse Urine	3-hydroxy-isovalerylcarnitine	0.806
15	KO	Mouse Urine	2-methyl-butyrylcarnitine	0.105
15	KO	Mouse Urine	pivaloylcarnitine	0.000
15	KO	Mouse Urine	tigloylcarnitine	0.015
15	KO	Mouse Urine	3-methyl-crotonylcarnitine	0.001
15	KO	Mouse Urine	hexanoylcarnitine	0.041
15	KO	Mouse Urine	R-3-hydroxy-hexanoylcarnitine	0.027
15	KO	Mouse Urine	S-3-hydroxy-hexanoylcarnitine	0.016
15	KO	Mouse Urine	phenylacetylcarnitine	0.002
15	KO	Mouse Urine	phenylpropionylcarnitine	0.001
15	KO	Mouse Urine	4-phenyl-butyrylcarnitine	0.000
15	KO	Mouse Urine	benzoylcarnitine	0.208
15	KO	Mouse Urine	4-methyl-hexanoylcarnitine	0.001
15	KO	Mouse Urine	octanoylcarnitine	0.027
15	KO	Mouse Urine	R-3-hydroxy-octanoylcarnitine	0.005

15	KO	Mouse Urine	S-3-hydroxy-octanoylcarnitine	0.008
15	KO	Mouse Urine	valproylcarnitine	0.000
15	KO	Mouse Urine	branched-chain C8	0.000
15	KO	Mouse Urine	cis-3,4-methylene-heptanoylcarnitine	0.018
15	KO	Mouse Urine	4-methyl-octanoylcarnitine	0.000
15	KO	Mouse Urine	2,6-dimethyl-heptanoylcarnitine	0.002
15	KO	Mouse Urine	decanoylcarnitine	0.012
15	KO	Mouse Urine	cis-4-decenoylcarnitine	0.020
15	KO	Mouse Urine	cis-3,4-methylene-nonanoylcarnitine	0.071
15	KO	Mouse Urine	R-3-hydroxy-decanoylcarnitine	0.001
15	KO	Mouse Urine	S-3-hydroxy-decanoylcarnitine	0.007
15	KO	Mouse Urine	5-decynoylcarnitine	0.007
15	KO	Mouse Urine	malonylcarnitine	6.734
15	KO	Mouse Urine	succinylcarnitine	5.151
15	KO	Mouse Urine	methyl-malonylcarnitine	2.365
15	KO	Mouse Urine	ethyl-malonylcarnitine	0.034
15	KO	Mouse Urine	glutaroylcarnitine	3.770
15	KO	Mouse Urine	adipoylcarnitine	3.375
15	KO	Mouse Urine	3-methyl-glutaroylcarnitine	0.526
15	KO	Mouse Urine	suberoylcarnitine	2.226
15	KO	Mouse Urine	sebacoylcarnitine	0.483
15	KO	Mouse Urine	sum_of_individual_acylcarnitines	64.198
15	KO	Mouse Urine	ratio:_sum/calculated	0.462
43	KO	Mouse Urine	total_carnitine	718.844
43	KO	Mouse Urine	free_carnitine	560.265

43	KO	Mouse Urine	calculated_acylcarnitines	158.579
43	KO	Mouse Urine	acyl/free	0.283
43	KO	Mouse Urine	butyrobetaine	32.649
43	KO	Mouse Urine	acetylcarnitine	32.911
43	KO	Mouse Urine	propionylcarnitine	0.546
43	KO	Mouse Urine	butyrylcarnitine	0.995
43	KO	Mouse Urine	isobutyrylcarnitine	0.161
43	KO	Mouse Urine	R-3-hydroxy-butyrylcarnitine	0.047
43	KO	Mouse Urine	S-3-hydroxy-butyrylcarnitine	0.092
43	KO	Mouse Urine	valerylcarnitine	0.017
43	KO	Mouse Urine	isovalerylcarnitine	0.060
43	KO	Mouse Urine	3-hydroxy-isovalerylcarnitine	0.926
43	KO	Mouse Urine	2-methyl-butyrylcarnitine	0.090
43	KO	Mouse Urine	pivaloylcarnitine	0.000
43	KO	Mouse Urine	tigloylcarnitine	0.015
43	KO	Mouse Urine	3-methyl-crotonylcarnitine	0.001
43	KO	Mouse Urine	hexanoylcarnitine	0.057
43	KO	Mouse Urine	R-3-hydroxy-hexanoylcarnitine	0.018
43	KO	Mouse Urine	S-3-hydroxy-hexanoylcarnitine	0.019
43	KO	Mouse Urine	phenylacetylcarnitine	0.002
43	KO	Mouse Urine	phenylpropionylcarnitine	0.001
43	KO	Mouse Urine	4-phenyl-butyrylcarnitine	0.000
43	KO	Mouse Urine	benzoylcarnitine	0.218
43	KO	Mouse Urine	4-methyl-hexanoylcarnitine	0.002
43	KO	Mouse Urine	octanoylcarnitine	0.041
43	KO	Mouse Urine	R-3-hydroxy-octanoylcarnitine	0.003
43	KO	Mouse Urine	S-3-hydroxy-octanoylcarnitine	0.003

43	KO	Mouse Urine	valproylcarnitine	0.000
43	KO	Mouse Urine	branched-chain C8	0.000
43	KO	Mouse Urine	cis-3,4-methylene-heptanoylcarnitine	0.034
43	KO	Mouse Urine	4-methyl-octanoylcarnitine	0.002
43	KO	Mouse Urine	2,6-dimethyl-heptanoylcarnitine	0.001
43	KO	Mouse Urine	decanoylcarnitine	0.022
43	KO	Mouse Urine	cis-4-decenoylcarnitine	0.042
43	KO	Mouse Urine	cis-3,4-methylene-nonanoylcarnitine	0.081
43	KO	Mouse Urine	R-3-hydroxy-decanoylcarnitine	0.002
43	KO	Mouse Urine	S-3-hydroxy-decanoylcarnitine	0.002
43	KO	Mouse Urine	5-decynoylcarnitine	0.019
43	KO	Mouse Urine	malonylcarnitine	5.713
43	KO	Mouse Urine	succinylcarnitine	3.732
43	KO	Mouse Urine	methyl-malonylcarnitine	1.286
43	KO	Mouse Urine	ethyl-malonylcarnitine	0.013
43	KO	Mouse Urine	glutaroylcarnitine	2.969
43	KO	Mouse Urine	adipoylcarnitine	2.680
43	KO	Mouse Urine	3-methyl-glutaroylcarnitine	0.164
43	KO	Mouse Urine	suberoylcarnitine	1.136
43	KO	Mouse Urine	sebacoylcarnitine	0.196
43	KO	Mouse Urine	sum_of_individual_acylcarnitines	54.365
43	KO	Mouse Urine	ratio:_sum/calculated	0.343
70	KO	Mouse Urine	total_carnitine	248.932
70	KO	Mouse Urine	free_carnitine	173.427
70	KO	Mouse Urine	calculated_acylcarnitines	75.505

70	KO	Mouse Urine	acyl/free	0.435
70	KO	Mouse Urine	butyrobetaine	6.135
70	KO	Mouse Urine	acetylcarnitine	10.753
70	KO	Mouse Urine	propionylcarnitine	0.329
70	KO	Mouse Urine	butyrylcarnitine	0.245
70	KO	Mouse Urine	isobutyrylcarnitine	0.183
70	KO	Mouse Urine	R-3-hydroxy-butyrylcarnitine	0.000
70	KO	Mouse Urine	S-3-hydroxy-butyrylcarnitine	0.009
70	KO	Mouse Urine	valerylcarnitine	0.007
70	KO	Mouse Urine	isovalerylcarnitine	0.071
70	KO	Mouse Urine	3-hydroxy-isovalerylcarnitine	0.375
70	KO	Mouse Urine	2-methyl-butyrylcarnitine	0.050
70	KO	Mouse Urine	pivaloylcarnitine	0.000
70	KO	Mouse Urine	tigloylcarnitine	0.014
70	KO	Mouse Urine	3-methyl-crotonylcarnitine	0.000
70	KO	Mouse Urine	hexanoylcarnitine	0.013
70	KO	Mouse Urine	R-3-hydroxy-hexanoylcarnitine	0.009
70	KO	Mouse Urine	S-3-hydroxy-hexanoylcarnitine	0.005
70	KO	Mouse Urine	phenylacetylcarnitine	0.002
70	KO	Mouse Urine	phenylpropionylcarnitine	0.000
70	KO	Mouse Urine	4-phenyl-butyrylcarnitine	0.000
70	KO	Mouse Urine	benzoylcarnitine	0.085
70	KO	Mouse Urine	4-methyl-hexanoylcarnitine	0.001
70	KO	Mouse Urine	octanoylcarnitine	0.009
70	KO	Mouse Urine	R-3-hydroxy-octanoylcarnitine	0.001
70	KO	Mouse Urine	S-3-hydroxy-octanoylcarnitine	0.002
70	KO	Mouse Urine	valproylcarnitine	0.000

70	KO	Mouse Urine	branched-chain C8	0.000
70	KO	Mouse Urine	cis-3,4-methylene-heptanoylcarnitine	0.009
70	KO	Mouse Urine	4-methyl-octanoylcarnitine	0.000
70	KO	Mouse Urine	2,6-dimethyl-heptanoylcarnitine	0.001
70	KO	Mouse Urine	decanoylcarnitine	0.007
70	KO	Mouse Urine	cis-4-decenoylcarnitine	0.008
70	KO	Mouse Urine	cis-3,4-methylene-nonanoylcarnitine	0.048
70	KO	Mouse Urine	R-3-hydroxy-decanoylcarnitine	0.001
70	KO	Mouse Urine	S-3-hydroxy-decanoylcarnitine	0.002
70	KO	Mouse Urine	5-decynoylcarnitine	0.005
70	KO	Mouse Urine	malonylcarnitine	2.372
70	KO	Mouse Urine	succinylcarnitine	2.003
70	KO	Mouse Urine	methyl-malonylcarnitine	1.123
70	KO	Mouse Urine	ethyl-malonylcarnitine	0.021
70	KO	Mouse Urine	glutaroylcarnitine	2.872
70	KO	Mouse Urine	adipoylcarnitine	2.237
70	KO	Mouse Urine	3-methyl-glutaroylcarnitine	0.144
70	KO	Mouse Urine	suberoylcarnitine	1.285
70	KO	Mouse Urine	sebacoylcarnitine	0.476
70	KO	Mouse Urine	sum_of_individual_acylcarnitines	24.800
70	KO	Mouse Urine	ratio:_sum/calculated	0.328
96	WT	Mouse Urine	total_carnitine	256.373
96	WT	Mouse Urine	free_carnitine	171.935
96	WT	Mouse Urine	calculated_acylcarnitines	84.438
96	WT	Mouse Urine	acyl/free	0.491

96	WT	Mouse Urine	butyrobetaine	15.111
96	WT	Mouse Urine	acetylcarnitine	9.677
96	WT	Mouse Urine	propionylcarnitine	0.219
96	WT	Mouse Urine	butyrylcarnitine	0.307
96	WT	Mouse Urine	isobutyrylcarnitine	0.066
96	WT	Mouse Urine	R-3-hydroxy-butyrylcarnitine	0.000
96	WT	Mouse Urine	S-3-hydroxy-butyrylcarnitine	0.005
96	WT	Mouse Urine	valerylcarnitine	0.004
96	WT	Mouse Urine	isovalerylcarnitine	0.027
96	WT	Mouse Urine	3-hydroxy-isovalerylcarnitine	0.333
96	WT	Mouse Urine	2-methyl-butyrylcarnitine	0.038
96	WT	Mouse Urine	pivaloylcarnitine	0.000
96	WT	Mouse Urine	tigloylcarnitine	0.009
96	WT	Mouse Urine	3-methyl-crotonylcarnitine	0.000
96	WT	Mouse Urine	hexanoylcarnitine	0.016
96	WT	Mouse Urine	R-3-hydroxy-hexanoylcarnitine	0.007
96	WT	Mouse Urine	S-3-hydroxy-hexanoylcarnitine	0.006
96	WT	Mouse Urine	phenylacetylcarnitine	0.002
96	WT	Mouse Urine	phenylpropionylcarnitine	0.000
96	WT	Mouse Urine	4-phenyl-butyrylcarnitine	0.000
96	WT	Mouse Urine	benzoylcarnitine	0.114
96	WT	Mouse Urine	4-methyl-hexanoylcarnitine	0.000
96	WT	Mouse Urine	octanoylcarnitine	0.014
96	WT	Mouse Urine	R-3-hydroxy-octanoylcarnitine	0.001
96	WT	Mouse Urine	S-3-hydroxy-octanoylcarnitine	0.001
96	WT	Mouse Urine	valproylcarnitine	0.000
96	WT	Mouse Urine	branched-chain C8	0.000

96	WT	Mouse Urine	cis-3,4-methylene-heptanoylcarnitine	0.010
96	WT	Mouse Urine	4-methyl-octanoylcarnitine	0.001
96	WT	Mouse Urine	2,6-dimethyl-heptanoylcarnitine	0.001
96	WT	Mouse Urine	decanoylcarnitine	0.006
96	WT	Mouse Urine	cis-4-decenoylcarnitine	0.008
96	WT	Mouse Urine	cis-3,4-methylene-nonanoylcarnitine	0.054
96	WT	Mouse Urine	R-3-hydroxy-decanoylcarnitine	0.001
96	WT	Mouse Urine	S-3-hydroxy-decanoylcarnitine	0.001
96	WT	Mouse Urine	5-decynoylcarnitine	0.005
96	WT	Mouse Urine	malonylcarnitine	2.830
96	WT	Mouse Urine	succinylcarnitine	3.622
96	WT	Mouse Urine	methyl-malonylcarnitine	1.706
96	WT	Mouse Urine	ethyl-malonylcarnitine	0.014
96	WT	Mouse Urine	glutaroylcarnitine	2.297
96	WT	Mouse Urine	adipoylcarnitine	2.306
96	WT	Mouse Urine	3-methyl-glutaroylcarnitine	0.170
96	WT	Mouse Urine	suberoylcarnitine	1.454
96	WT	Mouse Urine	sebacoylcarnitine	0.247
96	WT	Mouse Urine	sum_of_individual_acylcarnitines	25.591
96	WT	Mouse Urine	ratio:_sum/calculated	0.303
97	WT	Mouse Urine	total_carnitine	495.455
97	WT	Mouse Urine	free_carnitine	409.470
97	WT	Mouse Urine	calculated_acylcarnitines	85.985
97	WT	Mouse Urine	acyl/free	0.210
97	WT	Mouse Urine	butyrobetaine	15.903

97	WT	Mouse Urine	acetylcarnitine	21.824
97	WT	Mouse Urine	propionylcarnitine	0.573
97	WT	Mouse Urine	butyrylcarnitine	0.485
97	WT	Mouse Urine	isobutyrylcarnitine	0.176
97	WT	Mouse Urine	R-3-hydroxy-butyrylcarnitine	0.011
97	WT	Mouse Urine	S-3-hydroxy-butyrylcarnitine	0.016
97	WT	Mouse Urine	valerylcarnitine	0.006
97	WT	Mouse Urine	isovalerylcarnitine	0.053
97	WT	Mouse Urine	3-hydroxy-isovalerylcarnitine	0.899
97	WT	Mouse Urine	2-methyl-butyrylcarnitine	0.060
97	WT	Mouse Urine	pivaloylcarnitine	0.000
97	WT	Mouse Urine	tigloylcarnitine	0.016
97	WT	Mouse Urine	3-methyl-crotonylcarnitine	0.001
97	WT	Mouse Urine	hexanoylcarnitine	0.013
97	WT	Mouse Urine	R-3-hydroxy-hexanoylcarnitine	0.012
97	WT	Mouse Urine	S-3-hydroxy-hexanoylcarnitine	0.017
97	WT	Mouse Urine	phenylacetylcarnitine	0.006
97	WT	Mouse Urine	phenylpropionylcarnitine	0.001
97	WT	Mouse Urine	4-phenyl-butyrylcarnitine	0.000
97	WT	Mouse Urine	benzoylcarnitine	0.169
97	WT	Mouse Urine	4-methyl-hexanoylcarnitine	0.000
97	WT	Mouse Urine	octanoylcarnitine	0.011
97	WT	Mouse Urine	R-3-hydroxy-octanoylcarnitine	0.002
97	WT	Mouse Urine	S-3-hydroxy-octanoylcarnitine	0.003
97	WT	Mouse Urine	valproylcarnitine	0.000
97	WT	Mouse Urine	branched-chain C8	0.000
97	WT	Mouse Urine	cis-3,4-methylene-	0.013

			heptanoylcarnitine	
97	WT	Mouse Urine	4-methyl-octanoylcarnitine	0.001
97	WT	Mouse Urine	2,6-dimethyl-heptanoylcarnitine	0.001
97	WT	Mouse Urine	decanoylcarnitine	0.005
97	WT	Mouse Urine	cis-4-decenoylcarnitine	0.007
97	WT	Mouse Urine	cis-3,4-methylene- nonanoylcarnitine	0.050
97	WT	Mouse Urine	R-3-hydroxy-decanoylcarnitine	0.001
97	WT	Mouse Urine	S-3-hydroxy-decanoylcarnitine	0.003
97	WT	Mouse Urine	5-decynoylcarnitine	0.007
97	WT	Mouse Urine	malonylcarnitine	2.765
97	WT	Mouse Urine	succinylcarnitine	3.132
97	WT	Mouse Urine	methyl-malonylcarnitine	1.281
97	WT	Mouse Urine	ethyl-malonylcarnitine	0.014
97	WT	Mouse Urine	glutaroylcarnitine	1.766
97	WT	Mouse Urine	adipoylcarnitine	2.091
97	WT	Mouse Urine	3-methyl-glutaroylcarnitine	0.213
97	WT	Mouse Urine	suberoylcarnitine	1.714
97	WT	Mouse Urine	sebacoylcarnitine	0.303
97	WT	Mouse Urine	sum_of_individual_acylcarnitines	37.740
97	WT	Mouse Urine	ratio:_sum/calculated	0.439
98	WT	Mouse Urine	total_carnitine	0.181
98	WT	Mouse Urine	free_carnitine	0.522
98	WT	Mouse Urine	calculated_acylcarnitines	-0.341
98	WT	Mouse Urine	acyl/free	-0.653
98	WT	Mouse Urine	butyrobetaine	0.038
98	WT	Mouse Urine	acetylcarnitine	0.000

98	WT	Mouse Urine	propionylcarnitine	0.000
98	WT	Mouse Urine	butyrylcarnitine	0.000
98	WT	Mouse Urine	isobutyrylcarnitine	0.000
98	WT	Mouse Urine	R-3-hydroxy-butyrylcarnitine	0.000
98	WT	Mouse Urine	S-3-hydroxy-butyrylcarnitine	0.000
98	WT	Mouse Urine	valerylcarnitine	0.000
98	WT	Mouse Urine	isovalerylcarnitine	0.000
98	WT	Mouse Urine	3-hydroxy-isovalerylcarnitine	0.000
98	WT	Mouse Urine	2-methyl-butyrylcarnitine	0.000
98	WT	Mouse Urine	pivaloylcarnitine	0.000
98	WT	Mouse Urine	tigloylcarnitine	0.000
98	WT	Mouse Urine	3-methyl-crotonylcarnitine	0.000
98	WT	Mouse Urine	hexanoylcarnitine	0.000
98	WT	Mouse Urine	R-3-hydroxy-hexanoylcarnitine	0.000
98	WT	Mouse Urine	S-3-hydroxy-hexanoylcarnitine	0.000
98	WT	Mouse Urine	phenylacetylcarnitine	0.000
98	WT	Mouse Urine	phenylpropionylcarnitine	0.000
98	WT	Mouse Urine	4-phenyl-butyrylcarnitine	0.000
98	WT	Mouse Urine	benzoylcarnitine	0.000
98	WT	Mouse Urine	4-methyl-hexanoylcarnitine	0.000
98	WT	Mouse Urine	octanoylcarnitine	0.000
98	WT	Mouse Urine	R-3-hydroxy-octanoylcarnitine	0.000
98	WT	Mouse Urine	S-3-hydroxy-octanoylcarnitine	0.000
98	WT	Mouse Urine	valproylcarnitine	0.000
98	WT	Mouse Urine	branched-chain C8	0.000
98	WT	Mouse Urine	cis-3,4-methylene-heptanoylcarnitine	0.000

98	WT	Mouse Urine	4-methyl-octanoylcarnitine	0.000
98	WT	Mouse Urine	2,6-dimethyl-heptanoylcarnitine	0.000
98	WT	Mouse Urine	decanoylcarnitine	0.000
98	WT	Mouse Urine	cis-4-decenoylcarnitine	0.000
98	WT	Mouse Urine	cis-3,4-methylene- nonanoylcarnitine	0.000
98	WT	Mouse Urine	R-3-hydroxy-decanoylcarnitine	0.000
98	WT	Mouse Urine	S-3-hydroxy-decanoylcarnitine	0.000
98	WT	Mouse Urine	5-decynoylcarnitine	0.000
98	WT	Mouse Urine	malonylcarnitine	0.004
98	WT	Mouse Urine	succinylcarnitine	0.000
98	WT	Mouse Urine	methyl-malonylcarnitine	0.001
98	WT	Mouse Urine	ethyl-malonylcarnitine	0.000
98	WT	Mouse Urine	glutaroylcarnitine	0.000
98	WT	Mouse Urine	adipoylcarnitine	0.000
98	WT	Mouse Urine	3-methyl-glutaroylcarnitine	0.000
98	WT	Mouse Urine	suberoylcarnitine	0.000
98	WT	Mouse Urine	sebacoylcarnitine	0.000
98	WT	Mouse Urine	sum_of_individual_acylcarnitines	0.008
15	KO	Mouse Brain	total_carnitine	252.737
15	KO	Mouse Brain	free_carnitine	167.498
15	KO	Mouse Brain	calculated_acylcarnitines	85.239
15	KO	Mouse Brain	acyl/free	0.509
15	KO	Mouse Brain	butyrobetaine	4.071
15	KO	Mouse Brain	acetylcarnitine	83.157
15	KO	Mouse Brain	propionylcarnitine	2.897
15	KO	Mouse Brain	butyrylcarnitine	1.375

15	KO	Mouse Brain	isobutyrylcarnitine	0.130
15	KO	Mouse Brain	R-3-hydroxy-butyrylcarnitine	0.263
15	KO	Mouse Brain	S-3-hydroxy-butyrylcarnitine	0.597
15	KO	Mouse Brain	valerylcarnitine	0.042
15	KO	Mouse Brain	isovalerylcarnitine	0.639
15	KO	Mouse Brain	3-hydroxy-isovalerylcarnitine	0.571
15	KO	Mouse Brain	2-methyl-butyrylcarnitine	0.198
15	KO	Mouse Brain	pivaloylcarnitine	0.000
15	KO	Mouse Brain	tigloylcarnitine	0.007
15	KO	Mouse Brain	3-methyl-crotonylcarnitine	0.000
15	KO	Mouse Brain	hexanoylcarnitine	0.072
15	KO	Mouse Brain	R-3-hydroxy-hexanoylcarnitine	0.005
15	KO	Mouse Brain	S-3-hydroxy-hexanoylcarnitine	0.011
15	KO	Mouse Brain	phenylacetylcarnitine	0.002
15	KO	Mouse Brain	phenylpropionylcarnitine	0.000
15	KO	Mouse Brain	4-phenyl-butyrylcarnitine	0.000
15	KO	Mouse Brain	benzoylcarnitine	0.000
15	KO	Mouse Brain	4-methyl-hexanoylcarnitine	0.000
15	KO	Mouse Brain	octanoylcarnitine	0.018
15	KO	Mouse Brain	R-3-hydroxy-octanoylcarnitine	0.001
15	KO	Mouse Brain	S-3-hydroxy-octanoylcarnitine	0.006
15	KO	Mouse Brain	valproylcarnitine	0.000
15	KO	Mouse Brain	branched-chain C8	0.000
15	KO	Mouse Brain	cis-3,4-methylene-heptanoylcarnitine	0.002
15	KO	Mouse Brain	4-methyl-octanoylcarnitine	0.001
15	KO	Mouse Brain	2,6-dimethyl-heptanoylcarnitine	0.000

15	KO	Mouse Brain	decanoylcarnitine	0.029
15	KO	Mouse Brain	cis-4-decenoylcarnitine	0.009
15	KO	Mouse Brain	cis-3,4-methylene- nonanoylcarnitine	0.000
15	KO	Mouse Brain	R-3-hydroxy-decanoylcarnitine	0.000
15	KO	Mouse Brain	S-3-hydroxy-decanoylcarnitine	0.009
15	KO	Mouse Brain	5-decynoylcarnitine	0.002
15	KO	Mouse Brain	lauroylcarnitine	0.114
15	KO	Mouse Brain	trans-2-dodecenoylcarnitine	0.000
15	KO	Mouse Brain	R-3-hydroxy-lauroylcarnitine	0.003
15	KO	Mouse Brain	S-3-hydroxy-lauroylcarnitine	0.005
15	KO	Mouse Brain	myristoylcarnitine	0.676
15	KO	Mouse Brain	myristoleoylcarnitine	0.033
15	KO	Mouse Brain	cis-5-tetradecenoylcarnitine	0.000
15	KO	Mouse Brain	trans-2-tetradecenoylcarnitine	0.000
15	KO	Mouse Brain	cis,cis-5,8- tetradecadienoylcarnitine	0.028
15	KO	Mouse Brain	R-3-hydroxy-myristoylcarnitine	0.000
15	KO	Mouse Brain	S-3-hydroxy-myristoylcarnitine	0.000
15	KO	Mouse Brain	hydroxy-C14:1	0.007
15	KO	Mouse Brain	palmitoylcarnitine	1.738
15	KO	Mouse Brain	palmitoleoylcarnitine	0.138
15	KO	Mouse Brain	trans-2-hexadecenoylcarnitine	0.002
15	KO	Mouse Brain	R-3-hydroxy-palmitoylcarnitine	0.000
15	KO	Mouse Brain	S-3-hydroxy-palmitoylcarnitine	0.026
15	KO	Mouse Brain	hydroxy-C16:1	0.028
15	KO	Mouse Brain	stearoylcarnitine	1.418

15	KO	Mouse Brain	oleoylcarnitine	1.703
15	KO	Mouse Brain	linoleoylcarnitine	0.120
15	KO	Mouse Brain	alpha-linolenoylcarnitine	0.000
15	KO	Mouse Brain	gamma-linolenoylcarnitine	0.000
15	KO	Mouse Brain	R-3-hydroxy-stearoylcarnitine	0.000
15	KO	Mouse Brain	S-3-hydroxy-stearoylcarnitine	0.006
15	KO	Mouse Brain	hydroxy-C18:1	0.022
15	KO	Mouse Brain	hydroxy-C18:2	0.016
15	KO	Mouse Brain	hydroxy-C18:3	0.000
15	KO	Mouse Brain	malonylcarnitine	0.461
15	KO	Mouse Brain	succinylcarnitine	0.303
15	KO	Mouse Brain	methyl-malonylcarnitine	0.089
15	KO	Mouse Brain	ethyl-malonylcarnitine	0.001
15	KO	Mouse Brain	glutaroylcarnitine	0.168
15	KO	Mouse Brain	adipoylcarnitine	0.027
15	KO	Mouse Brain	3-methyl-glutaroylcarnitine	0.047
15	KO	Mouse Brain	suberoylcarnitine	0.043
15	KO	Mouse Brain	sebacoylcarnitine	0.003
15	KO	Mouse Brain	sum_of_individual_acylcarnitines	97.268
15	KO	Mouse Brain	ratio:_sum/calculated	1.141
15	KO	Mouse Fat	total_carnitine	57.346
15	KO	Mouse Fat	free_carnitine	31.845
15	KO	Mouse Fat	calculated_acylcarnitines	25.501
15	KO	Mouse Fat	acyl/free	0.801
15	KO	Mouse Fat	butyrobetaine	2.103
15	KO	Mouse Fat	acetylcarnitine	8.308
15	KO	Mouse Fat	propionylcarnitine	0.233

15	KO	Mouse Fat	butyrylcarnitine	0.236
15	KO	Mouse Fat	isobutyrylcarnitine	0.069
15	KO	Mouse Fat	R-3-hydroxy-butyrylcarnitine	0.152
15	KO	Mouse Fat	S-3-hydroxy-butyrylcarnitine	0.127
15	KO	Mouse Fat	valerylcarnitine	0.003
15	KO	Mouse Fat	isovalerylcarnitine	0.207
15	KO	Mouse Fat	3-hydroxy-isovalerylcarnitine	0.048
15	KO	Mouse Fat	2-methyl-butyrylcarnitine	0.050
15	KO	Mouse Fat	pivaloylcarnitine	0.000
15	KO	Mouse Fat	tigloylcarnitine	0.000
15	KO	Mouse Fat	3-methyl-crotonylcarnitine	0.000
15	KO	Mouse Fat	hexanoylcarnitine	0.022
15	KO	Mouse Fat	R-3-hydroxy-hexanoylcarnitine	0.005
15	KO	Mouse Fat	S-3-hydroxy-hexanoylcarnitine	0.021
15	KO	Mouse Fat	phenylacetylcarnitine	0.003
15	KO	Mouse Fat	phenylpropionylcarnitine	0.000
15	KO	Mouse Fat	4-phenyl-butyrylcarnitine	0.000
15	KO	Mouse Fat	4-methyl-hexanoylcarnitine	0.000
15	KO	Mouse Fat	octanoylcarnitine	0.010
15	KO	Mouse Fat	R-3-hydroxy-octanoylcarnitine	0.003
15	KO	Mouse Fat	S-3-hydroxy-octanoylcarnitine	0.004
15	KO	Mouse Fat	valproylcarnitine	0.000
15	KO	Mouse Fat	branched-chain C8	0.000
15	KO	Mouse Fat	cis-3,4-methylene-heptanoylcarnitine	0.000
15	KO	Mouse Fat	4-methyl-octanoylcarnitine	0.000
15	KO	Mouse Fat	2,6-dimethyl-heptanoylcarnitine	0.000

15	KO	Mouse Fat	decanoylcarnitine	0.004
15	KO	Mouse Fat	cis-4-decenoylcarnitine	0.000
15	KO	Mouse Fat	cis-3,4-methylene- nonanoylcarnitine	0.000
15	KO	Mouse Fat	R-3-hydroxy-decanoylcarnitine	0.000
15	KO	Mouse Fat	S-3-hydroxy-decanoylcarnitine	0.012
15	KO	Mouse Fat	5-decynoylcarnitine	0.000
15	KO	Mouse Fat	lauroylcarnitine	0.000
15	KO	Mouse Fat	trans-2-dodecenoylcarnitine	0.000
15	KO	Mouse Fat	R-3-hydroxy-lauroylcarnitine	0.000
15	KO	Mouse Fat	S-3-hydroxy-lauroylcarnitine	0.001
15	KO	Mouse Fat	myristoylcarnitine	0.064
15	KO	Mouse Fat	myristoleoylcarnitine	0.070
15	KO	Mouse Fat	cis-5-tetradecenoylcarnitine	0.000
15	KO	Mouse Fat	trans-2-tetradecenoylcarnitine	0.000
15	KO	Mouse Fat	cis,cis-5,8- tetradecadienoylcarnitine	0.000
15	KO	Mouse Fat	R-3-hydroxy-myristoylcarnitine	0.000
15	KO	Mouse Fat	S-3-hydroxy-myristoylcarnitine	0.000
15	KO	Mouse Fat	hydroxy-C14:1	0.009
15	KO	Mouse Fat	palmitoylcarnitine	0.098
15	KO	Mouse Fat	palmitoleoylcarnitine	0.000
15	KO	Mouse Fat	trans-2-hexadecenoylcarnitine	0.000
15	KO	Mouse Fat	R-3-hydroxy-palmitoylcarnitine	0.000
15	KO	Mouse Fat	S-3-hydroxy-palmitoylcarnitine	0.016
15	KO	Mouse Fat	hydroxy-C16:1	0.046
15	KO	Mouse Fat	stearoylcarnitine	0.069

15	KO	Mouse Fat	oleoylcarnitine	0.004
15	KO	Mouse Fat	linoleoylcarnitine	0.123
15	KO	Mouse Fat	alpha-linolenoylcarnitine	0.000
15	KO	Mouse Fat	gamma-linolenoylcarnitine	0.000
15	KO	Mouse Fat	R-3-hydroxy-stearoylcarnitine	0.000
15	KO	Mouse Fat	S-3-hydroxy-stearoylcarnitine	0.000
15	KO	Mouse Fat	hydroxy-C18:1	0.035
15	KO	Mouse Fat	hydroxy-C18:2	0.012
15	KO	Mouse Fat	hydroxy-C18:3	0.000
15	KO	Mouse Fat	malonylcarnitine	0.000
15	KO	Mouse Fat	succinylcarnitine	0.101
15	KO	Mouse Fat	methyl-malonylcarnitine	0.003
15	KO	Mouse Fat	ethyl-malonylcarnitine	0.001
15	KO	Mouse Fat	glutaroylcarnitine	0.000
15	KO	Mouse Fat	adipoylcarnitine	0.014
15	KO	Mouse Fat	3-methyl-glutaroylcarnitine	0.005
15	KO	Mouse Fat	suberoylcarnitine	0.022
15	KO	Mouse Fat	sebacoylcarnitine	0.000
15	KO	Mouse Fat	sum_of_individual_acylcarnitines	10.211
15	KO	Mouse Fat	ratio:_sum/calculated	0.400
15	KO	Mouse Heart	total_carnitine	964.287
15	KO	Mouse Heart	free_carnitine	704.870
15	KO	Mouse Heart	calculated_acylcarnitines	259.417
15	KO	Mouse Heart	acyl/free	0.368
15	KO	Mouse Heart	butyrobetaine	12.430
15	KO	Mouse Heart	acetylcarnitine	231.944
15	KO	Mouse Heart	propionylcarnitine	11.693

15	KO	Mouse Heart	butyrylcarnitine	8.580
15	KO	Mouse Heart	isobutyrylcarnitine	6.083
15	KO	Mouse Heart	R-3-hydroxy-butyrylcarnitine	5.067
15	KO	Mouse Heart	S-3-hydroxy-butyrylcarnitine	5.077
15	KO	Mouse Heart	valerylcarnitine	0.886
15	KO	Mouse Heart	isovalerylcarnitine	0.087
15	KO	Mouse Heart	3-hydroxy-isovalerylcarnitine	0.806
15	KO	Mouse Heart	2-methyl-butyrylcarnitine	0.661
15	KO	Mouse Heart	pivaloylcarnitine	0.000
15	KO	Mouse Heart	tigloylcarnitine	0.173
15	KO	Mouse Heart	3-methyl-crotonylcarnitine	0.000
15	KO	Mouse Heart	hexanoylcarnitine	0.794
15	KO	Mouse Heart	R-3-hydroxy-hexanoylcarnitine	0.135
15	KO	Mouse Heart	S-3-hydroxy-hexanoylcarnitine	0.361
15	KO	Mouse Heart	phenylacetylcarnitine	0.012
15	KO	Mouse Heart	phenylpropionylcarnitine	0.000
15	KO	Mouse Heart	4-phenyl-butyrylcarnitine	0.000
15	KO	Mouse Heart	benzoylcarnitine	0.039
15	KO	Mouse Heart	4-methyl-hexanoylcarnitine	0.004
15	KO	Mouse Heart	octanoylcarnitine	0.176
15	KO	Mouse Heart	R-3-hydroxy-octanoylcarnitine	0.052
15	KO	Mouse Heart	S-3-hydroxy-octanoylcarnitine	0.170
15	KO	Mouse Heart	valproylcarnitine	0.000
15	KO	Mouse Heart	branched-chain C8	0.000
15	KO	Mouse Heart	cis-3,4-methylene-heptanoylcarnitine	0.009
15	KO	Mouse Heart	4-methyl-octanoylcarnitine	0.000

15	KO	Mouse Heart	2,6-dimethyl-heptanoylcarnitine	0.000
15	KO	Mouse Heart	decanoylcarnitine	0.177
15	KO	Mouse Heart	cis-4-decenoylcarnitine	0.035
15	KO	Mouse Heart	cis-3,4-methylene- nonanoylcarnitine	0.000
15	KO	Mouse Heart	R-3-hydroxy-decanoylcarnitine	0.016
15	KO	Mouse Heart	S-3-hydroxy-decanoylcarnitine	0.112
15	KO	Mouse Heart	5-decynoylcarnitine	0.000
15	KO	Mouse Heart	lauroylcarnitine	0.231
15	KO	Mouse Heart	trans-2-dodecenoylcarnitine	0.000
15	KO	Mouse Heart	R-3-hydroxy-lauroylcarnitine	0.011
15	KO	Mouse Heart	S-3-hydroxy-lauroylcarnitine	0.051
15	KO	Mouse Heart	myristoylcarnitine	0.775
15	KO	Mouse Heart	myristoleoylcarnitine	0.272
15	KO	Mouse Heart	cis-5-tetradecenoylcarnitine	0.264
15	KO	Mouse Heart	trans-2-tetradecenoylcarnitine	0.000
15	KO	Mouse Heart	cis,cis-5,8- tetradecadienoylcarnitine	0.100
15	KO	Mouse Heart	R-3-hydroxy-myristoylcarnitine	0.003
15	KO	Mouse Heart	S-3-hydroxy-myristoylcarnitine	0.062
15	KO	Mouse Heart	hydroxy-C14:1	0.108
15	KO	Mouse Heart	palmitoylcarnitine	1.465
15	KO	Mouse Heart	palmitoleoylcarnitine	0.233
15	KO	Mouse Heart	trans-2-hexadecenoylcarnitine	0.034
15	KO	Mouse Heart	R-3-hydroxy-palmitoylcarnitine	0.061
15	KO	Mouse Heart	S-3-hydroxy-palmitoylcarnitine	0.205
15	KO	Mouse Heart	hydroxy-C16:1	0.270

15	KO	Mouse Heart	stearoylcarnitine	4.086
15	KO	Mouse Heart	oleoylcarnitine	2.931
15	KO	Mouse Heart	linoleoylcarnitine	1.005
15	KO	Mouse Heart	alpha-linolenoylcarnitine	0.009
15	KO	Mouse Heart	gamma-linolenoylcarnitine	0.000
15	KO	Mouse Heart	R-3-hydroxy-stearoylcarnitine	0.040
15	KO	Mouse Heart	S-3-hydroxy-stearoylcarnitine	0.190
15	KO	Mouse Heart	hydroxy-C18:1	0.622
15	KO	Mouse Heart	hydroxy-C18:2	0.321
15	KO	Mouse Heart	hydroxy-C18:3	0.088
15	KO	Mouse Heart	malonylcarnitine	5.286
15	KO	Mouse Heart	succinylcarnitine	19.812
15	KO	Mouse Heart	methyl-malonylcarnitine	0.930
15	KO	Mouse Heart	ethyl-malonylcarnitine	0.013
15	KO	Mouse Heart	glutaroylcarnitine	0.000
15	KO	Mouse Heart	adipoylcarnitine	0.013
15	KO	Mouse Heart	3-methyl-glutaroylcarnitine	0.009
15	KO	Mouse Heart	suberoylcarnitine	0.018
15	KO	Mouse Heart	sebacylcarnitine	0.002
15	KO	Mouse Heart	sum_of_individual_acylcarnitines	312.672
15	KO	Mouse Heart	ratio:_sum/calculated	1.205
15	KO	Mouse Kidney	total_carnitine	475.739
15	KO	Mouse Kidney	free_carnitine	347.970
15	KO	Mouse Kidney	calculated_acylcarnitines	127.769
15	KO	Mouse Kidney	acyl/free	0.367
15	KO	Mouse Kidney	butyrobetaine	4.727
15	KO	Mouse Kidney	acetylcarnitine	62.411

15	KO	Mouse Kidney	propionylcarnitine	3.744
15	KO	Mouse Kidney	butyrylcarnitine	3.433
15	KO	Mouse Kidney	isobutyrylcarnitine	0.651
15	KO	Mouse Kidney	R-3-hydroxy-butyrylcarnitine	1.525
15	KO	Mouse Kidney	S-3-hydroxy-butyrylcarnitine	1.025
15	KO	Mouse Kidney	valerylcarnitine	0.207
15	KO	Mouse Kidney	isovalerylcarnitine	0.245
15	KO	Mouse Kidney	3-hydroxy-isovalerylcarnitine	1.403
15	KO	Mouse Kidney	2-methyl-butyrylcarnitine	0.803
15	KO	Mouse Kidney	pivaloylcarnitine	0.000
15	KO	Mouse Kidney	tigloylcarnitine	0.010
15	KO	Mouse Kidney	3-methyl-crotonylcarnitine	0.000
15	KO	Mouse Kidney	hexanoylcarnitine	0.394
15	KO	Mouse Kidney	R-3-hydroxy-hexanoylcarnitine	0.065
15	KO	Mouse Kidney	S-3-hydroxy-hexanoylcarnitine	0.077
15	KO	Mouse Kidney	phenylacetylcarnitine	0.005
15	KO	Mouse Kidney	phenylpropionylcarnitine	0.000
15	KO	Mouse Kidney	4-phenyl-butyrylcarnitine	0.000
15	KO	Mouse Kidney	benzoylcarnitine	0.180
15	KO	Mouse Kidney	4-methyl-hexanoylcarnitine	0.004
15	KO	Mouse Kidney	octanoylcarnitine	0.142
15	KO	Mouse Kidney	R-3-hydroxy-octanoylcarnitine	0.029
15	KO	Mouse Kidney	S-3-hydroxy-octanoylcarnitine	0.112
15	KO	Mouse Kidney	valproylcarnitine	0.000
15	KO	Mouse Kidney	branched-chain C8	0.000
15	KO	Mouse Kidney	cis-3,4-methylene-heptanoylcarnitine	0.001

15	KO	Mouse Kidney	4-methyl-octanoylcarnitine	0.005
15	KO	Mouse Kidney	2,6-dimethyl-heptanoylcarnitine	0.000
15	KO	Mouse Kidney	decanoylcarnitine	0.171
15	KO	Mouse Kidney	cis-4-decenoylcarnitine	0.014
15	KO	Mouse Kidney	cis-3,4-methylene- nonanoylcarnitine	0.000
15	KO	Mouse Kidney	R-3-hydroxy-decanoylcarnitine	0.040
15	KO	Mouse Kidney	S-3-hydroxy-decanoylcarnitine	0.143
15	KO	Mouse Kidney	5-decynoylcarnitine	0.002
15	KO	Mouse Kidney	lauroylcarnitine	0.271
15	KO	Mouse Kidney	trans-2-dodecenoylcarnitine	0.000
15	KO	Mouse Kidney	R-3-hydroxy-lauroylcarnitine	0.023
15	KO	Mouse Kidney	S-3-hydroxy-lauroylcarnitine	0.168
15	KO	Mouse Kidney	myristoylcarnitine	1.427
15	KO	Mouse Kidney	myristoleoylcarnitine	0.149
15	KO	Mouse Kidney	cis-5-tetradecenoylcarnitine	0.135
15	KO	Mouse Kidney	trans-2-tetradecenoylcarnitine	0.012
15	KO	Mouse Kidney	cis,cis-5,8- tetradecadienoylcarnitine	0.080
15	KO	Mouse Kidney	R-3-hydroxy-myristoylcarnitine	0.000
15	KO	Mouse Kidney	S-3-hydroxy-myristoylcarnitine	0.377
15	KO	Mouse Kidney	hydroxy-C14:1	0.254
15	KO	Mouse Kidney	palmitoylcarnitine	8.315
15	KO	Mouse Kidney	palmitoleoylcarnitine	1.092
15	KO	Mouse Kidney	trans-2-hexadecenoylcarnitine	0.079
15	KO	Mouse Kidney	R-3-hydroxy-palmitoylcarnitine	0.053
15	KO	Mouse Kidney	S-3-hydroxy-palmitoylcarnitine	1.157

15	KO	Mouse Kidney	hydroxy-C16:1	0.392
15	KO	Mouse Kidney	stearoylcarnitine	5.240
15	KO	Mouse Kidney	oleoylcarnitine	8.057
15	KO	Mouse Kidney	linoleoylcarnitine	4.271
15	KO	Mouse Kidney	alpha-linolenoylcarnitine	0.101
15	KO	Mouse Kidney	gamma-linolenoylcarnitine	0.043
15	KO	Mouse Kidney	R-3-hydroxy-stearoylcarnitine	0.012
15	KO	Mouse Kidney	S-3-hydroxy-stearoylcarnitine	0.153
15	KO	Mouse Kidney	hydroxy-C18:1	0.955
15	KO	Mouse Kidney	hydroxy-C18:2	0.721
15	KO	Mouse Kidney	hydroxy-C18:3	0.117
15	KO	Mouse Kidney	malonylcarnitine	0.835
15	KO	Mouse Kidney	succinylcarnitine	0.332
15	KO	Mouse Kidney	methyl-malonylcarnitine	0.124
15	KO	Mouse Kidney	ethyl-malonylcarnitine	0.010
15	KO	Mouse Kidney	glutaroylcarnitine	1.094
15	KO	Mouse Kidney	adipoylcarnitine	1.496
15	KO	Mouse Kidney	3-methyl-glutaroylcarnitine	0.189
15	KO	Mouse Kidney	suberoylcarnitine	0.041
15	KO	Mouse Kidney	sebacoylcarnitine	0.005
15	KO	Mouse Kidney	sum_of_individual_acylcarnitines	114.622
15	KO	Mouse Kidney	ratio:_sum/calculated	0.897
15	KO	Mouse Liver	total_carnitine	412.023
15	KO	Mouse Liver	free_carnitine	297.247
15	KO	Mouse Liver	calculated_acylcarnitines	114.776
15	KO	Mouse Liver	acyl/free	0.386
15	KO	Mouse Liver	butyrobetaine	2.952

15	KO	Mouse Liver	acetylcarnitine	68.491
15	KO	Mouse Liver	propionylcarnitine	9.035
15	KO	Mouse Liver	butyrylcarnitine	3.999
15	KO	Mouse Liver	isobutyrylcarnitine	2.756
15	KO	Mouse Liver	R-3-hydroxy-butyrylcarnitine	8.323
15	KO	Mouse Liver	S-3-hydroxy-butyrylcarnitine	2.350
15	KO	Mouse Liver	valerylcarnitine	1.402
15	KO	Mouse Liver	isovalerylcarnitine	0.605
15	KO	Mouse Liver	3-hydroxy-isovalerylcarnitine	0.468
15	KO	Mouse Liver	2-methyl-butyrylcarnitine	1.300
15	KO	Mouse Liver	pivaloylcarnitine	0.000
15	KO	Mouse Liver	tigloylcarnitine	0.000
15	KO	Mouse Liver	3-methyl-crotonylcarnitine	0.000
15	KO	Mouse Liver	hexanoylcarnitine	0.724
15	KO	Mouse Liver	R-3-hydroxy-hexanoylcarnitine	0.045
15	KO	Mouse Liver	S-3-hydroxy-hexanoylcarnitine	0.047
15	KO	Mouse Liver	phenylacetylcarnitine	0.003
15	KO	Mouse Liver	phenylpropionylcarnitine	0.000
15	KO	Mouse Liver	4-phenyl-butyrylcarnitine	0.001
15	KO	Mouse Liver	benzoylcarnitine	0.006
15	KO	Mouse Liver	4-methyl-hexanoylcarnitine	0.026
15	KO	Mouse Liver	octanoylcarnitine	0.056
15	KO	Mouse Liver	R-3-hydroxy-octanoylcarnitine	0.009
15	KO	Mouse Liver	S-3-hydroxy-octanoylcarnitine	0.017
15	KO	Mouse Liver	valproylcarnitine	0.000
15	KO	Mouse Liver	branched-chain C8	0.000
15	KO	Mouse Liver	cis-3,4-methylene-	0.000

			heptanoylcarnitine	
15	KO	Mouse Liver	4-methyl-octanoylcarnitine	0.003
15	KO	Mouse Liver	2,6-dimethyl-heptanoylcarnitine	0.000
15	KO	Mouse Liver	decanoylcarnitine	0.006
15	KO	Mouse Liver	cis-4-decenoylcarnitine	0.003
15	KO	Mouse Liver	cis-3,4-methylene- nonanoylcarnitine	0.000
15	KO	Mouse Liver	R-3-hydroxy-decanoylcarnitine	0.001
15	KO	Mouse Liver	S-3-hydroxy-decanoylcarnitine	0.018
15	KO	Mouse Liver	5-decynoylcarnitine	0.000
15	KO	Mouse Liver	lauroylcarnitine	0.000
15	KO	Mouse Liver	trans-2-dodecenoylcarnitine	0.000
15	KO	Mouse Liver	R-3-hydroxy-lauroylcarnitine	0.001
15	KO	Mouse Liver	S-3-hydroxy-lauroylcarnitine	0.005
15	KO	Mouse Liver	myristoylcarnitine	0.193
15	KO	Mouse Liver	myristoleoylcarnitine	0.113
15	KO	Mouse Liver	cis-5-tetradecenoylcarnitine	0.000
15	KO	Mouse Liver	trans-2-tetradecenoylcarnitine	0.000
15	KO	Mouse Liver	cis,cis-5,8- tetradecadienoylcarnitine	0.000
15	KO	Mouse Liver	R-3-hydroxy-myristoylcarnitine	0.000
15	KO	Mouse Liver	S-3-hydroxy-myristoylcarnitine	0.000
15	KO	Mouse Liver	hydroxy-C14:1	0.021
15	KO	Mouse Liver	palmitoylcarnitine	0.811
15	KO	Mouse Liver	palmitoleoylcarnitine	0.154
15	KO	Mouse Liver	trans-2-hexadecenoylcarnitine	0.000
15	KO	Mouse Liver	R-3-hydroxy-palmitoylcarnitine	0.012

15	KO	Mouse Liver	S-3-hydroxy-palmitoylcarnitine	0.059
15	KO	Mouse Liver	hydroxy-C16:1	0.082
15	KO	Mouse Liver	stearoylcarnitine	1.029
15	KO	Mouse Liver	oleoylcarnitine	1.281
15	KO	Mouse Liver	linoleoylcarnitine	0.603
15	KO	Mouse Liver	alpha-linolenoylcarnitine	0.000
15	KO	Mouse Liver	gamma-linolenoylcarnitine	0.000
15	KO	Mouse Liver	R-3-hydroxy-stearoylcarnitine	0.000
15	KO	Mouse Liver	S-3-hydroxy-stearoylcarnitine	0.000
15	KO	Mouse Liver	hydroxy-C18:1	0.079
15	KO	Mouse Liver	hydroxy-C18:2	0.050
15	KO	Mouse Liver	hydroxy-C18:3	0.018
15	KO	Mouse Liver	malonylcarnitine	2.031
15	KO	Mouse Liver	succinylcarnitine	0.405
15	KO	Mouse Liver	methyl-malonylcarnitine	0.108
15	KO	Mouse Liver	ethyl-malonylcarnitine	0.000
15	KO	Mouse Liver	glutaroylcarnitine	1.166
15	KO	Mouse Liver	adipoylcarnitine	0.893
15	KO	Mouse Liver	3-methyl-glutaroylcarnitine	0.061
15	KO	Mouse Liver	suberoylcarnitine	0.030
15	KO	Mouse Liver	sebacoylcarnitine	0.029
15	KO	Mouse Liver	sum_of_individual_acylcarnitines	108.928
15	KO	Mouse Liver	ratio:_sum/calculated	0.949
15	KO	Mouse Lung	total_carnitine	631.837
15	KO	Mouse Lung	free_carnitine	412.819
15	KO	Mouse Lung	calculated_acylcarnitines	219.018
15	KO	Mouse Lung	acyl/free	0.531

15	KO	Mouse Lung	butyrobetaine	9.254
15	KO	Mouse Lung	acetylcarnitine	223.281
15	KO	Mouse Lung	propionylcarnitine	1.457
15	KO	Mouse Lung	butyrylcarnitine	5.106
15	KO	Mouse Lung	isobutyrylcarnitine	0.182
15	KO	Mouse Lung	R-3-hydroxy-butyrylcarnitine	1.738
15	KO	Mouse Lung	S-3-hydroxy-butyrylcarnitine	3.214
15	KO	Mouse Lung	valerylcarnitine	0.127
15	KO	Mouse Lung	isovalerylcarnitine	0.920
15	KO	Mouse Lung	3-hydroxy-isovalerylcarnitine	0.563
15	KO	Mouse Lung	2-methyl-butyrylcarnitine	0.414
15	KO	Mouse Lung	pivaloylcarnitine	0.000
15	KO	Mouse Lung	tigloylcarnitine	0.006
15	KO	Mouse Lung	3-methyl-crotonylcarnitine	0.000
15	KO	Mouse Lung	hexanoylcarnitine	0.390
15	KO	Mouse Lung	R-3-hydroxy-hexanoylcarnitine	0.064
15	KO	Mouse Lung	S-3-hydroxy-hexanoylcarnitine	0.309
15	KO	Mouse Lung	phenylacetylcarnitine	0.001
15	KO	Mouse Lung	phenylpropionylcarnitine	0.000
15	KO	Mouse Lung	4-phenyl-butyrylcarnitine	0.000
15	KO	Mouse Lung	benzoylcarnitine	0.018
15	KO	Mouse Lung	4-methyl-hexanoylcarnitine	0.000
15	KO	Mouse Lung	octanoylcarnitine	0.092
15	KO	Mouse Lung	R-3-hydroxy-octanoylcarnitine	0.080
15	KO	Mouse Lung	S-3-hydroxy-octanoylcarnitine	0.306
15	KO	Mouse Lung	valproylcarnitine	0.000
15	KO	Mouse Lung	branched-chain C8	0.000

15	KO	Mouse Lung	cis-3,4-methylene-heptanoylcarnitine	0.015
15	KO	Mouse Lung	4-methyl-octanoylcarnitine	0.003
15	KO	Mouse Lung	2,6-dimethyl-heptanoylcarnitine	0.000
15	KO	Mouse Lung	decanoylcarnitine	0.164
15	KO	Mouse Lung	cis-4-decenoylcarnitine	0.049
15	KO	Mouse Lung	cis-3,4-methylene-nonanoylcarnitine	0.014
15	KO	Mouse Lung	R-3-hydroxy-decanoylcarnitine	0.056
15	KO	Mouse Lung	S-3-hydroxy-decanoylcarnitine	0.293
15	KO	Mouse Lung	5-decynoylcarnitine	0.000
15	KO	Mouse Lung	lauroylcarnitine	0.406
15	KO	Mouse Lung	trans-2-dodecenoylcarnitine	0.009
15	KO	Mouse Lung	R-3-hydroxy-lauroylcarnitine	0.041
15	KO	Mouse Lung	S-3-hydroxy-lauroylcarnitine	0.187
15	KO	Mouse Lung	myristoylcarnitine	1.836
15	KO	Mouse Lung	myristoleoylcarnitine	0.157
15	KO	Mouse Lung	cis-5-tetradecenoylcarnitine	0.244
15	KO	Mouse Lung	trans-2-tetradecenoylcarnitine	0.036
15	KO	Mouse Lung	cis,cis-5,8-tetradecadienoylcarnitine	0.059
15	KO	Mouse Lung	R-3-hydroxy-myristoylcarnitine	0.140
15	KO	Mouse Lung	S-3-hydroxy-myristoylcarnitine	0.333
15	KO	Mouse Lung	hydroxy-C14:1	0.300
15	KO	Mouse Lung	palmitoylcarnitine	6.425
15	KO	Mouse Lung	palmitoleoylcarnitine	0.566
15	KO	Mouse Lung	trans-2-hexadecenoylcarnitine	0.112

15	KO	Mouse Lung	R-3-hydroxy-palmitoylcarnitine	0.234
15	KO	Mouse Lung	S-3-hydroxy-palmitoylcarnitine	0.683
15	KO	Mouse Lung	hydroxy-C16:1	0.351
15	KO	Mouse Lung	stearoylcarnitine	2.550
15	KO	Mouse Lung	oleoylcarnitine	3.990
15	KO	Mouse Lung	linoleoylcarnitine	1.272
15	KO	Mouse Lung	alpha-linolenoylcarnitine	0.044
15	KO	Mouse Lung	gamma-linolenoylcarnitine	0.027
15	KO	Mouse Lung	R-3-hydroxy-stearoylcarnitine	0.121
15	KO	Mouse Lung	S-3-hydroxy-stearoylcarnitine	0.091
15	KO	Mouse Lung	hydroxy-C18:1	0.884
15	KO	Mouse Lung	hydroxy-C18:2	0.351
15	KO	Mouse Lung	hydroxy-C18:3	0.094
15	KO	Mouse Lung	malonylcarnitine	0.238
15	KO	Mouse Lung	succinylcarnitine	0.469
15	KO	Mouse Lung	methyl-malonylcarnitine	0.061
15	KO	Mouse Lung	ethyl-malonylcarnitine	0.005
15	KO	Mouse Lung	glutaroylcarnitine	0.000
15	KO	Mouse Lung	adipoylcarnitine	0.104
15	KO	Mouse Lung	3-methyl-glutaroylcarnitine	0.008
15	KO	Mouse Lung	suberoylcarnitine	0.038
15	KO	Mouse Lung	sebacoylcarnitine	0.003
15	KO	Mouse Lung	sum_of_individual_acylcarnitines	261.333
15	KO	Mouse Lung	ratio:_sum/calculated	1.193
15	KO	Mouse Muscle	total_carnitine	264.841
15	KO	Mouse Muscle	free_carnitine	87.259
15	KO	Mouse Muscle	calculated_acylcarnitines	177.582

15	KO	Mouse Muscle	acyl/free	2.035
15	KO	Mouse Muscle	butyrobetaine	6.191
15	KO	Mouse Muscle	acetylcarnitine	121.490
15	KO	Mouse Muscle	propionylcarnitine	0.563
15	KO	Mouse Muscle	butyrylcarnitine	3.500
15	KO	Mouse Muscle	isobutyrylcarnitine	0.189
15	KO	Mouse Muscle	R-3-hydroxy-butyrylcarnitine	0.647
15	KO	Mouse Muscle	S-3-hydroxy-butyrylcarnitine	3.235
15	KO	Mouse Muscle	valerylcarnitine	0.022
15	KO	Mouse Muscle	isovalerylcarnitine	0.472
15	KO	Mouse Muscle	3-hydroxy-isovalerylcarnitine	0.652
15	KO	Mouse Muscle	2-methyl-butyrylcarnitine	0.192
15	KO	Mouse Muscle	pivaloylcarnitine	0.000
15	KO	Mouse Muscle	tigloylcarnitine	0.020
15	KO	Mouse Muscle	3-methyl-crotonylcarnitine	0.000
15	KO	Mouse Muscle	hexanoylcarnitine	0.338
15	KO	Mouse Muscle	R-3-hydroxy-hexanoylcarnitine	0.027
15	KO	Mouse Muscle	S-3-hydroxy-hexanoylcarnitine	0.058
15	KO	Mouse Muscle	phenylacetylcarnitine	0.000
15	KO	Mouse Muscle	phenylpropionylcarnitine	0.000
15	KO	Mouse Muscle	4-phenyl-butyrylcarnitine	0.000
15	KO	Mouse Muscle	benzoylcarnitine	0.016
15	KO	Mouse Muscle	4-methyl-hexanoylcarnitine	0.000
15	KO	Mouse Muscle	octanoylcarnitine	0.111
15	KO	Mouse Muscle	R-3-hydroxy-octanoylcarnitine	0.022
15	KO	Mouse Muscle	S-3-hydroxy-octanoylcarnitine	0.082
15	KO	Mouse Muscle	valproylcarnitine	0.000

15	KO	Mouse Muscle	branched-chain C8	0.000
15	KO	Mouse Muscle	cis-3,4-methylene-heptanoylcarnitine	0.012
15	KO	Mouse Muscle	4-methyl-octanoylcarnitine	0.000
15	KO	Mouse Muscle	2,6-dimethyl-heptanoylcarnitine	0.000
15	KO	Mouse Muscle	decanoylcarnitine	0.137
15	KO	Mouse Muscle	cis-4-decenoylcarnitine	0.015
15	KO	Mouse Muscle	cis-3,4-methylene-nonanoylcarnitine	0.007
15	KO	Mouse Muscle	R-3-hydroxy-decanoylcarnitine	0.039
15	KO	Mouse Muscle	S-3-hydroxy-decanoylcarnitine	0.044
15	KO	Mouse Muscle	5-decynoylcarnitine	0.000
15	KO	Mouse Muscle	lauroylcarnitine	0.226
15	KO	Mouse Muscle	trans-2-dodecenoylcarnitine	0.000
15	KO	Mouse Muscle	R-3-hydroxy-lauroylcarnitine	0.006
15	KO	Mouse Muscle	S-3-hydroxy-lauroylcarnitine	0.016
15	KO	Mouse Muscle	myristoylcarnitine	1.392
15	KO	Mouse Muscle	myristoleoylcarnitine	0.349
15	KO	Mouse Muscle	cis-5-tetradecenoylcarnitine	0.164
15	KO	Mouse Muscle	trans-2-tetradecenoylcarnitine	0.000
15	KO	Mouse Muscle	cis,cis-5,8-tetradecadienoylcarnitine	0.058
15	KO	Mouse Muscle	R-3-hydroxy-myristoylcarnitine	0.000
15	KO	Mouse Muscle	S-3-hydroxy-myristoylcarnitine	0.071
15	KO	Mouse Muscle	hydroxy-C14:1	0.029
15	KO	Mouse Muscle	palmitoylcarnitine	12.639
15	KO	Mouse Muscle	palmitoleoylcarnitine	2.629

15	KO	Mouse Muscle	trans-2-hexadecenoylcarnitine	0.022
15	KO	Mouse Muscle	R-3-hydroxy-palmitoylcarnitine	0.063
15	KO	Mouse Muscle	S-3-hydroxy-palmitoylcarnitine	0.438
15	KO	Mouse Muscle	hydroxy-C16:1	0.245
15	KO	Mouse Muscle	stearoylcarnitine	7.562
15	KO	Mouse Muscle	oleoylcarnitine	22.434
15	KO	Mouse Muscle	linoleoylcarnitine	6.579
15	KO	Mouse Muscle	alpha-linolenoylcarnitine	0.411
15	KO	Mouse Muscle	gamma-linolenoylcarnitine	0.062
15	KO	Mouse Muscle	R-3-hydroxy-stearoylcarnitine	0.000
15	KO	Mouse Muscle	S-3-hydroxy-stearoylcarnitine	0.179
15	KO	Mouse Muscle	hydroxy-C18:1	0.831
15	KO	Mouse Muscle	hydroxy-C18:2	0.374
15	KO	Mouse Muscle	hydroxy-C18:3	0.069
15	KO	Mouse Muscle	malonylcarnitine	0.497
15	KO	Mouse Muscle	succinylcarnitine	0.371
15	KO	Mouse Muscle	methyl-malonylcarnitine	0.106
15	KO	Mouse Muscle	ethyl-malonylcarnitine	0.000
15	KO	Mouse Muscle	glutaroylcarnitine	0.000
15	KO	Mouse Muscle	adipoylcarnitine	0.056
15	KO	Mouse Muscle	3-methyl-glutaroylcarnitine	0.005
15	KO	Mouse Muscle	suberoylcarnitine	0.043
15	KO	Mouse Muscle	sebacoylcarnitine	0.002
15	KO	Mouse Muscle	sum_of_individual_acylcarnitines	189.819
15	KO	Mouse Muscle	ratio:_sum/calculated	1.069
15	KO	Mouse Pancreas	total_carnitine	184.359
15	KO	Mouse Pancreas	free_carnitine	59.215

15	KO	Mouse Pancreas	calculated_acylcarnitines	125.144
15	KO	Mouse Pancreas	acyl/free	2.113
15	KO	Mouse Pancreas	butyrobetaine	7.360
15	KO	Mouse Pancreas	acetylcarnitine	45.458
15	KO	Mouse Pancreas	propionylcarnitine	1.943
15	KO	Mouse Pancreas	butyrylcarnitine	6.899
15	KO	Mouse Pancreas	isobutyrylcarnitine	2.010
15	KO	Mouse Pancreas	R-3-hydroxy-butyrylcarnitine	0.473
15	KO	Mouse Pancreas	S-3-hydroxy-butyrylcarnitine	1.547
15	KO	Mouse Pancreas	valerylcarnitine	0.185
15	KO	Mouse Pancreas	isovalerylcarnitine	2.295
15	KO	Mouse Pancreas	3-hydroxy-isovalerylcarnitine	0.134
15	KO	Mouse Pancreas	2-methyl-butyrylcarnitine	2.316
15	KO	Mouse Pancreas	pivaloylcarnitine	0.000
15	KO	Mouse Pancreas	tigloylcarnitine	0.004
15	KO	Mouse Pancreas	3-methyl-crotonylcarnitine	0.000
15	KO	Mouse Pancreas	hexanoylcarnitine	0.124
15	KO	Mouse Pancreas	R-3-hydroxy-hexanoylcarnitine	0.011
15	KO	Mouse Pancreas	S-3-hydroxy-hexanoylcarnitine	0.031
15	KO	Mouse Pancreas	phenylacetylcarnitine	0.000
15	KO	Mouse Pancreas	phenylpropionylcarnitine	0.000
15	KO	Mouse Pancreas	4-phenyl-butyrylcarnitine	0.000
15	KO	Mouse Pancreas	benzoylcarnitine	0.000
15	KO	Mouse Pancreas	4-methyl-hexanoylcarnitine	0.002
15	KO	Mouse Pancreas	octanoylcarnitine	0.020
15	KO	Mouse Pancreas	R-3-hydroxy-octanoylcarnitine	0.012
15	KO	Mouse Pancreas	S-3-hydroxy-octanoylcarnitine	0.030

15	KO	Mouse Pancreas	valproylcarnitine	0.000
15	KO	Mouse Pancreas	branched-chain C8	0.000
15	KO	Mouse Pancreas	cis-3,4-methylene-heptanoylcarnitine	0.000
15	KO	Mouse Pancreas	4-methyl-octanoylcarnitine	0.000
15	KO	Mouse Pancreas	2,6-dimethyl-heptanoylcarnitine	0.000
15	KO	Mouse Pancreas	decanoylcarnitine	0.009
15	KO	Mouse Pancreas	cis-4-decenoylcarnitine	0.002
15	KO	Mouse Pancreas	cis-3,4-methylene-nonanoylcarnitine	0.000
15	KO	Mouse Pancreas	R-3-hydroxy-decanoylcarnitine	0.014
15	KO	Mouse Pancreas	S-3-hydroxy-decanoylcarnitine	0.018
15	KO	Mouse Pancreas	5-decynoylcarnitine	0.000
15	KO	Mouse Pancreas	lauroylcarnitine	0.003
15	KO	Mouse Pancreas	trans-2-dodecenoylcarnitine	0.000
15	KO	Mouse Pancreas	R-3-hydroxy-lauroylcarnitine	0.002
15	KO	Mouse Pancreas	S-3-hydroxy-lauroylcarnitine	0.020
15	KO	Mouse Pancreas	myristoylcarnitine	0.164
15	KO	Mouse Pancreas	myristoleoylcarnitine	0.000
15	KO	Mouse Pancreas	cis-5-tetradecenoylcarnitine	0.000
15	KO	Mouse Pancreas	trans-2-tetradecenoylcarnitine	0.000
15	KO	Mouse Pancreas	cis,cis-5,8-tetradecadienoylcarnitine	0.000
15	KO	Mouse Pancreas	R-3-hydroxy-myristoylcarnitine	0.000
15	KO	Mouse Pancreas	S-3-hydroxy-myristoylcarnitine	0.034
15	KO	Mouse Pancreas	hydroxy-C14:1	0.051
15	KO	Mouse Pancreas	palmitoylcarnitine	1.788

15	KO	Mouse Pancreas	palmitoleoylcarnitine	0.056
15	KO	Mouse Pancreas	trans-2-hexadecenoylcarnitine	0.006
15	KO	Mouse Pancreas	R-3-hydroxy-palmitoylcarnitine	0.004
15	KO	Mouse Pancreas	S-3-hydroxy-palmitoylcarnitine	0.167
15	KO	Mouse Pancreas	hydroxy-C16:1	0.089
15	KO	Mouse Pancreas	stearoylcarnitine	1.799
15	KO	Mouse Pancreas	oleoylcarnitine	1.143
15	KO	Mouse Pancreas	linoleoylcarnitine	0.453
15	KO	Mouse Pancreas	alpha-linolenoylcarnitine	0.009
15	KO	Mouse Pancreas	gamma-linolenoylcarnitine	0.000
15	KO	Mouse Pancreas	R-3-hydroxy-stearoylcarnitine	0.000
15	KO	Mouse Pancreas	S-3-hydroxy-stearoylcarnitine	0.097
15	KO	Mouse Pancreas	hydroxy-C18:1	0.127
15	KO	Mouse Pancreas	hydroxy-C18:2	0.105
15	KO	Mouse Pancreas	hydroxy-C18:3	0.034
15	KO	Mouse Pancreas	malonylcarnitine	0.000
15	KO	Mouse Pancreas	succinylcarnitine	0.131
15	KO	Mouse Pancreas	methyl-malonylcarnitine	0.029
15	KO	Mouse Pancreas	ethyl-malonylcarnitine	0.000
15	KO	Mouse Pancreas	glutaroylcarnitine	0.000
15	KO	Mouse Pancreas	adipoylcarnitine	0.036
15	KO	Mouse Pancreas	3-methyl-glutaroylcarnitine	0.004
15	KO	Mouse Pancreas	suberoylcarnitine	0.013
15	KO	Mouse Pancreas	sebacoylcarnitine	0.009
15	KO	Mouse Pancreas	sum_of_individual_acylcarnitines	69.912
15	KO	Mouse Pancreas	ratio:_sum/calculated	0.559
15	KO	Mouse Spleen	total_carnitine	516.835

15	KO	Mouse Spleen	free_carnitine	213.966
15	KO	Mouse Spleen	calculated_acylcarnitines	302.870
15	KO	Mouse Spleen	acyl/free	1.416
15	KO	Mouse Spleen	butyrobetaine	8.085
15	KO	Mouse Spleen	acetylcarnitine	221.128
15	KO	Mouse Spleen	propionylcarnitine	7.456
15	KO	Mouse Spleen	butyrylcarnitine	29.179
15	KO	Mouse Spleen	isobutyrylcarnitine	1.620
15	KO	Mouse Spleen	R-3-hydroxy-butyrylcarnitine	4.800
15	KO	Mouse Spleen	S-3-hydroxy-butyrylcarnitine	7.040
15	KO	Mouse Spleen	valerylcarnitine	1.312
15	KO	Mouse Spleen	isovalerylcarnitine	2.004
15	KO	Mouse Spleen	3-hydroxy-isovalerylcarnitine	0.573
15	KO	Mouse Spleen	2-methyl-butyrylcarnitine	1.035
15	KO	Mouse Spleen	pivaloylcarnitine	0.000
15	KO	Mouse Spleen	tigloylcarnitine	0.023
15	KO	Mouse Spleen	3-methyl-crotonylcarnitine	0.000
15	KO	Mouse Spleen	hexanoylcarnitine	1.247
15	KO	Mouse Spleen	R-3-hydroxy-hexanoylcarnitine	0.080
15	KO	Mouse Spleen	S-3-hydroxy-hexanoylcarnitine	0.342
15	KO	Mouse Spleen	phenylacetylcarnitine	0.000
15	KO	Mouse Spleen	phenylpropionylcarnitine	0.000
15	KO	Mouse Spleen	4-phenyl-butyrylcarnitine	0.000
15	KO	Mouse Spleen	benzoylcarnitine	0.011
15	KO	Mouse Spleen	4-methyl-hexanoylcarnitine	0.016
15	KO	Mouse Spleen	octanoylcarnitine	0.217
15	KO	Mouse Spleen	R-3-hydroxy-octanoylcarnitine	0.085

15	KO	Mouse Spleen	S-3-hydroxy-octanoylcarnitine	0.328
15	KO	Mouse Spleen	valproylcarnitine	0.000
15	KO	Mouse Spleen	branched-chain C8	0.000
15	KO	Mouse Spleen	cis-3,4-methylene-heptanoylcarnitine	0.029
15	KO	Mouse Spleen	4-methyl-octanoylcarnitine	0.004
15	KO	Mouse Spleen	2,6-dimethyl-heptanoylcarnitine	0.000
15	KO	Mouse Spleen	decanoylcarnitine	0.161
15	KO	Mouse Spleen	cis-4-decenoylcarnitine	0.034
15	KO	Mouse Spleen	cis-3,4-methylene-nonanoylcarnitine	0.009
15	KO	Mouse Spleen	R-3-hydroxy-decanoylcarnitine	0.036
15	KO	Mouse Spleen	S-3-hydroxy-decanoylcarnitine	0.183
15	KO	Mouse Spleen	5-decynoylcarnitine	0.000
15	KO	Mouse Spleen	lauroylcarnitine	0.241
15	KO	Mouse Spleen	trans-2-dodecenoylcarnitine	0.003
15	KO	Mouse Spleen	R-3-hydroxy-lauroylcarnitine	0.011
15	KO	Mouse Spleen	S-3-hydroxy-lauroylcarnitine	0.085
15	KO	Mouse Spleen	myristoylcarnitine	1.519
15	KO	Mouse Spleen	myristoleoylcarnitine	0.242
15	KO	Mouse Spleen	cis-5-tetradecenoylcarnitine	0.091
15	KO	Mouse Spleen	trans-2-tetradecenoylcarnitine	0.000
15	KO	Mouse Spleen	cis,cis-5,8-tetradecadienoylcarnitine	0.100
15	KO	Mouse Spleen	R-3-hydroxy-myristoylcarnitine	0.000
15	KO	Mouse Spleen	S-3-hydroxy-myristoylcarnitine	0.127
15	KO	Mouse Spleen	hydroxy-C14:1	0.135

15	KO	Mouse Spleen	palmitoylcarnitine	12.324
15	KO	Mouse Spleen	palmitoleoylcarnitine	1.195
15	KO	Mouse Spleen	trans-2-hexadecenoylcarnitine	0.017
15	KO	Mouse Spleen	R-3-hydroxy-palmitoylcarnitine	0.005
15	KO	Mouse Spleen	S-3-hydroxy-palmitoylcarnitine	0.501
15	KO	Mouse Spleen	hydroxy-C16:1	0.233
15	KO	Mouse Spleen	stearoylcarnitine	5.377
15	KO	Mouse Spleen	oleoylcarnitine	15.900
15	KO	Mouse Spleen	linoleoylcarnitine	4.756
15	KO	Mouse Spleen	alpha-linolenoylcarnitine	0.129
15	KO	Mouse Spleen	gamma-linolenoylcarnitine	0.078
15	KO	Mouse Spleen	R-3-hydroxy-stearoylcarnitine	0.063
15	KO	Mouse Spleen	S-3-hydroxy-stearoylcarnitine	0.316
15	KO	Mouse Spleen	hydroxy-C18:1	0.725
15	KO	Mouse Spleen	hydroxy-C18:2	0.289
15	KO	Mouse Spleen	hydroxy-C18:3	0.056
15	KO	Mouse Spleen	malonylcarnitine	0.200
15	KO	Mouse Spleen	succinylcarnitine	0.108
15	KO	Mouse Spleen	methyl-malonylcarnitine	0.062
15	KO	Mouse Spleen	ethyl-malonylcarnitine	0.000
15	KO	Mouse Spleen	glutaroylcarnitine	0.000
15	KO	Mouse Spleen	adipoylcarnitine	0.034
15	KO	Mouse Spleen	3-methyl-glutaroylcarnitine	0.003
15	KO	Mouse Spleen	suberoylcarnitine	0.027
15	KO	Mouse Spleen	sebacoylcarnitine	0.000
15	KO	Mouse Spleen	sum_of_individual_acylcarnitines	323.903
15	KO	Mouse Spleen	ratio:_sum/calculated	1.069

96	WT	Mouse Brain	total_carnitine	123.794
96	WT	Mouse Brain	free_carnitine	103.547
96	WT	Mouse Brain	calculated_acylcarnitines	20.247
96	WT	Mouse Brain	acyl/free	0.196
96	WT	Mouse Brain	butyrobetaine	7.911
96	WT	Mouse Brain	acetylcarnitine	33.787
96	WT	Mouse Brain	propionylcarnitine	2.840
96	WT	Mouse Brain	butyrylcarnitine	1.051
96	WT	Mouse Brain	isobutyrylcarnitine	0.150
96	WT	Mouse Brain	R-3-hydroxy-butyrylcarnitine	0.082
96	WT	Mouse Brain	S-3-hydroxy-butyrylcarnitine	0.209
96	WT	Mouse Brain	valerylcarnitine	0.154
96	WT	Mouse Brain	isovalerylcarnitine	0.094
96	WT	Mouse Brain	3-hydroxy-isovalerylcarnitine	0.384
96	WT	Mouse Brain	2-methyl-butyrylcarnitine	0.263
96	WT	Mouse Brain	pivaloylcarnitine	0.000
96	WT	Mouse Brain	tigloylcarnitine	0.001
96	WT	Mouse Brain	3-methyl-crotonylcarnitine	0.000
96	WT	Mouse Brain	hexanoylcarnitine	0.059
96	WT	Mouse Brain	R-3-hydroxy-hexanoylcarnitine	0.001
96	WT	Mouse Brain	S-3-hydroxy-hexanoylcarnitine	0.002
96	WT	Mouse Brain	phenylacetylcarnitine	0.000
96	WT	Mouse Brain	phenylpropionylcarnitine	0.000
96	WT	Mouse Brain	4-phenyl-butyrylcarnitine	0.000
96	WT	Mouse Brain	benzoylcarnitine	0.000
96	WT	Mouse Brain	4-methyl-hexanoylcarnitine	0.000
96	WT	Mouse Brain	octanoylcarnitine	0.019

96	WT	Mouse Brain	R-3-hydroxy-octanoylcarnitine	0.000
96	WT	Mouse Brain	S-3-hydroxy-octanoylcarnitine	0.000
96	WT	Mouse Brain	valproylcarnitine	0.000
96	WT	Mouse Brain	branched-chain C8	0.000
96	WT	Mouse Brain	cis-3,4-methylene-heptanoylcarnitine	0.000
96	WT	Mouse Brain	4-methyl-octanoylcarnitine	0.000
96	WT	Mouse Brain	2,6-dimethyl-heptanoylcarnitine	0.000
96	WT	Mouse Brain	decanoylcarnitine	0.020
96	WT	Mouse Brain	cis-4-decenoylcarnitine	0.002
96	WT	Mouse Brain	cis-3,4-methylene-nonanoylcarnitine	0.000
96	WT	Mouse Brain	R-3-hydroxy-decanoylcarnitine	0.000
96	WT	Mouse Brain	S-3-hydroxy-decanoylcarnitine	0.008
96	WT	Mouse Brain	5-decynoylcarnitine	0.000
96	WT	Mouse Brain	lauroylcarnitine	0.123
96	WT	Mouse Brain	trans-2-dodecenoylcarnitine	0.000
96	WT	Mouse Brain	R-3-hydroxy-lauroylcarnitine	0.001
96	WT	Mouse Brain	S-3-hydroxy-lauroylcarnitine	0.001
96	WT	Mouse Brain	myristoylcarnitine	0.915
96	WT	Mouse Brain	myristoleoylcarnitine	0.000
96	WT	Mouse Brain	cis-5-tetradecenoylcarnitine	0.000
96	WT	Mouse Brain	trans-2-tetradecenoylcarnitine	0.000
96	WT	Mouse Brain	cis,cis-5,8-tetradecadienoylcarnitine	0.000
96	WT	Mouse Brain	R-3-hydroxy-myristoylcarnitine	0.000
96	WT	Mouse Brain	S-3-hydroxy-myristoylcarnitine	0.000

96	WT	Mouse Brain	hydroxy-C14:1	0.022
96	WT	Mouse Brain	palmitoylcarnitine	1.591
96	WT	Mouse Brain	palmitoleoylcarnitine	0.134
96	WT	Mouse Brain	trans-2-hexadecenoylcarnitine	0.000
96	WT	Mouse Brain	R-3-hydroxy-palmitoylcarnitine	0.000
96	WT	Mouse Brain	S-3-hydroxy-palmitoylcarnitine	0.014
96	WT	Mouse Brain	hydroxy-C16:1	0.021
96	WT	Mouse Brain	stearoylcarnitine	0.630
96	WT	Mouse Brain	oleoylcarnitine	1.132
96	WT	Mouse Brain	linoleoylcarnitine	0.134
96	WT	Mouse Brain	alpha-linolenoylcarnitine	0.000
96	WT	Mouse Brain	gamma-linolenoylcarnitine	0.000
96	WT	Mouse Brain	R-3-hydroxy-stearoylcarnitine	0.000
96	WT	Mouse Brain	S-3-hydroxy-stearoylcarnitine	0.000
96	WT	Mouse Brain	hydroxy-C18:1	0.011
96	WT	Mouse Brain	hydroxy-C18:2	0.000
96	WT	Mouse Brain	hydroxy-C18:3	0.003
96	WT	Mouse Brain	malonylcarnitine	0.155
96	WT	Mouse Brain	succinylcarnitine	0.213
96	WT	Mouse Brain	methyl-malonylcarnitine	0.015
96	WT	Mouse Brain	ethyl-malonylcarnitine	0.000
96	WT	Mouse Brain	glutaroylcarnitine	0.083
96	WT	Mouse Brain	adipoylcarnitine	0.014
96	WT	Mouse Brain	3-methyl-glutaroylcarnitine	0.018
96	WT	Mouse Brain	suberoylcarnitine	0.000
96	WT	Mouse Brain	sebacoylcarnitine	0.000
96	WT	Mouse Brain	sum_of_individual_acylcarnitines	44.358

96	WT	Mouse Brain	ratio:_sum/calculated	2.191
96	WT	Mouse Fat	total_carnitine	59.480
96	WT	Mouse Fat	free_carnitine	21.231
96	WT	Mouse Fat	calculated_acylcarnitines	38.249
96	WT	Mouse Fat	acyl/free	1.802
96	WT	Mouse Fat	butyrobetaine	1.774
96	WT	Mouse Fat	acetylcarnitine	4.971
96	WT	Mouse Fat	propionylcarnitine	0.187
96	WT	Mouse Fat	butyrylcarnitine	0.105
96	WT	Mouse Fat	isobutyrylcarnitine	0.147
96	WT	Mouse Fat	R-3-hydroxy-butyrylcarnitine	0.041
96	WT	Mouse Fat	S-3-hydroxy-butyrylcarnitine	0.067
96	WT	Mouse Fat	valerylcarnitine	0.002
96	WT	Mouse Fat	isovalerylcarnitine	0.127
96	WT	Mouse Fat	3-hydroxy-isovalerylcarnitine	0.040
96	WT	Mouse Fat	2-methyl-butyrylcarnitine	0.111
96	WT	Mouse Fat	pivaloylcarnitine	0.000
96	WT	Mouse Fat	tigloylcarnitine	0.000
96	WT	Mouse Fat	3-methyl-crotonylcarnitine	0.000
96	WT	Mouse Fat	hexanoylcarnitine	0.014
96	WT	Mouse Fat	R-3-hydroxy-hexanoylcarnitine	0.003
96	WT	Mouse Fat	S-3-hydroxy-hexanoylcarnitine	0.004
96	WT	Mouse Fat	phenylacetylcarnitine	0.000
96	WT	Mouse Fat	phenylpropionylcarnitine	0.000
96	WT	Mouse Fat	4-phenyl-butyrylcarnitine	0.000
96	WT	Mouse Fat	benzoylcarnitine	0.000
96	WT	Mouse Fat	4-methyl-hexanoylcarnitine	0.000

96	WT	Mouse Fat	octanoylcarnitine	0.002
96	WT	Mouse Fat	R-3-hydroxy-octanoylcarnitine	0.004
96	WT	Mouse Fat	S-3-hydroxy-octanoylcarnitine	0.002
96	WT	Mouse Fat	valproylcarnitine	0.000
96	WT	Mouse Fat	branched-chain C8	0.000
96	WT	Mouse Fat	cis-3,4-methylene-heptanoylcarnitine	0.000
96	WT	Mouse Fat	4-methyl-octanoylcarnitine	0.000
96	WT	Mouse Fat	2,6-dimethyl-heptanoylcarnitine	0.000
96	WT	Mouse Fat	decanoylcarnitine	0.000
96	WT	Mouse Fat	cis-4-decenoylcarnitine	0.000
96	WT	Mouse Fat	cis-3,4-methylene-nonanoylcarnitine	0.000
96	WT	Mouse Fat	R-3-hydroxy-decanoylcarnitine	0.000
96	WT	Mouse Fat	S-3-hydroxy-decanoylcarnitine	0.001
96	WT	Mouse Fat	5-decynoylcarnitine	0.000
96	WT	Mouse Fat	lauroylcarnitine	0.000
96	WT	Mouse Fat	trans-2-dodecenoylcarnitine	0.000
96	WT	Mouse Fat	R-3-hydroxy-lauroylcarnitine	0.000
96	WT	Mouse Fat	S-3-hydroxy-lauroylcarnitine	0.000
96	WT	Mouse Fat	myristoylcarnitine	0.000
96	WT	Mouse Fat	myristoleoylcarnitine	0.048
96	WT	Mouse Fat	cis-5-tetradecenoylcarnitine	0.000
96	WT	Mouse Fat	trans-2-tetradecenoylcarnitine	0.000
96	WT	Mouse Fat	cis,cis-5,8-tetradecadienoylcarnitine	0.005
96	WT	Mouse Fat	R-3-hydroxy-myristoylcarnitine	0.000

96	WT	Mouse Fat	S-3-hydroxy-myristoylcarnitine	0.000
96	WT	Mouse Fat	hydroxy-C14:1	0.004
96	WT	Mouse Fat	palmitoylcarnitine	0.000
96	WT	Mouse Fat	palmitoleoylcarnitine	0.019
96	WT	Mouse Fat	trans-2-hexadecenoylcarnitine	0.000
96	WT	Mouse Fat	R-3-hydroxy-palmitoylcarnitine	0.001
96	WT	Mouse Fat	S-3-hydroxy-palmitoylcarnitine	0.022
96	WT	Mouse Fat	hydroxy-C16:1	0.019
96	WT	Mouse Fat	stearoylcarnitine	0.000
96	WT	Mouse Fat	oleoylcarnitine	0.000
96	WT	Mouse Fat	linoleoylcarnitine	0.096
96	WT	Mouse Fat	alpha-linolenoylcarnitine	0.000
96	WT	Mouse Fat	gamma-linolenoylcarnitine	0.000
96	WT	Mouse Fat	R-3-hydroxy-stearoylcarnitine	0.000
96	WT	Mouse Fat	S-3-hydroxy-stearoylcarnitine	0.000
96	WT	Mouse Fat	hydroxy-C18:1	0.006
96	WT	Mouse Fat	hydroxy-C18:2	0.012
96	WT	Mouse Fat	hydroxy-C18:3	0.005
96	WT	Mouse Fat	malonylcarnitine	0.070
96	WT	Mouse Fat	succinylcarnitine	0.052
96	WT	Mouse Fat	methyl-malonylcarnitine	0.009
96	WT	Mouse Fat	ethyl-malonylcarnitine	0.000
96	WT	Mouse Fat	glutaroylcarnitine	0.000
96	WT	Mouse Fat	adipoylcarnitine	0.000
96	WT	Mouse Fat	3-methyl-glutaroylcarnitine	0.000
96	WT	Mouse Fat	suberoylcarnitine	0.000
96	WT	Mouse Fat	sebacoylcarnitine	0.002

96	WT	Mouse Fat	sum_of_individual_acylcarnitines	6.199
96	WT	Mouse Fat	ratio:_sum/calculated	0.162
96	WT	Mouse Heart	total_carnitine	1360.152
96	WT	Mouse Heart	free_carnitine	780.405
96	WT	Mouse Heart	calculated_acylcarnitines	579.747
96	WT	Mouse Heart	acyl/free	0.743
96	WT	Mouse Heart	butyrobetaine	22.150
96	WT	Mouse Heart	acetylcarnitine	504.800
96	WT	Mouse Heart	propionylcarnitine	8.049
96	WT	Mouse Heart	butyrylcarnitine	14.548
96	WT	Mouse Heart	isobutyrylcarnitine	10.411
96	WT	Mouse Heart	R-3-hydroxy-butyrylcarnitine	6.625
96	WT	Mouse Heart	S-3-hydroxy-butyrylcarnitine	17.252
96	WT	Mouse Heart	valerylcarnitine	0.653
96	WT	Mouse Heart	isovalerylcarnitine	0.079
96	WT	Mouse Heart	3-hydroxy-isovalerylcarnitine	1.498
96	WT	Mouse Heart	2-methyl-butyrylcarnitine	0.557
96	WT	Mouse Heart	pivaloylcarnitine	0.000
96	WT	Mouse Heart	tigloylcarnitine	0.286
96	WT	Mouse Heart	3-methyl-crotonylcarnitine	0.002
96	WT	Mouse Heart	hexanoylcarnitine	1.630
96	WT	Mouse Heart	R-3-hydroxy-hexanoylcarnitine	0.184
96	WT	Mouse Heart	S-3-hydroxy-hexanoylcarnitine	0.754
96	WT	Mouse Heart	phenylacetylcarnitine	0.000
96	WT	Mouse Heart	phenylpropionylcarnitine	0.000
96	WT	Mouse Heart	4-phenyl-butyrylcarnitine	0.000
96	WT	Mouse Heart	benzoylcarnitine	0.113

96	WT	Mouse Heart	4-methyl-hexanoylcarnitine	0.006
96	WT	Mouse Heart	octanoylcarnitine	0.431
96	WT	Mouse Heart	R-3-hydroxy-octanoylcarnitine	0.055
96	WT	Mouse Heart	S-3-hydroxy-octanoylcarnitine	0.289
96	WT	Mouse Heart	valproylcarnitine	0.000
96	WT	Mouse Heart	branched-chain C8	0.000
96	WT	Mouse Heart	cis-3,4-methylene-heptanoylcarnitine	0.007
96	WT	Mouse Heart	4-methyl-octanoylcarnitine	0.005
96	WT	Mouse Heart	2,6-dimethyl-heptanoylcarnitine	0.000
96	WT	Mouse Heart	decanoylcarnitine	0.518
96	WT	Mouse Heart	cis-4-decenoylcarnitine	0.062
96	WT	Mouse Heart	cis-3,4-methylene-nonanoylcarnitine	0.004
96	WT	Mouse Heart	R-3-hydroxy-decanoylcarnitine	0.073
96	WT	Mouse Heart	S-3-hydroxy-decanoylcarnitine	0.255
96	WT	Mouse Heart	5-decynoylcarnitine	0.000
96	WT	Mouse Heart	lauroylcarnitine	0.770
96	WT	Mouse Heart	trans-2-dodecenoylcarnitine	0.004
96	WT	Mouse Heart	R-3-hydroxy-lauroylcarnitine	0.025
96	WT	Mouse Heart	S-3-hydroxy-lauroylcarnitine	0.144
96	WT	Mouse Heart	myristoylcarnitine	2.291
96	WT	Mouse Heart	myristoleoylcarnitine	0.711
96	WT	Mouse Heart	cis-5-tetradecenoylcarnitine	0.740
96	WT	Mouse Heart	trans-2-tetradecenoylcarnitine	0.014
96	WT	Mouse Heart	cis,cis-5,8-tetradecadienoylcarnitine	0.525

96	WT	Mouse Heart	R-3-hydroxy-myristoylcarnitine	0.030
96	WT	Mouse Heart	S-3-hydroxy-myristoylcarnitine	0.179
96	WT	Mouse Heart	hydroxy-C14:1	0.223
96	WT	Mouse Heart	palmitoylcarnitine	6.833
96	WT	Mouse Heart	palmitoleoylcarnitine	1.107
96	WT	Mouse Heart	trans-2-hexadecenoylcarnitine	0.113
96	WT	Mouse Heart	R-3-hydroxy-palmitoylcarnitine	0.126
96	WT	Mouse Heart	S-3-hydroxy-palmitoylcarnitine	0.645
96	WT	Mouse Heart	hydroxy-C16:1	0.435
96	WT	Mouse Heart	stearoylcarnitine	5.602
96	WT	Mouse Heart	oleoylcarnitine	9.352
96	WT	Mouse Heart	linoleoylcarnitine	5.545
96	WT	Mouse Heart	alpha-linolenoylcarnitine	0.282
96	WT	Mouse Heart	gamma-linolenoylcarnitine	0.072
96	WT	Mouse Heart	R-3-hydroxy-stearoylcarnitine	0.113
96	WT	Mouse Heart	S-3-hydroxy-stearoylcarnitine	0.532
96	WT	Mouse Heart	hydroxy-C18:1	1.097
96	WT	Mouse Heart	hydroxy-C18:2	0.840
96	WT	Mouse Heart	hydroxy-C18:3	0.179
96	WT	Mouse Heart	malonylcarnitine	6.827
96	WT	Mouse Heart	succinylcarnitine	21.383
96	WT	Mouse Heart	methyl-malonylcarnitine	2.320
96	WT	Mouse Heart	ethyl-malonylcarnitine	0.000
96	WT	Mouse Heart	glutaroylcarnitine	0.000
96	WT	Mouse Heart	adipoylcarnitine	0.009
96	WT	Mouse Heart	3-methyl-glutaroylcarnitine	0.001
96	WT	Mouse Heart	suberoylcarnitine	0.002

96	WT	Mouse Heart	sebacoylcarnitine	0.001
96	WT	Mouse Heart	sum_of_individual_acylcarnitines	638.215
96	WT	Mouse Heart	ratio:_sum/calculated	1.101
96	WT	Mouse Kidney	total_carnitine	386.888
96	WT	Mouse Kidney	free_carnitine	270.807
96	WT	Mouse Kidney	calculated_acylcarnitines	116.081
96	WT	Mouse Kidney	acyl/free	0.429
96	WT	Mouse Kidney	butyrobetaine	8.451
96	WT	Mouse Kidney	acetylcarnitine	72.331
96	WT	Mouse Kidney	propionylcarnitine	3.427
96	WT	Mouse Kidney	butyrylcarnitine	4.640
96	WT	Mouse Kidney	isobutyrylcarnitine	0.766
96	WT	Mouse Kidney	R-3-hydroxy-butyrylcarnitine	0.933
96	WT	Mouse Kidney	S-3-hydroxy-butyrylcarnitine	2.040
96	WT	Mouse Kidney	valerylcarnitine	0.474
96	WT	Mouse Kidney	isovalerylcarnitine	0.224
96	WT	Mouse Kidney	3-hydroxy-isovalerylcarnitine	1.442
96	WT	Mouse Kidney	2-methyl-butyrylcarnitine	0.998
96	WT	Mouse Kidney	pivaloylcarnitine	0.000
96	WT	Mouse Kidney	tigloylcarnitine	0.033
96	WT	Mouse Kidney	3-methyl-crotonylcarnitine	0.000
96	WT	Mouse Kidney	hexanoylcarnitine	0.364
96	WT	Mouse Kidney	R-3-hydroxy-hexanoylcarnitine	0.025
96	WT	Mouse Kidney	S-3-hydroxy-hexanoylcarnitine	0.071
96	WT	Mouse Kidney	phenylacetylcarnitine	0.000
96	WT	Mouse Kidney	phenylpropionylcarnitine	0.000
96	WT	Mouse Kidney	4-phenyl-butyrylcarnitine	0.000

96	WT	Mouse Kidney	benzoylcarnitine	0.062
96	WT	Mouse Kidney	4-methyl-hexanoylcarnitine	0.009
96	WT	Mouse Kidney	octanoylcarnitine	0.134
96	WT	Mouse Kidney	R-3-hydroxy-octanoylcarnitine	0.011
96	WT	Mouse Kidney	S-3-hydroxy-octanoylcarnitine	0.055
96	WT	Mouse Kidney	valproylcarnitine	0.000
96	WT	Mouse Kidney	branched-chain C8	0.000
96	WT	Mouse Kidney	cis-3,4-methylene-heptanoylcarnitine	0.000
96	WT	Mouse Kidney	4-methyl-octanoylcarnitine	0.004
96	WT	Mouse Kidney	2,6-dimethyl-heptanoylcarnitine	0.000
96	WT	Mouse Kidney	decanoylcarnitine	0.136
96	WT	Mouse Kidney	cis-4-decenoylcarnitine	0.005
96	WT	Mouse Kidney	cis-3,4-methylene-nonanoylcarnitine	0.000
96	WT	Mouse Kidney	R-3-hydroxy-decanoylcarnitine	0.025
96	WT	Mouse Kidney	S-3-hydroxy-decanoylcarnitine	0.068
96	WT	Mouse Kidney	5-decynoylcarnitine	0.003
96	WT	Mouse Kidney	lauroylcarnitine	0.195
96	WT	Mouse Kidney	trans-2-dodecenoylcarnitine	0.000
96	WT	Mouse Kidney	R-3-hydroxy-lauroylcarnitine	0.011
96	WT	Mouse Kidney	S-3-hydroxy-lauroylcarnitine	0.043
96	WT	Mouse Kidney	myristoylcarnitine	1.128
96	WT	Mouse Kidney	myristoleoylcarnitine	0.209
96	WT	Mouse Kidney	cis-5-tetradecenoylcarnitine	0.000
96	WT	Mouse Kidney	trans-2-tetradecenoylcarnitine	0.000
96	WT	Mouse Kidney	cis,cis-5,8-	0.079

			tetradecadienoylcarnitine	
96	WT	Mouse Kidney	R-3-hydroxy-myristoylcarnitine	0.000
96	WT	Mouse Kidney	S-3-hydroxy-myristoylcarnitine	0.129
96	WT	Mouse Kidney	hydroxy-C14:1	0.066
96	WT	Mouse Kidney	palmitoylcarnitine	7.794
96	WT	Mouse Kidney	palmitoleoylcarnitine	0.972
96	WT	Mouse Kidney	trans-2-hexadecenoylcarnitine	0.047
96	WT	Mouse Kidney	R-3-hydroxy-palmitoylcarnitine	0.035
96	WT	Mouse Kidney	S-3-hydroxy-palmitoylcarnitine	0.540
96	WT	Mouse Kidney	hydroxy-C16:1	0.232
96	WT	Mouse Kidney	stearoylcarnitine	5.701
96	WT	Mouse Kidney	oleoylcarnitine	6.877
96	WT	Mouse Kidney	linoleoylcarnitine	4.979
96	WT	Mouse Kidney	alpha-linolenoylcarnitine	0.265
96	WT	Mouse Kidney	gamma-linolenoylcarnitine	0.024
96	WT	Mouse Kidney	R-3-hydroxy-stearoylcarnitine	0.019
96	WT	Mouse Kidney	S-3-hydroxy-stearoylcarnitine	0.131
96	WT	Mouse Kidney	hydroxy-C18:1	0.267
96	WT	Mouse Kidney	hydroxy-C18:2	0.439
96	WT	Mouse Kidney	hydroxy-C18:3	0.097
96	WT	Mouse Kidney	malonylcarnitine	0.733
96	WT	Mouse Kidney	succinylcarnitine	1.076
96	WT	Mouse Kidney	methyl-malonylcarnitine	0.126
96	WT	Mouse Kidney	ethyl-malonylcarnitine	0.000
96	WT	Mouse Kidney	glutaroylcarnitine	0.687
96	WT	Mouse Kidney	adipoylcarnitine	0.550
96	WT	Mouse Kidney	3-methyl-glutaroylcarnitine	0.092

96	WT	Mouse Kidney	suberoylcarnitine	0.012
96	WT	Mouse Kidney	sebacylcarnitine	0.002
96	WT	Mouse Kidney	sum_of_individual_acylcarnitines	121.837
96	WT	Mouse Kidney	ratio:_sum/calculated	1.050
96	WT	Mouse Liver	total_carnitine	327.240
96	WT	Mouse Liver	free_carnitine	184.576
96	WT	Mouse Liver	calculated_acylcarnitines	142.664
96	WT	Mouse Liver	acyl/free	0.773
96	WT	Mouse Liver	butyrobetaine	10.293
96	WT	Mouse Liver	acetylcarnitine	111.336
96	WT	Mouse Liver	propionylcarnitine	13.528
96	WT	Mouse Liver	butyrylcarnitine	6.376
96	WT	Mouse Liver	isobutyrylcarnitine	0.522
96	WT	Mouse Liver	R-3-hydroxy-butyrylcarnitine	4.112
96	WT	Mouse Liver	S-3-hydroxy-butyrylcarnitine	2.470
96	WT	Mouse Liver	valerylcarnitine	3.175
96	WT	Mouse Liver	isovalerylcarnitine	0.134
96	WT	Mouse Liver	3-hydroxy-isovalerylcarnitine	0.514
96	WT	Mouse Liver	2-methyl-butyrylcarnitine	1.088
96	WT	Mouse Liver	pivaloylcarnitine	0.000
96	WT	Mouse Liver	tigloylcarnitine	0.004
96	WT	Mouse Liver	3-methyl-crotonylcarnitine	0.000
96	WT	Mouse Liver	hexanoylcarnitine	1.428
96	WT	Mouse Liver	R-3-hydroxy-hexanoylcarnitine	0.040
96	WT	Mouse Liver	S-3-hydroxy-hexanoylcarnitine	0.141
96	WT	Mouse Liver	phenylacetylcarnitine	0.000
96	WT	Mouse Liver	phenylpropionylcarnitine	0.011

96	WT	Mouse Liver	4-phenyl-butyrylcarnitine	0.000
96	WT	Mouse Liver	benzoylcarnitine	0.017
96	WT	Mouse Liver	4-methyl-hexanoylcarnitine	0.030
96	WT	Mouse Liver	octanoylcarnitine	0.230
96	WT	Mouse Liver	R-3-hydroxy-octanoylcarnitine	0.015
96	WT	Mouse Liver	S-3-hydroxy-octanoylcarnitine	0.033
96	WT	Mouse Liver	valproylcarnitine	0.000
96	WT	Mouse Liver	branched-chain C8	0.000
96	WT	Mouse Liver	cis-3,4-methylene-heptanoylcarnitine	0.000
96	WT	Mouse Liver	4-methyl-octanoylcarnitine	0.003
96	WT	Mouse Liver	2,6-dimethyl-heptanoylcarnitine	0.000
96	WT	Mouse Liver	decanoylcarnitine	0.074
96	WT	Mouse Liver	cis-4-decenoylcarnitine	0.000
96	WT	Mouse Liver	cis-3,4-methylene-nonanoylcarnitine	0.000
96	WT	Mouse Liver	R-3-hydroxy-decanoylcarnitine	0.007
96	WT	Mouse Liver	S-3-hydroxy-decanoylcarnitine	0.016
96	WT	Mouse Liver	5-decynoylcarnitine	0.000
96	WT	Mouse Liver	lauroylcarnitine	0.000
96	WT	Mouse Liver	trans-2-dodecenoylcarnitine	0.000
96	WT	Mouse Liver	R-3-hydroxy-lauroylcarnitine	0.000
96	WT	Mouse Liver	S-3-hydroxy-lauroylcarnitine	0.000
96	WT	Mouse Liver	myristoylcarnitine	0.125
96	WT	Mouse Liver	myristoleoylcarnitine	0.029
96	WT	Mouse Liver	cis-5-tetradecenoylcarnitine	0.000
96	WT	Mouse Liver	trans-2-tetradecenoylcarnitine	0.000

96	WT	Mouse Liver	cis,cis-5,8-tetradecadienoylcarnitine	0.001
96	WT	Mouse Liver	R-3-hydroxy-myristoylcarnitine	0.000
96	WT	Mouse Liver	S-3-hydroxy-myristoylcarnitine	0.000
96	WT	Mouse Liver	hydroxy-C14:1	0.003
96	WT	Mouse Liver	palmitoylcarnitine	0.523
96	WT	Mouse Liver	palmitoleoylcarnitine	0.133
96	WT	Mouse Liver	trans-2-hexadecenoylcarnitine	0.000
96	WT	Mouse Liver	R-3-hydroxy-palmitoylcarnitine	0.000
96	WT	Mouse Liver	S-3-hydroxy-palmitoylcarnitine	0.024
96	WT	Mouse Liver	hydroxy-C16:1	0.024
96	WT	Mouse Liver	stearoylcarnitine	0.729
96	WT	Mouse Liver	oleoylcarnitine	0.571
96	WT	Mouse Liver	linoleoylcarnitine	0.531
96	WT	Mouse Liver	alpha-linolenoylcarnitine	0.024
96	WT	Mouse Liver	gamma-linolenoylcarnitine	0.000
96	WT	Mouse Liver	R-3-hydroxy-stearoylcarnitine	0.000
96	WT	Mouse Liver	S-3-hydroxy-stearoylcarnitine	0.002
96	WT	Mouse Liver	hydroxy-C18:1	0.032
96	WT	Mouse Liver	hydroxy-C18:2	0.016
96	WT	Mouse Liver	hydroxy-C18:3	0.003
96	WT	Mouse Liver	malonylcarnitine	1.066
96	WT	Mouse Liver	succinylcarnitine	0.653
96	WT	Mouse Liver	methyl-malonylcarnitine	0.086
96	WT	Mouse Liver	ethyl-malonylcarnitine	0.003
96	WT	Mouse Liver	glutaroylcarnitine	2.062
96	WT	Mouse Liver	adipoylcarnitine	0.811

96	WT	Mouse Liver	3-methyl-glutaroylcarnitine	0.082
96	WT	Mouse Liver	suberoylcarnitine	0.030
96	WT	Mouse Liver	sebacoylcarnitine	0.012
96	WT	Mouse Liver	sum_of_individual_acylcarnitines	152.877
96	WT	Mouse Liver	ratio:_sum/calculated	1.072
96	WT	Mouse Lung	total_carnitine	827.661
96	WT	Mouse Lung	free_carnitine	645.522
96	WT	Mouse Lung	calculated_acylcarnitines	182.139
96	WT	Mouse Lung	acyl/free	0.282
96	WT	Mouse Lung	butyrobetaine	16.292
96	WT	Mouse Lung	acetylcarnitine	190.537
96	WT	Mouse Lung	propionylcarnitine	1.775
96	WT	Mouse Lung	butyrylcarnitine	1.892
96	WT	Mouse Lung	isobutyrylcarnitine	0.890
96	WT	Mouse Lung	R-3-hydroxy-butyrylcarnitine	0.766
96	WT	Mouse Lung	S-3-hydroxy-butyrylcarnitine	1.499
96	WT	Mouse Lung	valerylcarnitine	0.076
96	WT	Mouse Lung	isovalerylcarnitine	1.214
96	WT	Mouse Lung	3-hydroxy-isovalerylcarnitine	0.815
96	WT	Mouse Lung	2-methyl-butyrylcarnitine	1.221
96	WT	Mouse Lung	pivaloylcarnitine	0.000
96	WT	Mouse Lung	tigloylcarnitine	0.025
96	WT	Mouse Lung	3-methyl-crotonylcarnitine	0.000
96	WT	Mouse Lung	hexanoylcarnitine	0.263
96	WT	Mouse Lung	R-3-hydroxy-hexanoylcarnitine	0.050
96	WT	Mouse Lung	S-3-hydroxy-hexanoylcarnitine	0.195
96	WT	Mouse Lung	phenylacetylcarnitine	0.008

96	WT	Mouse Lung	phenylpropionylcarnitine	0.000
96	WT	Mouse Lung	4-phenyl-butyrylcarnitine	0.000
96	WT	Mouse Lung	benzoylcarnitine	0.040
96	WT	Mouse Lung	4-methyl-hexanoylcarnitine	0.001
96	WT	Mouse Lung	octanoylcarnitine	0.047
96	WT	Mouse Lung	R-3-hydroxy-octanoylcarnitine	0.089
96	WT	Mouse Lung	S-3-hydroxy-octanoylcarnitine	0.092
96	WT	Mouse Lung	valproylcarnitine	0.000
96	WT	Mouse Lung	branched-chain C8	0.000
96	WT	Mouse Lung	cis-3,4-methylene-heptanoylcarnitine	0.000
96	WT	Mouse Lung	4-methyl-octanoylcarnitine	0.000
96	WT	Mouse Lung	2,6-dimethyl-heptanoylcarnitine	0.000
96	WT	Mouse Lung	decanoylcarnitine	0.057
96	WT	Mouse Lung	cis-4-decenoylcarnitine	0.020
96	WT	Mouse Lung	cis-3,4-methylene-nonanoylcarnitine	0.000
96	WT	Mouse Lung	R-3-hydroxy-decanoylcarnitine	0.030
96	WT	Mouse Lung	S-3-hydroxy-decanoylcarnitine	0.083
96	WT	Mouse Lung	5-decynoylcarnitine	0.000
96	WT	Mouse Lung	lauroylcarnitine	0.234
96	WT	Mouse Lung	trans-2-dodecenoylcarnitine	0.000
96	WT	Mouse Lung	R-3-hydroxy-lauroylcarnitine	0.012
96	WT	Mouse Lung	S-3-hydroxy-lauroylcarnitine	0.038
96	WT	Mouse Lung	myristoylcarnitine	0.937
96	WT	Mouse Lung	myristoleoylcarnitine	0.090
96	WT	Mouse Lung	cis-5-tetradecenoylcarnitine	0.012

96	WT	Mouse Lung	trans-2-tetradecenoylcarnitine	0.003
96	WT	Mouse Lung	cis,cis-5,8-tetradecadienoylcarnitine	0.064
96	WT	Mouse Lung	R-3-hydroxy-myristoylcarnitine	0.001
96	WT	Mouse Lung	S-3-hydroxy-myristoylcarnitine	0.054
96	WT	Mouse Lung	hydroxy-C14:1	0.064
96	WT	Mouse Lung	palmitoylcarnitine	4.120
96	WT	Mouse Lung	palmitoleoylcarnitine	0.318
96	WT	Mouse Lung	trans-2-hexadecenoylcarnitine	0.029
96	WT	Mouse Lung	R-3-hydroxy-palmitoylcarnitine	0.083
96	WT	Mouse Lung	S-3-hydroxy-palmitoylcarnitine	0.249
96	WT	Mouse Lung	hydroxy-C16:1	0.094
96	WT	Mouse Lung	stearoylcarnitine	1.334
96	WT	Mouse Lung	oleoylcarnitine	1.525
96	WT	Mouse Lung	linoleoylcarnitine	0.614
96	WT	Mouse Lung	alpha-linolenoylcarnitine	0.000
96	WT	Mouse Lung	gamma-linolenoylcarnitine	0.019
96	WT	Mouse Lung	R-3-hydroxy-stearoylcarnitine	0.169
96	WT	Mouse Lung	S-3-hydroxy-stearoylcarnitine	0.034
96	WT	Mouse Lung	hydroxy-C18:1	0.475
96	WT	Mouse Lung	hydroxy-C18:2	0.122
96	WT	Mouse Lung	hydroxy-C18:3	0.012
96	WT	Mouse Lung	malonylcarnitine	0.368
96	WT	Mouse Lung	succinylcarnitine	0.680
96	WT	Mouse Lung	methyl-malonylcarnitine	0.058
96	WT	Mouse Lung	ethyl-malonylcarnitine	0.001
96	WT	Mouse Lung	glutaroylcarnitine	0.000

96	WT	Mouse Lung	adipoylcarnitine	0.024
96	WT	Mouse Lung	3-methyl-glutaroylcarnitine	0.001
96	WT	Mouse Lung	suberoylcarnitine	0.010
96	WT	Mouse Lung	sebacoylcarnitine	0.000
96	WT	Mouse Lung	sum_of_individual_acylcarnitines	213.531
96	WT	Mouse Lung	ratio:_sum/calculated	1.172
96	WT	Mouse Muscle	total_carnitine	298.217
96	WT	Mouse Muscle	free_carnitine	131.089
96	WT	Mouse Muscle	calculated_acylcarnitines	167.128
96	WT	Mouse Muscle	acyl/free	1.275
96	WT	Mouse Muscle	butyrobetaine	8.071
96	WT	Mouse Muscle	acetylcarnitine	144.902
96	WT	Mouse Muscle	propionylcarnitine	0.617
96	WT	Mouse Muscle	butyrylcarnitine	3.174
96	WT	Mouse Muscle	isobutyrylcarnitine	0.193
96	WT	Mouse Muscle	R-3-hydroxy-butyrylcarnitine	0.672
96	WT	Mouse Muscle	S-3-hydroxy-butyrylcarnitine	4.603
96	WT	Mouse Muscle	valerylcarnitine	0.054
96	WT	Mouse Muscle	isovalerylcarnitine	0.074
96	WT	Mouse Muscle	3-hydroxy-isovalerylcarnitine	0.781
96	WT	Mouse Muscle	2-methyl-butyrylcarnitine	0.232
96	WT	Mouse Muscle	pivaloylcarnitine	0.000
96	WT	Mouse Muscle	tigloylcarnitine	0.083
96	WT	Mouse Muscle	3-methyl-crotonylcarnitine	0.000
96	WT	Mouse Muscle	hexanoylcarnitine	0.349
96	WT	Mouse Muscle	R-3-hydroxy-hexanoylcarnitine	0.020
96	WT	Mouse Muscle	S-3-hydroxy-hexanoylcarnitine	0.053

96	WT	Mouse Muscle	phenylacetylcarnitine	0.000
96	WT	Mouse Muscle	phenylpropionylcarnitine	0.000
96	WT	Mouse Muscle	4-phenyl-butyrylcarnitine	0.000
96	WT	Mouse Muscle	benzoylcarnitine	0.022
96	WT	Mouse Muscle	4-methyl-hexanoylcarnitine	0.000
96	WT	Mouse Muscle	octanoylcarnitine	0.129
96	WT	Mouse Muscle	R-3-hydroxy-octanoylcarnitine	0.008
96	WT	Mouse Muscle	S-3-hydroxy-octanoylcarnitine	0.041
96	WT	Mouse Muscle	valproylcarnitine	0.000
96	WT	Mouse Muscle	branched-chain C8	0.000
96	WT	Mouse Muscle	cis-3,4-methylene-heptanoylcarnitine	0.000
96	WT	Mouse Muscle	4-methyl-octanoylcarnitine	0.000
96	WT	Mouse Muscle	2,6-dimethyl-heptanoylcarnitine	0.000
96	WT	Mouse Muscle	decanoylcarnitine	0.157
96	WT	Mouse Muscle	cis-4-decenoylcarnitine	0.019
96	WT	Mouse Muscle	cis-3,4-methylene-nonanoylcarnitine	0.000
96	WT	Mouse Muscle	R-3-hydroxy-decanoylcarnitine	0.010
96	WT	Mouse Muscle	S-3-hydroxy-decanoylcarnitine	0.059
96	WT	Mouse Muscle	5-decynoylcarnitine	0.001
96	WT	Mouse Muscle	lauroylcarnitine	0.318
96	WT	Mouse Muscle	trans-2-dodecenoylcarnitine	0.000
96	WT	Mouse Muscle	R-3-hydroxy-lauroylcarnitine	0.003
96	WT	Mouse Muscle	S-3-hydroxy-lauroylcarnitine	0.025
96	WT	Mouse Muscle	myristoylcarnitine	1.431
96	WT	Mouse Muscle	myristoleoylcarnitine	0.310

96	WT	Mouse Muscle	cis-5-tetradecenoylcarnitine	0.231
96	WT	Mouse Muscle	trans-2-tetradecenoylcarnitine	0.000
96	WT	Mouse Muscle	cis,cis-5,8-tetradecadienoylcarnitine	0.104
96	WT	Mouse Muscle	R-3-hydroxy-myristoylcarnitine	0.000
96	WT	Mouse Muscle	S-3-hydroxy-myristoylcarnitine	0.078
96	WT	Mouse Muscle	hydroxy-C14:1	0.033
96	WT	Mouse Muscle	palmitoylcarnitine	10.543
96	WT	Mouse Muscle	palmitoleoylcarnitine	1.194
96	WT	Mouse Muscle	trans-2-hexadecenoylcarnitine	0.092
96	WT	Mouse Muscle	R-3-hydroxy-palmitoylcarnitine	0.093
96	WT	Mouse Muscle	S-3-hydroxy-palmitoylcarnitine	0.760
96	WT	Mouse Muscle	hydroxy-C16:1	0.156
96	WT	Mouse Muscle	stearoylcarnitine	4.789
96	WT	Mouse Muscle	oleoylcarnitine	9.539
96	WT	Mouse Muscle	linoleoylcarnitine	2.720
96	WT	Mouse Muscle	alpha-linolenoylcarnitine	0.204
96	WT	Mouse Muscle	gamma-linolenoylcarnitine	0.001
96	WT	Mouse Muscle	R-3-hydroxy-stearoylcarnitine	0.000
96	WT	Mouse Muscle	S-3-hydroxy-stearoylcarnitine	0.345
96	WT	Mouse Muscle	hydroxy-C18:1	0.993
96	WT	Mouse Muscle	hydroxy-C18:2	0.373
96	WT	Mouse Muscle	hydroxy-C18:3	0.044
96	WT	Mouse Muscle	malonylcarnitine	0.424
96	WT	Mouse Muscle	succinylcarnitine	0.625
96	WT	Mouse Muscle	methyl-malonylcarnitine	0.104
96	WT	Mouse Muscle	ethyl-malonylcarnitine	0.000

96	WT	Mouse Muscle	glutaroylecarnitine	0.000
96	WT	Mouse Muscle	adipoylcarnitine	0.005
96	WT	Mouse Muscle	3-methyl-glutaroylecarnitine	0.000
96	WT	Mouse Muscle	suberoylecarnitine	0.003
96	WT	Mouse Muscle	sebacoylcarnitine	0.000
96	WT	Mouse Muscle	sum_of_individual_acylcarnitines	191.790
96	WT	Mouse Muscle	ratio:_sum/calculated	1.148
96	WT	Mouse Pancreas	total_carnitine	44.823
96	WT	Mouse Pancreas	free_carnitine	44.477
96	WT	Mouse Pancreas	calculated_acylcarnitines	0.346
96	WT	Mouse Pancreas	acyl/free	0.008
96	WT	Mouse Pancreas	butyrobetaine	2.693
96	WT	Mouse Pancreas	acetylcarnitine	12.440
96	WT	Mouse Pancreas	propionylcarnitine	0.789
96	WT	Mouse Pancreas	butyrylcarnitine	0.584
96	WT	Mouse Pancreas	isobutyrylcarnitine	0.251
96	WT	Mouse Pancreas	R-3-hydroxy-butyrylcarnitine	0.087
96	WT	Mouse Pancreas	S-3-hydroxy-butyrylcarnitine	0.269
96	WT	Mouse Pancreas	valerylcarnitine	0.023
96	WT	Mouse Pancreas	isovalerylcarnitine	0.157
96	WT	Mouse Pancreas	3-hydroxy-isovalerylcarnitine	0.075
96	WT	Mouse Pancreas	2-methyl-butyrylcarnitine	0.151
96	WT	Mouse Pancreas	pivaloylcarnitine	0.000
96	WT	Mouse Pancreas	tigloylcarnitine	0.010
96	WT	Mouse Pancreas	3-methyl-crotonylcarnitine	0.000
96	WT	Mouse Pancreas	hexanoylcarnitine	0.042
96	WT	Mouse Pancreas	R-3-hydroxy-hexanoylcarnitine	0.002

96	WT	Mouse Pancreas	S-3-hydroxy-hexanoylcarnitine	0.007
96	WT	Mouse Pancreas	phenylacetylcarnitine	0.000
96	WT	Mouse Pancreas	phenylpropionylcarnitine	0.000
96	WT	Mouse Pancreas	4-phenyl-butyrylcarnitine	0.000
96	WT	Mouse Pancreas	benzoylcarnitine	0.000
96	WT	Mouse Pancreas	4-methyl-hexanoylcarnitine	0.000
96	WT	Mouse Pancreas	octanoylcarnitine	0.008
96	WT	Mouse Pancreas	R-3-hydroxy-octanoylcarnitine	0.002
96	WT	Mouse Pancreas	S-3-hydroxy-octanoylcarnitine	0.001
96	WT	Mouse Pancreas	valproylcarnitine	0.000
96	WT	Mouse Pancreas	branched-chain C8	0.000
96	WT	Mouse Pancreas	cis-3,4-methylene-heptanoylcarnitine	0.002
96	WT	Mouse Pancreas	4-methyl-octanoylcarnitine	0.001
96	WT	Mouse Pancreas	2,6-dimethyl-heptanoylcarnitine	0.000
96	WT	Mouse Pancreas	decanoylcarnitine	0.000
96	WT	Mouse Pancreas	cis-4-decenoylcarnitine	0.000
96	WT	Mouse Pancreas	cis-3,4-methylene-nonanoylcarnitine	0.001
96	WT	Mouse Pancreas	R-3-hydroxy-decanoylcarnitine	0.004
96	WT	Mouse Pancreas	S-3-hydroxy-decanoylcarnitine	0.009
96	WT	Mouse Pancreas	5-decynoylcarnitine	0.000
96	WT	Mouse Pancreas	lauroylcarnitine	0.000
96	WT	Mouse Pancreas	trans-2-dodecenoylcarnitine	0.000
96	WT	Mouse Pancreas	R-3-hydroxy-lauroylcarnitine	0.000
96	WT	Mouse Pancreas	S-3-hydroxy-lauroylcarnitine	0.000
96	WT	Mouse Pancreas	myristoylcarnitine	0.084

96	WT	Mouse Pancreas	myristoleoylcarnitine	0.000
96	WT	Mouse Pancreas	cis-5-tetradecenoylcarnitine	0.000
96	WT	Mouse Pancreas	trans-2-tetradecenoylcarnitine	0.000
96	WT	Mouse Pancreas	cis,cis-5,8-tetradecadienoylcarnitine	0.000
96	WT	Mouse Pancreas	R-3-hydroxy-myristoylcarnitine	0.000
96	WT	Mouse Pancreas	S-3-hydroxy-myristoylcarnitine	0.000
96	WT	Mouse Pancreas	hydroxy-C14:1	0.009
96	WT	Mouse Pancreas	palmitoylcarnitine	0.442
96	WT	Mouse Pancreas	palmitoleoylcarnitine	0.039
96	WT	Mouse Pancreas	trans-2-hexadecenoylcarnitine	0.000
96	WT	Mouse Pancreas	R-3-hydroxy-palmitoylcarnitine	0.000
96	WT	Mouse Pancreas	S-3-hydroxy-palmitoylcarnitine	0.033
96	WT	Mouse Pancreas	hydroxy-C16:1	0.014
96	WT	Mouse Pancreas	stearoylcarnitine	0.139
96	WT	Mouse Pancreas	oleoylcarnitine	0.236
96	WT	Mouse Pancreas	linoleoylcarnitine	0.173
96	WT	Mouse Pancreas	alpha-linolenoylcarnitine	0.002
96	WT	Mouse Pancreas	gamma-linolenoylcarnitine	0.000
96	WT	Mouse Pancreas	R-3-hydroxy-stearoylcarnitine	0.000
96	WT	Mouse Pancreas	S-3-hydroxy-stearoylcarnitine	0.000
96	WT	Mouse Pancreas	hydroxy-C18:1	0.036
96	WT	Mouse Pancreas	hydroxy-C18:2	0.056
96	WT	Mouse Pancreas	hydroxy-C18:3	0.015
96	WT	Mouse Pancreas	malonylcarnitine	0.121
96	WT	Mouse Pancreas	succinylcarnitine	0.189
96	WT	Mouse Pancreas	methyl-malonylcarnitine	0.020

96	WT	Mouse Pancreas	ethyl-malonylcarnitine	0.005
96	WT	Mouse Pancreas	glutaroylcarnitine	0.000
96	WT	Mouse Pancreas	adipoylcarnitine	0.005
96	WT	Mouse Pancreas	3-methyl-glutaroylcarnitine	0.001
96	WT	Mouse Pancreas	suberoylcarnitine	0.006
96	WT	Mouse Pancreas	sebacoylcarnitine	0.001
96	WT	Mouse Pancreas	sum_of_individual_acylcarnitines	16.546
96	WT	Mouse Pancreas	ratio:_sum/calculated	47.791
96	WT	Mouse Spleen	total_carnitine	419.610
96	WT	Mouse Spleen	free_carnitine	221.620
96	WT	Mouse Spleen	calculated_acylcarnitines	197.991
96	WT	Mouse Spleen	acyl/free	0.893
96	WT	Mouse Spleen	butyrobetaine	7.855
96	WT	Mouse Spleen	acetylcarnitine	145.812
96	WT	Mouse Spleen	propionylcarnitine	3.569
96	WT	Mouse Spleen	butyrylcarnitine	4.258
96	WT	Mouse Spleen	isobutyrylcarnitine	1.863
96	WT	Mouse Spleen	R-3-hydroxy-butyrylcarnitine	1.720
96	WT	Mouse Spleen	S-3-hydroxy-butyrylcarnitine	1.986
96	WT	Mouse Spleen	valerylcarnitine	0.268
96	WT	Mouse Spleen	isovalerylcarnitine	0.693
96	WT	Mouse Spleen	3-hydroxy-isovalerylcarnitine	0.647
96	WT	Mouse Spleen	2-methyl-butyrylcarnitine	1.217
96	WT	Mouse Spleen	pivaloylcarnitine	0.000
96	WT	Mouse Spleen	tigloylcarnitine	0.102
96	WT	Mouse Spleen	3-methyl-crotonylcarnitine	0.106
96	WT	Mouse Spleen	hexanoylcarnitine	0.690

96	WT	Mouse Spleen	R-3-hydroxy-hexanoylcarnitine	0.148
96	WT	Mouse Spleen	S-3-hydroxy-hexanoylcarnitine	0.220
96	WT	Mouse Spleen	phenylacetylcarnitine	0.110
96	WT	Mouse Spleen	phenylpropionylcarnitine	0.101
96	WT	Mouse Spleen	4-phenyl-butyrylcarnitine	0.100
96	WT	Mouse Spleen	benzoylcarnitine	0.134
96	WT	Mouse Spleen	4-methyl-hexanoylcarnitine	0.114
96	WT	Mouse Spleen	octanoylcarnitine	0.324
96	WT	Mouse Spleen	R-3-hydroxy-octanoylcarnitine	0.136
96	WT	Mouse Spleen	S-3-hydroxy-octanoylcarnitine	0.207
96	WT	Mouse Spleen	valproylcarnitine	0.000
96	WT	Mouse Spleen	branched-chain C8	0.000
96	WT	Mouse Spleen	cis-3,4-methylene-heptanoylcarnitine	0.111
96	WT	Mouse Spleen	4-methyl-octanoylcarnitine	0.114
96	WT	Mouse Spleen	2,6-dimethyl-heptanoylcarnitine	0.112
96	WT	Mouse Spleen	decanoylcarnitine	0.303
96	WT	Mouse Spleen	cis-4-decenoylcarnitine	0.226
96	WT	Mouse Spleen	cis-3,4-methylene-nonanoylcarnitine	0.115
96	WT	Mouse Spleen	R-3-hydroxy-decanoylcarnitine	0.171
96	WT	Mouse Spleen	S-3-hydroxy-decanoylcarnitine	0.288
96	WT	Mouse Spleen	5-decynoylcarnitine	0.117
96	WT	Mouse Spleen	lauroylcarnitine	0.475
96	WT	Mouse Spleen	trans-2-dodecenoylcarnitine	0.140
96	WT	Mouse Spleen	R-3-hydroxy-lauroylcarnitine	0.128
96	WT	Mouse Spleen	S-3-hydroxy-lauroylcarnitine	0.185

96	WT	Mouse Spleen	myristoylcarnitine	1.815
96	WT	Mouse Spleen	myristoleoylcarnitine	0.359
96	WT	Mouse Spleen	cis-5-tetradecenoylcarnitine	0.365
96	WT	Mouse Spleen	trans-2-tetradecenoylcarnitine	0.119
96	WT	Mouse Spleen	cis,cis-5,8-tetradecadienoylcarnitine	0.292
96	WT	Mouse Spleen	R-3-hydroxy-myristoylcarnitine	0.126
96	WT	Mouse Spleen	S-3-hydroxy-myristoylcarnitine	0.236
96	WT	Mouse Spleen	hydroxy-C14:1	0.087
96	WT	Mouse Spleen	palmitoylcarnitine	9.201
96	WT	Mouse Spleen	palmitoleoylcarnitine	0.846
96	WT	Mouse Spleen	trans-2-hexadecenoylcarnitine	0.175
96	WT	Mouse Spleen	R-3-hydroxy-palmitoylcarnitine	0.168
96	WT	Mouse Spleen	S-3-hydroxy-palmitoylcarnitine	0.509
96	WT	Mouse Spleen	hydroxy-C16:1	0.146
96	WT	Mouse Spleen	stearoylcarnitine	2.822
96	WT	Mouse Spleen	oleoylcarnitine	8.853
96	WT	Mouse Spleen	linoleoylcarnitine	5.626
96	WT	Mouse Spleen	alpha-linolenoylcarnitine	0.405
96	WT	Mouse Spleen	gamma-linolenoylcarnitine	0.172
96	WT	Mouse Spleen	R-3-hydroxy-stearoylcarnitine	0.194
96	WT	Mouse Spleen	S-3-hydroxy-stearoylcarnitine	0.235
96	WT	Mouse Spleen	hydroxy-C18:1	0.351
96	WT	Mouse Spleen	hydroxy-C18:2	0.370
96	WT	Mouse Spleen	hydroxy-C18:3	0.047
96	WT	Mouse Spleen	malonylcarnitine	0.351
96	WT	Mouse Spleen	succinylcarnitine	0.242

96	WT	Mouse Spleen	methyl-malonylcarnitine	0.159
96	WT	Mouse Spleen	ethyl-malonylcarnitine	0.099
96	WT	Mouse Spleen	glutaroylcarnitine	0.061
96	WT	Mouse Spleen	adipoylcarnitine	0.135
96	WT	Mouse Spleen	3-methyl-glutaroylcarnitine	0.125
96	WT	Mouse Spleen	suberoylcarnitine	0.131
96	WT	Mouse Spleen	sebacoylcarnitine	0.127
96	WT	Mouse Spleen	sum_of_individual_acylcarnitines	201.959
96	WT	Mouse Spleen	ratio:_sum/calculated	1.020

BIBLIOGRAPHY

- Adam, S., et al. (2013). "Dietary management of urea cycle disorders: European practice." Mol Genet Metab **110**(4): 439-445.
- Agarwala, S. S., et al. (2007). "Long-term outcomes with concurrent carboplatin, paclitaxel and radiation therapy for locally advanced, inoperable head and neck cancer." Ann Oncol **18**(7): 1224-1229.
- Atkinson, J., et al. (2011). "A mitochondria-targeted inhibitor of cytochrome c peroxidase mitigates radiation-induced death." Nat Commun **2**: 497.
- Baier, L. J. and R. L. Hanson (2004). "Genetic studies of the etiology of type 2 diabetes in Pima Indians: hunting for pieces to a complicated puzzle." Diabetes **53**(5): 1181-1186.
- Battaile, K. P., et al. (2002). "Crystal structure of rat short chain acyl-CoA dehydrogenase complexed with acetoacetyl-CoA: comparison with other acyl-CoA dehydrogenases." J Biol Chem **277**(14): 12200-12207.
- Battaile, KP, J. M.-C., R Paschke, M Wang, D Bennett, J Vockley, J-J Kim (2002). "Crystal structure of rat short shain acyl-CoA dehydrogenase complexed with acetoacetyl-CoA; comparison with other acyl-CoA dehydrogenases." J Biol Chem(12200-12207).
- Battaile, K. P., et al. (2004). "Structures of isobutyryl-CoA dehydrogenase and enzyme-product complex: comparison with isovaleryl- and short-chain acyl-CoA dehydrogenases." J Biol Chem **279**(16): 16526-16534.
- Battaile, KP, T. N., J Vockley, J-J Kim (2004). "Structures of isobutyryl-CoA dehydrogenase and enzyme-product complex: comparison with isovaleryl- and short-chain acyl-CoA dehydrogenases." J Biol Chem(269): 16526-16534.
- Behboo, R., et al. (1995). "Decreased nitric oxide generation following human islet culture in serum-free media." Transplant Proc **27**(6): 3380.
- Bian, F., et al. (2006). "Competition between acetate and oleate for the formation of malonyl-CoA and mitochondrial acetyl-CoA in the perfused rat heart." J Mol Cell Cardiol **41**(5): 868-875.

- Bian, L., et al. (2010). "Variants in ACAD10 are associated with type 2 diabetes, insulin resistance and lipid oxidation in Pima Indians." Diabetologia **53**(7): 1349-1353.
This is the reference in [My EndNote Library 9Dec13] on the lab computer.
- Coates, P. M. and K. Tanaka (1992). "Molecular basis of mitochondrial fatty acid oxidation defects." J Lipid Res **33**(8): 1099-1110.
- Cox, K. B., et al. (2001). "Gestational, pathologic and biochemical differences between very long-chain acyl-CoA dehydrogenase deficiency and long-chain acyl-CoA dehydrogenase deficiency in the mouse." Hum Mol Genet **10**(19): 2069-2077.
- Derks, TG, T. B., A van Assen, T Bos, J Ruiter, HR Waterham, KE Niezen-Koning, RJ Wanders, JM Rondeel, JG Loeber, LP Ten Kate, GP Smith (2008). "Neonatal screening for mediumchain acyl-CoA dehydrogenase (MCAD) deficiency in The Netherlands: the importance of enzyme analysis to ascertain true MCAD deficiency." J Inherit Metab Dis(31): 88-96.
- Diaz, G. A., et al. (2013). "Ammonia control and neurocognitive outcome among urea cycle disorder patients treated with glycerol phenylbutyrate." Hepatology **57**(6): 2171-2179.
- Eckersal, P. D. (2000). "Recent advances and future prospects for the use of acute phase proteins and markers of disease in animals." Revue Med. Vet. **151**(7): 577-584.
- Egger, G, A. A., SG Escobar, PA Jones (2007). "Inhibition of histone deacetylation does not block resilencing of p16 after 5-aza-2'-deoxycytidine treatment." Cancer Research(67): 346-353.
- Ensembl (2013). "Gene: ACAD10 ENSG00000111271."
- Ensenauer, R, M. H., JM Willard, ES Goetzman, TJ Corydon, BB Vandahl, A-W Mohsen, G Isaya, J Vockley (2005). "Human acyl-CoA dehydrogenase-9 plays a novel role in the mitochondrial beta-oxidation of unsaturated fatty acids." J Biol Chem(280): 32309-32316.
- Exil, V. J., et al. (2003). "Very-long-chain acyl-coenzyme a dehydrogenase deficiency in mice." Circ Res **93**(5): 448-455.
- Frerman, FE, S. G. (1985). "Fluorometric assay of acyl-CoA dehydrogenases in normal and mutant human fibroblasts." Biochem Med(33): 38-44.
- Fu, Z, M. W., R Paschke, KS Rao, FE Frerman, J-J Kim (2004). "Crystal structures of human glutaryl-CoA dehydrogenase with and without an alternate substrate: structural bases of dehydrogenation and decarboxylation reactions." Biochemistry(43): 9674-9684.
- GallusReactome (2010). "Mitochondrial Fatty Acid Beta-Oxidation [Homo sapiens]."

- Ghisla, S, C. T. (2004). "Acyl-CoA dehydrogenases. A mechanistic overview." Eur J Biochem(271): 494-508.
- Goodpaster, B. H. (2013). "Mitochondrial deficiency is associated with insulin resistance." Diabetes **62**(4): 1032-1035.
- Gore, SD L. W., S Zhai, WD Figg, RC Donehower, GJ Dover, M Grever, CA Griffin, LB Grochow, EK Rowinsky, Y Zabalena, AL Hawkins, K Burks, CB Miller (2001). "Impact of the putative differentiating agent sodium phenylbutyrate on myelodysplastic syndromes and acute myeloid leukemia." Clinical Cancer Res(8): 2330-2339.
- Graves, J. A., et al. (2012). "Mitochondrial structure, function and dynamics are temporally controlled by c-Myc." PLoS One **7**(5): e37699.
- Haga, Y., et al. (2011). "N-Glycosylation Is Critical for the Stability and Intracellular Trafficking of Glucose Transporter GLUT4." Journal of Biological Chemistry **286**(36): 31320-31327.
- Hashimoto, T., et al. (1999). "Peroxisomal and mitochondrial fatty acid beta-oxidation in mice nullizygous for both peroxisome proliferator-activated receptor alpha and peroxisomal fatty acyl-CoA oxidase. Genotype correlation with fatty liver phenotype." J Biol Chem **274**(27): 19228-19236.
- He, M., Pei, Z, Mohsen, A. W. Watkins, P. Murdoch, G. Van Veldhoven, P. P. Ensenauer, R. Vockley, J. (2011). "Identification and characterization of new long chain acyl-CoA dehydrogenases." Mol Genet Metab **102**(4): 418-429.
- Houten, S. M. and R. J. Wanders (2010). "A general introduction to the biochemistry of mitochondrial fatty acid beta-oxidation." J Inherit Metab Dis **33**(5): 469-477.
- Ibdah, J. A., et al. (2001). "Lack of mitochondrial trifunctional protein in mice causes neonatal hypoglycemia and sudden death." J Clin Invest **107**(11): 1403-1409.
- Ikeda, K. O.-I., K Tanaka (1985). "Purification and characterization of short-chain, medium-chain, long-chain acyl-CoA dehydrogenases from rat liver mitochondria. Isolation of the holo- and apoenzymes and conversion of the apoenzyme to the holoenzyme." J Biol Chem(260): 1311-1325.
- Ikeda, Y, C. D., K Tanaka (1983). "Separation and properties of five distinct acyl-CoA dehydrogenases from rat liver mitochondria." J Biol Chem(258): 1066-1076.
- Ikeda, Y D. H., K Okamura-Ikeda, K Tanaka (1985). "Mechanism of action of short-chain, medium-chain, and long-chain acyl-CoA dehydrogenases: Direct evidence for carbanion formation as an intermediate step using enzyme-catalyzed C-2 proton/deuteron exchange in the absence of C-3 exchange." J Biol Chem(260): 1326-1337.

- Ikeda, Y. K. O.-I., K Tanaka (1985). "Spectroscopic analysis of the interaction of rat liver short chain, medium chain and long chain acyl-CoA dehydrogenases with acyl-CoA substrates." Biochemistry(24): 7192-7199.
- Ikeda, Y., K. T. (1983). "Purification and characterization of 2-methyl-branched chain acyl Coenzyme A dehydrogenase, an enzyme involved in isoleucine and valine metabolism, from rat liver mitochondria." J Biol Chem(258): 9477-9487.
- Izai, K, Y. U., T Orii , S Yamamoto ,T Hashimoto (1992). "Novel fatty acid δ^2 -oxidation enzymes in rat liver mitochondria. 1. Purification and properties of very-long-chain acyl-Coenzyme A dehydrogenase." J Biol Chem(267): 1027-1033.
- Janssen, U. and W. Stoffel (2002). "Disruption of mitochondrial beta -oxidation of unsaturated fatty acids in the 3,2-trans-enoyl-CoA isomerase-deficient mouse." J Biol Chem **277**(22): 19579-19584.
- Ji, S., et al. (2008). "Homozygous carnitine palmitoyltransferase 1b (muscle isoform) deficiency is lethal in the mouse." Molecular Genetics and Metabolism **93**(3): 314-322.
- Katagiri, H., et al. (2002). "Acyl-coenzyme a dehydrogenases are localized on GLUT4-containing vesicles via association with insulin-regulated aminopeptidase in a manner dependent on its dileucine motif." Molecular Endocrinology **16**(5): 1049-1059.
- Kelley, D. E., et al. (1999). "Skeletal muscle fatty acid metabolism in association with insulin resistance, obesity, and weight loss." Am J Physiol **277**(6 Pt 1): E1130-1141.
- Kim J-J, M. W., R Paschke (1993). "Crystal structures of medium-chain acyl-CoA dehydrogenase from pig liver mitochondria with and without substrate." Proc Natl Acad Sci USA(90): 7523-7527.
- Koizumi, T., et al. (1988). "Infantile disease with microvesicular fatty infiltration of viscera spontaneously occurring in the C3H-H-2(0) strain of mouse with similarities to Reye's syndrome." Lab Anim **22**(1): 83-87.
- Kormanik, K., et al. (2012). "Evidence for involvement of medium chain acyl-CoA dehydrogenase in the metabolism of phenylbutyrate." Molecular Genetics and Metabolism **107**(4): 684-689.
- Kurtz, D. M., et al. (1998). "Targeted disruption of mouse long-chain acyl-CoA dehydrogenase gene reveals crucial roles for fatty acid oxidation." Proc Natl Acad Sci U S A **95**(26): 15592-15597.
- Kuwajima, M., et al. (1991). "Animal model of systemic carnitine deficiency: analysis in C3H-H-2 degrees strain of mouse associated with juvenile visceral steatosis." Biochem Biophys Res Commun **174**(3): 1090-1094.

- Lau, SM, C. T. (1987). "The nature of enzyme-substrate complexes in acyl-coenzyme A dehydrogenases." Biochem Biophys Acta(919): 171-174.
- Lehninger, N., and Cox (1982). "Principles of Biochemistry, 2nd edition."
- Liu, J., et al. (2013). "Vascular remodeling after ischemic stroke: Mechanisms and therapeutic potentials." Prog Neurobiol.
- Macheroux, P, C. S., H Büttner, V Kieweg, H Rüterjans, S Ghisla (1997). "Medium-chain acyl CoA dehydrogenase: evidence for phosphorylation." J Biol Chem(378): 1381-1385.
- Matsubara, Y. I., E Naito, H Ozasa, R Glassberg, J Vockley, Y Ikeda, J Kraus (1989). "Molecular cloning and nucleotide sequence of cDNAs encoding the precursors of rat long chain acyl- Coenzyme A, short chain acyl-Coenzyme A, and isovaleryl-Coenzyme A dehydrogenases. Sequence homology of four enzymes of the acyl-CoA dehydrogenase family." J Biol Chem(267): 16321-16331.
- McAndrew, R. P., et al. (2008). "Structural basis for substrate fatty acyl chain specificity: crystal structure of human very-long-chain acyl-CoA dehydrogenase." J Biol Chem **283**(14): 9435-9443.
- McAndrew, RP, Y. W., A-W Mohsen, M He, J Vockley, J-J Kim (2008). "Structural basis for substrate fatty acyl chain specificity: crystal structure of human very-long-chain acyl-CoA dehydrogenase." J Biol Chem(283): 9435-9443.
- McKean, MC, F. F., DM Mielke (1979). "General acyl-CoA dehydrogenase from pig liver. Kinetic and binding studies." J Biol Chem(254): 2730-2735.
- Mihalik, B., et al. (2003). "Endocytosis of the AT1A angiotensin receptor is independent of ubiquitylation of its cytoplasmic serine/threonine-rich region." Int J Biochem Cell Biol **35**(6): 992-1002.
- Mihalik, S. J., et al. (2010). "Increased levels of plasma acylcarnitines in obesity and type 2 diabetes and identification of a marker of glucolipototoxicity." Obesity (Silver Spring) **18**(9): 1695-1700.
- Miinalainen, I. J., et al. (2009). "Mitochondrial 2,4-dienoyl-CoA reductase deficiency in mice results in severe hypoglycemia with stress intolerance and unimpaired ketogenesis." PLoS Genet **5**(7): e1000543.
- Minkler, P. E., et al. (2008). "Quantification of carnitine and acylcarnitines in biological matrices by HPLC electrospray ionization-mass spectrometry." Clin Chem **54**(9): 1451-1462.
- Mohsen, A-W, J. V. (1995). "High-level expression of an altered cDNA encoding human isovaleryl-CoA dehydrogenase in Escherichia coli." Gene(160): 263-267.

- Mohsen, A-W, J. V. i. S. G., P. Kroneck, P. Macheroux, and H. Sund, eds.) (1999). "Flavins and Flavoproteins 1999, Rudolf Weber, New York 1999." 515-518.
- Mouse Specifics, I. (2010). "DigiGait™ Imaging System - Indices."
- Nasser, I, A.-W. M., I Jelesarov, J Vockley ,P Macheroux , S Ghisla (2004). "Thermal unfolding of medium-chain acyl-CoA dehydrogenase and iso(3)valeryl-CoA dehydrogenase: study of the effect of genetic defects on enzyme stability." Biochim Biophys Acta(1690): 22-32.
- National Center for Biotechnology Information, U. S. N. L. o. M. (2013). "ACAD10 acyl-CoA dehydrogenase family, member 10 [*Homo sapiens*]." from <http://www.ncbi.nlm.nih.gov/gene/80724>.
- Nguyen, T.V, B. A., TJ Corydon, S Ghisla, N Abd-El Razik, A-W Mohsen, SD Cederbaum, DS Roe, CR Roe, NJ Lench, J Vockley (2002). "Identification of isobutyryl-CoA dehydrogenase and its deficiency in humans." Mol Genet Metab(77): 68-79.
- Nyman, L. R., et al. (2005). "Homozygous carnitine palmitoyltransferase 1a (liver isoform) deficiency is lethal in the mouse." Molecular Genetics and Metabolism **86**(1-2): 179-187.
- Omura, T. (1998). "Mitochondria-targeting sequence, a multi-role sorting sequence recognized at all steps of protein import into mitochondria." J Biochem **123**(6): 1010-1016.
- Pike, ACW, V. H., C Smee ,FH Niesen ,KL Kavanagh ,C Umeano , AP Turnbull ,F Von Delft , J Weigelt,A Edwards ,CH Arrowsmith ,M Sundstrom , U Oppermann (2007). "Worldwide Protein Data Bank (PDB ID: 2JIF)."
- Pociask, D. A., et al. (2013). "IL-22 is essential for lung epithelial repair following influenza infection." Am J Pathol **182**(4): 1286-1296.
- Qi, X, T. H., Y Okuma, M Kaneko, Y Nomura (2004). "Sodium 4-phenylbutyrate protects against cerebral ischemic injury." Mol Pharmacol(66): 899-908.
- Rinaldo, P, J. O. S., PM Coates, DE Hale, CA Stanley, K Tanaka (1988). "Medium-chain acyl-CoA dehydrogenase deficiency. Diagnosis by stable-isotope dilution measurement of urinary Nhexanoylglycine and 3-phenylpropionylglycine." N Eng J Med(319): 1308-1313.
- Rozen, R, J. V., L Zhou, R Milos, J Willard, K Fu, C Vicaneck, L Low-Nang, E Torban, B Fournier (1994). "Isolation and expression of a cDNA encoding the precursor for a novel member (ACADSB) of the acyl-CoA dehydrogenase gene family." Genomics(24): 280-287.

- Reddy, J. K. and T. Hashimoto (2001). "Peroxisomal beta-oxidation and peroxisome proliferator-activated receptor alpha: an adaptive metabolic system." Annu Rev Nutr **21**: 193-230.
- Rehman, K. K., et al. (2005). "Efficient gene delivery to human and rodent islets with double-stranded (ds) AAV-based vectors." Gene Ther **12**(17): 1313-1323.
- Saito, Y, H. S., H Tsugawa, I Nakagawa, J Matsuzaki, Y Kanai, T Hibi (2009). "Chromatin remodeling at Alu repeats by epigenetic treatment activates silenced microRNA-512-5p with downregulation of Mcl-1 in human gastric cancer cells." Oncogene(38): 2738-2744.
- Schiffer, S. P., et al. (1989). "Organic aciduria and butyryl CoA dehydrogenase deficiency in BALB/cByJ mice." Biochem Genet **27**(1-2): 47-58.
- Schulz, H. (1974). "Long chain enoyl coenzyme A hydratase from pig heart." J Biol Chem(249): 2704-2709.
- Swigonova, Z., et al. (2009). "Acyl-CoA Dehydrogenases: Dynamic History of Protein Family Evolution." Journal of Molecular Evolution **69**(2): 176-193.
- Swigonova, Z., et al. (2009). "Acyl-CoA dehydrogenases: Dynamic history of protein family evolution." J Mol Evol **69**(2): 176-193.
- Tiffany, K. A., et al. (1997). "Structure of human isovaleryl-CoA dehydrogenase at 2.6 Å resolution: structural basis for substrate specificity." Biochemistry **36**(28): 8455-8464.
- Tiffany, KA, D. R., M Wang, R Paschke, A-W Mohsen, J Vockley, J-J Kim (1997). "Structure of human isovaleryl-CoA dehydrogenase at 2.6 angstrom resolution - basis for substrate specificity." Biochemistry(36): 8455-8464.
- Tolwani, R. J., et al. (2005). "Medium-chain acyl-CoA dehydrogenase deficiency in gene-targeted mice." PLoS Genet **1**(2): e23.
- Vilatoba, M, C. E., G Bilbao, CA Smyth, S Jenkins, JA Thompson, DE Eckhoff and C. JL (2005). "Sodium 4-phenylbutyrate protects against liver ischemia reperfusion injury by inhibition of endoplasmic reticulum-stress mediated apoptosis." Surgery(138): 342-351.
- Vockley, J. "ACAD10 & 11 Grant Renewal."
- Vockley, J., et al. (2002). "Diagnosis and management of defects of mitochondrial beta-oxidation." Curr Opin Clin Nutr Metab Care **5**(6): 601-609.
- Vockley, J. and D. A. Whiteman (2002). "Defects of mitochondrial beta-oxidation: a growing group of disorders." Neuromuscul Disord **12**(3): 235-246.

- Vockley, J, A.-W. M., B Binzak, J Willard, A Fauq (2000). "Mammalian branched-chain Acyl-CoA Dehydrogenases: Molecular cloning and characterization of the recombinant enzymes." Methods Enzymol(324): 241-258.
- Wang, Y., et al. (2010). "Evidence for physical association of mitochondrial fatty acid oxidation and oxidative phosphorylation complexes." J Biol Chem **285**(39): 29834-29841.
- Wood, P. A., et al. (1989). "Short-chain acyl-coenzyme A dehydrogenase deficiency in mice." Pediatr Res **25**(1): 38-43.
- Willard, J, C. V., KP Battaile, PP Vanveldhoven, AH Fauq, R Rozen, J Vockley "Cloning of a cDNA for short/branched chain acyl-coenzyme A dehydrogenase from rat and characterization of its tissue expression and substrate specificity." Arch Biochem Biophys(331): 127-133.
- Xin Ye, C. J., Li Zeng, Shaohua Gu, Kang Ying, Yi Xie, Yumin Mao (2004). "Cloning and characterization of a human cDNA ACAD10 mapped to chromosome 12q24.1." Molecular Biology Reports **31**: 191-195.
- Zhang, J, W. Z., D Zou, G Chen, T Wan, M Zhang, X Cao (2002). "Cloning and functional characterization of ACAD-9, a novel member of human acyl-CoA dehydrogenase family." Biochem Biophys Res Commun(297): 1033-1042.
- Zolman, B. K., et al. (2007). "IBR3, a novel peroxisomal acyl-CoA dehydrogenase-like protein required for indole-3-butyric acid response." Plant Mol Biol **64**(1-2): 59-72.